EXPERIMENTAL AND THEORETICAL INVESTIGATION OF A HORIZONTAL FREE TURBULENT DIFFUSION FLAME

by

Saadat Ali Syed, B.E(Mech), M.Eng.

A thesis submitted for the degree of Doctor of Philosophy of the University of London and for the Diploma of Imperial College.

June 1977

Mechanical Engineering Department,
Imperial College,
London, SW7

ABSTRACT

A prediction procedure for three-dimensional, turbulent, free-jet diffusion flames is described in this thesis along with a complimentary experimental programme.

The prediction procedure consists of a numerical method for solving the partial differential equations which govern the transport of mass and momentum in three-dimensional parabolic flows.

A two equation turbulence model which uses the kinetic energy of turbulence and its dissipation rate to calculate the eddy viscosity of turbulent flows is incorporated in the prediction procedure. This model is shown to predict a free, turbulent, round jet reasonably well. A combustion model which assumes a one step global reaction between fuel and oxidant, equality of exchange coefficients and fast chemical kinetics is also incorporated into the prediction procedure. Account is taken of the temporal behaviour of species mass fractions by a statistical approach which uses an assumed form of the probability density function for a mixing parameter to calculate mean values of species mass fractions, temperature, and density.

Measurements of mean temperature contours and mean oxygen concentration profiles have been made in a town gas horizontal, turbulent free-jet diffusion flames.

Predictions of the horizontal flame and some vertical flames are made. Reasonable agreement is obtained between experiments and predictions. It is argued that the descrepancies which do exist between experiments and prediction may be attributed to the inability of the turbulence model to predict the correct initial decay rate of the jet and to the underprediction of the mass fraction of fuel by the combustion model.

ACKNOWLEDGEMENTS

I am pleased to acknowledge the guidance and encouragement provided by my supervisor Dr. F.C. Lockwood. I owe much to his constructive criticism of my research method and my technical writing. Dr. A.D. Gosman maintained a constant interest in my work and guided in the developement of the computer program.

I have benefited from the advice and friendship provided by all my colleagues especially Drs. G. Bergeles, E. Khalil, A. Melling, D. Melling and N. Vlachos and Messrs. A. Morse, A. Salooja, S. Samaraweera and P. Watkins.

I would like to thank Messrs. R. Church, J. Laker, J. Pilmer and A. Robinson among the technical staff of the department who helped in the manufacture and assembly of my experimental rig.

I would also like to thank Miss E. Archer and Mrs. S. Boote for cheerfully allowing unlimited use of the library facilities, and Mrs. Hill for tracing the diagrams. For financial support I am indebted to N.E.D. Engineering College, Pakistan.

The understanding and help of my sister and her family have been a great support for my work; and to them I dedicate this thesis.

CONTENTS

		Page
ABSTRACT		1
ACKNOWLEDGEMENTS		2
CONTENTS		3
LIST OF TABLES		7
LIST OF FIGURES		8
1.0	INTRODUCTION	11
	1.1 The Problem	11
	1.2 Practical Importance	11
	1.3 Background	12
	1.4 Present Contribution	15
	1.5 Layout of the Thesis	17
2.0	EXPERIMENTAL PROGRAMME	18
	2.1 Introduction	18
	2.2 Design of Experiment	19
	2.2.1 Choice of Fuel, Burner and Reynolds Numbers	19
	2.2.2 Draught Screening and Flame Axis Alignment	22
	2.3 Mean Temperature	24
	2.3.1 Techniques of Temperature Measurement	24
	2.3.2 Thermocouple Probe	26
	2.3.2.1 Criteria for Selection of Thermocouple Material	27
	2.3.2.2 Estimation of and Compensation for Errors	28
	2.3.2.3 Thermocouple Fabrication	31
	2.3.3 Instrumentation	32

Page

2.4 Mean Oxygen Concentration Measurement 33

2.4.1 Techniques of Oxygen Concentration Measurement 33

2.4.1.2 Gas Analysis 35

2.4.2 Design of Sampling System 35

2.4.3 Instrumentation 36

2.5 Results and Discussion 36

2.6 Conclusions 39

3.0 MEAN FLOW EQUATIONS 40

3.1 Instantaneous Equations 40

3.2 Time Averaged Equations 42

3.2.1 Variable Density, Time Averaged Equations 42

3.2.2 Mean Flow Equations Neglecting Density Fluctuations 45

4.0 THE TURBULENCE MODEL 47

4.1 Introduction 47

4.2 Turbulence Models for Constant-Density Flows 48

4.2.1 Zero Equation Models 48

4.2.2 One Equation Models 50

4.2.3 Two Equation Models 52

4.2.4 Prediction of a Round Jet 57

4.2.5 Multi-Equation Models 57

4.3 A Two Equation Model for Reacting Flows 58

4.3.1 Turbulence Energy Equation for Reacting Flows 62

4.3.2 Transport Equations for Model I 65

4.4 Modelling of Density Fluctuations 66

4.4.1 Favre Averaging 67

4.4.2 Brays Approach 67

Page

4.4.3 Choice of the Method 71

4.5 The Transport and Dissipation of Scalar Fluctuations 74

5.0 THE COMBUSTION MODEL 77

5.1 Introduction 77

5.2 Some Historical Combustion Studies 80

5.3 Physical Picture of a Diffusion Flame 83

5.4 Simple Chemically Reacting System 87

5.4.1 Calculation of Instantaneous Thermodynamic Quantities 89

5.5 Modelling of Fluctuations in the Mixture Fraction 93

5.5.1 Simple Model for the Fluctuations in the Mixture Fraction 93

5.5.2 Periodic Model for the Fluctuations in the Mixture Fraction 94

5.5.3 Models Based on Random Fluctuations 95

5.6 Clipped Guassian Distribution Function 97

5.6.1 Calculation of Thermodynamic Quantities 99

5.7 Concluding Remarks 104

6.0 THE NUMERICAL PROCEDURE 106

6.1 Introduction 106

6.2 Simplification of the Transport Equations. Due to the Boundary Layer Nature of the Flow. 108

6.3 Transport Equations in the Curvi-linear Co-ordinate System 111

6.4 The Discretization of the Partial Differential Equations 113

6.4.1 The Grid System 114

6.4.2 Location of the Variables on the Grid 114

6.4.3 The Control Volumes 114

6.4.4 Integration of Partial Differential Equations 115

Page

6.4.4.1 Integration of the Continuity Equation 116

6.4.4.2 Integration of the General Φ Transport Equation 117

6.4.4.3 Integration of the Momentum Equations 124

6.5 Description of SIMPLE 124

6.6 Summary of the Solution Procedure 126

6.7 Specification of Initial and Boundary Conditions 128

6.8 Validation of the Computation Procedure 129

6.9 Closure 132

7.0 PREDICTION OF TURBULENT DIFFUSION FLAMES 134

7.1 Introduction 134

7.2 Specification of Initial and Boundary Conditions 135

7.3 Grid Specification 137

7.4 Prediction of Vertical Flames 137

7.5 Prediction of Horizontal Flames 145

7.6 Prediction of Vertical Flames with Model II 147

7.7 Concluding Remarks 149

8.0 CLOSURE 150

8.1 Attainment of Objectives 150

8.2 Suggestions for Future Work 151

8.2.1 Experimental Work 151

8.2.2. Theoretical Work 152

REFERENCES 154

NOMENCLATURE 163

APPENDICES 169

FIGURES 181

List of Tables

Table	Title	Page
2.1	Physical properties and volumetric composition of Town gas	23
2.2	Methods of determining temperature in flames	25
4.1	Comparison of turbulence models	49
4.2	List of dependent variables for the second equation	50
4.3	The turbulence model constants	56
4.4	List of flows for which K-ε model has been used	59
6.1	Extra terms added to Model I to obtain Model II	107
6.2	Boundary conditions for the prediction procedure	130
7.1	Boundary conditions for 2-D and 3-D flames	138
7.2	Values of adjustable constants used in present study	140
7.3	Values of adjustable constants used by Naguib	140

LIST OF FIGURES

Figure	Title	Page
2.1a	Burner tube and plug	182
2.1b	Burner tube and plugs (Half-sectioned view)	182
2.2	Experimental set-up	183
2.3	Calibration curve for radiation correction	184
2.4a	Thermocouple probe	185
2.4b	Thermocouple probe mounted on Cathetometer	185
2.5	Block diagram for temperature measurement	186
2.6	Gas sampling probe	187
2.7	Block diagram for oxygen concentration measurement	188
2.8a	Long time exposure photograph of flame I	189
2.8b	Long time exposure photograph of flame II	189
2.9	Horizontal turbulent diffusion flame	190
2.10	Temperature contours at Z/D = 34.5 (Flame I)	191
2.11	Temperature contours at Z/D = 47 (Flame I)	192
2.12	Temperature contours at Z/D = 29.0 (Flame II)	193
2.13	Temperature contours at Z/D = 35.4 (Flame II)	194
2.14	Temperature contours at Z/D = 47.0 (Flame II)	195
2.15	Temperature contours at Z/D = 59.0 (Flame II)	196
2.16a	Temperature profile along Y-axis at Z/D = 13.0 (Flame II)	197
2.16b	Oxygen concentration profile along Y-axis at Z/D = 13.0 (Flame II)	197
2.17a	Temperature profile along Y-axis at Z/D = 29.0 (Flame II)	198
2.17b	Oxygen concentration profile along Y-axis at Z/D = 29.0	198
2.18a	Temperature profile along Y-axis at Z/D = 34.0	199
2.18b	Oxygen concentration profile along Y-axis at Z/D = 34.0	199
2.19a	Temperature profile along Y-axis at Z/D = 47.0 (Flame II)	200

Figure	Title	Page
2.19b	Oxygen concentration profile along Y-axis at Z/D = 47.0 (Flame II)	200
2.20a	Temperature profile along Y-axis at Z/D = 59.0 (Flame II)	201
2.20b	Oxygen concentration profile along Y-axis at Z/D = 59.0 (Flame II)	201
4.1	Axial distribution of W_{CL}/W_{inlet}	202
4.2	Fully developed velocity profile	202
5.1a	Laminar flame front	203
5.1b	Wrinkled laminar flame	203
5.2a	Turbulent mixing of two fluids	204
5.2b	Control volume in a turbulent fluid	204
5.3	Mixture fraction VS various thermodynamic variables	205
5.4	Square wave fluctuation	206
5.5	Triangular wave fluctuation	206
5.6	Probability density function for a conserved scalar in a slightly heated round jet	207
5.7	Clipped Gaussian distribution function for the mixture fraction	208
6.1	Cylindrical co-ordinate grid system	209
6.2	Quasi-orthogonal co-ordinate grid system	209
6.3	Grid system in $\beta \sim \eta$ plane	210
6.4	Grid system in $\zeta \sim \eta$ plane	210
6.4	The staggered grid arrangement	211
6.6	The control volume used to derive the finite difference equations	212
6.7	Weighting factor for non-uniform grid	213
6.8a	First cross-stream plane	214
6.8b	Boundary conditions for the calculation procedure	214

Figure	Title	Page
6.9	Fully developed profile of axial velocity in a round pipe	215
6.10	Centre-line velocity development in a square duct	216
6.11	Fully developed velocity profile in a square duct (central plane)	216
6.12	Radial distribution of W	217
6.13	Radial distribution of V	217
7.1	Axial distribution of $W_{CL}/W_{O,CL}$	219
7,2	Radial profile of $\overline{W}/\overline{W}_{CL}$ at Z/D = 39.0	219
7.3	Axial distribution of mean temperature	220
7.4	Radial profile of mean temperature at Z/D = 10.0	221
7.5	Radial profile of mean temperature at Z/D = 40.0	222
7.6	Radial profile of mean temperature at Z/D = 90.0	223
7.7	Non-dimensional profile of mean temperature at Z/D = 90.0	224 224
7.8	Temperature profile along Y-axis at Z/D = 35.4	225
7.9	Temperature profile along Y-axis at Z/D = 47.0	225
7.10a	Temperature profile along Y-axis at Z/D = 13.0	226
7.10b	Oxygen concentration along Y-axis Z/D = 13.0	226
7.11a	Temperature profile along Y-axis at Z/D = 29.0	227
7.11b	Oxygen concentration profile along Y-axis at Z/D = 29.0	227
7.12a	Temperature profile along Y-axis at Z/D = 35.4	228
7.12b	Oxygen concentration profile along Y-axis at Z/D = 35.4	228
7.13a	Temperature profile along Y-axis at Z/D = 47.0	229
7.13b	Oxygen concentration profile along Y-axis at Z/D = 47.0	230
7.14	Radial profile of $\overline{f}$ at Z/D = 20.0	230
7.15	Radial profile of $\overline{T}$ at Z/D = 20.0	231

CHAPTER ONE

1. Introduction

1.1 The Problem

The work reported in this thesis comprises the experimental and theoretical investigation of a buoyancy-influenced, horizontal, round, free-jet, diffusion flame. The stream lines of the flow are curved because of cross stream buoyancy, the flow is asymmetric and consequently three dimensional.

The experiments were carried out on two horizontal town gas diffusion flames of Reynolds number 23000, and 32500, the diameter of the burner tube was 12.7 mm. Mean temperature contours were measured in planes perpendicular to the axis of the burner tube at various downstream stations. Mean oxygen concentration profiles were also measured in these planes along the diameter aligned with the gravity vector.

A computer program was developed for the prediction of the class of turbulent reacting flows which include the experimental flames. The computational procedure is based on a numerical scheme for solving the partial differential equations which govern the transport of mass, momentum and energy in such flows. It incorporates mathematical 'models' for both the turbulence and the combustion. The ability of the turbulence and combustion models to predict such flows has been assessed by comparing the experimental results with those obtained by the prediction procedure.

1.2 Practical Importance

The ability to predict three dimensional turbulent reacting flows successfully is the aim of the research effort in the field of combustion. This is of immense practical importance for two principal reasons. Firstly as an aid for determining the optimal design of combustion equipment such as furnaces, combustion chambers of gas turbines, internal combustion engines,

etc. and secondly, to understand the effect of combustion on the environment by studying the formation of pollutants by reaction and methods for minimizing them.

The present study is especially relevant to large industrial furnaces which are fired with fuel and air in the form of a round jet and in a mainly unpremixed state. The flame is asymmetric, primarily because the burner axis is normally not vertically oriented. In addition to this class of flows the calculation procedure can also be used to predict inert three-dimensional flows such as: flow through annular diffusers, fluids transported in ducts of irregular cross sections, river flows and other similar circumstances.

1.3 Background

A considerable quantity of research work has been done in this department over the past ten years on the development of general, efficient and reliable numerical prediction procedures for engineering fluid flows. The aim is to replace, at least partially, the expensive experiments that precede any new design of fluid flow equipment by computer experiments which are very much less time consuming and economical. For example the influence of the length, diameter, Reynolds number, velocity ratio, swirl number, cooling load, etc. on the performance of a furnace can be investigated by changing only a few cards of a computer program.

With this end in view two computer programs were first developed, one for two dimensional boundary layer flows, Patankar and Spalding (1970) and the other for two dimensional elliptic flows, Gosman et al (1969). The two programs were tested for various laminar flows against analytical solutions. The agreement obtained showed that the computational schemes were correct. These two powerful tools facilitated the work on the development of turbulence models for inert flows. Initially Prandtl's

mixing length hypothesis was used (Launder and Spalding, 1972) to predict some simple flows such as fully developed turbulent pipe flow, boundary layers on smooth walls etc.The main drawback to this approach is that the mixing length cannot always be prescribed, for example in the developing region of a co-flowing jet and in almost all recirculating flows. This led to the development of a 'two equation model' in which eddy viscosity was described as a function of kinetic energy of turbulence and its dissipation rate, both of these variables being determined from the modelled form of their transport equations.

Rodi (1972) among others used the two-equation model to investigate several free shear flows such as plane jet, plane wake, radial jet, round jet etc. He found that these flows could be reasonably well predicted. The model has been tested for isothermal furnace flows by Elgobashi and Pun (1973) and Khalil et al (1975), the agreement with the experiment was found to be reasonable.

The computer program used by Khalil et al was based on the'pressure-velocity' method of solution of the relevant differential equations described by Carretto et al (1972). The development of this method was initiated by the long term interest in devising three-dimensional prediction procedures; the vorticity stream function method of Gosman et al (1969) could not be extended to three dimensional flows. Also, the specification of boundary conditions for the pressure velocity method is much simpler than for the vorticity stream function method. The success in the prediction of two dimensional flows encouraged the application of the two equation model to three dimensional parabolic flows. It was used to predict flows in rectangular diffusers by Sharma (1974) and flow in curved pipes by Pratap (1975) with reasonable success.

Work on combustion modelling was also proceeding during this time on parallel lines. Some early predictions were reported by Pun and

Spalding(1967) for a hypothetical, two dimensional cylindrical furnace fired by unpremixed fuel and air. The deficiency of this work was the lack of realism in the physical modelling. The eddy viscosity was calculated by means of a simple algebraic relation involving the physical dimensions of the combustion chamber, the mass flow rate and the density of the fluid. The role of concentration fluctuations was ignored completely, thermodynamic relations were only approximately specified and thermal radiation which can play an important role in combustion chambers was neglected. Gosman and Lockwood (1973) used the two equation model and an alternative flux radiation model to obtain predictions for a large experimental furnace which they compared with the data. They also neglected the influence of concentration fluctuations and hence were unable to predict the 'unmixedness' phenomenon; also the calculated maximum temperatures were higher than the experimental ones.

Spalding (1971a) chose to simulate the concentration fluctuations by solving a modelled form of the transport equation for the square of concentration fluctuations. He obtained good agreement for non-reacting flows. Spalding (1971b) suggested a 'square wave' model for the simulation of the temporal behaviour of these fluctuations to obtain values of mean temperature, oxidant and fuel in diffusion flames. This model was applied by Gosman and Lockwood (1973) in an attempt to obtain better agreement with the experiment than their previous predictions but the improvement was only marginal. Spalding's approach was subsequently improved by Naguib (1975) who adopted a form of Gaussian probability distribution function to determine time averages of fluctuating properties for free turbulent diffusion flames. Elgobashi (1975) applied this approach to confined diffusion flames. Reasonable success was achieved in both the above cases.

Reliable experimental data is vital for the validation of all pre-

diction procedures. In the turbulent combustion field there is a general lack of simple experiments, even for two dimensional flows, with well defined initial and boundary conditions which are an essential input to any prediction procedure. Odidi (1974) measured time-mean and fluctuating temperature in methane diffusion flames and mean temperature in town gas diffusion flames. The flames were free and the exit conditions from the burner were those of a fully developed pipe flow. This data was used by Naguib for the validation of the combustion model for two dimensional flows.

1.4 Present Contribution

A natural extension to the development of the prediction program would be to apply the turbulence model, which had been successful in predicting three dimensional inert flows, and the combustion model, which had been found satisfactory for two dimensional flows, to three dimensional reacting flows. The need again arose for simple experiments. Since data from such experiments were scarce, it was decided to undertake an experimental program in which time-mean temperature and oxygen concentration were very carefully measured in horizontal free gaseous diffusion flames.

The flames would be large enough to be strongly influenced by cross stream buoyancy making them asymmetric and hence three dimensional. This experiment, it was thought, would also be useful in studying the influence of buoyancy and stream line curvature on turbulence and as such would provide a good test of the turbulence model. The surroundings would be stagnant air at ambient conditions, imposing no special difficulty in specifying the boundary conditions for the solution procedure. The burner tube would be long and round so that fully developed pipe flow initial conditions would prevail at its exit.

The techniques of measuring mean temperature and oxygen concentration

were fairly well established, so data of reasonable accuracy could be expected. It was decided to measure mean temperature and mean oxygen concentration contours in two flames of different fuel mass flow rates, so that the influence of the ratio of Reynolds number to Grashof number could also be investigated. It was found that very long times were required to measure temperature, especially at the 'edge' of the flame, because of large scale fluctuations. Moreover the thermocouples were fragile and broke frequently causing delays. The oxygen concentration measurements were even more time consuming. Since electronic integration could not be carried out with the instrument used, the system response time had to be increased in order to obtain repeatable readings.

For the prediction of the above experimental data a computer program was required which could solve three dimensional parabolic flows. Unfortunately no such program was available in the department. The computer programs used by Pratap and Sharma were the copyright of a private company whose permission for their use could not quickly be obtained. Hence it was decided to develop a new program for this purpose. A computer program to solve two dimensional elliptic flows (TEACH-2D) was available and it was decided to gain experience with the TEACH family of programs by first converting this program into a two dimensional parabolic procedure. This was done as a prelude to making the three dimensional elliptic program, which was then being developed by Vlachos and Humphrey (1975), applicable to three dimensional parabolic problems. The development of these three programs was time consuming and while valuable experience was gained from the development of the two dimensional parabolic program it did not contribute directly to this thesis. The routines for calculating the radial velocity at the free stream and the 'expanding grid' for the flow were first tried in the two dimensional program.

Only when the three-dimensional parabolic computer program had been developed and the combustion and turbulence models incorporated,

it was possible to start work on predicting the present experiment.

1.5 Layout of the Thesis

The remainder of this thesis is divided into seven chapters and four appendices. In the second chapter the experimental program is described, the details of the design of the experiment with the choice of fuel, burners and Reynolds numbers are given. The various techniques of mean temperature and oxygen concentration measurement are discussed and the reasons for the final choice of a thermocouple and a quartz microprobe with paramagnetic oxygen analyser are presented. The sources of errors in these measurements are identified and their likely magnitude is discussed. Chapter 2 closes with the presentation and discussion of the experimental results.

Chapter three gives two forms of the time-averaged governing partial differential transport equations, one in which the fluctuating density-velocity correlations have been neglected and the other in which they are not. These equations are in cylindrical coordinates and are derived from their instantaneous counter parts by Reynolds averaging.

Chapter four is concerned with modelling of Reynolds stresses and turbulent mass fluxes. Different models of turbulence used to represent Reynolds stresses in constant density turbulent flows are outlined and a two equation model suitable for the present flow is selected. Two methods for dealing with turbulent mass fluxes: Favre averaging and the approach used by Bray (1974) are given and reasons for selecting the latter method are also given.

Chapter five deals with the modelling of combustion for turbulent diffusion flames. Various methods are examined and a model to predict the present experimental flame is selected. This model is based on an assumed form of probability density function for the fluctuations of a

mixing parameter. A single one step irreversible reaction in which fuel and oxidant combine stiochemetrically to form products is also assumed. Relations for calculating the mean thermodynamic quantities with the help of the above assumption are given.

In chapter six the forms of the governing partial differential equations applicable to three dimensional boundary layer flows are recast into a more suitable quasi-orthogonal coordinate system. These differential equations are then converted into difference ones by integrating them over a small control volume. This chapter also describes the 'SIMPLE' method of solving pressure linked equations.

In chapter seven the predictions are presented. They are compared with the experimental data and the reasons for the discrepancy between experiment and predictions are discussed.

The final chapter discusses the extent to which the objectives of the research program stated in this chapter are attained and presents some suggestions for future work.

CHAPTER TWO

2. Experimental Programme

2.1 Introduction

In this chapter the experimental programme is described. An outline of the objective of the experiment and the measurements undertaken are presented in this section. In section 2.2 the design of the experiment including the choice of fuel, burners and Reynolds numbers is described. Section 2.3 is concerned with the technique of mean temperature measurement, the design and fabrication of the thermocouple probe and the estimation of errors; while section 2.4 details the method of obtaining the mean oxygen concentration. In section 2.5 the mean flow behaviour and turbulence structure suggested by the results is discussed. Concluding remarks appear in section 2.6.

The experimental programme was undertaken because, as discussed in Chapter 1, very little experimental information is available on reacting flows, and particularly on turbulent diffusion flames.

Measurements in horizontal diffusion flames where the influence of cross-stream buoyancy is not negligible are, to the best of the author's knowledge, not available in the literature. Since most industrial flames are large unpremixed ones, horizontally fired, or fired at a significant angle to the vertical, it was decided to undertake measurements in horizontal, turbulent diffusion flames. The flames were gaseous fuelled, large enough to be fully turbulent, but small enough for the radiation losses to be negligible. Apart from giving insight into the structure of the turbulent flame, the experiment also served the purpose of providing data for validating the prediction procedure. It was decided to make the flame unconfined so that the effects of the wall on turbulence and of radiation from it on the heat transfer should not complicate the flow.

Time mean temperature and oxygen concentrations were measured since the techniques of obtaining them are fairly well established. In the absence of any other, it was felt that these data would give a reasonable preliminary insight into the flame structure. The determination of the more interesting fluctuating quantities is very difficult in reacting flows. The measurement techniques are not well established and although such data would greatly assist in the understanding of the diffusion flame, the limited time and financial resources available ruled out this area of investigation.

The measurements were made in two town gas diffusion flames of Reynolds numbers 32500 and 23000,hence forth called flame I and flame II respectively. Temperature contours were obtained in planes at 35 and 47 diameters for flame I and at 29,35,47,59 diameters for flame II. Mean oxygen concentration profiles were measured on vertical y-axis at 13,29,35,47 and 59 diameters for flame II.

Oxygen was sampled by a quartz microprobe and analysed by a paramagnetic oxygen analyser. A rhodium 20% - platinum vs rhodium 40% - platinum thermocuple was used to sense the temperature.

2.2. Design of Experiment

2.2.1 Choice of Fuel, Burner and Reynolds Numbers

The fuel chosen was town gas which was available in the laboratory. The supply pressure was boosted by using a pump. Apart from being readily available and economical, town gas had the advantage that it contained a fairly large amount of hydrogen (40-60% by vol) and, in consequence, produced a largely soot free flame. This greatly simplified the prediction task since the simulation of soot formation and burn-out is very much on the frontiers of existing combustion modelling capabilities and

the tackling of this subject area was not an objective of the present work.

Town gas had the further advantage that its flame speed was much larger than that of hydrocarbon fuels. This was again due to the large hydrogen content. As a result, diffusion flames of reasonably high Reynolds numbers could be obtained without 'blow-off'. The principal disadvantage arising from the use of town gas was that its composition varied from day to day; this was overcome by obtaining the composition on a daily basis from the suppliers. The experiment was discontinued on the few occasions when there was a drastic change in composition.

The choice of burner was governed by the fact that prediction procedures require the initial profiles of mean velocity, species concentration, turbulence energy and temperature to be specified. Since fully developed turbulent pipe flows are well documented and profiles for this condition of all the above quantities are available, it was decided to use a circular tube burner which was long enough to ensure fully developed exit conditions. The selection of the burner diameter and Reynolds number was made after trials using tubes of various diameters and flow rates. The final choice was determined by three constraints:

1) A Reynolds number sufficiently large to produce a fully turbulent jet was required.
2) The flame had to be large enough to be significantly affected by cross stream buoyancy.
3) The total heat release had to be smaller than the capacity of the exhaust system of the laboratory.

An estimate of the ratio of initial momentum to total buoyancy force was made for different Reynolds numbers (based on burner exit conditions) and tube diameters. The buoyancy force was calculated from the volume occupied by the flame (which was estimated from the flame length and spreading angle) and its bulk mean temperature calculated by using

the magnitude of the total heat release. The minimum Reynolds number required for a turbulent inert jet is 1700 Hinze (1959), hence four burners having high buoyancy to momentum ratios at Reynolds number larger than the minimum were selected for testing. The upper limit on the Reynolds number was dictated by the maximum flow that could be obtained from the burners. This was limited by the blow-off velocity for the smaller diameter burners and acceptable maximum heat release for the larger ones. The diameters of the burners were 3/8", 1/2", 5/8" and 3/4". They were tested at Reynolds numbers ranging from 1700 to 40,000. Flames from the 5/8" and 3/4" diameter burner were strongly affected by buoyancy (as judged visually) but their size and heat release was too large for the laboratory. The flame from 3/8" burner was buoyant only at very low Reynolds numbers; in addition it was sooty and susceptable to draughts. The 1/2" burner was finally selected. It was fully turbulent and exhibited sufficient buoyancy.

The burner used for the experimental runs consisted of a thick walled stainless steel seamless tube 1/2" in diameter. Its straightness was checked with the aid of three cylindrical plugs, having small holes drilled along their axes, which were inserted in burner tube Fig. 2.1. A laser beam was aligned with the axial holes of the plugs, and the central one was moved from one end of the tube to the other. It was considered straight when the laser beam passed unhindered through the three plugs. The exit end of the tube was machined to a thickness of 0.025" to eliminate recirculation in the initial region of the jet. Fully developed pipe flow is achieved in an axial length of about 40 diameters, Schlichting (1968), the present burner was 4 ft, or more than 90 diameters, in length. The mean velocity and turbulence kinetic energy profiles at the burner exit could be obtained from the literature, Laufer (1953); the length scale could be calculated from the shear stress, kinetic energy and mean velocity profiles.

2.2.2 Draught Screening and Flame Axis Alignment

Screening of the flame from draughts was very important since it was rather large and lazy. However, care had to be taken to ensure that the screening did not result in confinement effects. An open top cloth tent was errected around the flame of dimensions 10 ft wide, 20 ft long and 10 ft high. Inside this tent a steel mesh enclosure was constructed having dimensions of 6.5 ft wide, 10 ft long and 10 ft high. The height and breadth of the screen enclosure was more than the expected diameter of turbulent jet at 200 burner diameters (based on growth rate of $Y_{\frac{1}{2}}/Z=0.1$ and width $=6.0Y_{\frac{1}{2}}$). Smoke tests were made in order to visualize the entrainment pattern of the flame and to check for any recirculation zone inside the enclosure. The entrainment pattern was uniform, some recirculation zones were found in the far corners of the enclosure but their influence in the region of interest was considered negligible.

The burner tube was mounted on a compound table, fig. 2.2, which could be traversed in the horizontal plane to an accuracy of 0.25 mm. The probe was on a cathetometer which could be positioned in the vertical direction to an accuracy of 0.1 mm.

The flame axis was positioned normal to the plane of measurements by passing a laser beam through the burner tube in the manner described in sec 2.2.1. A reference position for the probes was established by moving the probes until their tip obstructed the beam. In the case of thermocouple, this was done every time it had to be replaced, which was usually after about four hours of measurements. In order to minimize setting up times, the laser was maintained permanently in position. The flow rate of fuel was measured by a Rotameter caliberated for town gas. The composition and property values of the town gas were obtained from the manufacturers and are given in table 2.1.

Table 2.1

Physical Properties of Town Gas

Viscosity	1.273×10^{-5}	Kg/ms
Density	0.473	Kg/m^3
Specific Heat	2.5×10^3	J/Kg^oC
Calorific Value	5.4×10^7	J/Kg
Molecular Weight	8.12	(Fuel constituents only)

Volumetric Composition of Town Gas

Hydrogen	0.55
Methane	0.27
Carbon Monoxide	0.04
Ethane	0.02
Carbon Dioxide	0.08
Nitrogen	0.04

2.3 Mean Temperature

2.3.1 Techniques of Temperature Measurement

The basic statistical definition of temperature can be given by way of the Maxwell-Boltzman distribution law (Fristrom and Westenberg, 1965) which can be written as:

$$f_i(v_i) = n \left(\frac{m_i}{2\ kT}\right)^{3/2} - e^{\left(\frac{m_i v_i^2}{2kT}\right)} \qquad 2.1$$

Here temperature is a characteristic parameter of the system at equilibrium. Since gas molecules can have more than one degree of freedom, more than one temperature can be associated with a gas that is not in complete equilibrium. Hence temperature is not an accurately defined concept in the reaction zone of flame, where equilibrium does not exist Gaydon and Wolfhard (1970). However the departure from eqiulibrium for steady small scale laboratory flames of bunsen type is small, Gaydon and Wolfhard (1970). Consequently, any one of the translational, vibrational and rotational energies of the gas molecule in such flames may be used to indicate local instantaneous temperature. Since translational equilibrium is achieved locally in very few molecular collisions and translational temperature is used in the equation of state and transport property calculation, hence any device measuring translational temperature is preferable, Fristrom and Westenberg (1965). Thermocouples have this advantage.

Some of the techniques used to measure temperature are presented in table 2.2. It can be seen that the thermocouple method has the added advantage of high spatial resolution. It is also economical and does not require very elaborate instrumentation. The construction of a thermocouple probe is tedious and time consuming but when carried out with sufficient care the effort is rewarded by accurate results. Individual cali-

Technique	Upper temperature limit, ^{o}K	Spatial resolution, cm	Precision, ^{o}K or %	Position error, cm	Corrections	Effects in flames	Cost of apparatus
Thermocouple	3000	10 diam. (10^{-2})	1^{o}	5 diam. (5×10^{-3})	Radiation	Aerodynamic wake and catalysis	Moderate, low
Resistance thermometer	3000	10^{-1}	1^{o}	10^{-2}	Radiation	Aerodynamic wake and catalysis	Moderate
Aerodynamic measurements	3500	10^{-3}	3%	Slight	Acceleration lag and thermo-mechanical effects	Quenching	Moderate
Optical pyrometry	None	5×10^{-1}	5^{o}	None	Nonequilibrium effects	Additives	Moderate
Spectroscopic line intensity	None	5×10^{-1}	5^{o}	None	Nonequilibrium effects	None	High
Pneumatic	2500	10 diam. (10^{-2})	2%	5 diam. (5×10^{-3})	Orifice coefficients	Wake and catalysis	Low
X-ray absorption	None	5×10^{-1}	3%	None	Molecular weight	None	High
Interferometer	None	5×10^{-2}	1%	None	Molecular weight	None	High
Inclined slit	None	5×10^{-2}	1%	None	Molecular weight	None	Low

Table 2.2* Methods of Determining Temperatures in Flames

*Extracted from Fristrom and Westenberg (1965)

bration of thermocouples is not required. The calibration tables supplied by the manufacturers are accurate enough for the present experiment (0.05%). Hence the need for having elaborate calibration facilities does not arise. Because of these several advantages the thermcouple probe was selected as the temperature measurement technique.

2.3.2. Thermocouple Probe

One of the first measurements of temperature in flames using a thermocouple probe were performed by Klaukens and Wolfhard (1948). They used a Ni vs Ni-Cr thermocouple to obtain the temperature distribution in low pressure flat acetylene-air flames. Their results were open to uncertainties. First they had to correct for radiation loss some of their indicated temperatures by as much as 1500^{o}K. Since neither the convective heat transfer coefficient nor the emissivity of the thermocouple was known, the validity of such large corrections was doubtful. Second the diameter of their thermocouple bead was about one eighth of the visible flame thickness which was quite large. Third, the thermocouple was uncoated which could have resulted in catalytic errors. Friedman (1953) improved the technique by using very small diameter thermocouple wires (0.0005 cm). He measured temperature in laminar propane-air flames under lean and low pressure conditions in order to reduce their maximum temperatures. In this way the correction required for radiation loss was reduced to about 40^{o}K. The thermocouple was also coated with an anti-catalytic ceramic. Smith et al (1969) measured temperatures in turbulent diffusion flames at atmospheric pressure. An Irridium vs Irridium 60%-Rhodium 40% thermocouple was used which had a higher melting point than the maximum temperature obtained in the flame. It was given a Zirconia coating to avoid catalytic errors. This thermocouple was very brittle and had a very limited working life. Recently Odidi (1974) measured temperature in town gas turbulent diffusion

flames using a 100 μm diameter, 40% rhodium - 60% platinum versus 20% rhodium - 80% platinum thermocouple. Alumina was used as an anti-catalytic coating. His thermocouple being small, anticatalytic and of high tensile strength, was free from the errors described above.

2.3.2.1. Criteria for Selection of Thermocouple Material

The choice of thermocouple probe is subject to the following conditions:

1. The maximum permissible working temperature of the materials should be higher than the maximum temperature the probe is expected to attain in the flame. If the thermocouple is to be heated to correct for radiation losses the former should be about 150°C greater than the latter.
2. The EMF output per degree change in temperature should be as large as possible. This improves the signal to noise ratio and consequently the accuracy of measurement.
3. The variation in EMF output with temperature change should be linear since the time averaging circuits give the time averaged EMF and not time averaged temperature.
4. The requirements of high spatial resolution, small conduction loss and minimum interference to the flow dictate that the thermocouple should be of very small diameter. This means that the material should be both ductile and of high tensile strength so that the wire is strong and can be easily handled.
5. The metal should be able to withstand the strongly oxidizing atmosphere of the flame.

A thermocuple made from 40% Rh - 60% Pt vs 20% Rh - 80% Pt fulfills the above requirements and was selected. The maximum working temperature of the probe was 2120°K, its sensitivity was 3.3 μv/°K, it had an ultimate tensile strength of 4.1 Kg/mm^2, and its diameter was 100 μm.

2.3.2.2 Estimation of and Compensation for Errors

Thermocouples, like any immersion device, indicate their own temperature which, in general, is not equal to the flame temperature. For optimal accuracy the discrepancy must be theoretically determined or, if possible, the probe must be designed to minimize the difference. In this section, the errors, their causes and steps taken to compensate for them will be given. An estimate of the accuracy of temperature measured in this experiment will also be made. The reasons for the errors are as follows:

1. High flow velocities cause an error because kinetic energy is not completely transferred into thermal energy. Scotsmann (1970) provides a relation for estimating it:

$$\Delta T_v = T_g \left(\frac{0,5(\gamma-1)M^2}{1.0+0.5(\gamma-1)M^2}\right) \qquad 2.2$$

where T_g = gas temperature M = Mach number.

The maximum error is less than 0.2% for this flow.

2. The error due to heat conduction from the thermocouple junction along the wiresis given by Scotsmann (1970) as:

$$\Delta T_c = (T_g - T_m) \frac{1}{\cosh(al)} \qquad 2.3$$

where $a^2 = \frac{4h}{Kd}$

ℓ = length of wire, d = diameter, K thermal conductivity.

h = convective heat transfer coefficient.

The estimate of conduction error for the probe selected for this experiment is 0.2%.

3. The thermal inertia of a thermocouple varies with gas temperature, velocity and wire properties. The error caused in the measurement of mean temperature due to the variation of thermal inertia was estimated by Odidi (1974) to be less than 1% for his thermocouple

probe which was very similar to the one used in the present study.

4. The heat transfer by radiation from the hot probe to the surroundings is greater than the heat transfer from the surroundings to the probe. This causes a difference between probe and gas temperature. Since radiation loss remains one of the most serious sources of error, the method used for its compensation will be discussed in some detail. The technique used was developed by Berkenbush (1899) and recently used by Odidi (1974). The principle is given below.

The steady state equation of energy for an electrically heated wire in gaseous surroundings, neglecting conduction and absorption losses can be written as:

$$q + \frac{4h}{d}(T_G - T_c) = \frac{4\sigma}{d}\varepsilon T_c^4 \qquad 2.4$$

where q = Power used to heat the thermocouple/Unit Vol

T_c = Temperature of thermocouple

T_G = Temperature of surrounding gas

h = Convective heat transfer coefficient

σ = Stefan-Boltzman Constant

ε = Emissivity of thermocouple

d = Diameter of thermocouple

When there is no heating $q = 0$ and T_c is equal to temperature of unheated thermocouple in flame. When thermocouple is heated q increases and T_c approaches T_G. At the point where $T_c = T_G$ the convection loss is zero and

$$q = \frac{4\sigma\varepsilon T_G^4}{d} = \frac{4\sigma}{d}\varepsilon T_c^4 \qquad 2.5$$

where the value of q will be the same if the wire is heated to T_G in a vacuum. The gas temperature was obtained, using the above principle. Initially a radiation loss caliberation curve was obtained.

This was done by electrically heating the thermocouple and simultaneously measuring the power loss and probe temperature in high vacuum (5×10^{-6} torr). The resulting plot of probe temperature versus electrical power per unit length of probe is given in Fig. 2.3.

When the thermocouple was in the measuring position in the flame, it was heated electrically and the heating power and temperature were plotted on the calibration curve. The temperature at the point of intersection of the curve was the temperature of the flame.

Two major objections can be made against this method. One is that the radiant exchange between the probe and flame is not taken into account Rein and O'Laughlin (1967). The other is that an error is introduced if the effective time mean radiating temperature of the probe is not equal to the time averaged probe temperature. In this experiment the flame was clear and soot free hence the first objection did not apply. Odidi (1974) had shown that the difference between effective time mean radiating temperature and mean probe temperature, for a similar flame, was not more than 1%.

5. Error is introduced in the temperature measurement because of the catalytic reactions on the surface of the thermocouple wire in the combustion gases. The catalytic activity is quite high where hydrogen is a constituent of the fuel as in town gas. The thermocouple used was coated with an anticatalytic ceramic coating. The requirements of a ceramic coating were that it should be thin, even and strong enough to withstand the vibrations caused in flames. Different coatings have been used in flame measurements. Silica was used by Friedman and Burke (1954) and Kent (1970) used a mixture of Yitrium and Beryllia. Silica is known to react with platinum and Beryllia was poisonous, hence neither were considered for the present experiment. Odidi used an inexpensive mixture of M_gO and

commonly available alumina cement, but he did not control the particle size, which resulted in uneven and thick coating. In this experiment a calgoromate free alumina powder was used having a particle size of 1μm, which formed extremely thin and even layers. The method of applying the coating is described in sec. 2.3.2.3 below.

2.3.2.3 Thermocouple Fabrication

The sequence of steps in the fabrication of thermocouples is described below.

1. Preliminary Preparation

The wires were supplied in tight wound coils and were straightened by electrical heating. The method suggested by Knight and Rhys (1961) was used to clean the wires of any organic matter left on the surface. The required length of the wire was first degreased in carbon tetrachloride, washed with dilute hot nitric acid, distilled water, hot dilute hydrochloric acid and again washed with distilled water. Finally the wire was washed in acetone.

2. Welding

A hydrogen diffusion flame from a microtorch was used to flame-weld the thermocouple junction. Flame welding of noble metals does not present oxidation problems. The method has been described in detail by Fristrom and Westenberg (1965). The bead size was checked under a microscope and only thermocouples having a bead size less than 1.1 times the diameter of the wire were accepted.

3. Probe Mounting and Annealing

The support wires were of the same material as the thermocouple, 0.5 mm in diameter, and the thermocouple was stretched across a fork formed from these wires Fig. 2.4a. The support wire was then

threaded through a twin bore alumina tube which was further enclosed in a stainless steel tube. The thermocouple was subsequently annealed by heating it electrically to a temperature of 1300°C for a period of three minutes as recommended by Zysk (1962). Finally, the probe was fixed to the cathetometer by clamps formed by cutting V shaped wedges in stainless steel and perspex plates Fig. 2.4b.

4. Alumina Coating

The alumina coating was produced by the following procedure. One half gramme of calogromate free alumina powder, of particle size 1μm, was added to 100 CC of distilled water to form thin cream. The coating was applied by heating the wire to about 1000°C and towelling it with cotton wool which had been immersed in the cream. Several coatings were applied in this manner. The maximum final outside diameter of the thermocouple was 0.11 mm. The quality of the coating was observed with the aid of a travelling microscope. When a smooth continuous covering was obtained, it was fired by heating the wire to about 1800°C. The thermocouple was tested for catalytic activity in a premixed bunsen flame by passing it from the outer edge of the flame through the reaction zone and into the cool inner core. If the coating was satisfactory, the probe temperature fell quickly to the temperature of the inner core.

2.3.3 Instrumentation

The arrangement of the apparatus used in measuring mean temperatures is given in Fig. 2.5. It consists of two circuits: one used to electrically heat the thermocouple, and the other to monitor the EMF generated by the thermocuple.

The heating circuit consisted of: 1) an oscillator (Wyne-Kerr Video oscillator type 022D, 2) a power amplifier (type Z-50 sinclair

operated at 50 KHZ) and a DC power supply for this amplifier, and
3) an ammeter (solartron LM1242) to measure the heating current.

The EMF output measuring circuit consisted of:

1) a low pass low drift filter amplifier to filter out the heating current supplied at 50 KHZ and amplify the thermocouple E M F by an amplification ratio of 1000,
2) a DISA 52B30 true integrator to time average the thermocouple EMF, and
3) a solartron voltmeter LM1242.

2.4. Mean Oxygen Concentration Measurement

2.4.1 Techniques of Oxygen Concentration Measurement

Measurements of the concentration of oxygen and other stable species in diffusion flames are useful. They help in understanding of flame structure and provide information for validation procedures. Various techniques have been developed depending on the type of flame studied and the particular species for which concentration measurements are required. Conditions which any technique is required to satisfy are:

1) The extraction of the sample representative of the conditions at the measuring point in flow.
2) The conservation of the initial characteristics of the sample.
3) The separation of gaseous, liquid and solid phases.
4) The precise and, if possible, rapid analysis of the gaseous mixture.

The first and second conditions concern the design and selection of the sampling probe. The third condition is related to design of vapour traps, filters and heating and cooling devices to maintain the temperature of the sample. The fourth condition concerns the selection of the analysing technique. Two types of probes are generally used, water cooled probe and quartz microprobe. The main advantage of the water cooled probe is that sampling can be isokinetic (i.e. sampling velocity is equal to the velocity

at the measuring location), Isokinetic sampling ensures that stream lines of the flow are not distorted at the measuring location. The velocity of flow at the measuring point is some times difficult to determine and so this advantage is not very great. The disadvantages are as follows

1) The size of the probe is necessarily large which can cause disturbance to flow.

2) The probes are usually constructed from stainless steel tubes and stainless steel is suspect to catalytic activity. It has been shown by England et al (1973) that due to catalytic activity a stainless steel probe gave 40-220% lower levels of NO than a quartz probe.

3) A water cooled probe also represents a heat sink which can reduce temperature and enthalpy in the region being sampled.

The water cooled probe was not used in this experiment because of the above disadvantages. The quartz microprobe was selected for use in this experiment. It was small in size and did not disturb the flow. Quartz had the ability to withstand high temperatures and had no known catalytic effect on the flame gases. Since the probe was uncooled the question of it being a heat sink did not arise. Some uncertainty had been expressed about the quenching ability of the probe by expansion alone, Bilger and Beck (1974). It was argued that recompression can be caused by expansion shocks inside the sampling tube. There are however indications that this does not affect quenching. Friedman and Cyphers (1955) measured unreacted hydrogen and carbon monoxide along with large amounts of oxygen using a quartz microprobe. Lazzara and Biordi (1973) used a similar probe to measure free radicals in lean methane, oxygen argon flames. They found maximum values of the radicals which were substantially in excess of their equilibrium values. These experiments showed that reaction could be frozen in the quartz microprobe.

2.4.1.2 Gas Analysis

The problem of analysis of gas mixtures extracted from flames is very complicated. The sample consists of various constituents (nitrogen, carbon dioxide, carbon monoxide, oxygen, water vapour, hydrogen, hydrocarbon et and their concentrations may vary widely from one sampling point to another. A great variety of analysers each relying on different properties of the gases for their identification and measurement can be used. Methods of gas analyses are described in detail in the literature. Vardin (1973) A paramagnetic oxygen analyser was used for oxygen concentration measurement in this study. This instrument makes use of the paramagnetic property possessed by only a very few gases (oxygen, nitric oxide and nitric peroxide). For this reason it is least affected by the presence of background gases in the sample. The method is suitable for continuous analysis and has a very small response time.

2.4.2 Design of Sampling System

The quartz microprobe used to sample the gases is shown in Fig. 2.6. It consisted of a quartz glass tube 2 mm ID and 3 mm OD, the tip of the probe was reduced to an orifice of about 150 μm diameter which gave an expansion ratio of about 100. A vacuum of about 5 mm of mercury was maintained in the probe. Trials were made with the probe cooled and uncooled, but no difference in recorded concentrations could be detected. It was concluded that the sudden expansion provided sufficient quenching. The sample was dried by bubbling it through concentrated sulphuric acid and then led to a Beckman oxygen analyser, type E2.

The oxygen analyser had two ranges of oxygen concentration 0-25% and 0-5%, minimum increment was 0.25% on the former and 0.05% on the latter range. The instrument was calibrated by passing pure nitrogen and a mixture

of 5% O_2-95% N_2 for the smaller range and 25% O_2 - 75%N_2 for the larger range. The stability of calibration was checked each day and the drift was found to be no more than ±0.2%. The accuracy of instrument was ±1% of the maximum scale reading. The temperature of the gases entering the analyser was monitored by a thermocouple and it was found to be within the range of the instrument. A rotameter was used to regulate the flow rate of the gases.

The time scale of concentration fluctuations at the edge of the flame was quite large. The response of the probe alone was not sufficient to smooth the large fluctuations, but the system response time could be altered by regulating the volume occupied by the sample in the wash bottle Fig. (2.7). The level of acid was adjusted until the reading given by the oxygen analyser remained constant for about five minutes. This procedure gave reproducible results, but it had the disadvantage that sometimes more than one hour was necessary to obtain one reading.

2.4.3 Instrumentation

The gas analysis system is shown in Fig. 2.7, it consists of: 1) Quartz microprobe 2) Vacuum pump 3) Wash bottle 4) Vapour trap 5) By-pass valve 6) Flow meter 7) Thermocouple 8) Oxygen analyser.

2.5 Results and Discussion

The contours and profiles of mean temperature and profiles of oxygen concentration are presented in figures 2.10 to 2.20. . Photographs of flames I and II are shown in Fig. 2.8. These pictures show that near the exit of the burner buoyancy has very little effect and that the flames appear to be symmetric over the first few diameters. As the flame grows buoyancy becomes influential and the flame curls upwards.

A sketch of the flame is shown in Fig. 2.9. . It shows three regions

in the flame; the reaction zone which is product rich and is the hottest part of the flame, the inside core which contains unreacted fuel, and the outer envelope which is oxygen rich. The core or the 'centre' of the flame is the region where the fuel concentration is maximum and can be represented by the line ab in the figure. The surface through ab divides the flame into two parts. It will be seen from the results below, that the structure of the flame is different in these two regions. For the purpose of discussion they can be called upper region and lower region depending on whether they are above or below the surface. Since more data was obtained for flame II, the discussion below will be restricted to flame II although in general it is applicable to flame I as well.

The flame is similar to a vertical diffusion flame in many respects. Initially, as is clear from the temperature and concentration profiles at Z/D = 13, there is a cool fuel rich core separated from the surrounding ambient air by a hot product rich zone. There is no oxygen in the centre and since the temperature is also low it is an indication of unreacted fuel. The oxygen and products diffuse towards the centre of the flame with increasing Z/D. Ultimately the unreacted fuel core vanishes completely which is indicated by temperature and oxygen profiles at Z/D = 57. Maximum temperature together with some oxygen at the centre indicates a high temperature product rich reaction zone. This does not imply that reaction is complete at this point. Due to the 'unmixedness' of turbulent flames, Hawthorne et al (1949), the visible reaction zone, as shown by long exposure photography, extends far beyond this plane.

The horizontal flame exhibits several significant differences from the vertical flame of a detailed nature. One of the features is that the maximum temperature recorded in the lower region is less than the maximum temperature recorded in the upper region (e.g Z/D = 29,35). This gives rise to high temperature 'islands' in the upper region of temperature

contours Figs.(2.10, 2.11, 2.12, 2.13). The absence of these islands from Fig. 2.14 and Fig. 2.15 is due to the influence of buoyancy which further downstream becomes strong enough to make the contours similar to those of vertical flames. Another feature which might explain the discrepancy can also be seen in the oxygen profiles, Figs.2.16, 2.17, 2.18. The oxygen concentrations at the maxima in temperature in the upper and lower regions of the flame are not the same, this is most pronounced at Z/D = 29 where in the upper region the oxygen concentration is nearly zero, but in the lower region it is almost 20% of its value in air. This reveals a high degree of unmixedness in this region which may be the cause of the lower temperature.

The level of turbulence, as explained below can also be higher in the lower region which will increase the magnitude of temperature fluctuations resulting in lower mean temperature. No experimental evidence is available to show this but the following argument can be put forward. One effect of buoyancy on mean flow will be to generate strong cross stream velocities. These velocities will assist the momentum transport by diffusion in the upper region, but will oppose it in the lower region. This will cause steeper velocity gradients in the lower region of the flame. It can be seen from the production term in the kinetic energy equation, Eq. (4.22), that large velocity gradients increase turbulence energy. The location of maximum temperature coincides with the centre of the flame in about 60 diameters. The maximum temperature was reached in the centre of the Odidi flame (which used the same fuel and was turbulent, the only difference being that it was vertical) in about 100 diameters implying a slower diffusion of oxygen in his case. This again points to the role of the cross stream velocities in assisting the diffusion of oxygen in the horizontal flame and causing it to be shorter than the corresponding vertical one.

The maximum temperature recorded was about 350^{o}C below the adiabatic flame temperature. Higher mean temperature values were measured by

Odidi. This is indicative of the fact that the magnitudes of the temperature fluctuations in his case were lower than those encountered here. This can be explained by the fact that his flame was smaller and, due to the greater effect of diffusion between the relatively smaller scale hot and cool turbulent fluid 'parcels', the magnitudes of the fluctuations were less.

2.6 Conclusions

Measurements have been obtained of time-averaged temperature and oxygen concentration in a horizontal, free, turbulent diffusion flame. They are intended to assist in the validation of prediction procedures for flows such as furnace ones, in which buoyancy influences on the mean flow and turbulence structure are likely to be important.

The present measurements by themselves reveal several special features of this type of flow. The most important being unequal maximum temperatures measured in the upper and lower regions of the flame. This experiment also showed that the length of a horizontal flame is shorter than a comparable vertical one. It can be concluded that features observed in this flame which are different from vertical flames are due to buoyancy, because buoyancy affects turbulence which in turn affects reaction. Unfortunately mean velocities and turbulence quantities such as Reynolds stresses which are directly influenced by buoyancy were not measured. A useful future task would be to obtain these data and corroborate the findings of this experiment. It can also be concluded that solution procedures which do not take into account cross stream buoyancy are unlikely to be very successful in prediction of performance of large horizontally fired furnaces.

CHAPTER THREE

3. Mean Flow Equations

3.1 Instantaneous Equations

As a first step in the analysis, the differential equations describing the present flow are presented in this section. The equations are instantaneous and three dimensional with variable properties. In the following sections these equations will be time-averaged and two forms will be given. One in which the fluctuations in density are neglected and the other in which they are not. All the equations are presented in cylindrical co-ordinates

a) Continuity Equation

The equation of conservation of mass is:

$$\frac{\partial}{\partial r}(\hat{\rho}\hat{V}_r) + \frac{\hat{\rho}\hat{V}_r}{r} + \frac{1}{r}\frac{\partial}{\partial \theta}(\hat{\rho}\hat{V}_\theta) + \frac{\partial}{\partial z}(\hat{\rho}\hat{V}_z) = 0 \qquad 3.1$$

(b) Momentum Equations

r-direction

$$\hat{\rho}\hat{V}_r\frac{\partial \hat{V}_r}{\partial r} + \frac{\hat{\rho}\hat{V}_\theta}{r}\frac{\partial \hat{V}_r}{\partial \theta} + \hat{\rho}\hat{V}_z\frac{\partial \hat{V}_r}{\partial z} - \frac{\hat{\rho}\hat{V}_\theta^2}{r}$$

$$= \hat{\rho}g_r - \frac{\partial \hat{p}}{\partial r} + \frac{\partial}{\partial r}\left[2\hat{\mu}\frac{\partial \hat{V}_r}{\partial r} + (\tau + \frac{2}{3}\hat{\mu})\,\nabla.\hat{\vec{V}}\right]$$

$$+ \frac{1}{r}\frac{\partial}{\partial \theta}\left[\hat{\mu}\left(\frac{1}{r}\frac{\partial \hat{V}_r}{\partial \theta} + \frac{\partial \hat{V}_\theta}{\partial r} - \frac{\hat{V}_\theta}{r}\right)\right] + \frac{\partial}{\partial z}\hat{\mu}\left(\frac{\partial \hat{V}_r}{\partial z} + \frac{\partial \hat{V}_z}{\partial r}\right)$$

$$+ \frac{2\hat{\mu}}{r}\left(\frac{\partial \hat{V}_r}{\partial r} + \frac{1}{r}\frac{\partial \hat{V}_\theta}{\partial \theta} - \frac{\hat{V}_r}{r}\right) \qquad 3.2$$

θ-direction

$$\hat{\rho}\hat{V}_r\frac{\partial \hat{V}_\theta}{\partial r} + \frac{\hat{\rho}\hat{V}_\theta}{r}\frac{\partial \hat{V}_\theta}{\partial \theta} + \hat{\rho}\hat{V}_z\frac{\partial \hat{V}_\theta}{\partial z} + \frac{\hat{\rho}\hat{V}_r\hat{V}_\theta}{r}$$

$$= \hat{\rho} g_\theta - \frac{1}{r}\frac{\partial \hat{p}}{\partial \theta} + \frac{1}{r}\frac{\partial}{\partial \theta}\left[\frac{2\hat{\mu}}{r}\frac{\partial \hat{V}_\theta}{\partial \theta} + \left(\tau - \frac{2}{3}\hat{\mu}\right)\nabla.\hat{V}\right]$$

$$+ \frac{\partial}{\partial r}\left[\hat{\mu}\left(\frac{1}{r}\frac{\partial \hat{V}_r}{\partial \theta} + \frac{\partial \hat{V}_\theta}{\partial r} - \frac{\hat{V}_\theta}{r}\right)\right] + \frac{2\hat{\mu}}{r}\left[\frac{1}{r}\frac{\partial \hat{V}_r}{\partial \theta} + \frac{\partial \hat{V}_\theta}{\partial r} - \frac{\hat{V}_\theta}{r}\right]$$

$$+ \frac{\partial}{\partial z}\left[\hat{\mu}\left(\frac{1}{r}\frac{\partial \hat{V}_z}{\partial \theta} + \frac{\partial \hat{V}_\theta}{\partial z}\right)\right] \qquad 3.3$$

z-direction

$$\hat{\rho}\hat{V}_r\frac{\partial \hat{V}_z}{\partial r} + \frac{\hat{\rho}\hat{V}_\theta}{r}\frac{\partial \hat{V}_z}{\partial \theta} + \hat{\rho}\hat{V}_z\frac{\partial \hat{V}_z}{\partial z}$$

$$= \hat{\rho} g_z - \frac{\partial \hat{p}}{\partial z} + \frac{\partial}{\partial z}\left[2\hat{\mu}\frac{\partial \hat{V}_z}{\partial z} + \left(\tau - \frac{2}{3}\hat{\mu}\right)\nabla.V\right]$$

$$+ \frac{1}{r}\frac{\partial}{\partial r}\left[\hat{\mu} r \left(\frac{\partial \hat{V}_r}{\partial z} + \frac{\partial \hat{V}_z}{\partial r}\right)\right] + \frac{1}{r}\frac{\partial}{\partial \theta}\left[\hat{\mu}\left(\frac{1}{r}\frac{\partial \hat{V}_z}{\partial \theta} + \frac{\partial \hat{V}_\theta}{\partial z}\right)\right]$$

where r, θ, z are distances in the radial, circumferential and axial directions, $\hat{\rho}$ is the density, V_r, V_θ, V_z are velocities in the r, θ, z directions respectively, $\hat{\mu}$ is viscosity, τ is second co-efficient of viscosity, $\hat{}$ denotes instantaneous value and:

$$\nabla.V = \frac{1}{r}\frac{\partial}{\partial r}(r\hat{V}_r) + \frac{1}{r}\frac{\partial \hat{V}_\theta}{\partial \theta} + \frac{\partial \hat{V}_z}{\partial z} \qquad 3.5$$

(c) Conservation Equation of a Scalar

The conservation equation of a scalar such as a species concentration can be represented in a general form as:

$$\hat{\rho}\hat{V}_r\frac{\partial \hat{\Phi}}{\partial r} + \frac{\hat{\rho}\hat{V}_\theta}{r}\frac{\partial \hat{\Phi}}{\partial \theta} + \hat{\rho}V_z\frac{\partial \hat{\Phi}}{\partial z}$$

$$= \hat{\rho} D\left[\frac{1}{r}\frac{\partial \hat{\Phi}}{\partial r} + \frac{1}{r^2}\frac{\partial^2 \hat{\Phi}}{\partial \theta^2} + \frac{\partial^2 \hat{\Phi}}{\partial z^2} + \frac{\partial^2 \hat{\Phi}}{\partial r^2}\right] + S_\Phi \qquad 3.6$$

$\rightarrow \hat{e}\, S\phi$

where D = diffusion co-efficient assumed constant, and S_Φ is a source term which in the case of fuel represents rate of depletion of fuel or the rate of reaction.

3.2 The Time Averaged Equations

The flow can be calculated with the help of above equations if the flow is laminar i.e. in steady state the time-averaged value of property Φ is at any time equal to its instantaneous value. This is not the case in turbulent flow and because the important details of turbulence are small-scale in character we need values of the variables at a very large number of discrete points to solve the flow using a numerical procedure. This is not possible due to the storage limitations of the present computers.

The commonly adopted approach to overcome this problem is to work with time-averaged equations. This method is used here as well. The flow equations when time averaged contain extra terms involving correlations of fluctuating velocity and density. These terms are then evaluated using a 'turbulence model' which comprises of a set of equations which, when solved with mean-flow equations, allows the calculation of the relevant correlations and so simulating the behaviour of real fluids in important aspects. The formulation of the turbulence model forms a major part of the next Chapter.

The time-averaged equations that have been used for predicting reacting flows in many cases have been derived neglecting the fluctuations in density. If the fluctuations in density are taken into account many extra terms appear whose effect in some cases may not be negligible. In the next two sections both constant and variable density forms of the time-averaged equations are presented.

3.2.1 Variable Density, Time Averaged Equations

$$\frac{\partial}{\partial r}(\bar{\rho}\bar{V}_r + \overline{\rho' V_r'}) + \frac{\partial}{r\partial\theta}(\bar{\rho}\bar{V}_\theta + \overline{\rho' V_\theta'}) + \frac{\partial}{\partial z}(\bar{\rho}\bar{V}_z + \overline{\rho' V_z'})$$

$$+ \frac{\bar{\rho}\bar{V}_r + \overline{\rho' V_r'}}{r} = 0 \qquad 3.7$$

Momentum Equations

The momentum equations have been derived neglecting fluctuations in viscosity.

r-direction

$$(\bar{\rho}\bar{V}_r + \overline{\rho' V'_r})\frac{\partial \bar{V}_r}{\partial r} + (\bar{\rho}\bar{V}_\theta + \overline{\rho' V'_\theta})\frac{\partial \bar{V}_r}{r\partial\theta} + (\bar{\rho}\bar{V}_z + \overline{\rho' V'_z})\frac{\partial \bar{V}_r}{\partial z}$$

$$+ \frac{\partial}{\partial r}(\bar{\rho}\overline{V'_r V'_r} + \bar{V}_r\overline{\rho' V'_r} + \overline{\rho' V'_r V'_r}) + \frac{\partial}{r\partial\theta}(\bar{\rho}\overline{V'_\theta V'_r} + \bar{V}_\theta\overline{\rho' V'_r} + \overline{\rho' V'_\theta V'_r})$$

$$+ \frac{\partial}{\partial z}(\bar{\rho}\overline{V'_z V'_r} + \bar{V}_z\overline{\rho' V'_r} + \overline{\rho' V'_z V'_r}) +$$

$$\frac{\bar{\rho}\overline{V'_r V'_r} + \bar{V}_r\overline{\rho' V'_r} + \overline{\rho' V'_r V'_r} + \bar{\rho}\bar{V}_\theta^2 + \overline{\rho V'^2_\theta} + 2\bar{V}_\theta\overline{\rho' V'_\theta} + \overline{\rho' V'^2_\theta}}{r}$$

$$= \bar{\rho}g_r - \frac{\partial \bar{p}}{\partial r} + \frac{\partial}{\partial r}\left[\bar{\mu}\frac{\partial \bar{V}_r}{\partial r} + (\tau - \frac{2}{3}\bar{\mu})\nabla \cdot V\right] +$$

$$+ \frac{1}{r}\frac{\partial}{\partial\theta}\left[\bar{\mu}\left(\frac{1}{r}\frac{\partial \bar{V}_r}{\partial\theta} + \frac{\partial \bar{V}_\theta}{\partial r} + \frac{\bar{V}_\theta}{r}\right)\right] + \frac{\partial}{\partial z}\left[\bar{\mu}\left(\frac{\partial \bar{V}_r}{\partial z} + \frac{\partial \bar{V}_z}{\partial r}\right)\right]$$

$$+ \frac{2\mu}{r}\left(\frac{\partial \bar{V}_r}{\partial r} - \frac{1}{r}\frac{\partial \bar{V}_\theta}{\partial\theta} - \frac{\bar{V}_r}{r}\right) \qquad 3.8$$

θ-direction

$$(\bar{\rho}\bar{V}_r + \overline{\rho' V'_r})\frac{\partial \bar{V}_\theta}{\partial r} + (\bar{\rho}\bar{V}_\theta + \overline{\rho' V'_\theta})\frac{\partial \bar{V}_\theta}{r\partial\theta} + (\bar{\rho}\bar{V}_z + \overline{\rho' V'_z})\frac{\partial \bar{V}_\theta}{\partial z}$$

$$+ \frac{\partial}{\partial r}(\bar{\rho}\overline{V'_\theta V'_r} + \bar{V}_r\overline{\rho' V'_\theta} + \overline{\rho' V'_\theta V'_r}) + \frac{\partial}{r\partial\theta}(\bar{\rho}\overline{V'_\theta V'_\theta} + \bar{V}_\theta\overline{\rho' V'_\theta} + \overline{\rho' V'_\theta V'_\theta})$$

$$+ \frac{\partial}{\partial z}(\bar{\rho}\overline{V'_z V'_\theta} + \bar{V}_z\overline{\rho' V'_\theta} + \overline{\rho' V'_z V'_\theta}) +$$

$$\frac{2\bar{\rho}\overline{V'_r V'_\theta} + 2\bar{V}_r\overline{\rho' V'_\theta} + 2\overline{\rho' V'_r V'_\theta} + \bar{\rho}\bar{V}_r\bar{V}_\theta + \bar{V}_\theta\overline{\rho' V'_r}}{r}$$

$$= \bar{\rho} g_\theta - \frac{\partial \bar{p}}{r\partial\theta} + \frac{1}{r}\frac{\partial}{\partial\theta}\left[\frac{2\bar{\mu}}{r}\frac{\partial \bar{v}_\theta}{\partial\theta} + (\tau - \frac{2}{3}\bar{\mu})\ \nabla.v\right]$$

$$+ \frac{\partial}{\partial z}\left[\bar{\mu}\left(\frac{1}{r}\frac{\partial \bar{v}_z}{\partial\theta} + \frac{\partial \bar{v}_z}{\partial z}\right)\right] + \frac{\partial}{\partial r}\left[\bar{\mu}\left(\frac{1}{r}\frac{\partial \bar{v}_r}{\partial\theta} + \frac{\partial \bar{v}_\theta}{\partial r} - \frac{\bar{v}_\theta}{r}\right)\right]$$

$$+ \frac{2\bar{\mu}}{r}\left[\frac{1}{r}\frac{\partial \bar{v}_r}{\partial\theta} + \frac{\partial \bar{v}_\theta}{\partial r} - \frac{\bar{v}_\theta}{r}\right] \qquad 3.9$$

z-direction

$$(\bar{\rho}\bar{v}_r + \overline{\rho' v_r'})\frac{\partial \bar{v}_z}{\partial r} + (\bar{\rho}\bar{v}_\theta + \overline{\rho' v_\theta'})\frac{\partial \bar{v}_z}{r\partial\theta} + (\bar{\rho}\bar{v}_z + \overline{\rho' v_z'})\frac{\partial \bar{v}_z}{\partial z}$$

$$+ \frac{\partial}{\partial r}(\bar{\rho}\overline{v_z' v_r'} + \bar{v}_r\overline{\rho' v_z'} + \overline{\rho' v_r' v_z'}) + \frac{\partial}{r\partial\theta}(\bar{\rho}\overline{v_\theta' v_z'} + \bar{v}_\theta\overline{\rho' v_z'} + \overline{\rho' v_z' v_\theta'})$$

$$+ \frac{\partial}{\partial z}(\bar{\rho}\overline{v_z' v_z'} + \bar{v}_z\overline{\rho' v_z'} + \overline{\rho' v_z' v_z'}) + \frac{\bar{\rho}\overline{v_z' v_r'} + \bar{v}_r\overline{v_z'\rho'} + \overline{\rho' v_r' v_z'}}{r}$$

$$= \bar{\rho} g_z - \frac{\partial \bar{p}}{\partial z} + \frac{\partial}{\partial z}(2\bar{\mu}\frac{\partial \bar{v}_z}{\partial z} + (\tau - \frac{2}{3}\bar{\mu})\ \nabla.v)$$

$$+ \frac{1}{r}\frac{\partial}{\partial r}(\bar{\mu} r\ (\frac{\partial \bar{v}_r}{\partial z} + \frac{\partial \bar{v}_z}{\partial r})) + \frac{1}{r}\frac{\partial}{\partial\theta}\left[\bar{\mu}(\frac{1}{r}\frac{\partial \bar{v}_z}{\partial\theta} + \frac{\partial \bar{v}_\theta}{\partial z})\right] \qquad 3.10$$

Conservation Equation of a Scalar

$$(\bar{\rho}\bar{v}_r + \overline{\rho' v_r'})\frac{\partial \bar{\Phi}}{\partial r} + (\bar{\rho}\bar{v}_\theta + \overline{\rho' v_\theta'})\frac{\partial \bar{\Phi}}{r\partial\theta} + (\bar{\rho}\bar{v}_z + \overline{\rho' v_z'})\frac{\partial \bar{\Phi}}{\partial z}$$

$$\frac{\partial}{\partial r}(\bar{\rho}\overline{v_r'\Phi'} + \bar{v}_r\overline{\rho'\Phi'} + \bar{\rho}\overline{v_r'\Phi'}) + \frac{\partial}{r\partial\theta}(\bar{\rho}\overline{v_\theta'\Phi'} + \bar{v}_\theta\overline{\rho'\Phi'} + \overline{\rho' v_\theta'\Phi'})$$

$$+ \frac{\partial}{\partial z}(\bar{\rho}\overline{v_z'\Phi'} + \bar{v}_z\overline{\rho'\Phi'} + \overline{v_z'\rho'\Phi'}) + \frac{\bar{\rho}\overline{v_r'\Phi'} + \bar{v}_r\overline{\rho'\Phi'} + \overline{\rho' v_r'\Phi'}}{r}$$

$$= \frac{\bar{\rho} D\left[\frac{1}{r}\frac{\partial \bar{\Phi}}{\partial r} + \frac{1}{r^2}\frac{\partial^2 \bar{\Phi}}{\partial\theta^2} + \frac{\partial^2 \bar{\Phi}}{\partial z^2} + \frac{\partial^2 \bar{\Phi}}{\partial r^2}\right] + \rho' D\left[\frac{1}{r}\frac{\partial \Phi'}{\partial r} + \frac{1}{r^2}\frac{\partial^2 \Phi'}{\partial\theta^2} + \frac{\partial^2 \Phi'}{\partial z^2} + \frac{\partial^2 \Phi'}{\partial r^2}\right]}{} + \overline{S_\Phi} \qquad 3.11$$

Equation 3.11 has a term $\overline{S_\phi}$ which if Φ is an active species (fuel or oxidant), represents the mean reaction rate in a reacting flow. The modelling of this term forms the major portion of Chapter 5 on reaction modelling.

3.2.2 Mean Flow Equations Neglecting Density Fluctuations

The above equations reduce to comparatively simple forms if density fluctuations are neglected. In this section these equations are presented

a) Continuity Equation

$$\frac{\partial}{\partial r}(\bar{\rho}\bar{v}_r) + \frac{\partial}{r\partial\theta}(\bar{\rho}\bar{v}_\theta) + \frac{\partial}{\partial z}(\bar{\rho}\bar{v}_z) + \frac{\bar{\rho}\bar{v}_r}{r} = 0 \qquad 3.12$$

b) Momentum Equation

r-direction

$$\bar{\rho}\bar{v}_r\frac{\partial\bar{v}_r}{\partial r} + \bar{\rho}\bar{v}_\theta\frac{\partial\bar{v}_r}{r\partial\theta} + \bar{\rho}\bar{v}_z\frac{\partial\bar{v}_r}{\partial z} + \frac{\partial}{\partial r}(\bar{\rho}\overline{v'_r v'_r}) + \frac{\partial}{r\partial\theta}(\bar{\rho}\overline{v'_\theta v'_r}) +$$

$$\frac{\partial}{\partial z}(\bar{\rho}\overline{v'_z v'_r}) + \frac{\bar{\rho}\overline{v'_r v'_r} - \bar{\rho}\bar{v}_\theta^2 + \bar{\rho}\overline{v'^2_\theta}}{r}$$

$$= \bar{\rho}g_r - \frac{\partial\bar{p}}{\partial r} + \frac{\partial}{\partial r}\left[2\bar{\mu}\frac{\partial\bar{v}_r}{\partial r} + (\tau - \frac{2}{3}\bar{\mu})\nabla\cdot\bar{v}\right] +$$

$$\frac{1}{r}\frac{\partial}{\partial\theta}\left[\bar{\mu}(\frac{1}{r}\frac{\partial\bar{v}_r}{\partial\theta} + \frac{\partial\bar{v}_\theta}{\partial r} + \frac{\bar{v}_\theta}{r})\right] + \frac{\partial}{\partial z}\left[\bar{\mu}(\frac{\partial\bar{v}_r}{\partial z} + \frac{\partial\bar{v}_z}{\partial r})\right]$$

$$+ \frac{2\bar{\mu}}{r}(\frac{\partial\bar{v}_r}{\partial r} - \frac{1}{r}\frac{\partial\bar{v}_\theta}{\partial\theta} - \frac{\bar{v}_r}{r}) \qquad 3.13$$

θ-direction

$$\bar{\rho}\bar{v}_r\frac{\partial\bar{v}_\theta}{\partial r} + \bar{\rho}\bar{v}_\theta\frac{\partial\bar{v}_\theta}{r\partial\theta} + \bar{\rho}\bar{v}_z\frac{\partial\bar{v}_\theta}{\partial z} + \frac{\partial}{\partial r}(\bar{\rho}\overline{v'_\theta v'_r}) + \frac{\partial}{r\partial\theta}(\bar{\rho}\overline{v'_\theta v'_\theta})$$

$$+ \frac{\partial}{\partial z}(\bar{\rho}\overline{v'_z v'_\theta}) + \frac{2\bar{\rho}\overline{v'_r v'_\theta} + \bar{\rho}\bar{v}_r\bar{v}_\theta}{r}$$

$$= \bar{\rho}g_\theta - \frac{\partial \bar{p}}{r\partial\theta} + \frac{1}{r}\frac{\partial}{\partial\theta}\left[\frac{2\bar{\mu}}{r}\frac{\partial \bar{v}_\theta}{\partial\theta} + (\tau - \frac{2}{3}\bar{\mu})\ \nabla.v\right]$$

$$+ \frac{\partial}{\partial z}\left[\bar{\mu}\left(\frac{1}{r}\frac{\partial \bar{v}_z}{\partial\theta} + \frac{\partial \bar{v}_\theta}{\partial z}\right)\right] + \frac{\partial}{\partial r}\left[\bar{\mu}\left(\frac{1}{r}\frac{\partial \bar{v}_r}{\partial\theta} + \frac{\partial \bar{v}_\theta}{\partial r} - \frac{\bar{v}_\theta}{r}\right)\right]$$

$$+ \frac{2\bar{\mu}}{r}\left[\frac{1}{r}\frac{\partial \bar{v}_r}{\partial\theta} + \frac{\partial \bar{v}_\theta}{\partial r} - \frac{\bar{v}_\theta}{r}\right] \qquad 3.14$$

z-direction

$$\bar{\rho}\bar{v}_r\frac{\partial \bar{v}_z}{\partial r} + \bar{\rho}\bar{v}_\theta\frac{\partial \bar{v}_z}{r\partial\theta} + \bar{\rho}\bar{v}_z\frac{\partial \bar{v}_z}{\partial z} + \frac{\partial}{\partial r}(\bar{\rho}\overline{v'_z v'_r}) + \frac{\partial}{r\partial\theta}(\bar{\rho}\overline{v'_\theta v'_z})$$

$$+ \frac{\partial}{\partial z}(\bar{\rho}\overline{v'_z v'_z}) + \frac{\bar{\partial}\overline{v'_z v'_r}}{r} = \bar{\rho}g_z - \frac{\partial \bar{p}}{\partial z} + \frac{\partial}{\partial z}(2\bar{\mu}\frac{\partial \bar{v}_z}{\partial z} + (\tau - \frac{2}{3}\bar{\mu})\ \nabla.v)$$

$$+ \frac{1}{r}\frac{\partial}{\partial r}(\bar{\mu}r\ (\frac{\partial \bar{v}_r}{\partial z} + \frac{\partial \bar{v}_z}{\partial r})) + \frac{1}{r}\frac{\partial}{\partial\theta}\left[\bar{\mu}(\frac{1}{r}\frac{\partial \bar{v}_z}{\partial\theta} + \frac{\partial \bar{v}_\theta}{\partial z})\right] \qquad 3.15$$

C) Conservation Equation of a Scalar

$$\bar{\rho}\bar{v}_r\frac{\partial \bar{\Phi}}{\partial r} + \bar{\rho}\bar{v}_\theta\frac{\partial \bar{\Phi}}{r\partial\theta} + \bar{\rho}\bar{v}_z\frac{\partial \bar{\Phi}}{\partial z} + \frac{\partial}{\partial r}(\bar{\rho}\ \overline{v'_r\Phi'}) + \frac{\partial}{r\partial\theta}(\bar{\rho}\overline{v'_\theta\Phi'})$$

$$+ \frac{\partial}{\partial z}(\bar{\rho}\overline{v'_z\Phi'}) + \frac{\bar{\rho}\overline{v'_r\Phi'}}{r}$$

$$= \bar{\rho}D\left[\frac{1}{r}\frac{\partial \bar{\Phi}}{\partial r} + \frac{1}{r^2}\frac{\partial^2\bar{\Phi}}{\partial\theta^2} + \frac{\partial^2\bar{\Phi}}{\partial z^2} + \frac{\partial^2\bar{\Phi}}{\partial r^2}\right] + \overline{S_\Phi} \qquad 3.16$$

The above set of equations contains no extra terms as compared to their constant density forms hence the turbulence modelling required for reacting flows is the same as that for inert flows.

CHAPTER FOUR

4.0 The Turbulence Model

4.1 Introduction

The set of time averaged equations presented in Chapter 3 cannot be solved because the unknown turbulent correlations $\overline{u_i'u_j'}$ and $\overline{\rho'u_i'}$, respectively the Reynolds stresses and turbulent mass fluxes appear. In order to solve the equations some means of evaluating these terms have to be found.

Many proposals, or 'turbulence models' as they are called, have been put forward to approximate these correlations in terms of known quantities. They have achieved varied amounts of success depending on the complexity of the turbulence structure in the flow field as well as on the choice of the model.

In section 4.2 models applicable to constant density flows are discussed; these are described first because major developments in turbulence modelling have arisen out of attempts to solve constant-density flows. Moreover the models deviced to predict variable density flows, such as turbulent flames, have usually been extensions of constant-density models. In section 4.3 reasons for choosing a 'two equation' model for the present problem are given and an existing one is extended to three dimensional variable density flows where the density fluctuations are neglected. In section 4.4 the effect of the density fluctuations on the turbulence and mean flow are discussed along with proposals to account for them. Finally section 4.5 gives the modelled equation for the fluctuations of a passive scalar.

4.2 Turbulence Models for Constant-Density Flows

The development and classification of turbulence models, together with their advantages and disadvantages in different flow situations, have been discussed by Launder and Spalding (1972). A convenient classification of models is the number of differential equations which must be solved, in addition to those for the mean flow, to form a closed set. The models and their important features are listed in Table 4.1.

The zero, one and two equation models employ the eddy viscosity concept to relate the Reynolds stresses in the mean momentum equations (3.8-3.10) to the mean velocity gradient. For two-dimensional boundary layer flows the relation is expressed by:

$$-\rho\overline{u'v'} = \mu_t \frac{\partial \overline{U}}{\partial y} \qquad 4.1$$

where μ_t = proportionality factor or turbulent viscosity.

4.2.1 Zero Equation Models

In the zero equation models, an algebraic expression is used to determine the turbulent viscosity. It comprises a length scale depending on the geometry of flow and a velocity scale. Prandtl's (1925) mixing length hypothesis is a model of this type in which the turbulent viscosity is expressed as:

$$\mu_t = \overline{\rho}\ell^2 \frac{\partial \overline{U}}{\partial y} \qquad 4.2$$

where ℓ = length scale (usually determined as function of width of turbulent flow).

$\ell \left| \frac{\partial \overline{U}}{\partial y} \right|$ = a characteristic velocity scale.

This model does not need an extra differential equation to solve a turbulent flow hence it is called a zero equation model.

Table 4.1 Comparison of Turbulence Models

No. of Equation	Dependent Variable	Source	Comments	Examples of Prediction
0	-	Prandtl (1925)	Mixing length hypothesis; shear stress related to local mean flow conditions only. Empirical constants involved vary from one flow situation to another.	Many boundary layer flows such as plane jet, plane wake Rodi (1972)
1	K	Prandtl (1945)	$K^{1/2}$ used as representative velocity scale. Algebraic prescription of length scale required. Lacks universality. Performance not much better than mixing length hypothesis.	Fully developed flow in square duct; Launder and Ying (1973)
2	K,ε	Harlow & Nakayama (1967)	Velocity and length scale obtained from their respective transport equations. Useful in situations where length scale cannot be prescribed algebraically such as recirculating or reattaching flows.	Film cooling; Mathews & Whitelaw (1971) Confined jet; Elgobashi (1975) Isothermal furnace flows; Khalil et al (1975)
3	$K,\overline{u_1'u_2'},\varepsilon$		Eddy viscosity concept not used. Transport equation for shear stress solved as well. Superior to 2-equation models where transport of shear stress important.	Asymmetric channel flow, Hanjali and Launder (1971)
5	$\overline{u_1'^2},\overline{u_2'^2},\overline{u_3'^2},\overline{u_1'u_2'},\varepsilon$		Transport equations of normal stresses solved as well. Useful where transport of normal stresses important.	Plane jet, plane wake, asymmetri channel flows; Launder et al (19

4.2.2 One Equation Models

Three major one equation models of turbulence have been suggested. Prandtl (1945) proposed that the square root of turbulence kinetic energy K should be used as the velocity scale. Kinetic energy is defined as:

$$K = \frac{1}{2}(\overline{u_1'^2 + u_2'^2 + u_3'^2}) \qquad 4.3$$

If $K^{1/2}$ is substituted as velocity scale in Eq. 4.2 we have

$$\mu_t = \rho K^{1/2} \ell \qquad 4.4$$

Bradshaw and Ferris (1967) also suggested solution of a transport equation for K, but they did not make use of the eddy viscosity concept and assumed that the kinematic shear stress is directly proportional to turbulence kinetic energy. For most external boundary layers this is a reasonable assumption in agreement with experiments, but in other cases, for example along the axis of a pipe where the stress is zero, but turbulence energy finite, their model is evidently incorrect. Nee and Kavazney (1969) employed the effective viscosity concept with the effective viscosity itself appearing as the dependent variable of a differential equation.

The derivation and modelling of the K equation will be discussed in some detail here since one equation models which employ $K^{1/2}$ as velocity scale have been used in this department and also because the concepts formed with respect to approximating this equation are carried over to the two equation and five equation models as well. The exact form of K equation can be derived by multiplying the component of instantaneous velocity equation by its fluctuating part and summing up the three equations so formed. The kinetic energy equation can be written for constant density 2-D boundary layer flows as

$$(\bar{\rho}\frac{\partial K}{\partial x} + \bar{\rho}\,\bar{V}\,) = -\frac{\partial}{\partial y}(\bar{\rho}\,\overline{v'K'} + \overline{v'P'}) - \bar{\rho}\,\overline{u'v'}\,\frac{\partial \bar{U}}{\partial y} - \mu\,\Sigma(\overline{\frac{\partial u_i'}{\partial x_j}})^2 \qquad 4.5$$

convection diffusion production dissipation

The left hand side of this equation can be interpreted as the convective rate of change of kinetic energy along a streamline. The first term on the right hand side integrates to zero across a boundary layer which shows that it is diffusive in nature serving to redistribute the energy in space. The second term on the right hand side is usually called the production term. If the equation for the kinetic energy of the mean flow is derived, it is found that this term also appears in that equation but with a reverse sign. From this it can be deduced that the term expresses the rate at which mean kinetic energy is converted into turbulence energy by the working of the turbulent stress $-\rho\overline{u'v'}$, against the mean velocity gradient. The last term can be described as the rate at which turbulence energy is dissipated by the viscous action of small scale motions.

The turbulent diffusion of turbulence has been assumed by Prandtl (1945), Kolmogorov (1942) and other workers, to act like a molecular diffusion process and by analogy one can write:

$$-(\rho\overline{v'K'} + \overline{p'v'}) = \frac{\mu t}{\sigma_k}\frac{\partial K}{\partial y} \qquad 4.6$$

Where σ_k is the Prandtl number for the diffusion of turbulence kinetic energy. The production term is modelled according to the eddy viscisoty hypothesis as given in eq. 4.1 . In the modelling of the dissipation term it is argued that the dissipation rate is controlled not by the dissipative motions themselves (hence dispensing with the need to prescribe the length scale for smaller energy dissipating eddies), but by the process that transfers energy from larger to successively smaller eddies which is supposed to depend on the turbulence energy, density and length scale of energy containing eddies. Kolmogorov (1942) and others have adopted the following form for dissipation rate of turbulence:

$$\mu \cdot \Sigma \left(\frac{\overline{\partial u_i'}}{\partial x_j}\right)^2 = C_\mu \frac{\bar{\rho} K^{3/2}}{\ell} = \bar{\rho}\,\varepsilon \qquad 4.7$$

Hence the modelled form of K-equation becomes

$$\bar{\rho}\overline{U'} \frac{\partial K}{\partial x} + \bar{\rho}\,\bar{V} \frac{\partial K}{\partial y} = \frac{\partial}{\partial y} \frac{\mu_t}{\sigma_k} \frac{\partial K}{\partial y} + \bar{\rho}\mu_t \left(\frac{\partial \bar{U}}{\partial y}\right)^2 - \bar{\rho}\,\varepsilon \qquad 4.8$$

This model gives improved predictions over the mixing length model in some cases, e.g. plane wake Rodi (1972). Its principal limitation is the same as that of the mixing length model in that the length scale of energy containing eddies must be prescribed as an algebraic function of position.

4.2.3 Two Equation Models

The next logical stage in turbulence model evolution was to solve a differential equation for length scale itself. A means of constructing the equation of length scale is to define a variable

$$z = K^m \ell^n \qquad 4.9$$

and to derive the equation for Z from the Navier Stokes equation. Several variables depending on the values of indices m and n can be formed. Table 4.2 lists the variables adopted by different workers to determine the length scale.

In this department the practice is to use

$$\varepsilon = c_\mu K^{3/2}/\ell = \nu\left(\frac{\overline{\partial u_i'}}{\partial x_j}\right)^2 \qquad 4.10$$

as the dependent variable for length scale. The turbulent viscosity can then be found by substituting ℓ from equation 4.10 into Eq. 4.4.

$$\mu_t = \bar{\rho} c_\mu K^2/\varepsilon \qquad 4.11$$

Reasons for the choice of ε are given by Launder and Spalding (1973). The main reason being that the value of the Prandtl number for dissipation equation 4.16 remains the same for near wall flows as well as for

Table 4.2 List of dependent variables for the second equation.

Launder and Spalding (1972)

Proposer	Year	m	n	z
Kolmogorov	1942	0.5	-1	$K^{1/2}/\ell$
Harlow and Nakayama	1969	1.5	-1	$K^{3/2}/\ell$
Rotta	1951	0	1	ℓ
Rotta	1968	1	1	$K\ell$
Spalding	1969	1	-2	K/ℓ^2

free flows. Another reason is that the transport equation for ε contains fewer terms than for any other similar variable (e.g. $K\ell$, K/ℓ^2 etc.). Following Harlow and Nakayama (1967) an exact equation for ε can be derived for high Reynolds numbers by differentiating the instantaneous Navier-Stokes equations, multiplying throughout by $\frac{\partial u_i}{\partial x_j}$ and time averaging.

$$\frac{D\varepsilon}{Dt} = \underbrace{-2\nu \frac{\partial \bar{U}_i}{\partial x_k} \left(\overline{\frac{\partial u_i'}{\partial x_\ell} \cdot \frac{\partial u_k'}{\partial x_\ell}} + \overline{\frac{\partial u_\ell'}{\partial x_i} \cdot \frac{\partial u_\ell'}{\partial x_k}}\right)}_{\text{(i)}} \underbrace{- 2\nu \overline{\frac{\partial u_i'}{\partial x_k} \cdot \frac{\partial u_i'}{\partial x_\ell} \cdot \frac{\partial u_k'}{\partial x_\ell}}}_{\text{(ii)}}$$

$$\underbrace{- 2 \overline{\left[\nu \frac{\partial^2 u_i'}{\partial x_k \partial x_\ell}\right]^2}}_{\text{(iii)}} \underbrace{- \frac{\partial}{\partial x_k} \left[\overline{u_k' \varepsilon'} + \frac{2\nu}{\rho} \overline{\frac{\partial p'}{\partial x_\ell} \frac{\partial u_k'}{\partial x_\ell}}\right]}_{\text{(iv)}} \qquad 4.12$$

All terms on the R.H.S. of this equation contain unknown correlations which have to be approximated in terms of known quantities. Some of these correlations are impossible to measure directly hence the modelling of these terms is more of an 'art' than anything else and it remains one of the weakest links in turbulence research. The validation of the modelling of these terms is 'indirect' in the sense that a modelled form of this equation is used to predict the Reynolds stresses as well as mean flow properties in 'standard' flows (plane mixing layer, wall boundary layer). If these quantities are predicted correctly it is reasoned that the modelling of tne dissipation equation is also correct. This is not satisfactory but until reliable measurements are available for the terms in Eq. 4.12 it re-represents the only possible method of validation.

The following approximations are used for various terms in the dissipation equation.

Term (i) expresses the production of dissipation eddies through mean motion and can be called the 'production of dissipation', Launder and Spalding (1973) assumed that this term can be written as

$$\text{Production of } \varepsilon = -2\nu \frac{\partial \bar{U}_i}{\partial x_k}\left(\overline{\frac{\partial u_i'}{\partial x_\ell} \cdot \frac{\partial u_k'}{\partial x_\ell}} + \overline{\frac{\partial u_\ell'}{\partial x_i} \cdot \frac{\partial u_\ell'}{\partial x_k}}\right)$$

$$= C_{\varepsilon 1}\left(\frac{\bar{\rho}\,\overline{u_i'u_k'}}{K}\right)\varepsilon \frac{\partial \bar{U}_i}{\partial x_k} \qquad 4.13$$

Term (ii), which expresses the generation of dissipation through the self-stretching action of the turbulence, may be considered small as compared to term (i) and is neglected. Term (iii) represents the decay of the dissipation rate ultimately through the action viscosity and is modelled as, Launder and Spalding (1973).

$$2\nu\overline{\frac{\partial^2 u_i'^2}{\partial x_k x_\ell}} = C_{\varepsilon 2}\frac{\varepsilon^2}{K} \qquad 4.14$$

Term (iv) which accounts for the diffusion of ε from velocity fluctuations is treated in a manner analogus to its counterpart in the turbulence energy equation viz:

$$\frac{\partial}{\partial x_k}\overline{u_k'\varepsilon'} = \frac{\partial}{\partial x_k}\frac{\mu_{eff}}{\sigma_\varepsilon}\frac{\partial \varepsilon}{\partial x_k} \qquad 4.15$$

where σ_ε is the Prandtl number for dissipation.

Term (v), which represents the diffusional transport of pressure fluctuations, is neglected.

The final form of ε-equation can be written as:

$$\bar{\rho}\bar{U}_j\frac{\partial \varepsilon}{\partial x_j} = \frac{\partial}{\partial x_j}\frac{\mu_{eff}}{\sigma_\varepsilon}\frac{\partial \varepsilon}{\partial x_j} + C_{\varepsilon 1}\,\bar{\rho}\,\frac{\varepsilon}{k}\,\overline{u_i'u_j'}\frac{\partial \bar{U}_i}{\partial x_j} - \bar{\rho}\,C_{\varepsilon 2}\frac{\varepsilon^2}{k} \qquad 4.16$$

The equation contains three constants which must be assigned appropriate values together with C_μ & σ_k. Table 4.3 lists their computer optimized values which give reasonable predictions for most two-dimensional, constant density, boundary layer flows.

There are two major defects in the modelling of the dissipation equation. One of them is that the approximation of dissipation is based on local properties of the flow, and Pope (1976) has shown that

Table 4.3 The Turbulence Model Constants

Constant	Value used		Basis of choice
	Most free shear flow	Inert round jet	
C_{μ}	0.09	0.09	Measurements of shear stress near a wall. Launder and Spalding(1972).
$\sigma_{t,K}$	1.0	1.0	The values given are a result of fine tuning for a wide range of
$\sigma_{t,\varepsilon}$	1.3	1.3	flows. Launder and Spalding (1972).
σ_{f}	0.7	0.7	Prandtl/Schmidt number for scalar has been measured for
σ_{g}	0.7	0.7	various free shear flows to be around 0.7 Launder (1976).
$C_{\varepsilon 1}$	1.44	1.57	Measurement of turbulence near a wall. Constant tuned to give the correct spreading rate of an inert jet. Morse (1976).
$C_{\varepsilon 2}$	1.90	1.90	Decay of turbulence behind a grid Launder and Spalding (1972).
C_{g1}	2.8	2.8	Constant optimized by Spalding
C_{g2}	1.9	1.9	for inert jets.

this is strictly true in self-similar flows only. It follows that the ability of the modelled equation to predict practical flows which are not self similar is limited. The other defect is that the constants used in eq. 4.16 are very sensitive. Rodi (1972), who solved equations for K and for the quantity $K^{5/2}/\varepsilon$, examined the effect of changing the constants on the spreading rates of four free shear flows. He found that a 5% increase in the constants analogus to $C_{\varepsilon 1}$ and $C_{\varepsilon 2}$ resulted, on an average, in 15% and 8% increase in the spreading rate.

4.2.4 Prediction of a Round Jet

Prediction of round jets has always posed problems because the set of constants as given in table 4.3 gives a very high spreading rate in the self similar region. This was found by Launder et al (1972) who modified the two equation model to prĕdict the spreading rate and turbulence level correctly. Morse (1976) found that correct spreading rate could be predicted only by modifying $C_{\varepsilon 1}$ from 1.44 to 1.57. Using these values predictions of a round jet measured by Rose (1962) were made by the present author. Fig. 4.1 shows the decay of central line velocity, the agreement between measured and calculated values is reasonable. Fig. 4.2 shows the fully developed radial profile of axial velocity in a jet measured by Wygnansky and Fiedler (1969) and predictions, the agreement is quite reasonable.

4.2.5 Mutli-Equation Models

For flows which are highly anisotropic, such as jets with high swirl, effective viscosity models are not very successful. In these flows, the normal stresses are not equal as suggested by the two equation model. Also the shear stress is not correctly represented by the Boussinesq hypothesis. In order to predict these flows correctly all the Reynolds stresses must be calculated and hence their modelled trans-

port equations are required to be solved. Launder et al (1975) proposed a five equation model in which four stress equations ($\overline{u_1'^2}$, $\overline{u_2'^2}$, $\overline{u_3'^2}$, $\overline{u_1'u_2'}$) and the ε equation for two dimensional boundary layer flows were solved. Hanjelic and Launder (1971) proposed a three equation model in which the shear stress equation in addition to the equations for kinetic energy and dissipation was solved. This model was successful in calculation of boundary layers in which the shear stress and mean velocity gradient had opposite signs over a significant region of the flow (asymmetric channel). For other boundary layer flows, three equation models were not superior to two equation ones, Rodi (1972).

4.3 A Two Equation Model for Reacting Flows

The two equation (k-ε) model has been used to predict the present flow. This model, as mentioned earlier, does not require algebraic prescription of the length scale. It is economical since only two extra equations are required as opposed to as many as seven needed by a Reynolds stress model. It has been extensively tested in many different flow situations on inert as well as reacting flows. Table 4.4 shows some of the flows which have been solved using this model. In general the performance is good. Mean flow quantities such as velocity profiles, pressure drop, heat transfer rates and temperature are in most cases well predicted. Turbulence quantities such as k and μ_t also show agreement with measurements. This model is not able to predict properly flows where turbulence in highly non-isotropic, but the Reynolds stress model developed to overcome this failing have so far not been very successful Pope (1976).

Table 4.4 List of flows for which K-ε model has been used

	Author	Flow	Dimension	Recirculating or Parabolic	Inert or Reacting	Free or Confined	Remarks
1	Launder et al (1972)	Plane jet in a moving stream	2-D	Parabolic	Inert	Free	Good agreement with data throughout the region of measurement
2	Launder et al (1972)	Round jet in stagnant surroundings	2-D	Parabolic	Inert	Free	Constant C_μ and $C_{\varepsilon 2}$ were modified to get agreement.
3	Mathews and Whitelaw (1971)	Plane jet flows over a backward facing step	2-D	Recirculating	Inert	Free	Good agreement with measurements. Boundary values of ε at the lip and downstream face of the step were modified.
4	Priddin (1975)	Heat transfer around the pressure surface of a turbine blade	2-D	Parabolic	Inert	Free	Good agreement with measurement.
5	Jones and Launder (1971)	Flow in pipe	2-D	Parabolic	Inert	Confined	Low Reynolds number version of the model employed. Good prediction obtained without using 'wall functio
6	Elgobashi(1975)	Confined co-axial jets	2-D	Recirculating	Inert	Confined	Measured position and magnitude of recirculating zone well predicted.

	Author	Flow	Dimension	Recirculating or Parabolic	Inert or Reacting	Free or Confined	Remarks
7	Nielson (1976)	Cavity flow	2-D	Recirculating	Inert	Confined	Velocity contours in close agreement with experiment
8	Sharma (1974)	Flow in rectangular sectioned diffusers	3-D	Parabolic	Inert	Confined	Mean velocity profiles well predicted
9	Pratap (1975)	Flow in helically coiled pipes	3-D	Semi-Elliptic	Inert	Confined	
10	Mujamdar (1975)	Follow in rotating ducts	3-D	Parabolic	Inert	Confined	Agreement with experiment quite good when speed of rotation is not high.
11	Naguib (1975)	Diffusion and premixed flames	2-D	Parabolic	Reacting	Free	Temperature profiles quite well predicted.
12	Mason & Spalding (1973)		2-D	Recirculating	Reacting	Confined	
13	Elgobashi(1975)	Turbulent diffusion flames axisymmetrical cylindrical furnace	2-D	Recirculating	Reacting	Confined	Measured values of mixture fraction reasonably well predicted

	Author	Flow	Dimension	Recirculating or Parabolic	Inert or Reacting	Free or Confined	Remarks
14	Khalil (1975)	Flow in axisymmetric furnace with swirl.	2-D	Recirculating	Reacting	Confined	Radial velocity profile and centreline distribution of kinetic energy well predicted

4.3.1 Turbulence Energy Equation for Reacting Flows

The exact form of the turbulence energy equation for three dimensional variable density and constant viscosity flows is given below, Bray (1974).

$$\underset{1}{\overline{\rho}\bar{U}_j\frac{\partial K}{\partial x_j}} + \underset{2}{\overline{\rho' u_j'}\frac{\partial K}{\partial x_j}} = \underset{3}{g_i\overline{\rho' u_i'}} - \underset{4}{\overline{\rho}\,\overline{u_i' u_j'}\frac{\partial \bar{U}_i}{\partial x_j}} - \underset{5}{(\overline{\rho' u_i' u_j'} + U_j\overline{\rho' u_i'})\frac{\partial \tilde{U}_i}{\partial x_j}}$$

$$+ \underset{6}{\frac{\partial}{\partial x_j}\overline{f_{ij}u_i'}} + \underset{7}{\overline{p'\frac{\partial u_i'}{\partial x_i}}} - \underset{8}{\Phi} - \underset{9}{\frac{\partial}{\partial x_j}(\overline{\rho k' u_j'} + \overline{p' u_j'})} - \underset{10}{\frac{\partial}{\partial x_j}(U_j\,\overline{\rho' k'} + \overline{\rho' k' u_j'} - \overline{k\rho' u_j'})} \qquad 4.17$$

where $f_{ij} = -\frac{2}{3}\mu\frac{\partial \hat{u}_i}{\partial x_j}\delta_{ij} + \mu\left[\frac{\partial \hat{u}_i}{\partial x_j} + \frac{\partial \hat{u}_j}{\partial x_i}\right]$ 4.18

and $\Phi = \overline{f_{ij}\frac{\partial u_i'}{\partial x_i}} = \overline{\frac{\partial u_i'}{\partial x_i}\mu\left(\frac{\partial u_i'}{\partial x_j} + \frac{\partial u_j'}{\partial x_i}\right)} - \frac{2}{3}\mu\,\overline{\frac{\partial u_i'}{\partial x_i}\frac{\partial u_j'}{\partial x_j}}$ 4.19

The following meanings can be ascribed to the various terms of equation 4.17.

Term 1: Convective rate of change due to mean velocity

Term 2: Convective rate of change due to density-velocity correlation

Term 3: Production of turbulence energy due to gravity

Term 4: Production due to the action of the Reynolds stresses on mean velocity gradients

Term 5: Production due to the action of density-velocity correlation on mean velocity gradients

Term 6: Viscous diffusion

Term 7: If positive represents transfer of energy from enthalpy to turbulence

Term 8: Viscous dissipation

Term 9: Turbulent diffusion

Term 10: Turbulent diffusion due to density fluctuations

The above equation is complicated, but some simplifications can be made if the different terms appearing are studied more closely. One term that can easily be neglected is the viscous diffusion (term 6) since for high Reynold number flows this will be much smaller than the turbulent diffusion term. If the fluctuations in density are small then terms 2, 3, 5 and 10 may also be neglected. Naguib (1975), Elgobashi (1975) and Khalil (1977) have neglected these terms in the calculation of various reacting flows and have procured reasonable predictions. For the initial part of this study it was decided to neglect them as well (methods of modelling fluctuating density correlations will be discussed in section 4.4). Bray (1974) has shown that term 7 can be expressed as pressure-reaction rate co-variance the details are quite involed and are given in appendix 4.1 . An order of magnitude analysis also carried out by Bray shows that this term is equal to triple density fluctuation correlation (term 5). Since term (5) is neglected term (7) can also be neglected. Hence we are left with the following equation for high Reynolds numbers:

$$\overline{\rho}\overline{U_j}\frac{\partial K}{\partial x_j} = -\overline{\rho}\,\overline{u_i'u_j'}\frac{\partial \overline{U_i}}{\partial x_j} - \frac{\partial}{\partial x_j}\left(\overline{\rho k' u_j'} + \overline{p' u_j'}\right) - \mu\,\overline{\left(\frac{\partial u_i'}{\partial x_j}\right)^2} \qquad 4.20$$

The above relation is similar to eq. 4.5 and can be approximated accordingly:

$$\overline{\rho}\overline{U_j}\frac{\partial K}{\partial x_j} = -\overline{\rho}\,\overline{u_i'u_j'}\frac{\partial \overline{U_i}}{\partial x_j} + \frac{\partial}{\partial x_j}\left(\frac{\mu_t}{\sigma_k}\frac{\partial K}{\partial x_j}\right) - \overline{\rho}\varepsilon \qquad 4.21$$

The Reynolds stresses can be approximated by an expression similar to 4.7. For three dimensional flows the following is appropriate, Hinze (1959):

$$-\overline{\rho}\,\overline{u_i'u_j'} = \mu_t\left(\frac{\partial \overline{U_i}}{\partial x_j} + \frac{\partial \overline{U_j}}{\partial x_i}\right) - \frac{2}{3}\overline{\rho}k\delta_{ij} \qquad 4.22$$

For cylindrical coordinates and variable density these terms can be written as:

$$-\bar{\rho}\,\overline{v_r'v_r'} = 2\mu_t \left(\frac{\partial \bar{V}_r}{\partial r}\right) - \frac{2}{3}\left(\bar{\rho}K + \mu_t \,.\, (\nabla.\vec{V})\right) \qquad 4.22a$$

$$-\bar{\rho}\,\overline{v_\theta'v_\theta'} = 2\mu_t \left(\frac{1}{r}\frac{\partial \bar{V}_\theta}{\partial \theta} + \frac{\bar{V}_r}{r}\right) - \frac{2}{3}\left(\bar{\rho}K + \mu_t\,(\nabla.\vec{V})\right) \qquad 4.22b$$

$$-\bar{\rho}\,\overline{v_z'v_z'} = +\,2\mu_t \left(\frac{\partial \bar{V}_z}{\partial z}\right) - \frac{2}{3}\left(\bar{\rho}K + \mu_t\,(\nabla.\vec{V})\right) \qquad 4.22c$$

$$-\bar{\rho}\,\overline{v_r'v_\theta'} = \mu_t\left[\frac{1}{r}\frac{\partial \bar{V}_r}{\partial \theta} + \frac{\partial \bar{V}_\theta}{\partial r} - \frac{\bar{V}_\theta}{r}\right] \qquad 4.22d$$

$$-\bar{\rho}\,\overline{v_r'v_z'} = \mu_t\left[\frac{\partial \bar{V}_r}{\partial z} + \frac{\partial \bar{V}_z}{\partial r}\right] \qquad 4.22e$$

$$-\bar{\rho}\,\overline{v_\theta'v_z'} = \mu_t\left[\frac{1}{r}\frac{\partial \bar{V}_z}{\partial \theta} + \frac{\partial \bar{V}_\theta}{\partial z}\right] \qquad 4.22f$$

where

$$\nabla.\vec{V} = \frac{1}{r}\frac{\partial}{\partial r}(r\bar{V}_r) + \frac{1}{r}\frac{\partial \bar{V}_\theta}{\partial \theta} + \frac{\partial \bar{V}_z}{\partial z}$$

The $\overline{u_i'\Phi'}$ term in the scalar transport equation can also be modelled with the help of the gradient hypothesis so that

$$\bar{\rho}\,\overline{u_i'\Phi'} = -\frac{\mu_t}{\sigma_\Phi}\frac{\partial \bar{\Phi}}{\partial x_i} = \Gamma_{\Phi,t}\frac{\partial \bar{\Phi}}{\partial x_i} \qquad 4.23$$

where σ_Φ and $\Gamma_{\Phi\ t}$ are the Prandtl number for Φ and turbulent exchange coefficient of Φ respectively. Using eq. 4.22 and 4.23 a closed set of equations can now be formed from equations 3.12-3.16, eq. 4.11, 4.16 and 4.21. These equations are written below and, together with the equation for square of scalar fluctuation to be described in section 4.5, comprise Model I of the present study.

4.3.2 Transport equations for Model I

Continuity

$$\frac{\partial (r\bar{\rho}\bar{V}_r)}{\partial r} + \frac{\partial}{r\partial\theta}(\bar{\rho}\bar{V}_\theta) + \frac{\partial}{\partial z}(\bar{\rho}\bar{V}_z) = 0 \qquad 4.24$$

r-Momentum

$$\frac{1}{r}\frac{\partial (r\bar{\rho}\bar{V}_r\bar{V}_r)}{\partial r} + \frac{\partial (\bar{\rho}\bar{V}_\theta\bar{V}_r)}{r\partial\theta} + \frac{\partial (\bar{\rho}\bar{V}_z\bar{V}_r)}{\partial z} = \bar{\rho}g_r - \frac{\partial \bar{p}}{\partial r} + \frac{1}{r}\frac{\partial}{\partial r} r\mu_{eff}\frac{\partial \bar{V}_r}{\partial r}$$

$$+ \frac{\partial}{r\partial\theta}\mu_{eff}\left(\frac{\partial \bar{V}_r}{r\partial\theta}\right) + \frac{\partial}{\partial z}\mu_{eff}\left(\frac{\partial \bar{V}_r}{\partial z}\right) + \frac{1}{3}\mu_{eff}\frac{\partial}{\partial r}(\Delta\vec{V}) - \mu_{eff}\frac{\bar{V}_r}{r^2}$$

$$- 2\mu_{eff}\frac{\partial \bar{V}_\theta}{\partial\theta} + \frac{\bar{\rho}\bar{V}_\theta^2}{\partial r} - \frac{2}{3}\frac{\partial \bar{\rho}K}{\partial r} + \frac{\partial \mu_{eff}}{\partial r}^{r}\frac{\partial \bar{V}_r}{\partial r} + \frac{1}{r}\frac{\partial}{\partial\theta}\mu_{eff}\frac{\partial \bar{V}_\theta}{\partial r}$$

$$+ \frac{\partial \mu_{eff}}{\partial z}\frac{\partial \bar{V}_z}{\partial r} \qquad 4.25$$

θ-Momentum

$$\frac{1}{r}\frac{\partial (r\bar{\rho}\bar{V}_r\bar{V}_\theta)}{\partial r} + \frac{\partial (\bar{\rho}\bar{V}_\theta\bar{V}_\theta)}{r\partial\theta} + \frac{\partial (\bar{\rho}\bar{V}_\theta\bar{V}_z)}{\partial z} = \bar{\rho}g_\theta - \frac{\partial \bar{p}}{r\partial\theta}$$

$$+ \frac{\partial}{r\partial\theta}\left(\mu_{eff}\frac{\partial \bar{V}_\theta}{r\partial\theta}\right) + \frac{\partial}{\partial z}\left(\mu_{eff}\frac{\partial \bar{V}_\theta}{\partial z}\right) + \frac{1}{r}\frac{\partial}{\partial r}\left(r\mu_{eff}\frac{\partial \bar{V}_\theta}{\partial r}\right) - \frac{\bar{\rho}\bar{V}_r\bar{V}_\theta}{r}$$

$$+ \mu_{eff}\frac{2}{r^2}\frac{\partial \bar{V}_r}{\partial\theta} - \frac{2}{3}\frac{\partial \bar{\rho}K}{r\partial\theta} - \mu_{eff}\frac{\bar{V}_\theta}{r^2} + \frac{1}{3}\mu_{eff}\frac{\partial}{r\partial\theta}(\nabla.\vec{V}) +$$

$$\frac{\partial \mu_{eff}}{r\partial\theta}\frac{\partial \bar{V}_\theta}{r\partial\theta} + \frac{\partial \mu_{eff}}{\partial r}\frac{\partial \bar{V}_r}{r\partial\theta} + \frac{\partial \mu_{eff}}{\partial z}\frac{\partial \bar{V}_z}{r\partial\theta} \qquad 4.26$$

z-Momentum

$$\frac{1}{r}\frac{\partial (r\bar{\rho}\bar{V}_r\bar{V}_z)}{\partial r} + \frac{\partial (\bar{\rho}\bar{V}_\theta\bar{V}_z)}{r\partial\theta} + \frac{\partial (\bar{\rho}\bar{V}_z\bar{V}_z)}{\partial z} = \bar{\rho}g_z - \frac{\partial \bar{p}}{\partial z}$$

$$\frac{\partial}{r\partial\theta}\left(\mu_{eff}\frac{\partial\bar{V}_z}{r\partial\theta}\right) + \frac{\partial}{\partial z}\mu_{eff}\frac{\partial\bar{V}_z}{\partial z} + \frac{1}{r}\frac{\partial}{\partial r}\left(r\mu_{eff}\frac{\partial\bar{V}_z}{\partial r}\right) - \frac{2}{3}\frac{\partial\bar{\rho K}}{\partial z} +$$

$$+ \frac{1}{3}\mu_{eff}\frac{\partial}{\partial z}(\nabla.\vec{V}) + \frac{\partial\mu_{eff}}{r\partial\theta}\cdot\frac{\partial\bar{V}_\theta}{\partial z} + \frac{\partial\mu_{eff}}{\partial r}\cdot\frac{\partial\bar{V}_r}{\partial z} + \frac{\partial\mu_{eff}}{\partial z}\cdot\frac{\partial\bar{V}_z}{\partial z} \qquad 4.27$$

Φ-Equation

$$\frac{1}{r}\frac{\partial(r\bar{\rho}\bar{V}_r\bar{\Phi})}{\partial r} + \frac{\partial(\bar{\rho}\bar{V}_\theta\bar{\Phi})}{r\partial\theta} + \frac{\partial(\bar{\rho}\bar{V}_z\bar{\Phi})}{\partial z} = \frac{\partial}{r\partial\theta}\Gamma_{eff}\frac{\partial\bar{\Phi}}{r\partial\theta} + \frac{\partial}{\partial z}\Gamma_{eff}\frac{\partial\bar{\Phi}}{\partial z}$$

$$+ \frac{1}{r}\frac{\partial}{\partial r}r\,\Gamma_{eff}\frac{\partial\bar{\Phi}}{\partial r} + S\bar{\Phi} \qquad 4.28$$

where $\mu_{eff} = \mu_t + \mu_\ell$

$$\Gamma_{eff} = \Gamma_t + D_\Phi$$

4.4 Modelling of Density Fluctuations

In model I proposed in the previous section the terms involving the density fluctuations were assumed to be small and were neglected. There is evidence however that these quantities may in some cases be larger in magnitude than the usual Reynolds stresses. Stanford and Libby (1974) measured density fluctuation correlations and Reynolds stresses in air flow through a porous pipe with uniform helium injection through the walls. They found that $\bar{\rho}\overline{u'v'}$ was less than $\bar{u}\,\overline{\rho'v'}$ in some regions of the flow. In situations of this type the effect of extra terms on turbulence and transport of mass and momentum can be very important and the flow cannot be predicted correctly without proper modelling of these terms.

Unfortunately for the case of reacting flows there is little experimental evidence of the magnitude of $\overline{\rho'u_i'}$ and $\overline{\rho'\phi'}$ terms, and in the absence of such information the effect of these terms can only be guessed. If the Boussinesq hypothesis is assumed to be applicable to turbulent

mass fluxes as well and if the exchange coefficient for density is of the same order of magnitude as that for momentum then the ratio $\overline{\rho' u_j'} / \overline{u_i' u_j'} \simeq \frac{\overline{\partial \rho}}{\partial x_j} / \frac{\partial \bar{U}_i}{\partial x_j}$. In the reaction zone of the flame where the density gradient is much larger than the velocity gradient the density-velocity correlations can be important. It does not, however, necessarily follow that if $\overline{\rho' u_j'} > \overline{u_i' u_j'}$ its effect on turbulence will be greater because these quantities do not appear with the same variable e.g. $\overline{\rho' u_j'}$ appears as $\bar{u}_i \overline{\rho' u_j'}$ and $\overline{u_i' u_j'}$ as $\bar{\rho} \overline{u_i' u_j'}$. Also, the effect of these terms in different equations may be different. In the momentum equation $u_i \overline{\rho' u_j'}$ and $\bar{\rho} \overline{u_i' u_j'}$ appear as diffusion terms $\frac{\partial}{\partial x_j}(\bar{\rho} \overline{u_i' u_j'} + \bar{U}_j \overline{\rho' u_i'})$ hence their gradients are important in this situation. In the kinetic energy equation they appear as production terms $(\overline{\rho u_i' u_j'} + \bar{U}_j \overline{\rho' u_i'}) \frac{\partial \bar{U}_i}{\partial x_j}$ in this equation their relative magnitudes are important. So it is possible that these terms affect the different transport equations to a different extent.

The problem remains of modelling these terms, two different approaches have been suggested, one by Favre (1969) and the other by Bray (1974). In the next section both will be examined in detail.

4.4.1 Favre Averaging

Favre (1969) introduced a method of averaging which eliminated double correlations involving density fluctuations from the turbulent fluxes. This method consists of weighting the variables by the instantaneous density before averaging. The resulting equations are very similar in form to the transport equations for constant density.

Favre averaging of the transport equations can best be demonstrated by introducing the concept of Favre probability density function of a variable Φ, Bilger (1975).

$$\tilde{P}_{\Phi}(\Phi) \equiv \left(\frac{1}{\bar{\rho}}\right) \int_{0}^{\infty} \hat{\rho} P_{\rho\Phi}(\rho,\Phi) \, .d\rho \qquad 4.29$$

where $P_{\rho,\Phi}(\rho,\Phi)$ is the joint pdf of ρ and Φ. The Favre mean is defined as:

$$(\tilde{\Phi} \equiv \overline{\hat{\rho}\hat{\Phi}}/\bar{\rho}) \qquad 4.30$$

Hence $\tilde{\Phi}$ can be obtained by weighting $\tilde{P}_{\Phi}(\Phi)$ as

$$\tilde{\Phi} \equiv \frac{\overline{\hat{\rho}\hat{\Phi}}}{\bar{\rho}} = \frac{1}{\bar{\rho}} \int \hat{\rho}\hat{\Phi} P_{\rho,\Phi}(\rho,\Phi) \, . \, d\rho d\Phi$$

$$= \int \hat{\Phi} \tilde{P}_{\Phi}(\Phi) \, .d\Phi \qquad 4.31$$

The Favre variance can be written as:

$$\tilde{\Phi}''^{2} = \overline{(\hat{\Phi}-\tilde{\Phi})^{2}} = \frac{\overline{\hat{\rho}\Phi''^{2}}}{\bar{\rho}} = \int (\hat{\Phi}-\tilde{\Phi})^{2} \tilde{P}_{\Phi}(\Phi) \, . \, d\Phi \qquad 4.32$$

Similarly for any function $f(\Phi)$

$$\tilde{f(\Phi)} = \int f(\Phi) \tilde{P}_{\Phi}(\Phi) \, .d\Phi \qquad 4.33$$

Note that from eq. (4.30)

$$\tilde{\Phi} = \frac{\overline{\hat{\rho}\hat{\Phi}}}{\bar{\rho}} = \bar{\Phi} + \frac{\overline{\rho'\Phi'}}{\bar{\rho}} \qquad 4.34$$

With the above definition of Favre probability density function the continuity equation can be written as:

$$\frac{\partial \overline{\hat{\rho}\hat{U}_{i}}}{\partial x_{i}} = 0 \qquad 4.35$$

or

$$\frac{\partial}{\partial x_{i}} \left| \bar{\rho} \frac{1}{\bar{\rho}} \int \hat{\rho}\hat{u}_{i} \, P_{\rho,U_{i}}(\rho,U_{i}) \, . \, d\rho du_{i} \right. = 0 \qquad 4.36$$

substituting eq. 4.31 above we have

$$\frac{\partial}{\partial x_{i}} \bar{\rho}\tilde{U}_{i} = 0 \qquad 4.37$$

The three momentum, species transport and kinetic energy equations

can be similarly written. Bilger (1975) has derived these equations for two dimensional axisymmetric flows and they are given in Appendix 4.2. It can be seen that these equations apart from the kinetic energy equation are exactly the same as those used for uniform density flows except that Favre averages and Favre correlations ($\tilde{U}$, $\widetilde{U''V''}$) are used instead of the Reynolds averages and fluctuations ($\overline{U}$, $\overline{U'V'}$).

If density fluctuations are neglected from the transport equations, Favre averaged variables are solved instead of time averaged ones in variable density flows. This suggests that an easier way to account for density fluctuations would be to solve Favre averaged equations and obtain conventional averages from eq. 4.34 as follows:

$$\overline{U} = \tilde{u} - \overline{\rho'u'/\rho} \qquad 4.38$$

$$\overline{T} = \tilde{T} - \overline{\rho'T'/\rho}$$

This would require modelling of $\overline{\rho'u'}$ and $\overline{\rho'T'}$ to compare with experiments only if conventional averages are measured. Apart from being simple this method has an added advantage that the error in the estimation of $\overline{'u'}$, etc. is not propagated into the system of equations.

4.4.2 Bray' Approach

Bray (1974) has suggested that correlations involving density fluctuations should be incorporated, in their modelled form, directly into the transport equations. The advantage of this method is that the effect of density fluctuations on the individual transport equations can be investigated. Also modelling techniques developed for uniform

density-flows can be applied directly to reacting flows because these stresses are expected to influence the variable density flows in analogous manner to uniform density flows. The task of modelling as well as computing is significantly increased. Not only the double correlations are to be modelled but triple correlations such as $\overline{\rho' u_i' u_j'}$, $\overline{\rho' f' u_i'}$ and $\overline{\rho' K' u_i'}$ have to be approximated in equations 3.8, 3.9, 3.10, 4.18 and 4.34 as well. Computing time also increases because these correlations are to be solved throughout the flow field and not only at the measuring location as required by Favre averaging.

Bray (1974) has included the fluctuating density velocity correlations in the kinetic energy equation only and in the final modelled form of this equation he has neglected the triple correlation $\overline{\rho' u_i' u_j'}$. He has used the gradient hypothesis, eq. 4.30, to model $\overline{\rho' u_i'}$. If this approach is extended so that all the density fluctuation correlations are included in every equation, the following stages can be suggested:

(i) Include double correlations of density and velocity fluctuation in all transport equations by using the gradient hypothesis.

(ii) Include double correlations of density and scalar fluctuations in the scalar transport equations. These fluctuations are modelled using a suitable probability density function for the scalar.

(iii) Improve modelling of $\overline{\rho' u_i'}$ and $\overline{\rho' f'}$ etc. by solving their respective transport equations and model the triple correlations using the gradient hypothesis.

Use of the above procedure will result in the systematic investigation of the influence of density fluctuations on the transport of mass and momentum in a reacting flow. Since complications will be included gradually into the computational procedure it will allow the effect of the inclusion of the extra terms in different equations to be monitored carefully. This procedure will also allow the model to be tested in detail rather than by its global effect if all the terms are included at once.

In the next section the relative merits of the two ways in which density fluctuationscan be handled will be discussed and one method will be selected to be used in the prediction of the present problem.

4.4.3 Choice of the Method

The choice between Favre averaging and modelling of individual turbulent fluxes is not an easy one. Very little work, experimental and theoretical, has been done in this field so guidelines are not available. Both approaches have their advantages and limitations.

The major advantage of Favre averaging is its ease of computation, but in choosing a model of density fluctuations one must keep in mind the ability of the model to represent the physical process accurately. Indeed, ease of computations should not be an argument to gloss over other defects. The basic assumption that has to be applied to the Favre averaged equation is that the Favre averaged correlations model in the same way as Reynolds stresses in uniform density flows. The simplicity of Favre averaged equations is based on this assumption. Extensive work will be required to model the Favre correlations if this assumption is not true.

Favre averaged shear stress $\overline{\rho u''_i u''_j}$ is modelled as:

$$\overline{\rho u'' v''} = - \nu_{T,F} \left(\frac{\partial \tilde{U}}{\partial y} + \frac{\partial \tilde{V}}{\partial x} \right) \qquad 4.40$$

Here $\nu_{T,F}$ is the Favre averaged turbulent viscosity which is a function of Favre averaged turbulent kinetic energy $\tilde{u}_i^2$ and Favre averaged dissipation. If both sides of the above equations are written in conventional averaged form we have

$$\overline{\rho u'v'} + \left(\frac{\overline{\rho' u' v'}}{\bar{\rho}} - \frac{\overline{\rho' u'}}{\bar{\rho}} \frac{\overline{\rho' v'}}{\bar{\rho}} \right) = - \nu_{T,F} \left(\frac{\partial \bar{U}}{\partial y} + \frac{\partial \bar{V}}{\partial x} \right) +$$

$$\nu_{T,F} \left(\frac{\partial \overline{\rho' u'/\rho}}{\partial y} + \frac{\partial \overline{\rho' v'/\rho}}{\partial x} \right) \qquad 4.41$$

Assuming that density-velocity correlations will be related to density gradients, the above equation can be broken into two relations as:

$$\overline{u'v'} = -\nu_{T,F}\left(\frac{\partial \bar{U}}{\partial y} + \frac{\partial \bar{V}}{\partial x}\right) \qquad 4.42$$

$$\left(\frac{\overline{\rho'u'v'}}{\bar{\rho}} - \frac{\overline{\rho'u'}}{\bar{\rho}}\,\frac{\overline{\rho'v'}}{\bar{\rho}}\right) = \nu_{T,F}\left(\frac{\partial(\overline{\rho'u'}/\bar{\rho})}{\partial y} + \frac{\partial(\overline{\rho'v'}/\bar{\rho})}{\partial x}\right) \qquad 4.43$$

Equation 4.42 suggests that Reynolds stresses model differently in variable density flows which is not physically probable. Equation 4.43 shows that density fluctuation terms have been modelled in a way which is not at all consistent with conventional modellling of similar terms. The sign is incorrect and a term is missing from the right hand side. It is interesting to see that the equation 4.40 reduces to the equation for shear stress Equation 4.23 when density is uniform and hence it may be correct for small density fluctuations. But this equation as shown above is suspect if density fluctuations are significant.

To provide a check on the modelling of $\overline{u_i'' u_j''}$ this quantity will have to be measured in reacting flows and compared with its predicted value given by the model. Until this validation has been done in a variety of reacting flows the generality of the model will be suspect. To the best of author's knowledge this has not been done for any reacting flow.

The buoyant generation term in the Favre averaged kinetic energy equation contains the fluctuating density velocity correlation. For the prediction of buoyant flows this term will have to be modelled as well as the extra pressure gradient velocity fluctuation correlation.
So it is clear that modelling task is not exactly equal to that of constant density flows.

If the Favre averaged stresses are modelled using Equation 4.40 and the pressure gradient velocity fluctuation correlation is neglected

from the kinetic energy equation then the effect of density fluctuations is in a sense 'linearized'. The effect is only evident in equation 4.38 which does not seem physically plausible.

Bray's approach on the other hand seems a logical extension to reacting flows of the modelling techniques of uniform density flows. It also requires less basic modelling assumptions. The disadvantage is that the equations are more tedious and contain a greater number of terms that their constant density counterparts. But if the investigation is carried out systematically as outlined in the previous section, it should lead to better understanding of turbulence in reacting flows.

For the reasons discussed above it was decided to use Bray's approach in the present work.

Due to the limited time available, only the first of the three stages suggested in section 4.42 was incorporated in model II. The $\overline{\Phi}$ equation of model II then becomes:

$$\frac{1}{r}\frac{\partial(r\overline{\rho}\overline{V}_r\overline{\Phi})}{\partial r} + \frac{\partial(\overline{\rho}\overline{V}_\theta\overline{\Phi})}{r\partial\theta} + \frac{\partial(\overline{\rho}\overline{V}_z\overline{\Phi})}{\partial z} + \frac{1}{r}\frac{\partial}{\partial r}\left(r\overline{\Phi}\frac{\mu_{eff}}{\sigma_\rho}\frac{\partial\overline{\rho}}{\partial r}\right)$$

$$+ \frac{\partial}{r\partial\theta}\left(\overline{\Phi}\frac{\mu_{eff}}{\sigma_\rho}\frac{\partial\overline{\rho}}{r\partial\theta}\right) + \frac{\partial}{\partial z}\left(\overline{\Phi}\frac{\mu_{eff}}{\sigma_\rho}\frac{\partial}{\partial z}\overline{\rho}\right)$$

$$= \frac{\partial}{r\partial\theta}\Gamma_{eff}\frac{\partial\overline{\Phi}}{r\partial\theta} + \frac{\partial}{\partial z}\Gamma_{eff}\frac{\partial\overline{\Phi}}{\partial z} + \frac{1}{r}\frac{\partial\overline{\Phi}}{r}\Gamma_{eff}\frac{\partial\overline{\Phi}}{\partial r} + S\overline{\Phi} \qquad 4.44$$

The extra terms required to be added to model I to change it into model II are given in table 6.1. It would have been useful to predict the flow using Favre averaged equations as well so that comparisons could be made but the shortage of time ruled out this possibility.

The above arguments should not be viewed as implying that Favre's approach should not be pursued at all, rather they are intended to reveal its own short-comings which are often glossed over.

③ $\phi' \frac{\partial}{\partial x_j} \rho u_j' \phi' = \phi' \rho \frac{\partial u_j' \phi'}{\partial x_j} + \phi' u_j' \frac{\partial \rho \phi'}{\partial x_j} + \phi \phi' \frac{\partial \rho u_j'}{\partial x_j}$

$= \phi' \rho u_j' \frac{\partial \phi'}{\partial x_j} + \phi' \rho \phi' \frac{\partial u_j'}{\partial x_j} + \phi' u_j' \rho \frac{\partial \phi'}{\partial x_j} + \phi u_j' \phi' \frac{\partial \rho}{\partial x_j}$

$= 2\phi' \rho u_j' \frac{\partial \phi'}{\partial x_j} = \rho u_j' \frac{\partial \phi'^2}{\partial x_j}$

averaging:

$$A = \rho \overline{u_j} \frac{\partial \overline{\phi'^2}}{\partial x_j} + 2\rho \overline{\phi' u_j'} \frac{\partial \overline{\phi}}{\partial x_j} + \overline{\rho u_j' \frac{\partial \phi'^2}{\partial x_j}}$$

B) $\phi' \frac{\partial}{\partial x_j} \left(\Gamma \frac{\partial \overline{\phi}}{\partial x_j} + \Gamma \frac{\partial \phi'}{\partial x_j} \right)$

$\phi' \frac{\partial}{\partial x_j} \Gamma \frac{\partial \overline{\phi}}{\partial x_j}$ ① $+ \phi' \frac{\partial}{\partial x_j} \Gamma \frac{\partial \phi'}{\partial x_j}$ ②

$2\Gamma \left(\frac{\partial \phi'}{\partial x_j} \right)^2$

① $\frac{\partial}{\partial x_j} \phi' \left(\Gamma \frac{\partial \overline{\phi}}{\partial x_j} \right) = \phi' \frac{\partial}{\partial x_j} \Gamma \frac{\partial \overline{\phi}}{\partial x_j} + \Gamma \frac{\partial \phi'}{\partial x_j} \frac{\partial \overline{\phi}}{\partial x_j}$

$\frac{\partial}{\partial x_j} \left(\phi' \Gamma \frac{\partial \phi'}{\partial x_j} \right) = \underbrace{\phi' \frac{\partial}{\partial x_j} \Gamma \frac{\partial \phi'}{\partial x_j}}_{②} + \Gamma \frac{\partial \phi'}{\partial x_j} \frac{\partial \phi'}{\partial x_j}$

① + ②

$\frac{\partial}{\partial x_j} \phi' \Gamma \frac{\partial \overline{\phi}}{\partial x_j} = \Gamma \frac{\partial \overline{\phi}}{\partial x_j} \frac{\partial \phi'}{\partial x_j} + \lambda \left(\phi' \Gamma \frac{\partial \phi'}{\partial x_j} \right) - \Gamma \left(\frac{\partial \phi'}{\partial x_j} \right)^2$

averaging: $\overline{\phi' \Gamma \frac{\partial \phi'}{\partial x_j}} = 0$, $\overline{\Gamma \frac{\partial \overline{\phi}}{\partial x_j} \frac{\partial \phi'}{\partial x_j}} = 0$

$\frac{\partial}{\partial x_j} \left(\phi' \Gamma \frac{\partial \phi'}{\partial x_j} \right) = -\Gamma \left(\frac{\partial \phi'}{\partial x_j} \right)^2$

Crosley business forms by John Dickinson

4.5 The Transport and Dissipation of Scalar Fluctuations

If the flow is of uniform composition and isothermal it is completely defined by the continuity, momentum and turbulence equations such as K and ε. For flows of non-uniform composition such as turbulent diffusion flames, mean values of scalars (temperature, oxygen mass fractions, fuel mass fraction etc.) are also required. This combustion models suggested so far (chapter 5) require at least one scalar fluctuations correlation to be specified. In this section the exact equation for square of fluctuations of a passive scalar is written and modelled for constant and variable density-flows. This particular variable is chosen because the combustion model employed for the present study uses this correlation. Equations for other fluctuating quantities can of course be written and modelled along the same lines.

The equation can be obtained by multiplying the instantaneous equation of passive scalar f by f' and ensemble averaging.

$$\overset{1}{\bar{\rho}\bar{U}_j\frac{\partial\overline{f'^2}}{\partial x_j}} + \overset{2}{\overline{\rho' u_j'}\frac{\partial\overline{f'^2}}{\partial x_j}} = -2\Big(\overset{3}{\bar{\rho}\overline{f'u_j'}} + \overset{4}{\bar{U}_j\overline{\rho'f'}} + \overset{5}{\overline{\rho'f'u_j'}}\Big)\frac{\partial\bar{f}}{\partial x_j}$$

$$-\frac{\partial}{\partial x_j}\Big(\overset{6}{\bar{\rho}\overline{f'^2u_j'}} + \overset{7}{\bar{U}_j\overline{\rho'f'^2}} + \overset{8}{\overline{u_j'\rho'f'^2}} - \overset{9}{\overline{f'^2}\,\overline{\rho'u_j'}}\Big)$$

$$-\overset{10}{\overline{2\frac{\partial f'}{\partial x_j}\tilde{J}_f}} - \overset{11}{2\bar{\rho}D_f\overline{\frac{\partial f'}{\partial x_j}\frac{\partial f'}{\partial x_j}}} - \overset{12}{2\overline{\rho' D_f\frac{\partial f'}{\partial x_j}\cdot\frac{\partial f'}{\partial x_j}}} - \overset{13}{2\overline{\rho' D_f\frac{\partial f'}{\partial x_i}\frac{\partial\bar{f}}{\partial x_j}}} \qquad 4.45$$

where

$$\hat{J}_f = -\hat{\rho}D_f\frac{\partial\hat{f}}{\partial x_j} \qquad 4.46$$

Now if fluctuating density terms are neglected and defining

$$\overline{f'^2} \equiv g: \quad \text{then}$$

$$\bar{\rho}\bar{U}_j\frac{\partial g}{\partial x_j} = -2\,\bar{\rho}\overline{f'u_j'}\frac{\partial\bar{f}}{\partial x_j} - \frac{\partial}{\partial x_j}\,\bar{\rho}\overline{g'u_j'} - 2\,\overline{\frac{\partial f'J_f}{\partial x_j}}$$

$$-2\,\bar{\rho}D_f\overline{\frac{\partial f'}{\partial x_j}\frac{\partial f'}{\partial x_j}}\Big) \qquad 4.47$$

This equation is simplest of turbulence transport equations and, as Corrison (1952) has pointed out, resembles the turbulence kinetic energy equation except that the pressure fluctuation term is missing from this equation. As in the case of turbulence energy, equation 4.47 expresses the fact that the rate of change of $\overline{f'^2}$ following a mean stream line is equal to the generation rate of scalar fluctuations by gradients in f (term 2) minus the sum of diffusion by turbulent velocity fluctuation u_j' (term 3) and molecular dispersion (term 4), less the dissipation of fluctuations due to molecular diffusion in fine scale motions (term 5). Closure of the equation is also applied along the lines of k-equation in the two equation model, hence $\overline{f'u_j'}$ is represented as

$$-\overline{f'u_j'} = \frac{\mu_t}{\sigma_f} \frac{\partial \bar{f}}{\partial x_j} \qquad 4.48$$

and

$$-\overline{g'u_j'} = \frac{\mu_t}{\sigma_g} \frac{\partial g}{\partial x_j} \qquad 4.49$$

where σ_f and σ_g are exchange coefficients for f and g respectively. One way to approximate for the dissipation term, $2 D_f \overline{\frac{\partial f'}{\partial x_j} \frac{\partial f'}{\partial x_j}} = \varepsilon_f$, is to write a transport equation for it in a similar manner as is done for the dissipation of kinetic energy, ε. Launder (1976) has given the exact form of this equation and has suggested a closure for it.

Alternatively it can be expressed by way of time scale ratio Cg_2 for the decay of scalar and velocity fluctuations as:

$$\frac{\varepsilon_f}{\varepsilon} = Cg_2 \frac{g}{K} \qquad 4.50$$

so that

$$\varepsilon_f = Cg_2 \frac{\varepsilon}{K} g \qquad 4.51$$

Different values have been chosen for this ratio. Spalding (1971a) used 2.0. while Launder (1976) has suggested

that 1.25 will give the best results for buoyancy affected homogenous free shear flows. Hence the modelled from of eq. 4.47 is

$$\bar{\rho}\bar{U}_j \frac{\partial g}{\partial x_j} = \frac{2\mu_t}{\sigma_f}\left(\frac{\partial f}{\partial x_j}\right)^2 + \frac{\partial}{\partial x_j}\frac{\mu_t}{\sigma_g}\frac{\partial g}{\partial x_j} - Cg_2 \frac{\varepsilon}{K} g \qquad 4.52$$

Extra terms due to variable density can also be modelled in eq. 4.45 in the same manner as that modelled for the $\bar{\Phi}$ equation (eq. 4.44). Neglecting the scalar correlations (term 4), the triple correlations (terms 5 and 8), the dissipation due to density fluctuations (term 12), and the fluctuating-density-mixture fraction gradient correlation (term 13) we have:

$$\bar{\rho}\bar{U}_j \frac{\partial g}{\partial x_j} = 2\frac{\mu_t}{\sigma_f}\left(\frac{\partial f}{\partial x_j}\right)^2 + \frac{\mu_t}{\sigma_\rho}\frac{\partial \bar{\rho}}{\partial x_j}\cdot\frac{\partial g}{\partial x_j} + \frac{\partial}{\partial x_j}\left[\frac{\mu_t}{\sigma_g}\frac{\partial g}{\partial x_j}\right.$$

$$\left. - \frac{\mu_t}{\sigma_\rho} g \frac{\partial \bar{\rho}}{\partial x_j}\right] - Cg_2 \frac{\varepsilon}{K} g \qquad 4.53$$

CHAPTER FIVE

5.0 The Combustion Model

5.1 Introduction

The previous Chapter on turbulence modelling was concerned with the determination of the average velocity field only. The object of the present work is to predict a reacting flow, which also requires modelling of the combustion phenomenon. Combustion is a very complex process and hence difficult to model. If we consider the chemical kinetics of the system, the overall reaction from initial reactants to final products normally comprises many steps involving intermediate species and free radicals. It is difficult to incorporate all of the reactions taking place in a computational scheme even for very simple reacting systems, and at the same time avoid the combustion model becoming excessively cumbersome. For example it was established by Dixon-Lewis (1970) that seven principal reactions take place in a fuel rich hydrogen-oxygen-nitrogen laminar flame. The reaction mechanism for practical fuels such as gaseous hydrocarbons and furnace oils is even more complex.

Turbulence makes matters worse, since it influences the rate of mixing of the reactants and so affects the reaction rate and the transport of heat and radicals which determine the initiation of reaction in the unburnt regions of the gas mixture. For engineering purposes, it is the gross features of combustion, such as mean temperature, density and mass fraction of the fuel together with the total heat release, which are especially important. Fortunately these features are not very strongly dependent on the detailed chemistry of reaction and some very simple, and in many circumstances very satisfactory assumptions may be introduced to make the modelling problem tractable. In this chapter these assumptions will be introduced and a model of turbulent combustion applicable to the present problem will be developed.

The transport equation for the mass fraction of a chemical species, Φ_α, has been written for low Mach number flows by Williams (1965), among others as:

$$\frac{\partial \hat{\rho}\hat{\Phi}_\alpha}{\partial t} + \frac{\partial}{\partial x_i}(\hat{\rho}\hat{U}_i\hat{\Phi}_\alpha) = \frac{\partial}{\partial x_i}(\Gamma_\alpha \frac{\partial \hat{\Phi}_\alpha}{\partial x_i}) + \omega_\alpha(\hat{\underline{\Phi}}) \qquad 5.1$$

The last term in the above equation, $\omega_\alpha(\underline{\Phi})$ represents the reaction rate of species Φ_α which is the function of the set $(\Phi_1, \Phi_2 \ldots\ldots \Phi_n)$. There is no universal expression for $\hat{\omega}_\alpha(\underline{\Phi})$, but in some cases the instantaneous reaction rate can be expressed in the global second order Arrhenius form as:

$$\hat{\omega}_\alpha(\underline{\Phi}) = \hat{\rho}\nu_\alpha W_\beta^{-1}\hat{\Phi}_\alpha\hat{\Phi}_\beta \quad A \exp(E/R\hat{T}) \qquad 5.2$$

In the above equation ν_α is the stiochiometric coefficient of species α, W_β is the molecular weight of species β (where β varies from 1 to n), A the frequency factor, E the activation energy for reaction, R the universal gas constant and T is the temperature.

The steady state time-averaged equation for Φ_α can be written as:

$$\frac{\partial}{\partial x_i}(\bar{\rho}\bar{U}_i\bar{\Phi}_\alpha) = \frac{\partial}{\partial x_i}(\Gamma_\alpha \frac{\partial \bar{\Phi}_\alpha}{\partial x_i})$$

$$- \frac{\partial}{\partial x_i}(\overline{\rho u_i' \Phi_\alpha'} + \overline{\rho' u_i' \Phi_\alpha'} + \bar{\Phi}_\alpha \overline{\rho' u_i'} + \bar{u}_i \overline{\rho' \Phi_\alpha'}) + \overline{\omega_\alpha(\underline{\Phi})} \qquad 5.3$$

In equation 5.3 the term $\overline{\omega_\alpha(\underline{\Phi})}$ is the time-averaged reaction rate which, as can be seen from equation 5.2 is highly non-linear. The often-made assumption that

$$\overline{\omega_\alpha(\underline{\Phi})} = \omega_\alpha(\bar{\underline{\Phi}})$$

is clearly incorrect,

Indeed in turbulent flows the time-averaged reaction rate may even be independent of the chemical kinetic rate given by equation 5.2. This apparent anomaly can be explained in the following manner. If the reactants are introduced in a control volume where the temperature is

high enough for the reaction to take place and products are withdrawn in such a manner that the residence time is t_r. Then, if the reaction time t_k is much smaller than t_r, the time averaged reaction rate will only depend on t_r. This was suggested by Spalding (1971) for premixed flames in his eddy break up model (EBU).

Borghi (1974) obtained an expression for $\overline{\omega_\alpha(\underline{\Phi})}$ for carbon monoxide by time averaging the experimentally obtained expression for its instantaneous reaction rate, equation 5.4 below, using series expansions of exp(x) and $(1+x)^\gamma$, $x = \frac{T'}{\bar{T}}$

$$\omega_\alpha(\hat{\alpha},\beta) = \frac{-K\bar{p}^2\hat{\Phi}_\alpha\hat{\Phi}_\beta\hat{T}^{-3/2}\exp(-E/R\hat{T})}{W_\alpha W_\beta R^2} \qquad 5.4$$

where α and β are carbon monoxide and oxygen respectively. The time-averaged expression becomes

$$\overline{\omega_\alpha(\Phi_\alpha,\Phi_\beta)} = \left[\frac{-K\bar{p}^2\bar{\Phi}_\alpha\bar{\Phi}_\beta\bar{T}^{-3/2}\exp(-E/R\bar{T})}{W_\alpha W_\beta R^2}\right]$$

$$\left\{1 + \frac{\overline{\Phi'_\alpha\Phi'_\beta}}{\bar{\Phi}_\alpha\bar{\Phi}_\beta} + \frac{p_2+Q_2+p_1Q_1}{\bar{T}^2}\cdot\overline{T'^2} + (p_1+Q_1)\left(\frac{\overline{T'\Phi'_\alpha}}{\bar{T}\bar{\Phi}_\alpha} + \frac{\overline{T'\Phi'_\beta}}{\bar{T}\bar{\Phi}_\beta}\right)\right.$$

$$\left. + p_1\frac{\overline{T'\Phi'_\alpha\Phi'_\beta}}{\bar{T}\,\bar{\Phi}_\alpha\,\bar{\Phi}_\beta} + p_2\left(\frac{\overline{T'^2\Phi'_\alpha}}{\bar{T}^2\,\bar{\Phi}_\alpha} + \frac{\overline{T'^2\Phi'_\beta}}{\bar{T}^2\,\bar{\Phi}_\beta}\right) - - - - -\right\} \qquad 5.5$$

where p_n are polynomials of degree n in $(E/R\bar{T})$, n varying from 1 to ∞ and Q_n is a series in α and n (p_n and Q_n are defined in nomenclature). Expressions of similar nature can be obtained for the reaction rates of other species as well.

It can be seen that the above expression for $\overline{\omega_\alpha(\Phi_\alpha,\Phi_\beta)}$ is quite complicated and involves a series expansion of the exponential. If equation 5.5 is used for computations this series has to be truncated. This truncation could lead to large errors due to neglect of the exponential terms. Moreover even the truncated series contains higher order correlations

which must be modelled or obtained by solving their transport equation. Expression 5.5 is also not rigorous as it is derived from equation 5.4 which is obtained by 'curve fitting' to experimental results. Owing to the above mentioned difficulties involved in deriving an expression for time-mean reaction rate in terms of instantaneous reaction rate it is much simpler to obtain expressions for $\overline{\omega_\alpha(\underline{\Phi})}$ which are independent of $\omega_\alpha(\hat{\underline{\Phi}})$. Fortunately in the case of diffusion flames it is possible as will be seen later in this chapter.

In the following sections methods of modelling turbulent combustion are discussed. In section 5.2 some methods of calculating turbulent flame speed in terms of laminar flame speed are given. The flame speed gives the reaction rate in terms of the volume of reactants consumed per unit flame area per unit time.

In section 5.3 a physical picture of the diffusion flame is presented. It is shown that the flame consists of randomly moving eddies of oxidant, fuel and products, and reaction takes place where fuel and oxidant come together at the right temperature.

In section 5.4 the simple chemically reacting system is described. The assumption that this system applies to the present flame simplifies the physical picture. The instantaneous values of the species mass fraction, temperature density, etc. are then calculated.

In section 5.5 models to simulate the fluctuations in the mixture fraction are described and one is selected for the present predictions. In section 5.6 the model is used to derive expressions for the mean values of the species mass fractions and other thermodynamic quantities. Concluding remarks appear in section 5.7.

5.2 Some Historical Combustion Studies

Early work on modelling of turbulent combustion was restricted to finding an expression for the turbulent flame speed μ_t as a function

of the laminar flame speed u_ℓ and/or the fluctuating velocity u'. The work proceeded on these lines because laminar flame speed represented the rate of reaction of the combustible mixture for laminar flow, so it was tempting to imagine a turbulent flame speed depending on u_ℓ and u'. The analogy is similar to one commonly made between 'turbulent' and laminar viscosity, though the success achieved by the use of the turbulent viscosity concept in the calculation of the hydrodynamics is far greater than that of the turbulent flame speed in the analysis of reacting flows. The work done following the above approach is considerable and while the present study does not draw from it directly, it is reviewed here since it throws light on some interesting aspects of turbulent combustion. The experimental work performed to validate the flame speed models is also useful since it reveals apparently conflicting features of turbulent combustion in different situations.

Damkohler (1940) introduced a model based on the laminar flame speed called the 'wrinkled laminar flame model'. He assumed that the principal effect of turbulence was to increase the area of the laminar flame Fig. 5.1. He postulated that if the macroscale 'ℓ' of the turbulence, that is the average size of low frequency eddies, was much greater than the laminar flame thickness δ_ℓ than the sole effect of turbulence would be to increase the flame surface area. This increase in area can also be associated with the fluctuating velocity, u', as ℓ/u' gives the time scale of the large eddies.

There were two assumptions implicit in the wrinkled lam nar flame model. First, that the flame front propogated, relative to the unburnt gas, at the one dimensional laminar burning velocity. Second, that the laminar flame was stable to large velocity perturbations over a wide range of frequency.

Shelkien (1943) put forward a model in which the ratio of the area of turbulent flame A_T, to the laminar flame A_ℓ could be expressed as

$$A_t/A_\ell = u_t/u_\ell = \sqrt{1 + (u'/u_\ell)^2} \qquad 5.6$$

The above expression leads to the result that for large u', the turbulent flame speed is independent of the laminar flame speed.

The development of wrinkled laminar flame model, following the proposals of Damkholer and Shelkien, have taken place in a rather irregular manner. A model for turbulent flame speed was proposed, then some experiments showed that the model was not accurate for a certain flow situation, and the model was modified to take into account the experimental observation.

For example, experiments of Williams et al (1948) on confined flames suggested that the turbulence intensity of the approach flow had virtually no effect on u_t. Experiments carried out by Scurlock and Grover (1953) showed that the turbulent flame speed was greater in confined than in open flames.

Eikhoff (1973) found that there was a sharp drop in turbulence intensity in the combustion zone. These experiments showed that u_t depended more on flow configuration than on the chemistry of reactants. The wrinkled laminar flame model was progressively modified by various authors to predict u_t under different conditions. A review of such works is provided by Andrew et al (1975).

The failure to find a 'universal' expression for the turbulent flame speed showed that the analogy with the laminar flame speed was imperfect. One of the reasons being that the laminar flame speed is a chemical kinetic property, which is independent of flow field and mechanism of flame stabilization. On the other hand experiment has shown, as discussed above, that the turbulent flame speed is strongly influenced by several characteristics of the flow field in which the flame is stabilized. The assumption of the wrinkled laminar flame model, that the flame is stable to very large strain rates which occur

in small turbulent eddies is also incorrect for the wrinkled laminar flame can only remain a coherent structure if the scale of eddies is larger than the thickness of the laminar flame, δ_ℓ. If eddy sizes smaller than δ_ℓ exist in the flow, then these eddies can cause the break-up of the flame structure. The turbulence structure consists of eddies of various sizes Tennekes and Lumley (1972). The largest eddies have length scale comparable to the width of the flow and the smallest are of size of Kolmogorov length scale, η. Andrews et al (1975) have shown that the typical value of η for $R_\lambda \simeq 100$ (R_λ is the Reynolds number based on Taylor microscale) is about 0.1 which is one tenth of laminar flame thickness. Hence if the turbulent Reynolds number is high, which it is in most engineering applications, laminar flame structure is unlikely.

Due to the above mentioned uncertainties involved, modelling of turbulent combustion in terms of the turbulent flame speed was not persued further. Moreover in the context of the present work expressions for time-averaged reaction rate $\overline{\omega_\alpha(\underline{\Phi})}$ are more suitable than turbulent flame speed. Because $\overline{\omega_\alpha(\underline{\Phi})}$ can be used as a direct input to equation 5.3, where as u_t will have to be expressed as a function of $\overline{\omega_\alpha(\underline{\Phi})}$. It was possible to devise a method to obtain the time averaged reaction rate in terms of the turbulent flame velocity, but it was not attempted for the present study. It was thought that the method should be validated on simple systems first, and to the best of author's knowledge this had not been done.

5.3 Physical Picture of a Diffusion Flame

From the discussions in the previous two sections, following conclusions can be drawn. First, mathematical formulation of time-averaged reaction rate from the instantaneous reaction rate of a fuel-oxidant system leads to expressions that are complicated and difficult

to solve. Second, the models based on turbulent flame speed, apart from not being universal, cannot be incorporated easily in the present computational scheme. The need therefore is for a simple expression of $\overline{\omega_\alpha\ (\underline{\Phi})}$ or alternatively a system of equations in which $\overline{\omega_\alpha\ (\underline{\Phi})}$ does not appear explicitly. To arrive at such a formulation, the physical features of turbulent flow have to be looked into in more detail.

Turbulence is a complex phenomenon which is difficult to define precisely. The best that can be done is to describe its salient features. The turbulent motion comprises of eddies of various sizes, the largest restricted only by the size of the flow field and the smallest determined by the viscous forces, Bradshaw (1971). Turbulence energy is generated by the action of the mean velocity gradient on large scale eddies which is then transferred to smaller scales by the mechanism of vortex stretching. The stretching of a vortex in one direction gives rise to an increase in its kinetic energy of rotation as a consequence of the conservation of angular momentum. Thus, perpendicular to the axis of stretching, the turbulent length scales are reduced and the velocity components increased. These components increase small scale stretching along their own axis. In this way ever increasing vorticity, and velocity gradients are produced. Finally the velocity gradients become so high that viscosity dissipates the energy transferring it to heat. Through this cascade of turbulent energy, vortex stretching eradicates the original anisotropy of the large scale eddies and creates isotropy amongst the small scale eddies, Bradshaw (1971).

The random motion of the eddies increases the diffusivity of the turbulent flow. This can be explained by considering a mixing layer formed by two fluids A and B, fig. 5.2a. Turbulence will cause eddies to be formed in these fluids. Because of the random motion of the eddies, eddy A_1 will cross into fluid B. This eddy will undergo stretching and as its scale is reduced the concentration gradient will increase and

consequently molecular diffusion between A_1 and fluid B will increase. The diffusion process will, however, decrease the concentration gradient which will oppose the increase in gradient due to vortex stretching. In other words turbulence will increase the diffusion flux whereas diffusion itself tends to decrease it.

Now consider a control volume within the turbulent fluid Fig. 5.2b (Assume that no reaction takes place between fluids A and B). This control volume will contain eddies of various sizes straining against each other. The concentration of fluid A or B in this control volume will depend on the number of eddies of fluid A or B respectively. Since molecular diffusion is also taking place, there might be some eddies which contain fluid A and B mixed at molecular level (which can be called fluid AB). The eddies move in and out of the control volume randomly. Hence the number of eddies containing fluid A will vary with time which will give rise to fluctuations in its mass fraction m_A. The fluid properties associated with fluid A such as temperature will also fluctuate (assuming the temperature of stream A is different from that of stream B).

The mass fraction m_A at any time in the control volume can be divided into its mean and fluctuating parts ($\bar{m}_A, m_A'$). Similarly m_B and temperature will fluctuate between $\bar{m}_B \pm m_B'$ and $\bar{T} \pm T'$ respectively. The magnitude of the fluctuations of any property will depend on its mean value and the kinetic energy of turbulence, which can be represented by u'.

The case of turbulent diffusion flame can be studied by considering fluid A to be fuel and fluid B to be oxidant. If we now look at a control volume, the picture is much more complicated. The eddies that can be found inside the control volume consist of pure fuel, pure oxidant, products or a combination of any two of these three

(similar to fluid 'AB' in the inert mixing case). Combustion will take place when two eddies of such composition come together that diffusion of mass and/or heat can initiate reaction. For example two eddies, one containing products and fuel and the other containing oxidant and products can come together. Since both are hot, reaction will occur when oxidant and fuel diffuse into each other. On the other hand if one eddy contains premixed fuel and oxidant and the other only hot products reaction will also occur when hot products diffuse into the premixed eddy.

The magnitude of fluctuations of fuel and oxidant will be different from that of fluid A and B (inert mixing). The difference is due to the appearance of products and disappearance of fuel and oxidant because of reaction. The rate at which reaction occurs is open to speculation. The wrinkled laminar flame model implies that reaction propagates at the laminar flame speed. Recently Paauw and Bakker (1976) have suggested that the reaction zone can be likened to a well-stirred reactor. Infinite reaction rates have been assumed by several workers, Naguib (1975) among many.

In summary, the structure of a turbulent diffusion flame is made up of eddies of varying sizes and composition which are moving randomly. Combustion takes place only between those eddies whose temperature and composition is such that reaction can be sustained. It should be noted that the dissipation of kinetic energy of turbulence takes place in all eddies where as reaction occurs only in some of them. The ratio of the rate of destruction of fuel (due to reaction) to the dissipation rate will depend on the flow and cannot be constant for all flow configurations. Hence any expression that relates the reaction rate to the dissipation of energy, Ris (1976), must take the above fact into account. Failure to do so would result in the 'constant' associated with the reaction rate expression being different for different flows.

5.4 Simple Chemically Reacting System

The physical picture of a diffusion flame, as seen in the previous section, is complicated. To keep the modelling problem tractable, it is clear that some simplifying assumptions are needed. Many complexities of the chemical kinetics can be avoided by introducing the Simple Chemically Reacting System (SCRS), Spalding (1971c). This system was chosen for the present study and relations for instantaneous enthalpy, temperature, density, mixture composition and scalar correlations were derived with its help.

The central feature of the SCRS is the assumption that fuel and oxidant combine instantaneously in stiochiometric proportions to form products in a one step irreversible reaction:

$$1 \text{ Kg fuel} + S \text{ Kg oxidant} \rightarrow (1+S) \text{ Kg of Products} \qquad 5.7$$

Equation 5.7 implies that all intermediate reactions are ignored. The influence of intermediate species on the gross features of combustion should be insignificant. Another assumption of the SCRS is that the exchange coefficients for enthalpy and species are constant and equal.

It is also assumed that the flow is in chemical equilibrium. (7)

That the present flow is so and can be found by calculating its Damkohler number. The Damkohler number is the ratio of the time scale of reaction to the Kolmogorov time scale ($1/\gamma$) which is the smallest time scale of turbulence. If the reaction time is much less than the time required by the Kolmogorov eddy to break down the flow can be assumed to be in equilibrium.

We have:

$$\text{Damkohler number} = K/\gamma$$

where

$$\gamma = (\varepsilon/\nu)^{1/2}$$

ν = kinematic viscosity

ε = dissipation rate of turbulence energy

$$= \nu/2 \left[\overline{\frac{\partial u_i'}{\partial x_j} + \frac{\partial u_j'}{\partial x_i}}\right]^2$$

K = reaction rate constant

The minimum Damkohler number for the present flow was estimated using a maximum predicted value of $\varepsilon = 1.38 \times 10^5$ in an inert jet of Re = 50,000 (The value of ε for the present flow would be somewhat different but the above value was considered sufficiently accurate for initial estimates). The expressions for reaction rate constant are not universal. An expression for the reaction rate constant, K, given by Khalil et al (1975) was used as it was used by them in a similar combustion situation.

Hence

$$\varepsilon = 1.38 \times 10^5 \quad M^2/sec^3$$

$$K = \rho \, 10^{10}_e \, (-\frac{1.84 \times 10^4}{T}) \quad 1/sec$$

$$\nu = 1.23 \times 10^{-5} \quad m^2/sec$$

$$T = 2000^{\circ}K$$

This gave Damkohler number $\simeq 6$. So the flow was assumed to be in chemical equilibrium. The above assumption together with one step reaction dictatesthat oxygen and fuel cannot co-exist. The preceding statement means that in a control volume inside a turbulent diffusion flame eddies containing either products and or oxidant or products and/or fuel only are present. It should be noted however that this assumption may not be entirely realistic in some regions of the flame. For example in the initial region of the jet, due to very high shearing rates, the time scale of turbulence may be much smaller than at the centreline of the jet in the fully developed region. Another possibility is that

since the surface of a turbulent flame is broken and discontinuous some oxidant can be entrained through the 'gates' formed in the surface which has not been heated sufficiently and therefore does not initiate reaction when it mixes with the fuel.

5.4.1 Calculation of Instantaneous Thermodynamic Quantities

If a quantity Φ is defined such as

$$\hat{\Phi} = S\hat{m}_{fu} - \hat{m}_{ox}$$

where m_{fu} and m_{ox} are mass fractions of fuel and oxidant respectively and S is the stoichiometric ratio. Then the transport equation for Φ can be derived by multiplying the mass fraction of fuel equation by S and subtracting the m_{ox} equation from it. Equations for the mass fraction of fuel and oxidant can be written from equation 5.1. It can be seen that the reaction rate term for Φ is:

$$\omega_{\Phi} = S\omega_{fu} - \omega_{ox} = 0 \quad \text{(SCRS)}$$

Hence Φ is a passive scalar. The time averaged differential equation for Φ will be the same as equation 5.3 with $\overline{\omega_{\alpha}(\underline{\Phi})} = 0$
For computational purposes it is convenient to define a mixture fraction:

$$\hat{f} \equiv \frac{\hat{\Phi} - \Phi_O}{\Phi_1 - \Phi_O} \qquad 5.8$$

where Φ_1 and Φ_O are respectively values of Φ in the jet pipe and surrounding air for a free diffusion flame (or father or mother streams as

Spalding called them generally). The transport equations for $\bar{f}$ will be the same as equation for Φ and can be written in cylindrical co-ordinates as:

$$\frac{1}{r}\frac{\partial}{\partial r}(r\bar{\rho}\bar{V}_r\bar{f}) + \frac{\partial}{r\partial\theta}(\bar{\rho}\bar{V}_\theta\bar{f}) + \frac{\partial}{\partial z}(\bar{\rho}\bar{V}_z\bar{f}) = -\frac{\partial}{\partial r}(\bar{\rho}\overline{V_r'f'})$$

$$-\frac{\partial}{r\partial\theta}(\bar{\rho}\overline{V_\theta'f'}) + \frac{\partial}{\partial z}(\bar{\rho}\overline{V_z'f'}) + \frac{\overline{\rho V'f'}}{r} + \rho D_f\frac{1}{r}\frac{\partial\bar{f}}{\partial r} + \frac{\partial}{r\partial\theta}D_f\frac{\partial\bar{f}}{r\partial\theta}$$

$$+\frac{\partial}{\partial r}D_f\frac{\partial\bar{f}}{\partial r} + \frac{\partial}{\partial z}D_f\frac{\partial\bar{f}}{\partial z} \qquad 5.9$$

It should be noted that all passive scalars are governed by the same partial differential equation, if the assumption of equal exchange coefficients is applied. Hence all the passive scalars can be linearly related if their boundary conditions are similar.

Fig. 5.3 gives a diagram of the variation of composition (and enthalpy which is also a passive scalar for this system as shown later in this section) with the mixture fraction. Assuming chemical equilibrium the instantaneous values of m_{fu} and m_{ox} can be found from the following relations.

$$0 \leq \hat{f} \leq f_{st} \qquad \hat{m}_{fu} = 0, \quad \hat{m}_{ox} = m_{ox,o}\left(\frac{f_{st}-\hat{f}}{f_{st}}\right) \qquad 5.10$$

$$f_{st} \leq \hat{f} \leq 1 \qquad \hat{m}_{ox} = 0, \quad \hat{m}_{fu} = m_{fu,1}\left(\frac{\hat{f}-f_{st}}{1-f_{st}}\right) \qquad 5.11$$

where f_{st} is the stoichiometric value of mixture fraction

$$f_{st} = \frac{m_{ox,o}}{S m_{fu,1} + m_{ox,o}} \qquad 5.12$$

The instantaneous mass fraction of products can be found from:

$$0 \leq \hat{f} \leq f_{st} \quad \hat{m}_{pr} = (m_{ox,o} + (m_{fu,1} - m_{ox,o})\hat{f}) - m_{ox,o}\left(\frac{f_{st}-\hat{f}}{f_{st}}\right) \qquad 5.13$$

$$f_{st} \leq \hat{f} \leq 1 \quad \hat{m}_{pr} = (m_{ox,o} + (m_{fu,1} - m_{ox,o})\hat{f}) - m_{fu,1}\left(\frac{\hat{f}-f_{st}}{1-f_{st}}\right) \qquad 5.14$$

A chemically reacting system may contain inerts. The transport equations for their mass fractions are also the same as equation 5.9. Hence the mass fraction of J^{th} inert in the system $m_{in,j}$ can be deduced from equation 5.8 where $\hat{m}_{in,j} = \Phi$.

$$\hat{m}_{in,j} = m_{in,jo} + (m_{in,j1} - m_{in,jo})\,\hat{f} \qquad 5.15$$

Applying the assumption of the SCRS of equality of exchange co-efficients for mass, heat and momentum the energy equation can be written as:

$$\frac{\partial}{\partial x_j}(\hat{\rho}\hat{U}_j\,\hat{h}) = \frac{\partial}{\partial x_j}\left(\Gamma_h \frac{\partial \hat{h}}{\partial x_j}\right) + S_h \qquad 5.16$$

where S_h = Radiation + Kinetic heating + Shear work 5.17

and

$$\hat{h} = \hat{m}_{fu}H + \sum_j \int_{T_{ref}}^{T} m_j cp_j \, dT + 1/2\,\hat{U}_i\hat{U}_i + h_{ref} \qquad 5.18$$

where H = heat of reaction of fuel.

In the experiment which supports the present work, the radiation loss was small. Since the Mach number of the flow was very low kinetic heating and shear work could also be neglected. Hence h also becomes a passive scalar and it can be found from equation 5.8 by putting $h = \Phi$.

or $$\hat{h} = h_o + (h_1 - h_o)\hat{f} \qquad 5.19$$

For the present flow the kinetic heating term $\frac{1}{2}\hat{U}_i\hat{U}_i$ can be neglected, also

for convenience the reference temperature is taken as absolute zero where h_{ref} is zero, equation 5.18 can be written as:

$$\hat{h} = \hat{m}_{fu} H + \int_{O}^{T} \sum_{j} \hat{m}_{j} \hat{C}_{Pj} \, dT \qquad 5.20$$

Temperature can be easily deduced from eqn. 5.20 if specific heat does not vary with temperature and composition in that case

$$\hat{h} = \hat{m}_{fu} H + \bar{C}_{P} \hat{T} \qquad 5.21$$

or

$$\hat{T} = \frac{\hat{h} - \hat{m}_{fu} H}{\bar{C}_{P}} \qquad 5.22$$

However, C_P is not constant and varies with temperature and composition. The expression for the variable specific heat can be obtained from its experimental values to which higher order polynomials have been fitted, Tribus (1961)

$$\hat{C}_{P,j} = F_{j}(T) \qquad 5.23$$

so

$$\hat{h} = \hat{m}_{fu} H + \int_{O}^{T} \sum_{j} \hat{m}_{j} F_{j}(T) \, dT \qquad 5.24$$

It is evident that calculation of temperature from the above equation is complicated and it is convenient to define an average specific heat:

$$\bar{C}_{P,j} \equiv \frac{\int_{O}^{T} C_{P,j} \, dT}{T} \qquad 5.25$$

so that

$$\hat{h} = \hat{m}_{fu} H + \sum_{j} \hat{m}_{j} \bar{C}_{P,j} \, T \qquad 5.26$$

and

$$\hat{T} = \frac{\hat{h} - \hat{m}_{fu} H}{\sum_{j} \hat{m}_{j} \bar{C}_{P,j}} \qquad 5.27$$

Since h, m_{fu} and m_j (which includes m_{fu}, m_{ox}, m_{Pr} & $\sum_j m_{in,j}$) have been expressed as functions of f, temperature is also a function of f.

The density of the mixture may be found from the equation of state which can be written as

$$\hat{\rho} = \frac{\hat{P}}{R\hat{T} \sum_j \frac{\hat{m}_j}{W_j}} \qquad 5.28$$

where P is the pressure, R is the universal gas constant and W_j is the molecular weight of species j. Equation 5.28 reveals that density is also a function of the mixture fraction.

5.5 Modelling for Fluctuations in the Mixture Fraction

In the previous section it was seen that all the thermodynamic quantities can be related to the instantaneous value of the mixture fraction. Since the flow is turbulent and as discussed in section 5.4, m_{fu} and m_{ox} fluctuate with time. The mixture fraction f is a function of m_{fu} and m_{ox}, hence its value also varies with time. The mean values of thermodynamic quantities and species mass fractions that are non linear functions of f cannot therefore be directly related to the mean values of f. This problem can be solved if the temporal behaviour of f is known or can be modelled.

In the following sections various models of simulating the fluctuations in the mixture fraction will be examined and one will be selected to predict the present flow.

5.5.1 Simple Model for the Fluctuations in the Mixture Fraction

The simplest way to 'account' for the fluctuations in the mixture fraction is to ignore them, Pun and Spalding (1967). Hence the instantaneous value of f will be equal to its mean value. The mean value of f can be

found from equation 5,9 and equations 5,10 - 5,28 can be used to evaluate the mass fractions of species and other combustion variables.

Gosman and Lockwood (1973), among others, applied the above model to predict the flow in a large gas-fired furnace. Since the fluctuations in the mixture fraction were neglected, the model was unable to predict the experimentally observed phenomenon of 'unmixedness'. This phenomenon suggests that on time-averaged basis fuel and oxygen are co-present in a turbulent diffusion flame. Also the temperature predicted was its fully reacted value, whereas in reality it would lie between the fully reacted value and that value which would prevail when no reaction occurs. Consequently the predicted temperature profiles exhibited unrealistic 'peaks'.

5.5.2 Periodic Model for the Fluctuations in the Mixture Fraction

The work done by Gosman and Lockwood showed that in order to get realistic predictions of a turbulent diffusion flame, fluctuations in the mixture fraction have to be included in the model.

A periodic form for the fluctuations in the mixture fraction was chosen by Spalding (1971b). He assumed that the instantaneous concentrations, as characterized by the mixture fraction, exhibit minimum or maximum values during finite time intervals and pass zero time at all intermediate values. The form of fluctuations is sketched in fig. 5.4 . The above assumption together with the mean value of the mixture fraction and $\overline{f'^2}$ which could be obtained from equation 4.52 enabled the mean values of species mass fractions and other thermodynamic variables to be calculated. This model for the fluctuations, although a crude one, served the purpose of highlighting the influence of concentration fluctuations on the turbulent flame. The 'flame brush' could be predicted and the unrealistic peaks in the temperature profiles were smoothed out.

The aboye model was physically unrealistic as the concentration would not, in reality, change instantaneously between maximum and minimum values. Naguib (1975), among others have examined a triangular wave form for the fluctuations, fig. 5.5 , in which the concentrations vary linearly from minimum to maximum values. However, the experimental evidence as discussed in the next section is against any periodic form of fluctuations. It strongly suggests that they are random in nature. The periodic model for the fluctuations has therefore not been considered.

5.5.3 Models Based on Random Fluctuations

In order to choose a model for the concentration fluctuations which is physically realistic, one has to look into the experimental evidence in this regard. Unfortunately not many reliable measurements have been made in reacting flows. Odidi (1974) and Ballantyne et al (1976) have measured the probability density function (PDF) of temperature in free-jet diffusion flames. The Reynolds' numbers of the flames were rather low and it is doubtful whether they were fully turbulent. Nevertheless these experiments showed that the fluctuion were random in nature and that the probability density function was approximately Gaussian near the axis and near the burner. In regions further from the inner part of the flame a transition to bi-nodal shape occured. The transition signified the occurence of quiesient periods in the fluctuating temperature, due to the intermittent nature of the flame in this region.

Work done in non reacting flows also confirms the above findings. Tutu and Chevray (1973) measured the probability density function of temperature in a slightly heated round jet mixing with still air. The measurements are shown in Fig. 5.6 where the Gaussian PDF is also drawn. It can be seen that near the centre of the jet the density function can be approximated as a Gaussian.

Several workers have tried to simulate the concentration fluctuations by assuming different forms for the probability density function. This approach, as seen above, is quite near to physical reality. Although it is possible to set up and model a balance equation for the PDF Pope (1976), specifying it empirically is justified on two grounds: (i) the resulting formulation for the mean values of thermodynamic variables and species mass fractions is relatively simple. (ii) It is possible to obtain direct measurements of the PDF in flames, hence the assumed form of the PDF can be approximated to the measured one.

The minimum number of variables should be used to prescribe the form of the PDF. This is advantageous because more parameters mean more equations to be solved for further correlations which means more modelling assumptions to close the equation set. Moreover computer time and storage also increases with the number of equations being solved which soon renders the computations uneconomical. Most of the studies carried out until now have used two parameters for the specificatgion of the PDF.

Hawthorne et al (1948) in their pioneer study of the turbulent diffusion flame assumed a Gaussian PDF for the nozzle fluid concentration bounded by the limits $-\infty$ and $+\infty$. The assumption of normal distribution is borne out by experiments in the centre of free shear flows, though it does not hold true near the edge. Moreover the limits are not realistic since physically f can vary from 0 - 1 only. Richardson et al (1953) proposed a beta function PDF for the concentration fluctuation between limits of 0 and 1, but did not take into account the time spent at these limits. Bilger and Kent (1972) have employed a Gaussian PDF for atomic hydrogen concentrations arbitrarily truncated at -2 and +2 to predict a hydrogen diffusion flame. Recently Naguib (1975) has proposed a clipped Gaussian PDF. This PDF is Gaussian between 0 and 1 and is bounded by dirac-delta functions at $f = 0$ and $f = 1$ fig. 5.7.

The clipped Gaussian PDF is chosen to obtain the present predictions because the limits on the PDF are physically realistic and because its shape conforms with the experimental findings for most parts of a jet. The PDF is economical since it requires only two parameters for its specification. Also Naguib was able to predict a vertical diffusion flame with reasonable success using this model and there is no reason to believe that it will not give an equally realistic representation of the PDF of the present horizontal flame.

5.6 Clipped Gaussian distribution function

The equation for the Clipped Gaussian distribution function is expressed as:

$$P(f) = \frac{1}{\bar{\sigma}\sqrt{2\pi}} e^{-1/2\left(\frac{f-\bar{\mu}}{\bar{\sigma}}\right)} \left[U(f) - U(f-1) \right]$$

$$+ A\delta(0) + B\delta(1) \qquad 5.29$$

In the above equation $\bar{\mu}$ is the value of f for maximum probability, σ is the variance, U(f) is heaviside step function and $\delta(f)$ is the dirac delta function and

$$A \equiv \int_{-\infty}^{0} P_0(f)\, df \qquad 5.30$$

$$B \equiv \int_{1}^{\infty} P_1(f)\, df \qquad 5.31$$

Taking first and second moments about $f = 0$ and $f = \bar{f}$ respectively we obtain.

$$\bar{f} = \int_{-\infty}^{\infty} \hat{f} P(f)\, df \qquad 5.32$$

$$\bar{g} = \int_{-\infty}^{\infty} (\hat{f}-\bar{f})^2 P(f)\, df \qquad 5.33$$

In the equation written below the following abbreviations have been used

$$Z = \left(\frac{f-\bar{\mu}}{\bar{\sigma}}\right), \quad Z_{st} = \frac{f_{st}-\bar{\mu}}{\bar{\sigma}}, \quad Z_O = -\frac{\bar{\mu}}{\bar{\sigma}} \quad \text{and}$$

$$Z_1 = \left(\frac{1-\bar{\mu}}{\bar{\sigma}}\right) \;\&\; P(Z) = \frac{1}{\sqrt{2\pi}} \int_{-\infty}^{Z} e^{-Z^2/2}\, dz$$

Subsituting equation 5.29 in 5.32 and 5.33 and integrating we have

$$\bar{f} = 1 + (\bar{\mu} - 1)\, P(Z_1) - \bar{\mu} P(Z_O) + \frac{\sigma}{\sqrt{2\pi}} \left(e^{-1/2\, Z_O^2} - e^{-1/2\, Z_1^2}\right) \qquad 5.34$$

$$\bar{g} = 1 + (\bar{\sigma}^2 + \bar{\mu}^2 - 1)\, P(Z_1) - (\bar{\sigma}^2 + \bar{\mu}^2)\, P(Z_O)$$

$$+ \frac{\bar{\sigma}}{\sqrt{2\pi}} \left(Z_O e^{-1/2\, Z_O^2} - Z_1 e^{-1/2\, Z_1^2}\right) + \frac{2\bar{\sigma}\bar{\mu}}{\sqrt{2\pi}} \left[e^{-1/2\, Z_O^2} - e^{-1/2\, Z_1^2} \right] - \bar{f}^2 \qquad 5.35$$

Since $\bar{f}$ and $\bar{g}$ are known from the solution of their transport equations, $\bar{\mu}$ and $\bar{\sigma}$ can be obtained from the simultaneous solution of equation 5.34 and 5.35.

Since it is not possible to solve for these equations analytically a numerical solution procedure was adopted. It consisted of generating a table of values of $\bar{f}$ and $\bar{g}$ for given values of $\bar{\mu}$ and $\bar{\sigma}$. This table was then inverted to give values of $\bar{\mu}$ and $\bar{\sigma}$ against $\bar{f}$ & $\bar{g}$.

The table was searched for values of $\bar{\mu}$ & $\bar{\sigma}$ with given values of $\bar{f}$ and $\bar{g}$ obtained from the solution of their transport equations. The values $\bar{\sigma}$ and $\bar{\mu}$ at a point in the flow defined the Pdf at that point. Knowing P(f) the Pdf of any dependent variable $\Phi(f)$ can be obtained from

$$P\left[\Phi\ (f)\right] = P(f)\, \frac{df}{d\Phi} \qquad 5.36$$

and knowing $P[\Phi(f)]$ moments of the variable Φ can be obtained from relations similar to 5.32 and 5.33.

Hence;

$$\overline{\Phi} = \int_{-\infty}^{+\infty} \Phi(f) \, P\left[\Phi(f)\right] d\Phi \qquad 5.37$$

Using equation 5.36

$$\overline{\Phi} = \int_{-\infty}^{+\infty} \Phi(f) \, P(f) . \, df \qquad 5.38$$

and substituting for P(f)

$$\overline{\Phi} = \left[\frac{1}{\overline{\sigma}\sqrt{2\pi}} \int_{0}^{1} \varphi(f) . \, e^{-1/2 \left(\frac{f-\overline{\mu}}{\overline{\sigma}}\right)^2} . \, df\right] + A\Phi(0) + B\Phi(1) \qquad 5.39$$

Higher moments of Φ can be similarly calculated.

5.6.1 Calculation of Thermodynamic Quantities

The instantaneous values of the thermodynamic quantities were derived in section 5.4, their mean values can now be obtained using equation 5.39.

(a) Oxygen Concentration

Using equations 5.10 and 5.39 we have

$$\overline{m_{ox}} = Am_{ox,o} + \frac{m_{ox,o}}{\overline{\sigma}\sqrt{2\pi}} \int_{o}^{f_{st}} \frac{f_{st} - \hat{f}}{f_{st}} \, e^{-1/2 \, z^2} . df.$$

$$= Am_{ox,o} + \frac{m_{ox,o}}{\overline{\sigma}\sqrt{2\pi}} \left[\int_{o}^{f_{st}} e^{-1/2 \, z^2} . df - \int_{o}^{f_{st}} \frac{\hat{f}}{f_{st}} e^{-1/2 \, z^2} . df\right]$$

$$\overline{m_{ox}} = m_{ox,o} \left[\left(1 - \frac{\overline{\mu}}{f_{st}}\right) P(Z_{st}) + \frac{\overline{\mu}}{f_{st}} P(Z_o) - \frac{\overline{\sigma}}{f_{st}} \left(e^{-1/2 \, z_o^2} - e^{-1/2 \, z_{st}^2}\right)\right] \qquad 5.40$$

(b) Fuel Concentration

Using equations 5.11 and 5.39 we have

$$\bar{m}_{fu} = Bm_{fu,1} + \frac{m_{fu,1}}{\bar{\sigma}\sqrt{2\pi}} \int_{f_{st}}^{1} \frac{\hat{f}-f_{st}}{1-f_{st}} \cdot e^{-1/2\ z^2} \cdot df \qquad 5.41$$

$$= Bm_{fu,1} + \frac{m_{fu,1}}{\bar{\sigma}\sqrt{2\pi}} \left\{ \int_{f_{st}}^{1} \frac{\hat{f}}{1-f_{st}} \cdot e^{-1/2\ z^2} \cdot df - \int_{f_{st}}^{1} \frac{f_{st}}{1-f_{st}} e^{-1/2\ z^2} \cdot df \right. \qquad 5.42$$

$$= m_{fu,1} + \left[Sm_{ox,o}\left(\frac{\bar{\mu}}{f_{st}} - 1\right) - m_{fu,1}\right] P(z_1)$$

$$+ Sm_{ox,o}\left[1 - \frac{\bar{\mu}}{f_{st}}\right] P(Z_{st}) + \frac{\bar{\sigma}}{Sf_{st}\sqrt{2\pi}}\left(e^{-1/2\ Z_{st}^2} - e^{-1/2\ z_1^2}\right) \qquad 5.43$$

The J^{th} inert concentration.

Using equation 5.15, 5.32 and 5.36

$$m_{in,\bar{j}} = \int_{-\infty}^{\infty} (m_{in,jo} - (m_{in,jl} - m_{in,jo})\hat{f})\ P(f) \cdot df.$$

$$= m_{in,jo} - (m_{in,jl} - m_{in,jo})\bar{f} \qquad 5.44$$

(c) Products Concentration

Using 5.13, 5.16, 5.39

$$\bar{m}_{pr} = Am_{Pr,o} + Bm_{Pr,1} + \frac{1}{\bar{\sigma}\sqrt{2\pi}} \left\{ \int_{0}^{1} (m_{ox,o} + (m_{fu,1} - m_{ox,o})\hat{f}) e^{-1/2\ z^2} \cdot df \right.$$

$$\left. - \int_{o}^{f_{st}} m_{ox,o}\left(\frac{f_{st}-\hat{f}}{f_{st}}\right) e^{-1/2\ z^2} \cdot df - \int_{f_{st}}^{1} m_{fu,1}\left(\frac{\hat{f}-f_{st}}{1-f_{st}}\right) \cdot e^{-1/2\ z^2} \cdot dz \right\}$$

$$\bar{m}_{pr} = m_{ox,o}\ (P(Z_1) - P(Z_0)) + (m_{fu,1} - m_{ox,o}) \left\{ \mu(P(Z_1) - P(Z_0)) \right.$$

$$\left. + \frac{\bar{\sigma}}{\sqrt{2\pi}} \left(e^{-1/2\ z_1^2} - e^{-1/2\ z_0^2}\right) \right\} - (\bar{m}_{fu} - m_{fu,1}) - (\bar{m}_{ox} - \bar{m}_{ox,o}) \qquad 5.45$$

Equations 5.40, 5.43, 5.44, and 5.45 have to satisfy the constraint:

$$\sum_{j=1}^{n} \bar{m}_{in,j} + \bar{m}_{fu} + \bar{m}_{ox} + \bar{m}_{pr} = 1 \qquad 5.46$$

When P(Z) is numerically calculated Eq. 5.46 can serve as a useful check of the numerical consistency of the computations.

(d) Mean Temperature

Using 5.27 and 5.39 we have

$$\overline{T} = \frac{1}{\overline{\sigma}\sqrt{2\pi}} \int_o^1 \left[\frac{\hat{h} - \hat{m}_{fu} H}{\sum_j m_j \overline{C}_{p,j}} \right] . e^{-1/2\ z^2} \ .df. + AT(o) + BT(1) \qquad 5.47$$

substituting the value of h from eq. 5.26 and expanding the denominator we have

$$\overline{T} = \frac{1}{\overline{\sigma}\sqrt{2\pi}} \int_o^1 \frac{h_o + \hat{f}(h_1 - h_o) - \hat{m}_{fu} H}{\hat{m}_{fu} \overline{C}_{pfu} + \hat{m}_{ox} \overline{C}_{pox} + \hat{m}_{pr} \overline{C}p_{pr} + \sum_{j=1}^{n} \hat{m}_{in,j} \overline{C}p_{in,j}} . e^{-1/2\ z^2} .df$$

$$+ A\ T(O) + BT(1)$$

$$\overline{T} = \frac{1}{\overline{\sigma}\sqrt{2\pi}} \left[\int_o^{f_{st}} \frac{h_o + \hat{f}(h_1 - h_o)}{\hat{m}_{ox} \overline{C}p_{ox} + \hat{m}_{pr} \overline{C}p_{pr} + \sum_{j=1}^{n} \hat{m}_{in,j} \overline{C}p_{in,j}} e^{-1/2\ z^2} .df \right.$$

$$\left. + \int_{f_{st}}^1 \frac{h_o + \hat{f}(h_1 - h_o) - \hat{m}_{fu} H}{\hat{m}_{fu} \overline{C}_{pfu} + \hat{m}_{pr} \overline{C}p_{pr} + \sum_{j=1}^{n} \hat{m}_{in,j} \overline{C}p_{in,j}} . e^{-1/2\ z^2} .df \right]$$

$$+ AT(O) + BT(1) \qquad 5.48$$

This can be further simplified to:

$$T = \frac{1}{\sqrt{2\pi}} \left[\int_o^{f_{st}} \frac{a_1 + b_1 \hat{f}}{(\alpha_1 + \beta_1 \hat{f})} e^{-1/2\ z^2} .dz + \int_{f_{st}}^1 \frac{a_2 + b_2 \hat{f}}{\alpha_2 + \beta_2 \hat{f}} e^{-1/2\ z^2} .dz \right]$$

$$+ AT(O) + BT(1) \qquad 5.49$$

Values of a_1, b_1, α_1, β_1 etc. are given in Appendix 5.1.

(e) Mean Square of Temperature Fluctuation

We have

$$\overline{\hat{T}^2} = \overline{(\bar{T}+T')^2} = \bar{T}^2 + \overline{T'^2}$$

$$\overline{T'^2} = \overline{\hat{T}^2} - \bar{T}^2$$

$$\overline{T'^2} = \int_{-\infty}^{+\infty} \hat{T}^2 P(f).df - \bar{T}^2$$

$$\overline{T'^2} = A\,T(O)^2 + BT(1)^2 + \int_O^1 \frac{1}{\bar{\sigma}\sqrt{2\pi}} \left(\frac{\hat{h} - \hat{m}_{fu} H}{\sum_j \bar{C}_{p,j} \hat{m}_j}\right)^2 e^{-1/2\, z^2}.df$$

Using equations 5.48 and 5.39 we have

$$\overline{T'^2} = AT(O)^2 + BT(1)^2 + \frac{1}{\sqrt{2\pi}} \int_O^{f_{st}} \left(\frac{a_1 + b_1\hat{f}}{\alpha_1 + \beta_1\hat{f}}\right)^2 e^{-1/2\, z^2} dz +$$

$$\int_{f_{st}}^1 \left(\frac{a_2 + b_2\hat{f}}{\alpha_2 + \beta_2\hat{f}}\right)^2 e^{-1/2\, z^2}\, dz - \bar{T}^2 \qquad 5.50$$

(f) Mean Density of the Mixture

Using equations 5.28 and 5.39 we have

$$\bar{\rho} = \left| \frac{1}{\sigma\sqrt{2\pi}} \int_O^1 \frac{\bar{p}}{R\hat{T} \sum_j \frac{\hat{m}_j}{W_j}} .e^{-1/2\, z^2}.df \right| + A\rho(O) + B\rho(1)$$

Where R is the Universal Gas Constant p is the pressure m_j is the mass fraction of species including oxidant, products and fuel and W_j is the molecular weight of the species. Appendix 5.1 gives the detailed derivation of the expression for mean density. The final form is

$$\bar{\rho} = A\rho(O) + B\rho(1) + \frac{\bar{\rho}}{R\sqrt{2\pi}} \int_O^{f_{st}} \frac{(\alpha_1+\beta_1) e^{-1/2\, z^2}}{(a_1+b_1\hat{f})(\alpha_3+\beta_3\hat{f})}.df$$

$$+ \int_{f_{st}}^1 \frac{(\alpha_2+\beta_2) e^{-1/2\, z^2}.df}{(a_2+b_2\hat{f})(\alpha_4+\beta_4\hat{f})} \qquad 5.51$$

(g) Scalar Fluctuation Correlations

In the transport equation for the mixture fraction f and the square of its fluctuations (model II) the scalar correlations $\overline{\rho' f'}$, $\overline{\rho' g'}$ arise. It is interesting to note that expressions to calculate these correlations can be derived with the help of equations 5.28 and 5.39. The magnitude of the correlations so obtained will be dependent on the accuracy with which the assumption of clipped Gaussian distribution applies.

$$\overline{\hat{\rho}\hat{f}} = \overline{(\bar{\rho}+\rho')(\bar{f}+f')} = \bar{\rho}\bar{f} + \overline{\rho' f'} \quad .$$

$$\overline{\rho' f'} = \overline{\hat{\rho}\hat{f}} - \bar{\rho}\bar{f} \qquad 5.52$$

From equation 5.28 we have

$$\hat{\rho}\hat{f} = \frac{\overline{p\hat{f}}}{R\hat{T}\sum_j \frac{\hat{m}_j}{W_j}} \qquad 5.53$$

Using equations 5.39, 5.52 and 5.53

$$\overline{\rho' f'} = \frac{1}{\bar{\sigma}\sqrt{2\pi}} \int \left(\frac{p\hat{f}}{R\hat{T}\sum_j \frac{\hat{m}_j}{W_j}}\right) e^{-z^2/2} \, .df + A\rho f(0) + B\rho f(1) - \bar{\rho}\bar{f}$$

or

$$\overline{\rho' f'} = A\rho f(0) + B\rho f(1) + \frac{p}{R\bar{\sigma}\sqrt{2\pi}} \left[\int_0^{f_{st}} \frac{(\alpha_1+\beta_1\hat{f})\hat{f}\, e^{-z^2/2}}{(a_1+b_1\hat{f})(\alpha_3+\beta_3\hat{f})} .df \right.$$

$$\left. + \int_{f_{st}}^{1} \frac{(\alpha_2+\beta_2\hat{f})\hat{f}\, e^{-z^2/2}}{(a_2+b_2\hat{f})(\alpha_4+\beta_4\hat{f})} .df \right] - \bar{\rho}\bar{f} \qquad 5.54$$

Similarly $\overline{\rho' g'}$ can be written as:

$$\overline{\rho' g'} = A\rho g(0) + B\rho g(1) + \frac{p}{R\bar{\sigma}\sqrt{2\pi}} \left[\int_0^{f_{st}} \frac{(\alpha_1+\beta_1\hat{f})\hat{f}^2\, e^{-z^2/2}}{(a_1+b_1\hat{f})(\alpha_3+\beta_3\hat{f})} . df \right.$$

$$\left. + \int_{f_{st}}^{1} \frac{(\alpha_2+\beta_2\hat{f})\hat{f}^2\, e^{-z^2/2}}{(a_2+b_2\hat{f})(\alpha_4+\beta_4\hat{f})} . df \right] - \bar{\rho}\bar{f}^2 - \bar{\rho}\bar{g} - 2\overline{\rho' f'}\,\bar{f} \qquad 5.55$$

The above expressions for $\bar{T}$, $\overline{T'^2}$, $\bar{\rho}$, $\overline{\rho'f'}$ and $\overline{\rho'g'}$ cannot be integrated analytically, hence $\bar{T}$, $\overline{T'^2}$, $\bar{\rho}$ were solved numerically using the Newton-Coats method of integration described in Hamming (1962). Expressions for $\overline{\rho'f'}$ and $\overline{\rho'g'}$ were not included in the computations of the present flame due to the short time available for computations.

(h) Triple Correlations

It is interesting to note that triple correlation $\overline{\rho'f'u_i'}$ and $\overline{\rho'g'u_i'}$ can also be calculated with the help of Boussinesque hypothesis and equation 5.54 and 5.55 as:

$$\overline{\rho'f'u_i'} = -\frac{\mu_t}{\sigma_{\rho_f}} \frac{\partial\overline{\rho'f'}}{\partial x_i} \quad \text{and} \quad \overline{\rho'g'u_i'} = -\frac{\mu_t}{\sigma_{\rho_g}} \frac{\partial\overline{g'\rho'}}{\partial x_i} \qquad 5.56$$

Although similar formulation has been used to calculate triple correlations in the Reynolds stress equations Launder et al (1975), it is not clear whether this formulation will be the accurate representation of the processes involved in the above correlations.

5.7 Concluding Remarks

In this Chapter different models for calculating the time-averaged reaction rate have been examined, and one has been selected to predict the present experimental flame.

Models which attempt to calculate the turbulent flame speed do not give the local time-averaged reaction rate directly, and are not suitable for the present flame. The physical picture of a turbulent diffusion flame shows that the flame consists mostly of randomly moving eddies of oxidant, products and fuel, and reaction takes place when fuel and oxidant come into contact at a sufficiently high temperature. The fluctuating structure of the flame necessitates modelling of the temporal behaviour of the mixture fraction.

Experiments show the fluctuations are random in nature and that the probability density function of temperature is Gaussian in the centre of the flame and bi-nodal near its edge. Hence a combustion model based on an assumed form of probability density function of the fluctuations is chosen. This model of the PDF, which approximates closely to the experimentally measured one, has been used for predicting two-dimensional boundary layer reacting flows with reasonable success. It is assumed that the reaction is single step and irreversible so that fuel and oxidant combine stiochiometrically to form products without any intermediate species being formed. The assumption that the system is in equilibrium, which means that either fuel and products or products and oxidant are present at a point, has also been applied.

The probability density function, together with the above two assumptions, is then used to calculate the mean values of scalars and their fluctuations which depend solely on the mixture fraction.

CHAPTER SIX

6.0 The Numerical Procedure

6.1 Introduction

In this Chapter the calculation procedure employed to solve the set of equations contained in Models I and II which were formulated in Chapter 4 will be described. Examination of the partial differential equations in any of the above sets show that they are three dimensional, elliptic, non-linear equations of the second order. They are also strongly coupled and, though the number of dependent variables is equal to the number of equations, pressure does not appear as the dependent variable of any of these equations. This fact reveals that analytical solutions of these sets of equations cannot be obtained and a numerical scheme will be required to solve them. Some simplification of the equations is, however, possible due to the boundary layer nature of the flow. In section 6.2 these assumptions are detailed and the resulting simplified set of transport equations is given for model I, which was described in section 4.3. Equations for model II can be developed by adding the extra terms to the finite difference equations as 'source terms'; these are given in table 6.1.

The streamlines in the present flow diverge, with increasing distance from the nozzle exit. The cylindrical co-ordinate system is not economical of computer time and storage for this type of flow. In section 6.3 the equations are recast into a curvilinear co-ordinate system in which the grid lines follow the flow more closely. Section 6.4 is concerned with the procedure by which the partial differential equations are discretized to give the finite difference equations. In section 6.5 the 'SIMPLE' algorithm used to solve the finite difference equations is described. A summary of the solution procedure is contained in section 6.6. The treatment of boundary conditions for the variables is presented in section 6.7. Section 6.8 closes the chapter with

Table 6.1

Extra terms added to Model I to obtain Model II

Equation	Terms
r-direction	$\frac{\mu_{eff}}{\sigma_\rho}\left(\frac{\partial\bar{\rho}}{\partial r}\cdot\frac{\partial\bar{V}_r}{\partial r}+\frac{\partial\bar{\rho}}{\partial z}\cdot\frac{\partial\bar{V}_r}{\partial z}+\frac{\partial\bar{V}_r}{r}\frac{\partial\bar{\rho}}{\partial r}\right)$
	$+\ \frac{\partial}{\partial r}\left(\frac{\bar{V}_r\,\mu_{eff}}{\sigma_\rho}\cdot\frac{\partial\bar{\rho}}{\partial r}\right)$
z-direction	$\frac{\mu_{eff}}{\sigma_\rho}\left(\frac{\partial\bar{\rho}}{\partial r}\cdot\frac{\partial\bar{V}_z}{\partial r}+\frac{\partial\bar{\rho}}{\partial z}\cdot\frac{\partial\bar{V}_z}{\partial z}+\frac{\bar{V}_r}{r}\cdot\frac{\partial\bar{\rho}}{\partial z}\right)$
	$+\ \frac{\partial}{\partial r}\left(\frac{\mu_{eff}\,\bar{V}_r}{\sigma_\rho}\cdot\frac{\partial\rho}{\partial z}\right)$
f-equation	$\frac{\mu_{eff}}{\sigma_\rho}\left(\frac{\partial\bar{\rho}}{\partial r}\cdot\frac{\partial\bar{f}}{\partial r}+\frac{\partial\bar{\rho}}{\partial z}\cdot\frac{\partial\bar{f}}{\partial z}\right)$
g-equation	$\frac{\mu_{eff}}{\sigma_\rho}\left(\frac{\partial\bar{\rho}}{\partial r}\cdot\frac{\partial g}{\partial r}+\frac{\partial\bar{\rho}}{\partial z}\cdot\frac{\partial g}{\partial z}\right)-\frac{\partial}{\partial r}\,g\,\frac{\mu_{eff}}{\sigma_\rho}\frac{\partial\bar{\rho}}{\partial r}-\frac{1}{r}\ \frac{\mu_{eff}}{\sigma_\rho}\,g\,\frac{\partial\bar{\rho}}{\partial r}$
k-equation	$\frac{\mu_{eff}}{\sigma_\rho}\left(\frac{\partial\bar{\rho}}{\partial r}\cdot\frac{\partial k}{\partial r}+\frac{\partial\bar{\rho}}{\partial z}\cdot\frac{\partial k}{\partial z}+V_r\frac{\partial\bar{\rho}}{\partial r}\cdot\frac{\partial\bar{V}_r}{\partial r}+V_z\frac{\partial\bar{\rho}}{\partial r}\frac{\partial\bar{V}_r}{\partial z}\right.$
	$\left.+\,V_r\frac{\partial\bar{\rho}}{\partial z}\cdot\frac{\partial\bar{V}_z}{\partial r}+V_z\frac{\partial\bar{\rho}}{\partial z}\cdot\frac{\partial\bar{V}_z}{\partial z}-\frac{K}{r}\frac{\partial\bar{\rho}}{\partial r}\right)$
	$-\frac{\partial}{\partial r}\left(\frac{\mu_{eff}}{\sigma_\rho}\,K.\,\frac{\partial\bar{V}_r}{\partial r}\right)$

Note:- Extra terms were not added to continuity and dissipation equation because addition resulted in unstable procedure

the description of the solution of some 'test case' flows.

6.2 Simplification of the Transport Equations Due to the Boundary Layer Nature of the Flow

The term 'boundary layer' in the numerical computations of three dimensional flows has been extended by Patankar and Spalding (1972) to encompass all flows which obey the following conditions;

i) Only one predominant flow direction (PFD) exists.

ii) Events downstream of any location along the PFD have negligible influence on this location.

The latter implies that recirculation along the PFD does not occur, the diffusion of momentum and energy along the PFD is negligible, and that the downstream pressure field does not have any influence on the upstream flow field.

The flame of the present experiment fulfills the above requirements quite well. There is only one predominant flow direction, this will be denoted by co-ordinate z, and no recirculation. This can be seen from the photographs of the flame as well, Fig. 2.8 . Since the flame is free the axial pressure gradient is zero and the question of downstream pressure influencing the upstream flow field does not arise. The velocity gradients in the flow direction are expected to be small hence diffusion in this direction can also be neglected. The above assumptions are expressed mathematically by:

$$\frac{dp}{dz} = 0; \quad w > 0; \quad \frac{\partial}{\partial z}\left(\Gamma_\Phi \frac{\partial \bar{\Phi}}{\partial r}\right) \quad , \frac{\partial}{\partial r}\left(\Gamma_\Phi \frac{\partial \Phi}{\partial z}\right)$$

and similar other terms are zero.

Applying these assumptions to equations of model I (section 4.3) we have

Continuity:

$$\frac{\partial(\bar{\rho}\bar{V}_\theta)}{r\partial\theta} + \frac{1}{r}\frac{\partial}{\partial r}(r\bar{\rho}\bar{V}_r) + \frac{\partial(\bar{\rho}\bar{V}_z)}{\partial z} = 0 \qquad 6.1$$

r-momentum

$$\frac{\partial(\bar{\rho}\bar{V}_\theta\bar{V}_r)}{r\partial\theta} + \frac{1}{r}\frac{\partial(\bar{r}\,\bar{V}_r\bar{V}_r)}{\partial r} + \frac{\partial(\bar{\rho}\bar{V}_z\bar{V}_r)}{\partial z} = \frac{\partial}{r\partial\theta}\mu_{eff}\left(\frac{\partial\bar{V}_r}{r\partial\theta}\right) + \frac{1}{r}\frac{\partial}{\partial r}\mu_{eff}\, r\frac{\partial\bar{V}_r}{\partial r} +$$

$$\bar{\rho}g_r - \frac{\partial p}{\partial r} - \mu_{eff}\frac{\bar{V}_r}{r^2} - \mu_{eff}\frac{\partial\bar{V}_\theta}{\partial\theta} - \frac{\bar{V}_\theta^2}{r} - \frac{2}{3}\frac{\partial\bar{\rho}K}{\partial r} + \frac{1}{3}\mu_{eff}\frac{\partial}{\partial r}\nabla\vec{V} \qquad 6.2$$

θ-momentum

$$\frac{\partial(\bar{\rho}\bar{V}_\theta\bar{V}_\theta)}{r\partial\theta} + \frac{1}{r}\frac{\partial(r\bar{\rho}\bar{V}_r\bar{V}_\theta)}{\partial r} + \frac{\partial\bar{\rho}\bar{V}_z\bar{V}_\theta}{\partial z} = \frac{\partial}{r\partial\theta}\mu_{eff}\left(\frac{\partial\bar{V}_\theta}{r\partial\theta}\right) + \frac{1}{r}\frac{\partial}{\partial r}\mu_{eff}\, r\frac{\partial\bar{V}_\theta}{\partial\theta}$$

$$+ \bar{\rho}g_\theta - \frac{\partial\bar{p}}{r\partial\theta} - \frac{\bar{V}_r\bar{V}_\theta}{r} + \mu_{eff}\frac{2}{r^2}\frac{\partial\bar{V}_r}{\partial\theta} - \frac{2}{3}\frac{\partial\bar{\rho}K}{r\partial\theta} - \mu_{eff}\frac{\bar{V}_\theta}{r^2} + \frac{1}{3}\mu_{eff}\frac{\partial(\nabla.\vec{V})}{r\partial\theta} \qquad 6.3$$

z-momentum

$$\frac{\partial(\bar{\rho}\bar{V}_\theta\bar{V}_z)}{r\partial\theta} + \frac{1}{r}\frac{\partial r\bar{\rho}\bar{V}_r\bar{V}_z}{\partial r} + \frac{\partial}{\partial z}(\bar{\rho}\bar{V}_z\bar{V}_z) = \frac{\partial}{r\partial\theta}\mu_{eff}\frac{\partial\bar{V}_z}{r\partial\theta} + \frac{1}{r}\frac{\partial}{\partial r}\mu_{eff}\, r\frac{\partial\bar{V}_z}{\partial r} \qquad 6.4$$

Mixture Fraction Equation

$$\frac{1}{r}\frac{\partial(\bar{\rho}\bar{V}_\theta\bar{f})}{\partial\theta} + \frac{\partial}{r\partial r}(r\bar{\rho}\bar{V}_r\bar{f}) + \frac{\partial}{\partial z}(\bar{\rho}\bar{V}_z\bar{f}) = \frac{\partial}{r\partial\theta}\Gamma_{eff,f}\frac{\partial\bar{f}}{r\partial\theta} + \frac{1}{r}\frac{\partial}{\partial r}r\Gamma_{eff,f}\frac{\partial\bar{f}}{\partial r}$$

6.5

g-equation

$$\frac{1}{r}\frac{\partial}{\partial\theta}(\bar{\rho}\bar{V}_\theta g) + \frac{\partial}{r\partial r}(r\bar{\rho}\bar{V}_r g) + \frac{\partial}{\partial z}(\bar{\rho}\bar{V}_z g) = \frac{\partial}{r\partial\theta}\Gamma_{eff,g}\frac{\partial g}{r\partial\theta} + \frac{1}{r}\frac{\partial}{\partial r}r\,\Gamma_{eff,g}\frac{\partial g}{\partial r}$$

$$+ 2\,\Gamma_{eff,f}\left[\left(\frac{\partial\bar{f}}{r\partial\theta}\right)^2 + \left(\frac{\partial\bar{f}}{\partial r}\right)^2\right] - C_{g2}\frac{\varepsilon}{k}g \qquad 6.6$$

K-equation

$$\frac{1}{r}\frac{\partial}{\partial\theta}(\bar{\rho}\,\bar{V}_\theta K) + \frac{\partial}{r\partial r}(r\bar{\rho}\bar{V}_r K) + \frac{\partial}{\partial z}(\bar{\rho}\bar{V}_z K) = \frac{\partial}{r\partial\theta}\Gamma_{eff,K}\frac{\partial K}{r\partial\theta} + \frac{1}{r}\frac{\partial}{\partial r}\,r\,\Gamma_{eff,K}$$

$$\frac{\partial K}{\partial r} + \{2\mu_t\left[\left(\frac{\partial\bar{V}_r}{\partial r}\right)^2 + \left(\frac{\partial\bar{V}_\theta}{r\partial\theta}\right)^2\right] + \mu_t\left[\frac{1}{r}\frac{\partial\bar{V}_r}{\partial\theta} + \frac{\partial\bar{V}_\theta}{\partial r} - \frac{\bar{V}_\theta}{r}\right]\left[\frac{\partial\bar{V}_r}{r\partial\theta} + \frac{\partial\bar{V}_\theta}{\partial r}\right]$$

$$+ \mu_t\left[\frac{1}{r}\frac{\partial\bar{V}_z}{\partial\theta}\right]^2 + \mu_t\left[\frac{\partial\bar{V}_z}{\partial r}\right]^2 - \frac{2}{3}(\bar{\rho}K)\left[\frac{\partial\bar{V}_r}{\partial r} + \frac{\partial\bar{V}_\theta}{r\partial\theta}\right]$$

$$- \frac{2}{3}\mu_t\frac{\partial}{\partial r}(\nabla.\bar{\vec{V}})\cdot\frac{\partial\bar{V}_r}{\partial r} - \frac{2}{3}\mu_t\frac{\partial}{r\partial\theta}(\nabla.\bar{\vec{V}})\cdot\frac{\partial\bar{V}_\theta}{r\partial\theta}\} - \bar{\rho}\varepsilon \qquad 6.7$$

Term in curly brackets = PK

ε-equation

$$\frac{1}{r}\frac{\partial}{\partial\theta}(\bar{\rho}\,\bar{V}_\theta\varepsilon) + \frac{\partial}{r\partial r}(r\bar{\rho}\,\bar{V}_r\varepsilon) + \frac{\partial}{\partial z}(\bar{\rho}\,\bar{V}_z\varepsilon) = \frac{\partial}{r\partial\theta}\,\Gamma_{eff,\varepsilon}\,\frac{\partial\varepsilon}{r\partial\theta} +$$

$$\frac{1}{r}\frac{\partial}{\partial r}(r\Gamma_{eff,\varepsilon}\frac{\partial\varepsilon}{\partial r}) + C_{\varepsilon 1}\,(PK)\,\frac{\varepsilon}{K} - \bar{\rho}C_{\varepsilon 2}\frac{\varepsilon^2}{K} \qquad 6.8$$

In the above equations terms containing gradients of viscosity have also been neglected. Inspection of eqns. 6.2 - 6.8 show that they can be written as

$$\frac{1}{r}\frac{\partial}{\partial\theta}(\bar{\rho}\,\bar{U}\,\bar{\Phi}) + \frac{1}{r}\frac{\partial(r\bar{\rho}\bar{V}\bar{\Phi})}{\partial r} + \frac{\partial(\bar{\rho}\bar{W}\bar{\Phi})}{\partial z} = \frac{\partial}{r\partial\theta}\,\Gamma_{eff,\Phi}\,\frac{\partial\bar{\Phi}}{r\partial\theta} + \frac{1}{r}\,\frac{\partial}{\partial r}$$

$$(r\,\Gamma_{eff,}\,\frac{\partial\bar{\Phi}}{\partial r}) + S_\Phi \qquad 6.9$$

where Φ stands for any of the variables V_θ, V_r, V_z, f, g, K, ε and S_Φ is the source term which contains the extra terms in the Φ equations also for convenience $U = V_\theta$, $V = V_r$, $W = V_z$.

6.3 Transport Equations in the Curvilinear Co-ordinate System

As the jet of fuel emerges from the burner it expands into the surrounding stagnant air, and as the distance from the burner exit increases the region of interest also increases in size. A cylindrical co-ordinate system is not economical for computing this type of flow because near the exit a large number of grid points lie in the surrounding stagnant atmosphere, away from the region of interest, Fig. 6.1. In the computation of the present problem a quasi-orthogonal system is adopted in which the radius R(Z) fig. 6.2 of the computational grid increases with the distance from the burner exit. A similar system is used by Sharma (1974) and Bergeles (1976) for a Cartesian type grid. In this section their system will be applied to transform the cylindrical co-ordinate system (r,θ, z) to a (η,β,ζ) co-ordinate system as described below. This system is still not the optimum one because the grid lines do not exactly follow the stream lines. It is not conceptually difficult to devise a co-ordinate system that maps the flow more economically but the time required to make the additional modifications to the computer program was not available.

In this co-ordinate system, η is the dimensionless radius normalized by the maximum radius R(Z) of the calculation domain, Fig. 6.3 . Angle β is the same as angle θ in the (r,θ,z) system. The constant η lines cut the constant β lines at right angles everywhere in the field. The third co-ordinate direction ζ is at angle γ with the z direction, Figure 6.4, and is not orthogonal to the planes defined by β,η co-ordinates. The relation between the co-ordinate directions of the two systems can be expressed as:

$$\begin{aligned} \eta &= r/R(Z) \\ \beta &= \theta \\ \zeta &= z/\cos\gamma. \end{aligned} \qquad 6.10$$

As the angle γ between the z & ζ directions is increased the error introduced in assuming ζ to be orthogonal to β,η plane increases. The maximum value of γ for which the error would be 5% was worked out by Bergeles (1976) for a Cartesian type of co-ordinate system. This will now be determined for the present curvilinear co-ordinate system, also relation will be derived to convert eqns. 6.1 and 6.9 to this co-ordinate system. The co-ordinates (β,η,ζ) are related to (θ,r,z) by the following relations.

$$\frac{\partial}{\partial\theta} = \frac{\partial}{\partial\beta}\cdot\frac{\partial\beta}{\partial\theta} + \frac{\partial}{\partial\eta}\cdot\frac{\partial\eta}{\partial\theta} + \frac{\partial}{\partial\zeta}\cdot\frac{\partial\zeta}{\partial\theta}$$

$$\frac{\partial}{\partial r} = \frac{\partial}{\partial\beta}\frac{\partial\beta}{\partial r} + \frac{\partial}{\partial\eta}\cdot\frac{\partial\eta}{\partial r} + \frac{\partial}{\partial\zeta}\cdot\frac{\partial\zeta}{\partial r} \qquad 6.11$$

$$\frac{\partial}{\partial z} = \frac{\partial}{\partial\beta}\cdot\frac{\partial\beta}{\partial z} + \frac{\partial}{\partial\eta}\cdot\frac{\partial\eta}{\partial z} + \frac{\partial}{\partial\zeta}\frac{\partial\zeta}{\partial z}$$

Substituting eqn. 6.10 in 6.11 we obtain.

$$\frac{\partial\beta}{\partial\theta} = 1;\quad \frac{\partial\eta}{\partial r} = \frac{1}{R};\quad \frac{\partial\zeta}{\partial z} = \left(\frac{1}{\cos\gamma} - z/\cos\gamma^2\right)\sin'\gamma\cdot\frac{\partial\gamma}{\partial z}$$

$$\frac{\partial\eta}{\partial z} = \frac{-r}{R^2}\cdot\frac{\partial R}{\partial z};\quad \frac{\partial\zeta}{\partial r} = -\frac{z}{\cos\gamma^2}\cdot\sin\gamma\frac{\partial\gamma}{\partial r} \qquad 6.12$$

The following order of magnitude relations can be assumed

$$\frac{\partial\gamma}{\partial z} = O(\gamma)$$

(where O( ) stands for the order of magnitude)

$$\frac{\partial\gamma}{\partial y} = O(\gamma)\cdot O\left(\frac{1}{R}\right) \qquad 6.13$$

$$\frac{\partial R}{\partial z} = O(\gamma)$$

Substituting equations 6.13 in 6.12, ignoring terms of $O(\gamma^2)$ and assuming $\cos\gamma \simeq 1$ we have

$$\frac{\partial\beta}{\partial\theta} = 1, \quad \frac{\partial\eta}{\partial r} = \frac{1}{R}, \quad \frac{\partial\zeta}{\partial z} = 1$$

$$\frac{\partial\eta}{\partial z} = \frac{-r}{R^2}\cdot\frac{\partial R}{\partial z}, \quad \frac{\partial\zeta}{\partial r} = 0 \qquad 6.14$$

The accuracy of above relations depends on the value of γ_{max}. In the present procedure γ_{max} was kept to 18°, this gives maximum error of 5%. The relations 6.11 can now be reduced to

$$\frac{\partial}{\partial\theta} = \frac{\partial}{\partial\beta}$$

$$\frac{\partial}{\partial r} = \frac{1}{R}\frac{\partial}{\partial\eta} \qquad 6.15$$

$$\frac{\partial}{\partial z} = \frac{\partial}{\partial\zeta} - \eta\,\frac{1}{R}\frac{\partial R}{\partial z}\cdot\frac{\partial}{\partial\eta}$$

The above equations are used to transform eqn. 6.1 and 6.9 into (β,η,ζ) co-ordinate system.

$$\frac{\partial(\bar{\rho}\bar{U})}{R\eta\partial\beta} + \frac{\partial(\eta\bar{\rho}\bar{V})}{R\eta\partial\eta} + \frac{\partial(\bar{\rho}\bar{W})}{\partial\zeta} - \frac{\eta}{R}\frac{dR}{dz}\frac{\partial(\bar{\rho}\bar{W})}{\partial\eta} = 0 \qquad 6.16$$

$$\frac{1}{R\eta}\frac{\partial(\bar{\rho}\bar{U}\bar{\Phi})}{\partial\beta} + \frac{\partial(\eta\bar{\rho}\bar{V}\bar{\Phi})}{R\eta\partial\eta} + \frac{\partial(\bar{\rho}\bar{W}\bar{\Phi})}{\partial\zeta} - \frac{\eta}{R}\frac{dR}{dz}\frac{\partial(\bar{\rho}\bar{W}\bar{\Phi})}{\partial\eta}$$

$$= \frac{\partial}{R\eta\partial\beta}\Gamma_{eff,\Phi}\frac{\partial\bar{\Phi}}{R\eta\partial\beta} + \frac{1}{R\eta d\eta}\partial(\eta\Gamma_{eff,\Phi}\frac{\partial\bar{\Phi}}{R\partial\eta}) + S_{\Phi} \qquad 6.17$$

6.4 The Discretization of the Partial Differential Equations

The next stage in the development of the numerical solution procedure is to convert eqns. 6.16, 6.17 into finite difference equations. This is accomplished in the following steps:

a) Specification of a grid system

b) Location of variables on the grid

c) Control volumes for the variables

d) Integration of the partial differential equations over the appropriate control volume.

6.4.1 The Grid System

The grid was formed by lines which were parallel to the co-ordinate directions. The points of intersection of the grid lines were termed grid nodes. No restriction was placed on the spacing of the grid lines in any direction. The number of grid nodes in the constant-ζ plane was determined by the number of nodes required to give a grid independent solution. The increment in the ζ direction, or the forward step size, was governed by the minimum increment required to achieve a forward step size independent solution.

6.4.2 Location of the Variables on the Grid

All the variables were stored at the grid nodes except the velocities U and V. The U velocities were located exactly midway between the grid nodes in the β direction and the V velocities were located midway between grid nodes in the η direction.Fig. 6.5 shows the grid system in the $\beta \sim \eta$ plane together with locations at which different variables were stored. The 'staggered' location of the U and V velocities is in line with other workers e.g. Amsden and Harlow (1970),Sharma (1974). The advantages of this practice will be discussed in the next section.

6.4.3 The Control Volumes

The control volume for variables located at grid node P is shown in Fig. 6.6 . The n, s, e and w faces are formed by $\eta \sim \zeta$ and $\beta \sim \zeta$

planes passing midway between the grid nodes. The other two faces (U and D) coincide with two constant ζ planes called the upstream plane (U) and the downstream plane (D). In the upstream plane the values of all the variables are known. Values in the downstream plane are unknown and are calculated by the integration of their partial differential equations over this control volume. Since the V and U velocities are stored halfway between the grid nodes the convective fluxes from n, s, e and w faces can be calculated without recourse to averaging of any of these velocities. Another advantage of the staggered location is that the pressure gradients that appear in the U and V momentum equations can also be calculated without averaging pressures.

The control volumes of the U and V velocities are formed by η - ζ and β ~ζ planes passing through the grid nodes. The velocities required to calculate the convection coefficients for these control volumes are obtained as weighted averages from the neighbouring locations. The weighting factors depend on the relative distance of the neighbouring locations. The averaging procedure will be explained in more detail in the next section.

6.4.4 Integration of Partial Differential Equations

The following assumptions are made in discretizing the transport equation,

i) The variation in the ζ direction of the values of the variables θ η, U, V, W etc, is stepwise. The downstream value prevailing from ζ_u to ζ_D except at ζ_u where the upstream value prevails.

ii) The variation of the variables in the β,η direction is assumed to be linear, so that when a variable is required at a location other than the one at which it is stored a weighted average is used to arrive at the value of the variable. The weighting depends on the relative distance of the neighbouring locations

from that point. For example radial velocity $\bar{V}$ is stored at n and s fig. 6.7. If $\bar{v}_p$ is required it is calculated from the relation:

$$\bar{V}_p = \left(\frac{\Delta r_{np}}{\Delta r_{np}+\Delta r_{ps}}\right)\bar{V}_s + \left(\frac{\Delta r_{ps}}{\Delta r_{np}+\Delta r_{ps}}\right)\bar{V}_n \qquad 6.18$$

If the grid spacing is uniform i.e. $\Delta r_{np} = \Delta r_{ps}$ this reduces to

$$\bar{V}_p = (\bar{V}_s + \bar{V}_n)/2 \qquad 6.19$$

6.4.4.1 Integration of the Continuity Equation

Using the above assumptions the continuity equation 6.16 is integrated over the control volume shown in fig. 6.6 as follows:

$$\int_V \frac{\partial(\bar{\rho}\bar{U})}{R\eta d\beta} \cdot dV + \int_V \left[\frac{1}{R}\,\frac{\partial(\eta\bar{\rho}\bar{V})}{\eta\partial\eta} - \eta\,\frac{dR}{dZ}\,\frac{\partial(\bar{\rho}\bar{W})}{\partial\eta}\right] dV + \int_V \frac{\partial}{\partial\zeta}(\bar{\rho}\bar{W}).dV = 0 \qquad 6.20$$

where $$\int_V dV = \int_{\beta w}^{\beta e}\int_{\eta s}^{\beta n}\int_{\zeta u}^{\beta p} R^2\eta d\beta d\eta d\zeta \qquad 6.21$$

After carrying out the integration one obtains:

$$(\bar{\rho}\bar{U})_e a'^{\Phi}_e - (\bar{\rho}\bar{U})_w a'^{\Phi}_w + (\bar{\rho}\bar{V})_n a'^{\Phi}_n - (\bar{\rho}\bar{V})_s a'^{\Phi}_s - (\bar{\rho}\bar{W})_n a'^{\Phi}_{xn}$$

$$+ (\bar{\rho}\bar{W})_s a'^{\Phi}_{xs} + (\bar{\rho}\bar{W})_p a'^{\Phi}_p - (\bar{\rho}\bar{W})_u a'^{\Phi}_u = 0.0 \qquad 6.22$$

The notation $(\bar{\rho}\bar{U}_e)_e$ denotes the values of variables ρ, U at the e, face of the control volume. The coefficients in equation 6.22 are defined by:

$$a_e'^{\Phi} \equiv (R\Delta\eta\Delta\zeta)_e , \qquad a_w'^{\Phi} \equiv R\Delta\eta\Delta\zeta$$

$$a_n'^{\Phi} \equiv \eta_n (R\Delta\beta\Delta\zeta), \qquad a_s'^{\Phi} \equiv \eta_s (R\Delta\beta\Delta\zeta)$$

$$a_u'^{\Phi} \equiv \eta_u (R_u^2\Delta\beta\Delta\eta), \qquad a_p'^{\Phi} \equiv \eta_p (R_p^2\Delta\beta\Delta\eta)$$

$$(ax)_n'^{\Phi} \equiv \eta_n^2 R\, \Delta\beta\, (R_u - R_p)$$

$$(ax)_s'^{\Phi} \equiv \eta_s^2 R\, \Delta\beta\, (R_u - R_p)$$

where

$$R = (R_u + R_p)/2$$

In the calculation of the mass fluxes $(\overline{\rho W})_p$ and $(\overline{\rho W})_u$ densities calculated in the previous step were used.

This approximation is necessary because downstream density can only be calculated after solving all the transport equations including $\bar{f}$ and $\bar{g}$. Iteration at every plane is necessary if the density at that plane is to be used. It was found that at least 20 iterations were required before convergence could be achieved. This made the procedure very expensive of computer time. It was found however that the use of upstream densities did not affect the accuracy of the solution if the forward step size was small, hence this practice was used throughout the computations. It was also less expensive than the iterative procedure.

6.4.4.2 Integration of the General Φ Transport Equation

The general Φ transport equation (eqn. 6.17) has a source term S_Φ. Its integral can be expressed in a linearised form as

$$\int_V S_\Phi . dV = S^\Phi_{u,\Phi} + S^\Phi_{p,\Phi} \Phi_p$$

Integrating eqn. 6.17 we have

$$\int_V \frac{1}{R\eta} \frac{\partial \bar{\rho}\bar{U}\bar{\Phi}}{\partial \beta} . dV + \int_V \frac{\partial (\eta \bar{\rho}\bar{V}\bar{\Phi})}{R\eta \partial \eta} . dV + \int_V \frac{\partial (\bar{\rho}\bar{w}\bar{\Phi})}{\partial \zeta} . dV$$

$$- \frac{1}{R} \int_V \eta \frac{dR}{dZ} \frac{\partial (\bar{\rho}\bar{w}\bar{\Phi})}{\partial \eta} . dV = \int_V \frac{\partial}{R\eta \partial \beta} \Gamma_{eff,\Phi} \frac{\partial \bar{\Phi}}{R\eta \partial \beta} . dV$$

$$+ \int_V \frac{1}{R\eta \partial \eta} \partial (\eta \Gamma_{eff,\Phi} \frac{\partial \bar{\Phi}}{\partial \eta}) . dV + \int_V S_\Phi . dV \qquad 6.23$$

Which yields

$$(\bar{\rho}\bar{U}\bar{\Phi})_e a'^\Phi_e - (\bar{\rho}\bar{U}\bar{\Phi})_w a'^\Phi_w + (\bar{\rho}\bar{V}\bar{\Phi})_n a'^\Phi_n - (\bar{\rho}\bar{V}\bar{\Phi})_s a'^\Phi_s$$

$$- (\bar{\rho}\bar{w}\bar{\Phi})_n (ax)'^\Phi_n + (\bar{\rho}\bar{w}\bar{\Phi})_s (ax)'^\Phi_s = (\Gamma_{eff,\Phi} \frac{\partial \bar{\Phi}}{R\eta \partial \beta})_e a'^\Phi_e - (\Gamma_{eff,\Phi} \frac{\partial \bar{\Phi}}{R\eta \partial \beta})_w a'^\Phi_w$$

$$+ (\eta \Gamma_{eff,\Phi} \frac{\partial \bar{\Phi}}{\partial \eta})_n a'^\Phi_n - (\eta \Gamma_{eff,\Phi} \frac{\partial \bar{\Phi}}{R \partial \eta})_s a'^\Phi_s + S^\Phi_{u,\Phi} + S^\Phi_{p,\Phi} \Phi_p \qquad 6.24$$

The above equation is written in a simplified form below

$$C_E \Phi_e - C_W \Phi_w + C_N \Phi_n - C_S \Phi_s + C_P \Phi_p - C_U \Phi_u$$

$$= D_E(\Phi_E - \Phi_P) - D_W(\Phi_p - \Phi_W) + D_N(\Phi_N - \Phi_P) - D_S(\Phi_P - \Phi_S)$$

$$+ S_{u,\Phi} \Phi_\Phi + S^\Phi_{p,\Phi} \Phi_p \qquad 6.25$$

where C_E, C_W, etc. are 'convection coefficients' as defined below

$$C_E = (\bar{\rho}\bar{U})_e a'^\Phi_e \ , \ C_W = (\bar{\rho}\bar{U})_w a'^\Phi_w \ , \ C_N = (\bar{\rho}\bar{V})_n a'^\Phi_n - (\bar{\rho}\bar{W})_n (ax)'^\Phi_n \ .$$

Similarly C_s, C_u and C_p.

D_E, D_w etc, are 'diffusion coefficents' and are expressed as:

$$D_E = \left(\frac{\Gamma_{eff,\Phi}}{R\eta\Delta\beta}\right) a'^{\Phi}_{e} \qquad , D_W = \left(\frac{\Gamma_{eff,\Phi}}{R\eta\Delta\beta}\right) a'^{\Phi}_{w} \qquad \text{etc.}$$

Now Φ_e, Φ_w, Φ_n, Φ_s can be evaluated from the one dimensional counterpart of the differential equation or

$$\frac{1}{R\eta} \frac{\partial(\overline{\rho U \Phi})}{\partial \overline{\rho}\beta} - \frac{1}{R\eta \partial\beta} \Gamma_{eff,\Phi} \frac{\partial \overline{\Phi}}{\partial \beta} = 0 \qquad 6.25a$$

From above equation

$$\Phi_e = g_E \Phi_E + (1 - g_E)\Phi_p$$

where $$g_E = (\exp(\tfrac{1}{2}Pe_e)-1)/(\exp(Pe_e)-1) \qquad 6.25b$$

where Pe_e is the Peclet number defined by eqn. 6.27a below.

Substituting the values of Φ_e, Φ_w etc. in eqn. 6.25 we have

$$C_E(g_E\Phi_E + (1-g_E)\Phi_p) - C_w(g_W\Phi_p + (1-g_W)\Phi_W)$$

$$+ C_N(g_N\Phi_N + (1-g_N)\Phi_p) - C_S(g_s\Phi_p + (1-g_s)\Phi_s) + C_p\Phi_p - C_u\Phi_u$$

$$= D_E(\Phi_E - \Phi_p) - D_W(\Phi_p - \Phi_W) + D_N(\Phi_N - \Phi_p) - D_S(\Phi_p - \Phi_S)$$

$$+ S_p^{\Phi}\Phi_p + S_u^{\Phi} \qquad 6.26a$$

This equation can be rewritten as

$$C_E(f_e\Phi_p + (1-f_e)\Phi_E) - C_W(f_w\Phi_W + (1-f_w)\Phi_p)$$

$$C_N(f_n\Phi_p + (1-f_n)\Phi_N) - C_S(f_s\Phi_S + (1-f_s)\Phi_p)$$

$$+ \Phi_p C_p - \Phi_u C_u = S^{\Phi}_{p,\Phi}\Phi_p + S^{\Phi}_{u,\Phi} \qquad 6.26b$$

where

$$f_e = 1 - g_E + \frac{1}{Pe_e}$$

$$f_w = 1 - g_W + \frac{1}{Pe_w}$$

$$f_s = 1 - g_S + \frac{1}{Pe_s} \qquad 6.27$$

$$f_n = 1 - g_N + \frac{1}{Pe_n}$$

where Pe is the Peclet number of the control volume defined as:

$$Pe_e = C_E/D_E = \frac{(\overline{\rho U})_e \, \eta_R \Delta\beta}{\Gamma_{eff,\Phi e}} \qquad \text{similarly for } Pe_w \text{ etc.}$$

6.27a

Equation 6.26 can be rearranged with the help of the continuity equation as follows

$$a_P^\Phi \Phi_P = a_N^\Phi (\Phi_N - \Phi_p) + a_S^\Phi (\Phi_S - \Phi_p) + a_E^\Phi (\Phi_E - \Phi_P)$$

$$+ a_W^\Phi (\Phi_W - \Phi_p) + \Phi_u a_u^\Phi + s_{u,\Phi}^\Phi \qquad 6.28$$

where

$$a_p^\Phi = C_u - s_p^\Phi , \qquad a_u^\Phi = C_u$$

$$a_N^\Phi = C_N(f_n - 1) , \qquad a_S^\Phi = C_S f_s ; \qquad a_E^\Phi = C_E(f_e - 1), \qquad a_W^\Phi = C_W f_w$$

6.29

(For the full details of the derivation of the above equation see Appendix 6.1).

Equation 6.27 can be simplified to give normalized coefficients

$$\Phi_p = A_N^\Phi \Phi_N + A_S^\Phi \Phi_S + A_E^\Phi \Phi_E + A_W^\Phi \Phi_W + A_u^\Phi \Phi_u + S_{u,}^\Phi \qquad 6.30$$

where

$$A_N^{\Phi} = a_N^{\Phi}/a_{pp}^{\Phi} \text{ etc.,} \qquad S_{u,\Phi}^{\Phi} = s_u^{\Phi}/a_{pp}^{\Phi}$$

and

$$a_{pp}^{\Phi} = a_p^{\Phi} + a_N^{\Phi} + a_S^{\Phi} + a_E^{\Phi} + a_W^{\Phi}$$

To solve eqn. 6.30 the finite difference equation for Φ_p, weighting factors f_e, f_w etc. have to be calculated which in turn requires evaluation of factors g_E, g_W etc. It can be seen from eqn. 6.25b that this involves exponentials which are costly to compute, moreover the values of g_E etc. given by eqn. 6.25b are the linearized one dimensional solutions which may not be true in the three dimensional non linear situation. The 'exact' calculation of g_E etc. can also cause the numerical scheme to become unstable as well. The practise followed in this computational procedure, which makes it economical as well as stable, is based on the hybrid differencing scheme (HDS) proposed by Spalding (1972). This method uses either central differencing (CDS) or Upwind differencing (UDS) depending on the Peclet number of the control volume. The weighting factors (g's) take different values for CDS and HDS. The central differencing scheme assumes a linear variation in the value of Φ for both convection as well as diffusion fluxes.

For CDS $\quad g = 1/2 \quad$ (From eqn. 6.26a)

$$f = \frac{1}{2} + \frac{1}{Pe} \quad \text{(From eqn. 6.27)}$$

From eqn. 6.27a and 6.29,

$$a_N^{\Phi} = \frac{C_N}{Pe_n} - \frac{C_N}{2} = D_N - \frac{C_N}{2}$$

$$a_S^{\Phi} = \frac{C_S}{Pe_s} + \frac{C_S}{2} = D_S + \frac{C_S}{2}$$

Similarly for a_E^{Φ} and a_W^{Φ}.

The upwind differencing scheme assumes linear variation in Φ for the diffusion flux only. For the convection flux account is taken of the local flow direction; the value of Φ convected across a cell face is

taken to be the nodal value on the upwind side of the face.

For UDS $\quad g = 0, \quad f = 1 + \frac{1}{Pe} \quad$ when $P_e \geq 0$

$\quad g = 1, \quad f = \frac{1}{Pe} \quad$ when $P_e < 0$

so $\quad a_N^\Phi = D_N \; ; \quad a_S^\Phi = C_S + D_S \quad$ when $Pe > 0$

$\quad a_N^\Phi = D_N - C_N ; \quad a_S^\Phi = D_S \quad$ when $Pe < 0$

similarly for a_E and a_W.

In the hybrid differencing scheme CDS is used for values of the Peclet number between +2 and -2, and UDS is used for all other values with one modification that diffusion flux is neglected.

The limiting values of +2 and -2 on Peclet number were determined by comparing the exact solution of the one dimensional equation (eqn. 6.25a) with solution obtained from central differencing and upwind differencing. It was found that CD gave realistic values for $|Pe| > 2$ and UD for all other values.

for HDS $\quad g = 1/2, \quad f = \frac{1}{2} + \frac{1}{Pe} \quad$ for $\quad -2 \leq Pe \leq 2$

$\quad g = 0, \quad f = 1 \quad$ for $\quad Pe > 2$

$\quad g = 1, \quad f = 0 \quad$ for $\quad Pe < 2$

values of the coefficients a_N^Φ; a_S^Φ, a_E^Φ, a_W^Φ can be calculated from the above relations, for example for a_N we have.

$Pe < 2 \qquad a_N^\Phi = C_N$

$-2 \leq Pe \leq 2 \qquad a_N^\Phi = D_N - \frac{C_N}{2}$

$Pe > 2 \qquad a_N^\Phi = 0$

The velocities used to calculate the convection coefficients are the upstream velocities for all the Φ equation and the momentum equations to be described below. This practice was adopted to ensure uniformity

in the calculation of coefficients for all equations. The densities and exchange coefficients were also the upstream ones.

6.4.4.3 Integration of the Momentum Equations

As explained in section 6.2 the momentum equations can be expressed in the same form as Φ equation with the extra terms, such as the pressure gradient, being absorbed by the linearized source term. In analogy with equation 6.30 the momentum equation becomes:

W-Momentum Equation

$$W_P = A^{\Phi}_W W_W + A^{\Phi}_E W_E + A^{\Phi}_S W_S + A^{\Phi}_N W_N + A^{\Phi}_u W_u + S^{\Phi}_{u,w} \qquad 6.31$$

U-Momentum Equation

$$U_P = A^U_W U_{WU} + A^U_E U_{EU} + A^U_S U_{SU} + A^U_N U_{NU} + A^U_U U_{UU} + S^U_{U,U} + DU(P_W - P_P) \qquad 6.32$$

V-Momentum Equation

$$V_P = A^V_W V_{WV} + A^V_E V_{EV} + A^V_S V_{SV} + A^V_N V_{NV} + A^V_U V_{UV} + S^V_{U,V} + DV(P_S - P_P) \qquad 6.33$$

where $DU = a'^{\Phi}_W / a^U_{PP}$, $DV = a'^{\Phi}_S / a^V_{PP}$

Here superscripts Φ, U, V show that the variables such as ρ, u, etc. are calculated with reference to Φ, U, V control volumes respectively. Also subscript WU denotes W side of U control volume similarly EU, WV etc.

6.5 Description of SIMPLE

In this solution procedure the velocities are obtained before the solution of any Φ field is attempted. The calculation of the velocity field requires solution of the three momentum equations and the continuity equation. This could be achieved very easily if the pressure field was known, which it is not. Patankar and Spalding (1972) have devised an algorithm named SIMPLE (Semi implicit method for pressure linked

equations) which they employed for the computation of 3-D boundary layer flows. The essence of SIMPLE is that a pressure field is guessed in the η-β plane (usually the upstream pressure field) to calculate the velocities and then it is corrected in such a way that the velocity field so obtained satisfies the continuity equation. SIMPLE is described in more detail below.

The W momentum equation is solved first, and since for the present problem $d\bar{p}/dz = 0$, the W velocities so obtained are exact. The V and U momentum equations 6.32 and 6.33 are then solved using the guessed pressure field which yields

$$V_P^* = A_N^V V_{NV}^* + A_S^V V_{SV}^* + A_E^V V_{EV}^* + A_W^V V_{WV}^* + A_U^V V_{UV}^* + S_{UV} + DV\,(P_S^* - P_P^*) \qquad 6.34$$

$$U_P^* = A_N^U U_{NU}^* + A_S^U U_{SU}^* + A_E^U U_{EU}^* + A_W^U U_{WU}^* + A_U^U U_{UU}^* + S_{UU} + DU\,(P_W^* - P_P^*) \qquad 6.35$$

where the (*) superscript denotes the values obtained from solving the momentum equations using the guessed pressure field. The 'starred' velocities will only satisfy the continuity equation if the guessed pressure is correct. An incorrect guess will give rise to a 'mass source' in each cell which can be calculated from equation 6.22 with guessed velocities replacing the exact values. Hence

$$M_P = (\bar{\rho}\bar{U}^*)_e\ a_e'^{\Phi} - (\bar{\rho}\bar{U}^*)_w\ a_w'^{\Phi} + (\bar{\rho}\bar{V}^*)_n\ a_n'^{\Phi} - (\bar{\rho}\bar{V}^*)_s\ a_S'^{\Phi} - (\bar{\rho}\bar{W})_n\,(ax)_n'^{\Phi} + (\bar{\rho}\bar{W})_s\,(ax)_s'^{\Phi} + (\bar{\rho}\bar{W})_P a_P'^{\Phi} - (\bar{\rho}\bar{W})_u a_u'^{\Phi} \qquad 6.36$$

where M_P is the mass source in the cell. If the above equation is substracted from 6.22 we have

$$- M_P = a'^{\Phi}_e \left(\bar{\rho}(\bar{U}-\bar{U}^*)\right)_e - a'^{\Phi}_w \left(\bar{\rho}(\bar{U}-\bar{U}^*)\right)_w$$

$$+ a'^{\Phi}_n \left(\bar{\rho}(\bar{V}-V^*)\right)_n - a'^{\Phi}_s \left(\bar{\rho}(\bar{V}-\bar{V}^*)\right)_s \qquad 6.37$$

or

$$-M_P = a'^{\Phi}_e \bar{\rho}U'_e - a'^{\Phi}_w \bar{\rho}U'_w + a'^{\Phi}_n \bar{\rho}V'_n$$

$$- a'^{\Phi}_s \bar{\rho}V'_s \qquad 6.38$$

Note that in the above equation U'_e is the velocity correction for the <u>east</u> side of the Φ control volume. Hence:

$$U'_e = (\bar{U}-U^*)_e \qquad \text{etc.}$$

Velocity corrections (U'_e etc.) can be calculated from their respective momentum equations. Substracting eqn. 6.35 from eqn. 6.32.

$$(\bar{U}_{PU} - U^*_{PU}) = U'_{W\Phi} = A^U_N U'_{NU} + A^U_E U'_{EU} + A^U_S U'_{SU} + A^U_W U'_{WU} + DU_W (P'_W - P'_P) \qquad 6.39$$

where $P'_S = \bar{P}_S - P^*_S$, similarly equations $U_{e\Phi}$ etc. can be written. The above velocity correction equation is not linear in the sense that it involves velocity corrections at the neighbouring nodes as well. This equation was linearized according to Patankar and Spalding (1972) so that

$$U'_{PU} = U'_{W\Phi} = DU_W (P'_W - P'_P) \qquad 6.40$$

and similarly

$$V'_{PV} = V'_{S\Phi} = DV_S (P'_S - P'_P) \qquad 6.41$$

Substituting equations for $U'_{W\Phi}$ and $V'_{S\Phi}$ and similarly equations for $U'_{e\Phi}$, $V'_{n\Phi}$ in equation 6.38 we have after simplification

$$P'_P = A^P_N P'_N + A^P_S P'_S + A^P_E P'_E + A^P_W P'_W + S^P_U \qquad 6.42$$

Where

$$A_N^P = (a_n'^{\Phi} \rho n_{\Phi} \; DV_N)/A_{PP}^P)$$

similarly A_S^P, A_E^P, A_W^P can be calculated.

$$S_{U\Phi}^{\Phi} = -M_P/A_{PP}^P$$

where $A_{PP}^P = a_e'^{\Phi} \rho_e \; DU_E + a_w'^{\Phi} \; \rho w \; DV_W + a_n'^{\Phi} \; \rho_n \; DV_N + a_S'^{\Phi} \; \rho_S \; DV_S$

Equation 6.42 is called the 'pressure correction equation' and this is solved to yield values of P', equations 6.40 - 6.41 are used to calculate the values of P', V' and U' are in turn used to obtain corrected velocities, and pressures as follows:

$$P_P = P_P^* + P_P'$$

$$U_{PU} = U_{PU}^* + U_{PU}'$$

$$V_{PV} = V_{PV}^* + V_{PV}'$$

6.6 Summary of the Solution Procedure

The solution for the various variables at a particular cross stream plane involves the following steps:

1) The W momentum equation is solved to yield the stream wise velocity field in the calculation plane. Since the stream wise pressure gradient is assumed to be zero, these velocities do not require correction.

2) The U and V momentum equations are then solved using a guessed cross stream pressure field which is the upstream pressure field. DV and DU are also calculated. The solution yields approximate velocity values U* and V*.

3) The pressure correction equation is then solved to give values of pressure corrections at every point in the field. The pressure corrections are in turn used to correct the cross stream velocities and pressures. The velocity field so obtained satisfies the continuity equation exactly, but the momentum equations are not. This inaccuracy is inherent to a marching procedure and can be minimized by taking small forward steps.

4) The finite difference equations for K, ε, $\bar{f}$ and $\bar{g}$ are solved in that order.

5) Knowing K and ε the turbulent viscosity is calculated.

6) Knowing $\overline{f}$ and $\overline{g}$ the probability distribution function is evaluated.

7) With the help of this PDf, time-mean values of m_{fu}, m_{ox}, m_{pr} temperature, and density are calculated.

8) This completes the solution in one cross-stream plane and a forward step is taken.

9) Steps 1-8 are repeated until the length of the solution domain is covered.

No iterations are performed in the cross stream plane, which means that steps 1-7 are performed once only at every step. This saves a great amount of computer time but necessitates approximations in the calculation procedure which are given below.

a) The use of upstream velocities and densities to evaluate convection coefficients. This practice assumes, as explained in section 6.4.4, that the variation in variables is stepwise in the ζ direction, which is not realistic.

b) At the end of each step the velocity field satisfies the continuity equation but does not necessarily satisfy the cross-stream momentum equation as well.

The above two errors will be negligible when a forward step size indpendent solution is obtained. It was found that at least four times

as much computer time was required when implicit coefficients were used with iterations at every step to achieve solutions of accuracy comparable with the present procedure. The use of implicit coefficients usually leads to a more stable solution procedure but instabilities were not a major problem in the present flow calculation. Hence the more expensive implicit coefficient method was not used.

6.7 Specification of Initial and Boundary Conditions

We now require to specify the initial and boundary conditions. Figure 6.8a shows the first cross stream plane at which the initial conditions were specified. The plane was divided into two parts, the inner circle bounded by the thick line representing the opening of the burner pipe. Grid nodes were provided in the stagnant surroundings as well as shown by the outer circle. This was done so that boundary conditions could be prescribed far away from the flow in the stagnant surroundings where they were known. More than one row of grid points in the outer circle was necessary to make the computational procedure stable. For the nodes in the inner half circle the variable fields were specified as fully developed pipe flow. In the outer circle zero values were given to all variables except the w-velocity which was given a very small value (0.1% of the maximum velocity in the cross stream plane). This was done to stabilize the calculation procedure

Boundary conditions were required at every cross stream plane for the boundaries AOB, ACB and O Fig. 6.8b. The boundary AOB was the plane of symmetry so that the U-velocity was zero and gradients of all other variables were also zero. At the point O, the centre of the grid, values of any variable stored were not required because the area is zero for this face of the cell.

The radial velocity V was however required at this point to calculate the mass flux at the south face of the first V-Cell. This velocity was calculated by assuming that the v-velocity at the centre was the mean of the velocities at the top and bottom V-nodes (V_a and V_b respectively) and in the OA direction.

$$V_O = \frac{V_a + V_b}{2} \qquad 6.43$$

The size of the first cell was also kept very small so that the error in calculation of the mass flux from the south face, because of inaccurate V_o, did not affect the accuracy of computations.

The boundary conditions for all variables at the free boundary ACB were those of the free stream except for the V-velocity which was calculated in the following manner. A momentum equation for V_B was solved assuming that P_N was known (free stream pressure). It was also assumed that the diffusion in the NS direction was negligible for this cell so AN = O. Now V_B^* and DV_B^V can be calculated from eqn. 6.34.

$$V_B^* = A_S^V V_{SV} + A_E^V V_{EV} + A_W^V V_{WV} + S_U^V + A_U^V V_{UV} + DV_B (P_B - P_{\text{free stream}})$$

The correction to V_B^* was calculated on the assumption that no pressure correction was required at the free stream or $P'_{\text{free stream}} = 0$ so that

$$V'_B = DV_B (P'_B) \qquad 6.44$$

and

$$\overline{V}_B = V_B^* + V'_B \qquad 6.45$$

Table 6.2 gives the summary of all the boundary conditions.

6.8 Validation of the Computation Procedure

In this section predictions of flows are reported which were made using the calculation procedure described in the previous sections. The purpose of these predictions was to test the computational accuracy of

Boundary	U	V	W	K	ε	f	g	ρ
Free stream	0	Eq. 6.45	0.1%	0	0	0	0	$\rho_{\text{free stream}}$
Centre of the grid	$\partial U/\partial r = 0$	Eq. 6.43	$\partial W/\partial r = 0$	$\partial K/\partial r = 0$	$\partial \varepsilon/\partial r = 0$	$\partial f/\partial r = 0$	$\partial g/\partial r = 0$	$\partial \rho/\partial r = 0$
Plane of Symmetry	0	$\partial V/\partial \beta = 0$	$\partial W/\partial \beta = 0$	$\partial K/\partial \beta = 0$	$\partial \varepsilon/\partial \beta = 0$	$\partial f/\partial \beta = 0$	$\partial g/\partial \beta = 0$	$\partial \rho/\partial \beta = 0$

Table 6.2

Boundary conditions for the prediction procedure

the procedure as well as the programming of the finite difference equations. Three types of flows were investigated.

- Flows for which analytical solutions are available.
- Flows for which predictions are available in the literature
- Flows for which reliable experiments are available in the literature.

Laminar Pipe Flow

Analytical solution of the fully developed velocity profile is available in the literature, Bird et al (1960), and since it also provided a test for the programming of the extra terms for the cylindrical co-ordinate system, this flow is first predicted. The three momentum equations together with the pressure correction equation are solved. Fluid properties are assumed constant and the axial pressure gradient is calculated using the procedure suggested by Patankar and Spalding (1972).

A plug flow velocity profile is given for the W velocity as initial condition. Initially V and U are given zero values. Fig. 6.9 shows the comparison between analytical axial velocity profile and the predicted profile, the agreement is almost perfect.

Developing Flow in a Square Duct

Equations solved and the initial conditions for this problem are the same as that for the pipe flow problem, except that changes are made to take into account the different geometry of the flow. Since no analytical solution is available for this developing flow, comparison with experiments Goldstein and Kreid (1967) are shown in Fig. 6.10.The agreement is quite reasonable. The fully developed velocity profile is also compared with the analytical solution fig, 6.11. The slight discrepancy is due to the predictions not being in the fully developed region.

Fully Developed Laminar Jet

In order to test the treatment of the free boundary described in section 6.7 a fully developed laminar jet was predicted. The results were compared with the analytical solution of these equations, Schilichting (1968). Fig. 6.12 and 6.13 show the comparisons for the radial profiles for the axial velocity and the radial profiles for the radial velocity respectively. In these figures Y_{max} denotes the width of the computational grid. Since the analytical solution is not valid in the developing region of the jet, fully developed W and V velocity profiles were calculated from the analytical solution and provided as initial conditions for the calculation procedure. Since the computational grid does not extend to infinity, the axial velocity is not zero at the free boundary. This velocity was calculated from the analytical solution as

$$W_{\text{free boundary}} = \frac{3}{8\pi} \frac{K'}{\nu z} \left(\frac{1}{(1+0.25\varepsilon^2)^2}\right)$$

$$\varepsilon = \sqrt{\frac{3}{16\pi}} \sqrt{\frac{K'}{\nu}} \frac{y_{max}}{z} \quad , \quad K' = 2\pi \int_0^\infty W^2 y \, dy$$

As can be seen from the figures agreement between the analytical solution and computations is almost perfect.

6.9 Closure

In this Chapter a numerical scheme has been presented to solve three dimensional boundary layer transport equations. It consists of expressing the transport equations in a quasi-orthogonal co-ordinate system in which the co-ordinate lines closely follow the stream lines. This set of equations is then converted to finite difference ones by integrating over a small control volume. The flow field is then calculated using Spalding's method of solving pressures linked equations. This

scheme has been applied to solve some test cases and the results obtained show that it is accurate. It will be used to compute the experimental flow in the turbulent diffusion flames in Chapter 7.

CHAPTER SEVEN

7.0 Prediction of Turbulent Diffusion Flames

7.1 Introduction

The numerical solution procedure developed in Chapter 6 has been used, in conjunction with the turbulence models described in Chapter 4 and the combustion model of chapter 5, to obtain prediction of turbulent jet diffusion flames. It is the purpose of this chapter to present these predictions and to compare them with experimental data. Predictions of a vertical diffusion flame have been compared with the data of Odidi (1974) and Asalor (1976). Predictions of a horizontal diffusion flame have been compared with the experimental data obtained in this study and presented in Chapter 2.

One of the purposes of predicting a vertical diffusion flame was to assess the ability of the turbulence and combustion models in this relatively simpler situation before going on to the more complicated horizontal diffusion flame. In this way it was thought that the deficiencies of the models that were due to the the three-dimensionality of the problem could be separated from their general short comings. For example, if the spreading rate of the temperature profile was underpredicted for both vertical and horizontal flames then the reason would be unlikely to lie in the modelling of the terms that arise solely in the transport equations of the horizontal flame. The vertical diffusion flame has been predicted by Naguib (1975) using virtually the same turbulence and combustion models. The results presented in his thesis did not include radial profiles of temperature and velocity in the initial region of the flame and hence were of little use in the detailed assessment of the models.

Two turbulence models have been presented in Chapter 4. Model I neglects the fluctuating density-velocity correlations whereas model II includes them. Model I has been used to predict both vertical and horizontal flames. Model II has been applied to the vertical flame only. The number of extra terms arising from density fluctuations reduces sub-

stantially in a two-dimensional situation, section 7.6, hence a vertical flame is more suitable to test this model than a horizontal one.

In the following section the procedure used to determine initial and boundary conditions is described. The initial conditions (fully developed pipe flow) and boundary condition (stagnant surroundings) are the same for vertical and horizontal flames.

Section 7.3 specifies the grid chosen for the predictions. Section 7.4 is concerned with the prediction of vertical flames. Mean temperature and velocity profiles are compared respectively with Odidi's (1974) data and Asalor's (1976) measurements in town gas diffusion flames. Predictions of horizontal town gas diffusion flames of Reynolds numbers 32500 and 23000 appear in section 7.5. Mean temperature and oxygen concentration profiles are compared with the data of the present study. The effect of including density fluctuations in the transport equation of the mixture fraction is studied in section 7.6. Concluding remarks appear in section 7.7.

7.2 Specification of Initial and Boundary Conditions

The initial conditions for all the flames were those of fully developed pipe flow. The specification of initial mean velocity profile was made by using the n^{th} power law, Shlichting (1968).

$$\frac{\bar{w}}{w_{max}} = (y/R)^{\frac{1}{n}} \qquad 7.1$$

Here

w_{max} = maximum velocity

y = distance from the pipe wall

R = radius of the pipe

The index n depends on the Reynolds number of flows and for Re = 23000 it takes a value of 6.6.

The mean initial kinetic energy profile was specified using the

experimental data of Laufer (1953). This data was normalized by the friction velocity w_τ. Hence to obtain the actual kinetic energy profiles w_τ for the present experiments had to be calculated. The friction velocity was calculated from the universal velocity-distribution law for smooth pipes

$$\frac{\bar{w}}{w_\tau} = \frac{1}{K} \ell n\left(\frac{w_\tau y E}{\nu}\right) \qquad 7.2$$

where

$$K = 0.42$$

$$E = 9.8$$

The velocity $\bar{w}$ at a given y was calculated from equations 7.1 and the value of w_τ was calculated by trial and error.

Experimental values for the dissipation of kinetic energy of turbulence in smooth pipes were not available, so this quantity could only be approximately specified. The shear stress at the wall, $\overline{w'v'}$, can be calculated from the following relation, Shlichting (1968):

$$\overline{w'v'} = \rho w_\tau^2 \qquad 7.3$$

Hence the production of kinetic energy, p_K, near the wall can be determined from:

$$p_K = \overline{w'v'} \frac{\partial \bar{w}}{\partial y} = \frac{\rho w_\tau^3}{Ky} \qquad 7.4$$

Where $\frac{\partial \bar{w}}{\partial y}$ is calculated from equation 7.2.

Assuming that the equilibrium relation

$$p_K = \rho \varepsilon \qquad 7.5$$

is valid throughout the pipe and also assuming a linear shear stress variation:

$$\overline{w'v'} = \rho w_\tau^2 \left(\frac{R-y}{R}\right) \qquad 7.6$$

we have:

$$\varepsilon(y) = \frac{w_\tau^3}{Ky}\left(\frac{R-y}{R}\right) \qquad 7.7$$

The above relation for ε is exactly true near the wall only. The sensitivity of the predictions to the initial profile of ε was tested by varying the value

of ε near the centre of the pipe by ±20%. The effect on predictions 13 burner diameters downstream (The first station at which predictions were compared with experiment) was negligible. The initial profile for the mixture fraction was uniform. The profiles for radial velocity $\bar{V}$, and tangential velocity $\bar{U}$, were uniform and zero.

The boundary values of all the variables were those of the free stream The entrainment velocity $\bar{V}_b$ was calculated from equation 6. In order to ensure numerical stability, $\bar{w}$ was given a value of $0.001W_{CL}$ at the free boundary. The gradients of all the variables at the axis of symmetry were zero for the vertical flames. The gradients of all the variables except $\bar{U}$ were zero at the plane of symmetry for the horizontal flame. The tangential velocity U was zero at the plane of symmetry. Table 7.1 summarizes these boundary conditions.

7.3 Grid Specification

The grid selected for the prediction of vertical flames had 17 grid nodes in the radial direction. The grid points were uniformly spaced. Tests were made for grid independence using up to 30 grid nodes. The initial forward step size was 1% of the half width ($y_{1/2}$) of the jet, the half width being the radius at which the velocity was 50% of the centre line velocity. It was found that computer time could be reduced considerably without affecting the accuracy by increasing the forward step size gradually to a maximum of 5% of $y_{1/2}$.

Grid dependency tests were conducted for the horizontal flame case and a uniformly spaced grid having 17 nodes in the radial and 9 nodes in the circumferential direction was found to be satisfactory. The forward step size was the same as that for the vertical flame.

7.4 Prediction of Vertical Flames

The results of the prediction of vertical diffusion flames presented in this section were obtained using the turbulence model, model I, described

Table 7.1

Boundary Condition for the Prediction Procedure (2-D Flame)

Variable	Axis of Symmetry	Stagnant Ambient
v	$dv/dr = 0$	Calculated from Eq. 6.45
w	$dw/dr = 0$	0.1% of centre line value
k	$dk/dr = 0$	0
ε	$d\varepsilon/dr = 0$	0
g	$dg/dr = 0$	0
f	$df/dr = 0$	0

Boundary Conditions for 3-D Flame

Variable	Centre of the Grid	Plane of Symmetry	Stagnant Ambient
v	Calculated from Eq. 6.43	$dv/d\theta = 0$	Calculated from Eq. 6.45
u	No specification required as area of the cell face is zero	0	0
w	"	$dw/d\theta = 0$	0.1% of centre line value
k	"	$dk/d\theta = 0$	0
ε	"	$d\varepsilon/d\theta = 0$	0
g	"	$dg/d\theta = 0$	0
f	"	$df/d\theta = 0$	0

in section 4.3. The constants used are listed in table 7.2. Before the results are presented it would be appropriate to discuss the basis of selection of the turbulence constants. Naguib (1975) had predicted vertical flames and initial guidance in selecting the constants was obtained from his work. Table 7.3 gives the constants used by him. The value of the constant associated with the production of dissipation, $C_{\varepsilon 1}$, chosen by him was 1.44, the value for a plane jet. As pointed out in section 4.2.4, $C_{\varepsilon 1}$ had to be changed to 1.57 to obtain the correct spreading rate in the fully developed region of an inert round jet. Hence it was decided to 'anchor' C_1 to 1.57 and predict Odidi's flame keeping all other constants the same as used by Naguib.

The temperature profiles thus obtained were similar to those presented in fig. 7.3 to 7.7 (Fig. 7.3 to 7.7 are discussed below). It was then decided to predict Asalor's flame to check the predictions of mean velocity. It was found that the centre-line velocity decay was too slow and consequently the spreading rate of the velocity was also lower than the experimental one. In order to correct this error $C_{\varepsilon 2}$ was gradually increased. The constant $C_{\varepsilon 2}$ was modified, instead of $C_{\varepsilon 1}$, as an increase in its value brought it near to its 'inert' value. It was found that with $C_{\varepsilon 2} = 1.92$ the error in the centre line velocity decay although still large in the initial region of the flame (Z/D <40) was small further downstream. The value of $C_{\varepsilon 2}$ could not be increased further because then the decay rate of velocity in the downstream region was overpredicted. This modification to $C_{\varepsilon 2}$ ruined completely the prediction of axial distribution of temperature. To bring the temperature distribution nearer to experiment σ_f and σ_g had to be increased from 0.7 to 0.9. These constants are different from those used by Naguib but gave better predictions of both velocity and temperature. They were subsequently used to predict both the vertical and horizontal flames.

The axial distribution of mean velocity is given in Fig. 7.1, whereas

Table 7.2

Values of Adjustable Constants Used in the Present Study

Constant	C_μ	$C_{\varepsilon 1}$	$C_{\varepsilon 2}$	C_{g1}	C_{g2}	σ_ρ	σ_f
	0.09	1.57	1.92	2.8	1.92	4.0	0.9

Constant	σ_g	σ_k	σ_ε
	0,9	1,0	1.3

Table 7.3

Values of Adjustable Constants Used by Naguib (1975)

Constant	C_μ	$C_{\varepsilon 1}$	$C_{\varepsilon 2}$	C_{g1}	C_{g2}	σ_ρ	σ_f
	0.09	1.44	1.78	2.8	1.78	-	0.7

Constant	σ_g	σ_k	σ_ε
	0,7	1.0	1.3

Fig. 7.2 shows the radial profile of mean axial velocity at Z/D = 39. Experimental profiles at stations further downstream were not available. These figures show that the initial centre-line velocity decay is much faster than predicted. Consequently the spreading rate of mean velocity is underpredicted. This defect, as can be seen from Fig. 4.2, is present in the prediction of inert flows as well, though to a much lesser extent.

The axial distribution of mean temperature is presented in Fig. 7.3. The temperature profile can be divided into three parts. One, from 0-30 diameters where the temperature is underpredicted. Two, from 30 to about 110 diameters where the temperature is overpredicted. Three, from 110 diameters onwards where the temperature is again underpredicted. The discrepancy between maximum temperature calculated and measured is about 50°K. In overall terms this profile shows that the predicted flame is shorter which means that the fuel is being consumed more rapidly than the measurements suggest. This is also evident from the higher temperature predicted in region 2.

The radial distribution of mean temperature at 10, 40 and 90 diameters is presented in Figs. 7.4 to 7.6. The measured profile at ten diameters exhibits a sharp peak in the mean temperature which is absent from the predicted profile. The absence is perhaps due to the concentration fluctuations being over predicted. Measurements of the mean values of mixture fraction and its fluctuation would have been helpful to substantiate the observation made above, but unfortunately they are not available. In fact reliable measurements of $\bar{f}$ and g will help greatly in the better understanding of combustion.

Mean temperature profiles at Z/D = 40 and Z/D = 90 show that the predicted spreading rate is less than the measured one. The shape of the temperature profile is, however, predicted correctly. This can be seen from fig. 7.7 in which the non-dimensional predicted and measured profiles are presented at Z/D = 90. The radius is normalized by $R_{T,1/2}$, which is the distance from the centre to the point where the temperature is

half its maximum value. The ratio of $R_{T,1/2}$ measured to $R_{T,1/2}$ predicted is about 1.28 which gives some idea of the relative spreading rates.

The following points emerge from the above discussion regarding the performance of the prediction procedure for vertical flames.

1) The maximum temperature levels are equal to those measured.
2) The shape of the temperature profile is correct.
3) The spreading rate of velocity is low.
4) The centre line decay of axial velocity is low in the initial regions of the jet.
5) The rate of increase in the centre line temperature in most parts of the flame is higher than measured.
6) The spreading rate of temperature is low.

The deficiency in the model which gave rise to points 3 and 4 could be corrected if it was independent of the temperature predictions. In fact Morse (1976) has introduced a modification to the disssipation equation (using a five equation turbulence model) which correctly predicts the centre line velocity decay for the initial region as well as the final part of the jet. But point 5 is in apparent conflict with 3 and 4. The conflict arises because if the velocity spread is increased it will mean increased mixing which in turn means even higher centre line temperatures.

The reasons which may cause the above conflict are listed below.

1) The relation, $\Gamma_f = \frac{\mu}{\sigma_f}$, does not hold true, hence mixing of momentum is different from the mixing of scalars. In which case an equation for $\overline{u'f'}$ has to be solved. There is little evidence to show that this is the case in free turbulent jets. The actual value of σ_f may be in doubt but the shape of the profile is the same as that of velocity is confirmed by many experiments. Also, Naguib (1975) predicted reasonably correctly the radial profile for the mixture fraction in inert jets using a constant value of σ_f.

2) The fluctuations in the mixture fraction are larger than those predicted. Larger fluctuations in the mixture fraction will lead to larger fluctuations in temperature and will consequently decrease the mean value of temperature. The fluctuations in mixture fraction were increased by reducing C_{g2} (The constant associated with dissipation term of $\overline{f'^2}$ equation) from 1.92 to 1.4 but there was no appreciable decrease in the mean temperature at the centre line in the initial region of the flame. Also the shape of the assumed Pdf in the central region of the jet is very near to reality, section 6. This possibility is therefore excluded.

3) The actual mean value of the fuel concentration is greater than that predicted by the combustion model. It has been argued above that the mean value of the mixture fraction seems to be correctly predicted, so if fuel is underpredicted it means that combustion does not necessarily take place when fuel and oxident come together. Unfortunately mean concentration of fuel was not measured for the present flame, but Kent and Bilger (1976), who have used virtually the same combustion model, have als underpredicted the mean value of fuel concentration at X/D = 80 by about 40% in a hydrogen diffusion flame. It is interesting to note that their estimate of mean temperature is also generally similar to the present predictions.

The under estimation of the fuel concentration seems to the author to be the most probable cause of the defect in the combustion model and as such needs further explanation.

In the present combustion model there are two basic assumptions:

1) Combustion takes place whenever fuel and oxident are mixed, that is the reaction is mixing controlled.

2) The products formed are CO_2 and H_2O without any intermediates.

In a diffusion flame, situations can arise where either or both of these assumptions do not hold true.

In the initial region of the flame, near the nozzle exit, the shear is very high and it is possible that these high stretching rates of fuel and oxident eddies cause the mixing times to be shorter than the reaction time. The phenomenon of a lifted diffusion flame, it has been argued, Paauw and Bakker (1976), occurs because reactant input into the reaction zone which can be assumed to be a fully stirred reactor becomes larger than the critical limit. Although the present flame was not lifted, it was operating near the lift-off limit and the combustion efficiency in the initial region may well have been less than 100%.

The flame surface in a turbulent flame is broken and continously fluctuating. This may give rise to 'gates' in the flame surface where the instantaneous temperature is much lower than the flame temperature. It is possible for a pocket of oxidant to be engulfed through one of these gates so that it remains cool when it comes in contact with a fuel packet and no reaction is initiated. These two packets (and several of this kind) will mix to form eddies of different fuel air ratios. Combustion will only occur when these eddies are heated to the ignition temperature of that particular fuel-air ratio. The premixing of fuel and oxident can give rise to eddies having a fuel-air ratio which is beyond the flammability limits of the mixture and they will have to await further break-up before combustion can occur.

Measurements which would yield direct evidence of premixing in a diffusion flame have yet to be made. Instantaneous measurement of fuel and oxident would reveal it, but such measurements are almost impossible to perform in practical situations. It is nevertheless evident that if premixing occurs in diffusion flames to a large extent the present combustion model is incapable of handling it. Determination of mean species concentration in a diffusion flame show that combustion does occur in premixed eddies. For example measurements of Lenze et al (1975) in city gas diffusion flames, which are essentially clear and soot free, show that substantial

amounts of carbon monoxide are produced during combustion. If reaction takes place only at the boundary of the reactant eddies, fuel and oxidant will burn at or near stiochemetric ratio and very little carbon monoxide will be produced in the downstream region of the flame. The fact that experiments show production of CO points to, in the opinion of this author, premixing of fuel and oxidant in diffusion flames.

The phenomenon of premixing also produces stable intermediates such as carbon monoxide. The production of CO occurs, if chemical kinetics is fast, only when fuel rich packets burn and there is insufficient oxygen to convert all CO to CO_2. The intermediate CO will reduce the amount of heat release and in consequence the temperature will be lower than it would be if only one step reaction took place.

The removal of the above mentioned defects involved substantial modifications to the procedure and was not attempted.

7.5 Prediction of Horizontal Flames

The results of the prediction of horizontal flames presented in this section were obtained using the turbulence and combustion model and the constants employed to predict the vertical flames in section 7.4.

There are several notable points of agreement between the data and predictions. The distribution of mean temperature along the vertical y-axis for flame I (Re No. = 32500) at Z/D = 35.4 and 47.0 is shown in Figs. 7.8 and 7.9. In these and all the following figures for horizontal flames the right-hand side (or + ve side) of the graph represents the top half of the flame and left-hand side represents the bottom half. It can be seen that the shape of the profiles is similar to the measured ones. Maximum temperature is also predicted only in the top half of the flame (Y > 0) as was measured experimentally. This also accounted for the high temperature island shown in Figs. 2.10 and 2.11. Again, as measured

experimentally the gradients in the temperature profiles are predicted to be steeper in the lower half of the flame than in the upper half. The maximum temperature predicted is also not at Y = 0 but is shifted upwards as was found experimentally.

The quantitative agreement is only fair and the reasons are, one can suppose, the same as those which caused the discrepancies in the prediction of vertical flames. If the top half of the temperature profile is examined, fig. 7.8, it can be seen that the predicted and measured radial profiles are very similar to those of the vertical flame, fig. 7.2. The spread of the temperature profile is, on the whole, underpredicted and its magnitude at the centre is also higher than measured. Hence it can be assumed that the modifications to the turbulence and combustion model providing better quantitative predictions of a two-dimensional flame will also improve the predictions of a three-dimensional one.

Note that the fact that the spread of the predicted profile for the lower portion of the three-dimensional flame, figs. 7.8 and 7.9, is apparently somewhat greater than the measured one, does not invalidate the above conclusion. This simply reflects the smaller buoyancy of the predicted flame consequent of its smaller cross section. If the predicted profile in Fig. 7.8 is shifted by about one diameter to the right it will be seen that the comparison between predicted and measured profiles at the bottom will also become similar to that of the two-dimensional flame discussed in the previous section. The maximum temperature predicted is about 100°K higher than its measured value. This was also true for a two-dimensional flame, but it is, in itself, not an important cause of disagreement between experiment and prediction.

Predictions of mean temperature and oxygen concentration for flame II (Re = 23000) are presented in figs. 7.10 to 7.13. In general the performance of the combustion and turbulence models is the same that for flame I. The prediction of another scalar ($\overline{m_{ox}}$) also follows the same trend. We

see qualitative agreement between experiment and predictions. The particular feature of the maximum temperature occuring at the top is predicted. The effect of gravity on the stream lines is also evident.

The deficiencies of the model are also apparent. The spread of mean temperature is underpredicted and consequently the predicted values of $\overline{m}_{ox}$ are higher than the measured ones. At Z/D = 13 and 29 figs. 7.10 and 7.11 the maximum predicted temperature is lower than its actual value. The reason is perhaps the same that caused the maximum temperature to be underpredicted at Z/D = 10 for a two-dimensional flame, viz. the fluctuations in concentration being overpredicted.

7.6 Prediction of Vertical Flames with Model II

In Chapter 4, model II was described which took into account the effect of density fluctuations on turbulent reacting flows. This model was used to predict the vertical flame of Odidi.

The essential feature of model II, as explained in Chapter 4, is that it retains all the terms containing double fluctuating density-velocity correlations, $\overline{\rho'u'}$ for example, in all the transport equations. These correlations were modelled using Bousenesq's hypothesis. The triple fluctuating density-velocity correlations such as $\overline{\rho'u'v'}$ and fluctuating scalar-density correlations such as $\overline{\rho'f'}$ were dropped from all equations. It decided to use this model to predict a vertical flame as in this case $\frac{d\overline{V}}{d\theta}$ was zero and $\frac{d\overline{W}}{dz}$ could be neglected. This reduced the number of extra terms appearing in the transport equations and made the computational task simpler than it would have been if a three-dimensional flame was predicted.

Model II also required specification of σ_ρ, and initially following recommendation of Bray (1974) it was assigned a value of unity. When predictions were made using this value it was found that the calculation procedure was unstable and σ_ρ had to be increased greatly to obtain stable

predictions. The minimum value of σ_ρ that gave stable solution was 4. The results so obtained are not very different from those of model I, particularly at Z/D 40 where density gradients are less severe. The results were understandable as σ_ρ was so large that it reduced the effect of density fluctuations by a factor of four as compared to $\sigma_\rho = 1$.

The likely reason for the predictions being unstable for $\sigma_\rho = 1$ can be seen from fig. 7.14, where the radial profile of the mixture fraction at Z/D = 20 is plotted for three cases: 1. fluctuations in density are neglected; 2. when they are included with $\sigma_\rho = 4$; and 3. when $\sigma_\rho = 1$. To isolate the effect of density fluctuations on the mixture fraction, density fluctuations were neglected in all other equations during these tests.

It can be seen from fig. 7.12 that when $\sigma_\rho = 4$ the predictions are similar to those obtained by neglecting density fluctuations. The predictions of temperature, fig. 7.14, are also similar for the two cases. When $\sigma_\rho = 1$ there is a curious dip in the $\overline{f}$ profile at R/D $\simeq$ 1.45. Since the mixture fraction is a conserved property, the effect of including density fluctuation terms can only be to redistribute $\overline{f}$. Hence the reduction in $\overline{f}$ at R/D $\simeq$ 1.45 increases its value at R/D $>$ 1.45. This distribution of the mixture fraction causes an unnatural dip in density which is fed back to the momentum equations and causes instabilities.

The above exercise suggests that all density fluctuation terms ($\rho' f'$ in $\overline{f}$ equation for example) will have to be included in the transport equations to investigate the effect of lower values of σ_ρ. The $\overline{\rho' f'}$ terms may be expected to compensate for the dip in $\overline{f}$ profile for $\sigma_\rho = 1$. There is also a possibility that σ_ρ is high, but this should await experimental verification.

7.7 Concluding Remarks

Predictions of vertical flames have been made with and without including density fluctuations. Predictions of horizontal flames have also been made neglecting the fluctuations in density.

The results are in qualitative agreement with experiment; all important features of both vertical and horizontal flames are predicted. The error in the prediction of maximum temperature in both flames is less than 5%. Quantitative agreement is not very good, due to two major reasons: 1. the turbulence model underpredicts the centre line velocity decay in the initial regions of the jet; 2. the combustion model underpredicts the mass fraction of fuel on the centre line which in consequence overpredicts the temperature.

The effect of including density fluctuations is negligible at high values of σ_ρ, the lower values can not be investigated as they result in an unstable computational procedure. Lower values of σ_ρ can only be investigated if all the density fluctuation terms are included in the model.

CHAPTER EIGHT

8.0 Closure

8.1 Attainment of Objectives

A statement of the objectives of the work of this thesis was made in chapter 1; for convenience they are now restated:

1) To obtain reliable measurements of mean scalar quantities in buoyancy influenced free-jet diffusion flames.

2) To predict these flames using turbulence and combustion models which have been used to predict two dimensional flames and to assess their applicability to three-dimensional situations.

The work reported is now summarized with a view to showing the extent to which the objectives of the research program have been attained. Chapter two is concerned with the experimental program which includes the design and fabrication of the experimental rig and the measuring systems for the mean temperature and oxygen concentration. Results obtained from these experiments are also presented. The accuracy of measurements is estimated to be $\pm 3.0\%$. The experimental work reported shows that the first objective is achieved.

The prediction of the flow constitutes the second objective and the procedure requires three main components.

1) The turbulence model.

Chapter 4 is concerned with the selection of a suitable turbulence model. An effective viscosity model (model I) is selected which employs two parameters (kinetic energy of turbulence and its dissipation) to obtain the turbulent viscosity of the flow. The Reynolds stresses are then obtained using a modified form of Boussinesq hypothesis for variable density flows. Model II takes into account the effect of density-velocity fluctuations by approximating them as being proportional to the gradient in density.

2) The Combustion Model

Chapter 5 describes the combustin model which is based on single step irreversable chemical reaction. Mixing between oxidant and fuel is described by the mixture fraction which is formulated in such a way as to contain no source term. A clipped Gaussian distribution function is used to simulate the temporal behaviour of the mixture fraction. This model is used to calculate the species mass fractions, temperature and density.

3) The Numerical Scheme

Chapter 6 describes the numerical scheme employed to solve the set of partial differential equations of model I and II. The equations are cast into a curvilinear co-ordinate system and discretized by integrating over a control volume. The finite-difference equations so obtained are then solved using SIMPLE method of solving pressure linked equations.

The turbulence model and the combustion model are incorporated in the numerical scheme to predict the horizontal diffusion flame. Predictions of vertical flames are also made in order to assess the models in more detail. Comparison of predictions of horizontal and vertical flames shows that the models are able to predict the horizontal flame as successfully as they predict the vertical one. Important features of the horizontal flame observed in experiments are also predicted.

8.2 Suggestions for Future Work

8.2.1 Experimental Work

The present study reports measurements of mean temperature and oxygen concentration. There is a need to extend the experimental work to obtain mean values of fuel and mixture fraction. These measurements will lend experimental support to the conclusion that the present combustion model underpredicts the fuel concentration on the axis of the flame. Mean values of

velocities and turbulence quantities shear and normal stresses are also required. These quantities will help in judging the performance of the turbulence model directly, because only indirect assessment is possible by the prediction of scalars such as mean temperature.

Measurement of the Pdf of temperature and other scalars in flames will enable a more realistic form of the function to be chosen. To determine the importance of density fluctuations measurement of its correlation with velocity and scalars is essential. These measurements should preferably be carried out in simple situations such as a hot vertical jet before venturing into a horizontal flame.

8.2.2 Theoretical Work

1) Turbulence Model

It was seen that the turbulence model was unable to predict the correct centre-line decay of mean velocity in the initial region of the jet. This defect in the model was one of the major causes for the unsatisfactory predictions of the horizontal as well as the vertical flames. Though this defect can be removed by modifying the constants in the dissipation equation, Morse (1976), the resulting model then fails in predicting other flows such as a plane jet. Work on turbulence is therefore required to formulate a model which predicts at least a class of turbulent flows, such as 'free turbulent boundary layers', equally well. Otherwise practical flows which are often a combination of simple flows will not be predicted correctly.

The role of density fluctuations in turbulent reacting flows in unclear. The best way to model these fluctuations is also debatable. There is therefore a need to predict a 'test flow', such as a vertical diffusion flame, using both Favre averaging and Bray's approach. The results can then be compared with experiment to evaluate the merits of both approachs.

2) Combustion Model

The combustion model employed to predict the present flames assumes that combustion takes place whenever fuel and oxidant are mixed, regardless of the temperature and fuel-air ratio of the resulting mixture, and that no intermediate products are formed during combustion. It has been argued in Chapters five and seven that in practical flames the above assumptions are not always applicable. In future predictions the combustion model should be modified to take into account the stretching rates of the eddies, the flamability limits of the fuel-air mixture and the possibility that intermediates can be produced if reaction takes place in eddies which are fuel rich.

3) Numerical Scheme

There is a need for the transport equations to be solved in a general curvilinear co-ordinate system, so that complex geometries that occur in practical situations can be handled economically. It will then be possible to follow the flame boundary closely even when the curvature in the flame is large. This computational procedure will also be able to predict flows in practical furnaces where a circular burner discharges fuel into a rectangular furnace.

LIST OF REFERENCES

Amsden, A.A. and Harlow, F.H.(1970) "The SMAC method: a numerical technique for calculating incompressible fluid flows", Los Alamos Scientific Laboratory, LA-4370.

Andrew, G.E., Bradley, D. and Levakabamba, J.B. (1975) "Turbulence and flame propagation - a critical appraisal" Combustion and Flame, 24, 285.

Asalor, J.O. (1976) "Local properties in turbulent flames" Ph.D. Thesis, London University.

Ballantyne, A., Boon, D.J. and Moss, J.B. (1976) "Measurements of fluctuating temperature in open diffusion flames using fine wire thermocouples" University of Southampton, Department of Aeronautics and Astronautics Memo No. 76/3.

Bergeles, G. (1976) "Three dimensional discrete-hole cooling processes. An experimental and theoretical study" Ph.D. Thesis, London University.

Berkenbush, F. (1899) "Radiation error corrections by the emmissivity method calibration in vaccum", Weid Ann. 67, p. 649.

Bilger, R.W. (1975) "Turbulent jet diffusion flames" Progress in Energy and Combustion" Vol I, Pergamon.

Bilger, R.W. and Beck, R.E. (1974) "Further experiments in turbulent jet diffusion flames" Fifteenth International Symposium on Combustion, The Combustion Institute.

Bilger, R.W. and Kent, J.H. (1972) "Concentration fluctuations in turbulent jet diffusion flames" Charles Kolling Research Laboratory, Tech. Note, F-46, Sydney,Australia.

Bird, R.B., Stewart, W.E. and Lightfoot, E.N. (1960) "Transport Phenonmenon" Wiley International Edition.

Borghi, R. (1974) "Chemical reactions calculations in turbulent flows: Application to a co-containing turbojet plume" Advances in Geophysics, Academic Press, 18B, p. 349.

Bradshaw, P., Ferris, D.H. and Alwell, N.P. (1967) "Calculation of boundary layer development using the turbulent energy equation" J. Fluid Mech. 28, 593.

Bradshaw, P. (1971) "An Introduction to Turbulence and its Measurement" Pergamon, Oxford.

Bray, K.N.C. (1974) "Kinetic energy of turbulence in flames" University of Southampton, Department of Aeronautics and Astronautics Report AASU No. 332.

Carretto, L.S., Gosman, A.D., Patankar, S.V. and Spalding, D.B. (1972) "Two calculation procedures for steady three-dimensional flows with recirculating" Proceedings of the Third International Conference on Numerical Methods in Fluid Mechanics.

Corrison, S. (1952) "Heat transfer in isotropic turbulence" J. Appl. Phys, 23, 113.

Damokohler, G. (1940) "The effect of turbulence on flame velocity in gas mixtures" Z. Elektrochem. Vol. 46, No. 11 English Translation NACA TM1112.

Dixon-Lewis, G. (1970) "Flame structure and flame reaction kinetics V. Investigation of reaction mechanism in a rich hydrogen-oxygen-nitrogen flame by solution of conservation equations" Proc. Roy. Soc. Lond. A.317, 235-263.

Eikoff, H.E. (1973) "Experimental investigation of the influence of combustion on turbulent transport in jet diffusion flames" Combustion Institute European Symposium p. 513.

Elgobashi, S.E., Pun, W.M. and Spalding, D.B. (1973) "Concentration fluctuations in isothermal turbulent confined co-axial jets" Imperial College, Mech. Eng. Dept. Rpt. HTS/73/54.

Elgobashi, S.E. (1975) "Characteristics of gaseous turbulent diffusion flames in cylindrical chambers, a theoretical and experimental investigation". Ph.D. Thesis, London University.

England, C., Houseman, J. and Teixeira, D.P. (1973) "Sampling nitric oxide from combustion gases" Combustion and Flame Vol. 20 No. 3.

Favre, A. (1969) "Statistical equations of turbulent gases" Problems of Hydrodynamics and Continui Mechanics, Society for Industrial and Applied Mechanics, Philadelphia, P.A. p. 231.

Friedman, R. (1953) "Measurement of temperature profile in a laminar flame" Fourth International Symposium on Combustion, The Combustion Institute.

Friedman, R. and Bruke, (1954) "Measurement of temperature distribution in low-pressure flat flame" J. Chemical Physics, 22, 824.

Friedman, R. and Cyphers, J.A. (1955) "Flame structure studies III, Gas sampling in low-pressure Propane-Air flame" The Journal of Chemical Physics Vol. 23 No. 10.

Fristrom, R.M. and Westenberg, A.A. (1965) "Flame Structure" McGraw Hill New York,

Gaydon, A.G. and Wolfhard, H.G. (1970) Flames: Their Structure Radiation and Temperature Chapman and Hall Ltd.,

Goldstein, R.J. and Kried, D.K. (1967) "Measurement of laminar flow development in a square duct using a laser doppler flowmeter" J. Appl. Mech. (ASME) 34, p. 813.

Gosman, A.D. Pun, W.M., Runchal, A.K., Spalding, D.B. and Wolfshtein, R. (1969) Heat and Mass Transfer in Recirculating Flows Academic Press.

Gosman, A.D. and Lockwood, F.C. (1973) "Predictions of the influence of turbulent fluctuations on flow and heat transfer in furnaces" Imperial College, Dept. of Mech. Eng. Rpt. HTS/73/52.

Hamming, R.W. (1962) Numerical Methods for Scientists and Engineers, McGraw Hill, New York,

Hawthorne, W.R., Weddell, D.S. and Hottel, H.C. (1949) "Mixing and Combustion in turbulent gas jets" Third Symposium (International) on Combustion. The Combustion Institute.

Hanjalic, K. and Launder, B.E. (1971) "A Reynolds stress model of turbulence and its application to asymmetric boundary layer". Imperial College, Dept. of Mech. Eng. Rpt. No TM/TN/A/8.

Harlow, F.H. and Nakayoma, P.I. (1967) "Transport or turbulence energy decay rate" Los Alamos Science Lab., University of California Rpt. LA3859.

Hinze, J.O. (1959) Turbulence McGraw Hill Inc.

Kent, J.H. (1970) "A non-catalytic coating for platinum-rhodium thermocouples" Combustion and Flame. 14, p. 279.

Kent, J.H. and Bilger, R.W. (1976) "The prediction of turbulent diffusion flame fields and nitric oxide formation", Charles Kolling Research Lab., Tech. Note F-82 Sydney, Australia.

Khalil, E..E., Spalding, D.B, and Whitelaw, J.H. (1975) "The calculation of local flow properties in two dimensional furnaces" Int. J. Heat Mass Transfer, 18, p. 775.

Khalil, E.E. (1977) "Flow and combustion in axi-symmetric furnaces", Ph.D. Thesis, University of London.

Klaukens, H. and Wolfhard, H.G. (1948) "Measurements in the reaction zone of a bunsen flame" Proc. Royal Society A193, 512.

Knight, J.R, and Rhys, D.W. (1961) The Platinum Metals in Thermometry Engelhard Industries Ltd, U.K.

Kolmogorov, A.N. (1942) "Equation of turbulent motion of an incompressible turbulent" Izv. Akad. Nauk. SSSR ser Phys. VI, No. 1-2, 56.

Laufer, J. (1953) "The structure of turbulence in fully developed pipe flow" NACA TN 2954.

Jones, W.P. and Launder, B.E. (1972) "The calculation of low Reynolds number phenomenon with a two-equation model of turbulence" Imperial College, Mech. Eng. Dept., Rpt. TM/TN/A/17.

Launder, B.E., Morse, A.P., Rodi, W. and Spalding, D.B. (1972) "The prediction of free shear flows - a comparison of six turbulence models" NASA Report SP-311, p. 361.

Launder, B.E., Reece, G.J. and Rodi, W. (1975) "Progress in the development of a Reynolds-stress turbulence closure", J. Fluid Mech. 68, p. 537.

Launder, B.E. (1976) "Heat and mass transport" Turbulence: Topics in Applied Physics. Editor P. Bradshaw, Springer-Verlag-Berlin.

Launder, B.E. and Spalding, D.B. (1972) Mathematical Models of Turbulence Academic Press, London.

Launder, B.E. and Spalding, D.B. (1973) "The numerical computations of turbulent flows" Imperial College, Mech. Eng. Dept. Rpt. HTS/73/2.

Launder, B.E. and Ying, W.M. (1972) "Prediction of flow and heat transfer in ducts of square cross-section" Proc. I. Mech. E. Vol. 187 p. 455.

Lazara, C.P. and Biordi, J.C. (1973) "Concentration profiles of radical species in a Methane-Oxygen-Argon flame" Combustion and Flame Vol. 21, p. 371.

Lenze, B., Milano, M.E. and Gunther, R. (1975) "The mutual influence of multiple jet diffusion flames" Combustion Science and Technology, vol. 11, 1.

Mathews, L. and Whitelaw, J.H. (1971a) "Plane jet over backward facing step" Imperial College, Mech. Eng. Dept. Rpt. HTS/71/29.

Mathews, L. and Whitelaw, J.H. (1971b) "The prediction of film cooling in the presence of recirculating flows with two equation model" Imperial College, Mech. Eng. Dept. Rpt. HTS/71/31.

Mason, H.B. and Spalding, D.B. (1973) "Prediction of reaction rates in turbulent premixed boundary layer flow" Imperial College, Mech. Eng. Dept. Rpt. HTS/73/11.

Morse, A.P. (1976) Private Communication.

Mujumdar, A.K. and Spalding, D.B. (1975) "The numerical computation of flow in rotating ducts by a parabolic procedure". Imperial College Mech. Eng. Dept. Rpt. HTS/75/14.

Naguib, A.S. (1975) "The prediction of axisymmetrical free jet, turbulent reacting flows" Ph.D. Thesis, University of London.

Nee, V.W. and Kovazney, L.S.G. (1969) "The calculation of the incompressible boundary layer by a simple theory" Physics of Fluids, Vol. 12, p. 473.

Nielson, P.V. (1976) "Flow in air conditioned rooms" (English translation of Ph.D. Thesis from Technical University of Denmark, Copenhagen) Danfoss A/S, Denmark.

Odidi, A.O.O. (1974) "The influence of turbulence on the time mean rate of reaction" Ph.D. Thesis, University of London.

Paauw, Th.T.A. and Bakker, R.P.W. (1976) "USe of well stirred reactor concept for the prediction of flame stabilization" 4th Members Conference, International Flame Research Foundation.

Patankar, S.V. and Spalding, D.B. (1970) Heat and Mass Transfer in Boundary Layers Intertext Books, London.

Patankar, S.V. and Spalding, D.B. (1972) "A calculation procedure for heat, mass and momentum transfer in three-dimensional parabolic flows" Int. J. Heat Mass Transfer, Vol. 15, p. 1787.

Pope, S.B. (1976) "The calculation of flows behind bluff bodies with and without combustion" Ph.D. Thesis University of London.

Prandtl, L. (1925) "Uber die Ausgebildete Turbulenz" Zamm 5, p. 136.

Prandtl, L. (1945) "Uber ein neves Formel system fur die ausgebildete Turbulenz" Nachr, Akad. Wiss., Gothingen, Math. Phys. Kl. p. 6.

Pratap, V.S. (1975) "Flow and heat transfer in curved ducts" Ph.D. Thesis. University of London.

Priddin, C.H. (1975) "The behaviour of the turbulent boundary layer on curved, porous walls" Ph.D. Thesis, University of London.

Pun, W.M. and Spalding, D.B. (1967) "A procedure for predicting the velocity and temperature distributions in a confined, steady, turbulent, gaseous, diffusion flame" 18th International Astronautical Congress, Belgrade.

Richardson, J.N., Howard, Jr. H.C. and Smith, Jr. R.W. (1953) "The relation between sampling-tube measurements and concentration fluctuations in a turbulent gas jet", Proc. 4th Symposium (International) on Combustion, The Combustion Institute, p. 814.

Rein, C.R. and O'Laughlin, J.R. (1967) "Correction for radiation absorbed by electrically heated wire temperature sensors in flames" AIAA Journal Vol. 5 (10).

Ris, J. De. (1976) Private Communication to Dr. F.C. Lockwood.

Rodi, W. (1972) "The prediction of free turbulent boundary layers by use of a two equation model of turbulence" Ph.D. Thesis - University of London.

Rose, W.G. (1962) "A swirling round turbulent jet. Mean flow measurements" J. Appl. Mech. Vol. 29, 615.

Rouse, H. (1959) Advanced Mechanics of Fluids Wiley, New York, p. 520.

Schlichting, H. (1968) "Boundary Layer Theory" McGraw Hill Book Co.

Scotsmann, P. (1970) "Temperature measurement by thermocouples including errors caused by catalytic effects" AGARAD-CP-73-71 Agarad Proceedings No. 73 on High Temperature Turbines.

Scurlock, A.C. and Grover, J.H. (1953) "Propagation of turbulent flames" Fourth Symposium (International) on Combustion p. 645.

Sharma, D. (1974) "Turbulent convective phenomena in straight rectangular sectioned diffusers" Ph.D. Thesis, University of London.

Shelkin, K.L. (1943) "On combustion in a turbulent flow" J. Tech. Phys. (USSR), 13, 250, English translation NACA TM 1110.

Smith, R., Stafford, C.M. and Winifordner, J.D. (1969) "Temperature profiles of turbulent hydrogen diffusion flames used in atomic flourescence spectrometry" Analytical chemistry Vol. 41, p. 946.

Spalding, D.B. (1971) "The calculation of combustion processes: Turbulent kinetically influenced flames" Imperial College, Mech. Eng. Dept. Rpt. No. RF/TN/A/6.

Spalding, D.B. (1971a) "Concentration fluctuations in a round turbulent free jet", Chem. Eng. Sc. 26, p. 95.

Spalding, D.B. (1971b) "The calculation of combustion processes: Turbulent, physically-controlled, combustion processes" Imperial College, Mech. Eng. Dept. Rpt. RF/TN/A/4.

Spalding, D.B. (1971c) "The calculation of combustion processes: Laminar physically controlled flames" Imperial College, Mech. Eng. Dept. Rpt. No. RF/TN/A/3.

Spalding, D.B. (1972) "A novel finite-difference formulation for differential expressions involving both first and second derivatives" Int. J. Num. Methods in Engg, Vol. 4, p. 551.

Stanford, R.A. and Libby, P.A. (1974) "Further application of hot-wire anemometry to turbulence measurement in helium-air mixtures" Physics of Fluids Vol. 17, p. 537.

Tennekes, H. and Lumley, J.H. (1972), A First Course in Turbulence. M.I.T. Press, Cambridge, Mass.

Tribus, M. (1961) Thermostatics and Thermodynamics Von Nostrand New York:

Tutu, N.K. and Chevray, R. (1973) Bull. Am. Phys. Soc. II, 18, 11. Data quoted by Bilger (1975).

Vlachos, N.S. and Humphrey, P. (1975) Private Communication.

Verdin, A. (1973) Gas Analysis Instrumentation McMillan Book Co. London.

Williams, F.A. (1965) Combustion Theory. Addison-Wesley, Reading, Mass.

Williams, G.C., Hottel, H.C. and Scurlock, A.C. (1948) "Flame stabilization and propagation in high velocity gas streams" Third Symposium (International) on Combustion, The Combustion Institute, p. 21.

Wygnanski, I. and Fiedler, H.E. (1969) "Some measurements in the self-preserving jet" J. Fluid Mech., Vol. 38, p. 577.

Zysk, E.D. (1962) "Platinum metal thermocouples" Temperature: Its measurement and control in science and industry" Vol. III, Part 2, Reinhold Publishing Co. p. 135.

NOMENCLATURE

Symbol	Meaning	Location of first occurrence
A	Frequency factor.	5.2
A_N^{Φ}	Normalised hybrid co-efficient of the discretized equation for Φ control volume.	6.30
	Similarly for S,E,W, V and P grid nodes.	6.30
A_N^U	Normalized hybrid co-efficient of the discretized equation for U control volume.	
	Similarly for S,E,W, U and P grid nodes	6.32
A_N^V	Normalized hybrid co-efficient of the discretized equation for V control volume.	
	Similarly for S,E,W, U and P grid nodes.	6.33
A_ℓ	Area of laminar flame.	
A_T	Area of turbulent flame.	
a_N^{Φ}	Hybrid co-efficient of the discretized equation for Φ control volume. Similarly for S,E,W, U and P grid nodes.	6.28
$a_n'^{\Phi}$	Co-efficient for the finite difference equation of Φ control volume, represents area of north face. Similarly for s,e,w,faces.	6.22
$a_{xn}'^{\Phi}$	Extra area to be added to north face because of grid expansion. Similarly for s face.	6.22
C_{g2}	Constant for mixture fraction fluctuation (g) equation.	4.50
C_N	Convection co-efficient for the north face of control volume. Similarly for S,E,W, u and P faces.	6.25

Symbol	Meaning	Location of first occurrence
C_P	Specific heat at constant pressure.	5.18
$C_{\varepsilon 1}$	Constant associated with the production term of the dissipation equation.	4.13
$C_{\varepsilon 2}$	Constant associated with the dissipation term of the dissipation equation.	4.14
C_μ	Constant associated with the dissipation term in turbulence energy equation.	4.7
D	Diffusivity.	3.6
D	Relating the downstream plane.	
D_E	Diffusion co-efficient for the east side of control volume similarly for W,N,S.	6.25
d	Diameter,	2.3
E	Activation energy.	5.2
f	Mixture fraction,	4.45
f_e	Function of Peclet number,	6.27
g	Acceleration due to gravity.	3.2
g	Mean square of mixture fraction fluctuations.	4.47
g_E	Function of cell Peclet number.	6.25b
H	Heat of reaction of fuel	5.18
h	Convective heat transfer co-efficient.	2.3
h	Enthalpy	5.10
J	Diffusion flux.	4.46
K	Thermal conductivity.	2.3
K	Turbulence energy.	4.3
k	Boltzman constant,	2.1
ℓ	Length.	2.3
ℓ	Length scale,	4.2
M	Mach number.	2.2

Symbol	Meaning	Location of first occurrence
M_P	Mass source in control volume.	6.36
m	Molecular mass of species.	2.1
m	Mass fraction.	5.10
n	Total number of density of molecules.	2.1
P_n	Polynomial of degree n in (E/RT)	5.5
Pe	Cell Peclet number.	6.27a
P*	Guessed pressure.	6.34
P'	Pressure correction.	6.39
p	Pressure.	3.2
Q	Series expansion.	5.5
q	Power used to heat a thermocouple.	2.4
q	Favre turbulence energy.	4.2
R	Maximum radius of calculation domain.	6.10
R	Universal gas constant.	5.2
R_λ	Reynolds number bssed on Taylor microscale.	
r	Radial co-ordinate direction.	3.2
S	Stiochiometric fuel-air ratio.	5.12
S	Source term in Φ transport equation.	3.6
S_P	Implicit source term in discretized equation.	6.25
S_u	Explicit source term in discretized equation.	6.25
T	Temperature,	5.2
t	Time,	5.1
U	Velocity component.	4.8
U	Relates to upstream plane.	
U*	Guessed velocity.	6.35
U'	Velocity correction.	6.38
U( )	Heaviside step function.	5.29
u_ℓ	Laminar flame speed.	5.6
u_t	Turbulent flame speed.	5.6

Symbol	Meaning	Location of first occurrence
μ	Maximum probable value.	5.29
μ_{eff}	Effective or eddy viscosity.	
σ	Prandtl number.	4.6
σ	Variance.	5.29
ν	Kinematic viscosity	4.10
ν	Stoichiometric co-efficient.	5.2
ρ	Density.	3.1
χ	Dissipation of scalar fluctuations.	
Φ	Scalar quantity.	3.6
ω_α	Reaction rate of species.	5.1

Subscript	Pertaining to
D	Downstream plane
E,N,S,W	Grid nodes east, north, south and west of control volume.
EU,NU,SU,WU	Grid nodes east, north, south and west of U control volume.
EV,NV,SV,WV	Grid nodes east, north, south and west of V control volume.
EΦ,NΦ,SΦ,WΦ	Grid nodes east, north, south and east of Φ control volume.
e,n,s,w	East, north, south and west faces of the control volume.
eff	Effective value.
fu	Fuel.
i,j	Tensor subscript taking values 1,2,3.
in,J	J^{th} inert species.
ℓ	Laminar value.
ox	Oxidant.
pr	Product.
U	Upstream plane.
U	U-velocity control volume.

Symbol	Meaning	Location of first occurrence
V	Velocity component.	4.8
V_r, V_θ, V_z	Velocity components in r,θ, z directions respectively.	3.1
v	Molecular velocity.	2.1
v'	Fluctuating velocity component.	
W	Molecular weight.	5.2
W_τ	Friction velocity.	7.2
W_{CL}	Centre line velocity.	7.2
Y_{max}	Width of computation grid.	

Greek Symbols

β	Curvilinear co-ordinate direction.	6.10
Γ	Exchange coefficient.	
γ	Ratio of specific heats.	2.2
γ	Angle between z and ζ co-ordinate directions.	6.12
δ_ℓ	Laminar flame thickness.	5.6
$\delta(\ )$	Dirac delta function.	5.29
ε	Emissivity.	2.4
ε	Dissipation of turbulence.	4.7
ζ	Curvilinear co-ordinate direction.	
ζ	Molar concentration.	
ζ	Second co-efficient of viscosity.	3.2
η	Curvilinear co-ordinate direction.	
η	Kolmogorov length scale.	
λ	Taylor microscale.	
μ	Laminar viscosity.	3.2
μ_t	Turbulent viscosity.	4.1

Subscript	Pertaining to
V	V-velocity control volume.
Φ	Φ-control volume.
st	Stoichiometric value.
O,1	Fuel and oxidant streams.

Superscript	
-	Mean value.
'	Fluctuating value.
^	Instantaneous value.
~	Favre mean value.
"	Faver fluctuating value.

Appendix 4.1

The thermal equation of state can be written as

$$\hat{P} = R\hat{T} \sum_{\alpha=1}^{n} \hat{\zeta}_\alpha \qquad 1$$

where R = Universal gas constant and $\hat{\zeta}$ is molar concentration.

The caloric equation of state is

$$\hat{h} = \frac{1}{\hat{\rho}} \sum_{\alpha=1}^{n} \hat{h}_\alpha \hat{\zeta}_\alpha \qquad 2$$

where $\hat{h}$ is the specific enthalpy of the mixture and $\hat{h}_\alpha$ is the molar enthalpy of species α which is assumed to be

$$\hat{h}_\alpha = C_{p\alpha}\hat{T} + H_\alpha \qquad 3$$

where $C_{p,\alpha}$ and H_α are molar heat capacity at constant pressure and molar heat of formation which are assumed to be constant.

If we define frozen specific heat for the mixture as

$$C_p = \frac{1}{\rho} \sum_{\alpha=1}^{n} \zeta_\alpha C_{p,\alpha} \qquad 4$$

The ratio of specific heats γ can be defined if the specific heats are assumed constant as

$$\frac{\gamma-1}{\gamma} = \frac{R \sum_{\alpha=1}^{n} \zeta_\alpha}{\sum_{\alpha=1}^{n} C_{p,\alpha}\zeta_\alpha} \qquad 5$$

subsitute eq. 3 in eq. 2.

$$\hat{h} = \frac{1}{\hat{\rho}} \sum_{=1}^{n} (C_{p,\alpha}\hat{T}_\alpha + H_\alpha)\hat{\zeta}_\alpha \qquad 6$$

or

$$h = \frac{\hat{T}}{\hat{\rho}} \sum_{\alpha=1}^{n} C_{p,\alpha}\hat{\zeta}_\alpha + \frac{1}{\hat{\rho}} \sum_{\alpha=1}^{n} H_\alpha \hat{\zeta}_\alpha$$

Using eq.5

$$\hat{h} = \frac{\hat{p}}{\hat{\rho}} \left(\frac{\gamma}{\gamma-1}\right) + \frac{1}{} \sum_{\alpha=1}^{n} H_\alpha \hat{\zeta}_\alpha$$

$$\hat{P} = \frac{\gamma-1}{\gamma} \hat{\rho} \left(\hat{h} \frac{1}{\hat{\rho}} \sum_{\alpha=1}^{n} \hat{\zeta}_\alpha H_\alpha\right) \qquad 7$$

Transport equation of ζ_α can be written as

$$\frac{\partial \hat{\zeta}_\alpha}{\partial t} + \hat{u}_j \frac{\partial \hat{\zeta}_\alpha}{\partial x_j} = -\hat{\zeta}_\alpha \frac{\partial \hat{u}_j}{\partial x_j} - \frac{1}{W_\alpha} \frac{\partial j_{\alpha' j}}{\partial x_j} + \frac{w_\alpha}{W_\alpha} \qquad 8$$

Where W_α is the molecular weight and w_α is the rate of formation of species α.

The transport equation for static enthalpy can be written as (neglecting radiation):

$$\hat{\rho} \frac{\partial \hat{h}}{\partial t} + \hat{\rho} u_j \frac{\partial h}{\partial x_j} = \hat{u}_j \frac{\partial \hat{p}}{\partial x_j} + \Phi + \frac{\partial \hat{p}}{\partial t} \qquad 9$$

where $\Phi = \hat{f}_{ij} \frac{\partial \hat{u}_i}{\partial x_j}$

and the continuity equation is

$$\frac{\partial \hat{u}_i}{\partial x_i} = -\frac{\partial \hat{\rho}}{\partial x_i} - \frac{\partial \hat{\rho}}{\partial t} \qquad 10$$

An expression for divergence of velocity $\frac{\partial \hat{u}_i}{\partial x_i}$ can be obtained from the above equations.

$$\frac{\partial \hat{u}_i}{\partial x_i} = -\left[\frac{1}{\gamma \hat{p}} \frac{\partial \hat{p}}{\partial t} + \hat{u}_i \frac{\partial \hat{p}}{\partial x_i}\right] + \frac{\gamma-1}{\gamma} \frac{1}{\hat{p}} \Phi - \frac{\gamma-1}{\gamma} \frac{1}{\hat{p}} \sum_{=1}^{n} \frac{H\alpha}{W\alpha} \left[w_\alpha - \frac{\partial j_{\alpha,i}}{\partial x_i}\right]$$

11

Assuming steady state and

Time averaging

$$\frac{\partial \bar{u}_i}{\partial x_i} = -\frac{1}{\gamma \bar{p}} \left[\bar{u}_i \frac{\partial \bar{p}}{\partial x_i} + \frac{\partial}{\partial x_i} \overline{p' u_i'} \right.$$

$$+ \frac{\gamma-1}{\gamma} \frac{1}{\bar{p}} \left[\bar{\dot{\Phi}} - \sum_{\alpha=1}^{n} \frac{H_\alpha}{W_\alpha} \bar{w}_\alpha - \overline{\frac{\partial j_{\alpha,i}}{\partial x_i}} \right]$$

$$+ \frac{\gamma-1}{\gamma} \frac{1}{\bar{p}^2} \left[\bar{u}_i \frac{\partial}{\partial x_i} \frac{1}{2} \overline{p'^2} + \overline{p' u_i'} \frac{\partial \bar{p}}{\partial x_i} + \frac{\partial}{\partial x_i} \frac{1}{2} \overline{p'^2 u_i'} - \frac{1}{2} \overline{p'^2 \frac{\partial u_i'}{\partial x_i}} \right]$$

$$\left. - \left[\frac{\gamma-1}{\gamma} \right]^2 \frac{1}{\bar{p}^2} \left[\overline{p'\Phi'} - \sum_{\alpha=1}^{m} \frac{H_\alpha}{W_\alpha} \overline{p' w_\alpha'} - \overline{p' \frac{\partial}{\partial x_i} j_{\alpha,i}} \right] \right] \qquad 12 \; 13$$

assuming

$$\frac{1}{p} \approx \frac{1}{\bar{p}} \left[1 - \frac{p'}{\bar{p}} \right]$$

The correlation between instantaneous pressure can be written as

$$\overline{\hat{p} \frac{\partial \hat{u}_i}{\partial x_i}} = \overline{p' \frac{\partial u_i'}{\partial x_i}} + \bar{p} \frac{\partial \bar{u}_i}{\partial x_i}$$

Hence

$$\overline{p' \frac{\partial u_i'}{\partial x_i}} = \overline{\hat{p} \frac{\partial \hat{u}_i}{\partial x_i}} - \bar{p} \frac{\partial \bar{u}_i}{\partial x_i} \qquad 13 \; 14$$

Appendix 4,2

Transport equations in Favre averaged form

Continuity

$$\frac{\partial}{\partial x_i}\left(\overline{\rho}\tilde{U}_i\right) = 0$$

Nomentum (neglecting laminar diffusion)

$$\overline{\rho}U_i \frac{\partial \tilde{u}_i}{\partial x_j} = - \frac{d\bar{p}}{dx} - \frac{\partial}{\partial x_j} \overline{\rho} \widetilde{u_i'' u_j''}$$

Mixture Fraction

$$\rho\tilde{U}_j \frac{\partial \tilde{f}}{\partial x_j} = - \frac{\partial}{\partial x_j} \overline{\rho} \widetilde{f''u_j''}$$

Turbulent Kinetic Energy

$$\overline{\rho}\tilde{U}_j \frac{\partial}{\partial x_j}\left(\frac{1}{2} q^2\right) = \rho g_i \overline{u_i''} - \overline{\rho} \widetilde{u_i'' u_j''} \frac{\partial \tilde{U}_i}{\partial x_j} - \overline{\rho} \widetilde{\frac{u_i}{\rho} \frac{\partial p}{\partial x_i}}$$

$$- \frac{\partial}{\partial x_i}\left(\frac{1}{2} \overline{\rho} \widetilde{u_i'' q''}\right) - \overline{\rho\varepsilon}$$

f''^2-equation

$$\overline{\rho}\tilde{U} \frac{\partial}{\partial x_j} \tilde{f''^2} = -2\overline{\rho} \tilde{u_j''f''} \frac{\partial \tilde{f}}{\partial x_j} - \frac{\partial}{\partial x_j} \overline{\rho} \widetilde{u_j'' f''^2} - \overline{\rho\chi}$$

where $q^2 = \tilde{u''}^2 + \tilde{v''}^2 + \tilde{w''}^2$

$$\varepsilon = \frac{1}{2} \nu \widetilde{\left(\frac{\partial u_i''}{\partial x_j} + \frac{\partial u_j''}{\partial x_i}\right)\left(\frac{\partial u_i''}{\partial x_j} + \frac{\partial u_j''}{\partial x_i}\right)}$$

$$\chi = 2D \overline{\frac{\partial f''}{\partial x_k} \frac{\partial f''}{\partial x_k}}$$

Now from eqn. ~~12~~ 11

$$\overline{\hat{p}\frac{\partial \hat{u}_i}{\partial x_i}} = -\frac{1}{\gamma}\left[\hat{u}_i \frac{\partial \hat{p}}{\partial x_i}\right] + \frac{\gamma-1}{\gamma}\hat{\Phi} - \frac{\gamma-1}{\gamma}\sum_{\alpha=1}^{n}\frac{H_\alpha}{W_\alpha}\left[w_\alpha - \frac{\partial j_{\alpha,i}}{\partial x_i}\right]$$

or

$$\overline{\hat{\rho}\frac{\partial \hat{u}_i}{\partial x_i}} = -\frac{1}{\gamma}\left[\bar{u}_i \frac{\partial \bar{p}}{\partial x_i} + \overline{u_i' \frac{\partial p'}{\partial x_i}}\right] + \frac{\gamma-1}{\gamma}\bar{\Phi} - \frac{\gamma-1}{\gamma}\sum_{\alpha=1}^{n}\frac{H_\alpha}{W_\alpha}\left[\bar{w}_\alpha - \frac{\partial j_{\alpha,i}}{\partial x_i}\right]$$

~~15~~ 14

Using eqns. ~~15~~ 14 and ~~13~~ 12 we can write eqn. ~~14~~ 13 as

$$\overline{p'\frac{\partial u_i'}{\partial x_i}} = -\frac{1}{\gamma\bar{p}}\,\bar{u}_i \frac{\partial}{\partial x_i}\frac{1}{2}\overline{p'^2} + \overline{p'u_i'}\frac{\partial \bar{p}}{\partial x_i} + \overline{u_i'\frac{\partial}{\partial x_i}\frac{1}{2}p'^2}$$

$$+ \frac{\gamma-1}{\gamma}\frac{1}{\bar{p}}\left[\overline{p'\Phi'} - \sum_{\alpha=1}^{n}\frac{H_\alpha}{W_\alpha}\right]\left[\overline{p'w_\alpha'} - p'\frac{\partial j_{\alpha,i}}{\partial x_i}\right] \qquad \text{~~16~~ 15}$$

Appendix 5.1

From equation 5.55

(A)

$$T = \frac{1}{\sigma\sqrt{2\pi}} \int_{o}^{f_{st}} \frac{| h_o + \hat{f}(h_1 - h_o)| \, e^{-z^2/2}}{\hat{m}_{ox}\,\bar{C}_{P_{ox}} + \hat{m}_{Pr} \cdot C_{P_{Pr}} + \sum_{j=1}^{n} \hat{m}_{in,j} C_{P_{in,j}}} .df$$

(B)

$$\int_{f_{st}}^{1} \frac{|(h_o + \hat{f})\,(h_1 - h_o) - \hat{m}_{fu}\, H|\; e^{-z^2/2}}{\hat{m}_{fu}\,\bar{C}_{P_{fu}} + \hat{m}_{Pr}\,\bar{C}_{P_{Pr}} + \sum_{j=1}^{n} \hat{m}_{in,j}\,\bar{C}_{P_{in,j}}} .df \quad + \; AT(O) + BT(O)$$

1

Substituting for $\hat{m}_{ox}$, $\hat{m}_{Pr}$, $\hat{m}_{in,j}$ in term A above and assuming that

$$a_1 = h_o \qquad 2$$

$$b_1 = h_1 - h_o \qquad 3$$

we have

$$\text{TERM A} = \frac{1}{\sigma\sqrt{2\pi}} \int_{o}^{f_{st}} \frac{(a_1 + b_1\hat{f}) e^{-z^2/2} .df}{\{\bar{C}_{P_{ox}}\, m_{ox,o}(\frac{f_{st}-\hat{f}}{f_{st}}) + \bar{C}_{P_{Pr}} | m_{ox,o} + (m_{fu,1} - m_{ox,o})\hat{f}) - m_{ox,o}(\frac{f_{st}-\hat{f}}{f_{st}})|}$$

$$+ \sum_{j=1}^{n} (m_{in,jo} + \hat{f}(m_{inj,o} - m_{inj,1}) \quad \bar{C}_{P_{in,j}} \}$$

$$\text{TERM A} = \frac{1}{\sigma\sqrt{2\pi}} \int_{o}^{f_{st}} \frac{(a_1 + b_1 f) e^{-z^2/2} .df}{\{((\bar{C}_{P_{ox}} - \bar{C}_{P_{Pr}}) m_{ox,o} + \bar{C}_{P_{Pr}}\, m_{ox,o} + \sum_{j=1}^{n} \bar{C}_{P_{in,j}}\, m_{inj,o})}$$

$$+ ((\bar{C}_{P_{Pr}} - \bar{C}_{P_{ox}}) m_{ox,o}/f_{st} + C_{Pr}(m_{fu,1} - m_{ox,o}) + \sum_{j=1}^{n} \bar{C}_{P_{in,j}} (m_{in,j,o} - m_{in,j,1}))\}$$

If $$\alpha_1 = \bar{C}_{P_{ox}} m_{ox,o} + \sum_{j=1}^{n} \bar{C}_{P_{in,j}} m_{in,j,o}$$

$$\beta_1 = (\bar{C}_{P_{Pr}} - \bar{C}_{P_{ox}}) m_{ox,o} \Big/ f_{st} + C_{Pr}(m_{fu,1} - m_{ox,o}) + \sum_{j=1}^{n} \bar{C}_{P_{in,j}} (m_{in,j,o} - m_{in,j,1})$$

$$\text{TERM A} = \frac{1}{\sigma\sqrt{2\pi}} \int_{o}^{f_{st}} \frac{(a_1 + b_1 f) e^{-z^2/2}}{(\alpha_1 + \beta_1 f)} .df \qquad .4$$

$$\text{TERM B} = \frac{1}{\sigma\sqrt{2\pi}} \int_{f_{st}}^{1} \frac{(h_o + \hat{f}(h_1 - h_o) - m_{fu,1}(\frac{\hat{f} - f_{st}}{1 - f_{st}}) H) e^{-z^2/2} .df}{\{ m_{fu,1}(\frac{\hat{f} - f_{st}}{1 - f_{st}}) \bar{C}_{P_{fu}} + \bar{C}_{P_{Pr}} (m_{ox,o} + (m_{fu,1} - m_{ox,o}) \hat{f}$$

$$- m_{fu,1}(\frac{\hat{f} - f_{st}}{1 - f_{st}})) + \sum_{j=1}^{n} (m_{in,j,o} + \hat{f}(m_{in,j,o} - m_{in,j,1}) \bar{C}_{P_{in,j}} \}$$

$$\text{TERM B} = \frac{1}{\sigma\sqrt{2\pi}} \int_{f_{st}}^{1} \frac{(h_o + m_{fu,1} H(f_{st}/1 - f_{st})) + ((h_1 - h_o) - m_{fu,1} H/1 - f_{st}) \hat{f} e^{-z^2/2} .df}{\{((\bar{C}_{P_{Pr}} - \bar{C}_{P_{fu}}) (m_{fu,1}(f_{st}/1 - f_{st}) + \bar{C}_{P_{Pr}} m_{ox,o} + \sum_{j=1}^{n} m_{in,j,o} \bar{C}_{P_{in,j}}$$

$$+ ((\bar{C}_{P_{fu}} - \bar{C}_{P_{Pr}})/(1 - f_{st}) + \bar{C}_{P_{Pr}}(m_{fu,1} - m_{ox,o}) + \sum_{j=1}^{n} \bar{C}_{P_{in,j}} (m_{in,j,o} - m_{in,j,1})) \hat{f} \}$$

$$a_2 = h_o + m_{fu,1} H(f_{st}/1 - f_{st}) \qquad 5$$

$$b_2 = (h_1 - h_o) - m_{fu,1} H/(1 - f_{st}) \qquad 6$$

$$\alpha_2 = (\bar{C}_{P_{Pr}} - \bar{C}_{P_{fu}}) (m_{fu,1}(f_{st}/(1 - f_{st})) + C_{P_{Pr}} m_{ox,o} + \sum_{j=1}^{n} m_{in,j,o} C_{P_{in,j}}$$

7

$$\beta_2 = (\bar{C}_{P_{fu}} - \bar{C}_{P_{Pr}})/(1.0-f_{st}) + \bar{C}_{P_{Pr}}(m_{fu,1} - m_{ox,o}) + \sum_{j=1}^{n} \bar{C}_{P_{in,j}}(m_{in,jo} - m_{in,j,1})$$

.8

Hence

$$\text{TERM B} \qquad \frac{1}{\sigma\sqrt{2\pi}} \int_{f_{st}}^{1} \frac{(a_2+b_2\hat{f})e^{-z^2/2}}{(\alpha_2+\beta_2\hat{f})} .df \qquad 9$$

Put .8 and .9 in .1

$$\bar{T} = \frac{1}{\bar{\sigma}\sqrt{2\pi}} \int_{o}^{f_{st}} \left(\frac{a_1+b_1\hat{f}}{\alpha_1+\beta_1\hat{f}}\right) e^{-z^2/2} .df + \frac{1}{\sigma\sqrt{2\pi}} \int_{f_{st}}^{1} \left(\frac{a_2+b_2\hat{f}}{\alpha_2+\beta_2\hat{f}}\right) e^{-z^2/2} .df$$

$$+ \quad Af(O) + Bf(1) \qquad 10$$

Mean Density of the Mixture

Using equations 5.36 and 5.47 we have

$$\bar{\rho} = \left[\frac{1}{\bar{\sigma}\sqrt{2\pi}} \frac{\bar{P}}{\bar{R}} \int_{o}^{1} \frac{1}{\hat{T} \sum_j \frac{\hat{m}_j}{W_j}} e^{-z^2/2} .df \right] + A\rho(O) + B\rho(1)$$

Substituting for T from equation 5.37.

$$\bar{\rho} = \left| \frac{1}{\sigma\sqrt{2\pi}} \frac{\bar{P}}{\bar{R}} \int_{o}^{1} \frac{\sum_j m_j \bar{C}_{P_j} e^{-z^2/2} .df}{(\hat{h}-\hat{m}_{fu}H)\sum_j \frac{\hat{m}_j}{W_j}} \right. + A\rho(O) + B\rho(1)$$

or

$$\bar{\rho} = \left| \frac{1}{\sigma\sqrt{2\pi}} \frac{\bar{P}}{\bar{R}} \int_{o}^{1} \frac{(\hat{m}_{fu}\bar{C}_{P_{fu}} + \hat{m}_{ox}\bar{C}_{P_{ox}} + \hat{m}_{P_r}\bar{C}_{P_{Pr}} + \sum_{j=1}^{n} \hat{m}_{in,j}\bar{C}_{P_{in,j}}) e^{-z^2/2} .df}{(h_o + \hat{f}(h_1-h_o) - \hat{m}_{fu}H)\left[\frac{\bar{m}_{fu}}{W_{fu}} + \frac{\bar{m}_{ox}}{W_{ox}} + \frac{\bar{m}_{P_r}}{W_{Pr}} + \sum_{j}^{n} \frac{\bar{m}_{in,j}}{W_{in,j}} \right]} \right.$$

$$+ A\rho(O) + B\rho(1) \qquad 11$$

The expression under the integral sign can be written as follows:

$$A = \int_{o}^{f_{st}} \frac{(\hat{m}_{ox}\bar{C}_{P_{ox}} + \hat{m}_{Pr}\bar{C}_{Pr} + \sum_{j=1}^{n}\hat{m}_{in,j}\bar{C}_{P_{in,j}})e^{-z^2/2}.df}{(h_o - \hat{f}(h_1-h_o))\left[\frac{\hat{m}_{ox}}{W_{ox}} + \frac{\hat{m}_{Pr}}{W_{Pr}} + \sum_{j}^{n}\frac{\hat{m}_{in,j}}{W_{in,j}}\right]}$$

B

$$+ \int_{f_{st}}^{1} \frac{(\hat{m}_{fu}\bar{C}_{fu} + \hat{m}_{Pr}\bar{C}_{PPr} + \sum_{j=1}^{n}\hat{m}_{in,j}\bar{C}_{P_{in,j}})e^{-z^2/2}.df}{(h_o - \hat{f}(h_1-h_o) - \hat{m}_{fu}H)\left[\frac{\hat{m}_{fu}}{W_{fu}} + \frac{\hat{m}_{Pr}}{W_{Pr}} + \sum_{j=1}^{n}\frac{\hat{m}_{in,j}}{W_{in,j}}\right]} \qquad 12$$

C

Substituting for values $m_{ox}, m_{fu}, m_{Pr}, m_{in,j}$ from equations 5.18, 5.19, 5.21, 5.22 and 5.23 in Term B and C of the above equation we have

$$B = \int_{o}^{f_{st}} \frac{\{m_{ox,o}(\frac{f_{st}-\hat{f}}{f_{st}})C_{P_{ox}} + \left[m_{ox,o} + (m_{fu,1}-m_{ox,o})\hat{f} - m_{ox,o}(\frac{f_{st}-\hat{f}}{f_{st}})\right]\bar{C}_{P_{Pr}} + \sum_{j=1}^{n}(m_{in,j,o} + (m_{in,j,1}-m_{in,j,o})\hat{f})C_{P_{in,j}}\}e^{-z^2/2}.df}{(h_o+\hat{f}(h_1-h_o))\{\frac{m_{ox,o}}{W_{ox}}(\frac{f_{st}-\hat{f}}{f_{st}}) + (m_{ox,o}+(m_{fu,1}-m_{ox,o})\hat{f} - m_{ox,o}\frac{f_{st}-\hat{f}}{f_{st}})\frac{1}{W_{Pr}} + \sum_{j=1}^{n}(m_{in,j,o}+(m_{in,j,1}-m_{in,j,o})\hat{f})\frac{1}{W_{in,j}}\}}$$

$$B = \int \frac{(m_{ox,o}C_{P_{ox}} + \sum_{j=1}^{n} m_{in,j,o}C_{P_{in,j}}) + \hat{f}\{(C_{P_{ox}}-C_{P_{Pr}})\frac{m_{ox,o}}{f_{st}} + C_{Pr}(m_{fu,1}-m_{ox,o}) + \sum_{j=1}^{n} C_{P_{in,j}}(m_{in,j,1}-m_{in,j,o})e^{-z^2/2}.df}{(h_o+(h_1-h_o)\hat{f})\{(\frac{m_{ox,o}}{W_{ox}} + \sum_{j=1}^{n}\frac{m_{in,j,o}}{W_{in,j,o}}) + \hat{f}\{(\frac{1}{W_{Pr}} - \frac{1}{W_{ox}})\frac{m_{ox,o}}{f_{st}} + (\frac{m_{fu,1}-m_{ox}}{W_{Pr}}) + \sum_{j=1}^{n}(\frac{m_{in,j,1}-m_{in,j,o}}{W_{in,j}})}$$

$$B = \int_{o}^{f_{st}} \frac{(\alpha_1 + \beta_1 \hat{f}) e^{-z^2/2} \, .df}{(a_1 + b_1 \hat{f})(\alpha_3 + \beta_3 \hat{f})} \qquad 13$$

where

$$\alpha_3 = \frac{m_{ox,o}}{W_{ox}} + \sum_{j=1}^{n} \frac{m_{in,j,o}}{W_{in,j,o}}$$

$$\beta_3 = \left(\frac{1}{W_{Pr}} - \frac{1}{W_{ox}}\right) \frac{m_{ox,o}}{f_{st}} + \frac{m_{fu,1} - m_{ox,o}}{W_{Pr}} + \sum_{j=1}^{n} \frac{(m_{in,j,1} - m_{in,j,o})}{W_{in,j}}$$

Similarly term C in equation 12 can be expressed as:

$$C = \int_{f_{st}}^{1} \frac{\{m_{fu,1}\left(\frac{\hat{f}-f_{st}}{1-f_{st}}\right)\bar{C}_{P_{fu}} + (m_{ox,o} + (m_{fu,1} - m_{ox,o})\hat{f} - m_{fu,1}\left(\frac{\hat{f}-f_{st}}{1-f_{st}}\right)\bar{C}_{Pr} + \sum_{j=1}^{n} (m_{in,j,o} + (m_{in,j,1} - m_{in,j,o})\hat{f})\bar{C}_{P_{in,j}}\} e^{-z^2/2} \, .df}{\left[h_o - \hat{f}(h_1 - h_o) - m_{fu,1}\left(\frac{\hat{f}-f_{st}}{1-f_{st}}\right)\right]\left\{\frac{m_{fu,1}}{W_{fu}}\left(\frac{\hat{f}-f_{st}}{1-f_{st}}\right) + \left[(m_{ox,o} + (m_{fu,1} - m_{ox,o})\hat{f} - m_{fu,1}\left(\frac{\hat{f}-f_{st}}{1-f_{st}}\right)\right]\frac{1}{W_{Pr}} + \sum_{j=1}^{n} (m_{in,j,o} + (m_{in,j,1} - m_{in,j,o})\hat{f})\frac{1}{W_{in,j}}\right\}}$$

$$C = \int_{o}^{1} \frac{\left\{\left[\frac{(\bar{C}_{Pr} - \bar{C}_{fu})m_{fu,1} f_{st}}{1-f_{st}} + (\bar{C}_{Pr} m_{ox,o} + \sum_{j=1}^{n} m_{in,j,o}\bar{C}_{P_{in,j}})\right] + \left[(\bar{C}_{P_{fu}} - \bar{C}_{Pr})\frac{m_{fu,1}}{1-f_{st}} + (m_{fu,1} - m_{ox,o})\bar{C}_{Pr} + \sum_{j=1}^{n} (m_{in,j,1} - m_{in,j,o})\bar{C}_{P_{in,j}}\right]\hat{f}\right\} e^{-z^2/2} .df}{\left\{\left[(h_o + \frac{m_{fu,1} H(f_{st})}{(1-f_{st})}) + ((h_1 - h_o) - \frac{m_{fu,1} H}{(1-f_{st})})\hat{f}\right]\left\{\left[\frac{(\frac{1}{W_{Pr}} - \frac{1}{W_{fu}})m_{fu,1} f_{st}}{1-f_{st}}\right.\right.\right.$$

$$\left.\begin{array}{l} \dfrac{m_{ox,o}}{W_{Pr}} + \sum_{j=1}^{n} \dfrac{m_{in,j,o}}{W_{in,j}} \Big] + \Big[\Big(\dfrac{1}{W_{fu}} - \dfrac{1}{W_{Pr}}\Big) \dfrac{m_{fu,1}}{1-f_{st}} + \dfrac{(m_{fu,1}-m_{ox,o})}{W_{Pr}} \\ \\ + \sum_{j=1}^{n} \dfrac{(m_{in,j,1}-m_{in,j,o})}{W_{in,j}} \Big] \hat{f} \Big\} \Big] \end{array}\right\rangle_{f_{st}}$$

or

$$c = \int_{f_{st}}^{1} \frac{(\alpha_2+\beta_2\hat{f})\, e^{-z^2/2}.df}{(a_2+b_2\hat{f})(\alpha_4+\beta_4\hat{f})}$$

where

$$\alpha_4 = \Big(\frac{1}{W_{Pr}} - \frac{1}{W_{fu}}\Big) \frac{m_{fu,1} f_{st}}{1-f_{st}} + \frac{m_{ox,o}}{W_{Pr}} + \sum_{j=1}^{n} \frac{m_{in,j,o}}{W_{in,j}}$$

$$\beta_4 = \Big(\frac{1}{W_{fu}} - \frac{1}{W_{Pr}}\Big) \frac{m_{fu,1}}{1-f_{st}} + \frac{(m_{fu,1}-m_{ox,o})}{W_{Pr}} + \sum_{j=1}^{n} \frac{(m_{in,j,1}-m_{in,j,o})}{W_{in,j}}$$

Hence

$$\bar{\rho} = \frac{1}{\sigma\sqrt{2\pi}} \frac{\bar{p}}{R} \Big[\int_{o}^{f_{st}} \frac{(\alpha_1 + \beta_1\hat{f}) e^{-z^2/2}.df}{(a_1+b_1\hat{f})(\alpha_3+\beta_3\hat{f})} + \frac{(\alpha_2+\beta_2\hat{f}) e^{-z^2/2}.df}{(a_2+b_2 f)(\alpha_4+\beta_4\hat{f})}$$

$$+ A\rho(O) + B\rho(O) \qquad 14$$

Appendix 6.1

Using the definition of convection coefficients, the continuity equation, eq. 6.22, can be written as:

$$C_E - C_W + C_N - C_S + C_P - C_U = 0.0 \qquad 1$$

Hence

$$\Phi_P(C_W - C_E + C_S - C_N + C_U - C_P) = 0.0 \qquad 2$$

Also eq. 6.26b can be written as

$$C_E\Phi_P f_e + C_E\Phi_E - C_E\Phi_E f_e - C_W f_w \Phi_W - C_W\Phi_P + C_W f_w \Phi_P$$

$$+ C_N f_n \Phi_P + C_N\Phi_N - C_N f_n \Phi_N - C_S f_s \Phi_S - C_S\Phi_P + C_S f_s \Phi_P$$

$$+ \Phi_P C_P - \Phi_u C_u = S^{\Phi}_{P,\Phi}\Phi_P + S^{\Phi}_{u,\Phi} \qquad 3$$

Adding eqns. 1 and 2 and simplifying we have

$$(C_u - S^{\Phi}_P)\Phi_P = C_N(f_n - 1)(\Phi_N - \Phi_P) + C_S f_s(\Phi_S - \Phi_P)$$

$$+ C_E(f_e - 1)(\Phi_E - \Phi_P) + C_W f_w(\Phi_W - \Phi_P)$$

$$+ C_u\Phi_u + S^{\Phi}_{u,\Phi} \qquad 4$$

or

$$a^{\Phi}_P\Phi_P = a^{\Phi}_N(\Phi_N - \Phi_P) + a^{\Phi}_S(\Phi_S - \Phi_P) + a^{\Phi}_E(\Phi_E - \Phi_P)$$

$$+ a^{\Phi}_W(\Phi_W - \Phi_P) + a^{\Phi}_u\Phi_u + S^{\Phi}_{u,\Phi} \qquad 5$$

Where the co-efficients a_P etc. are defined by eq. 6.29.

FIGURES

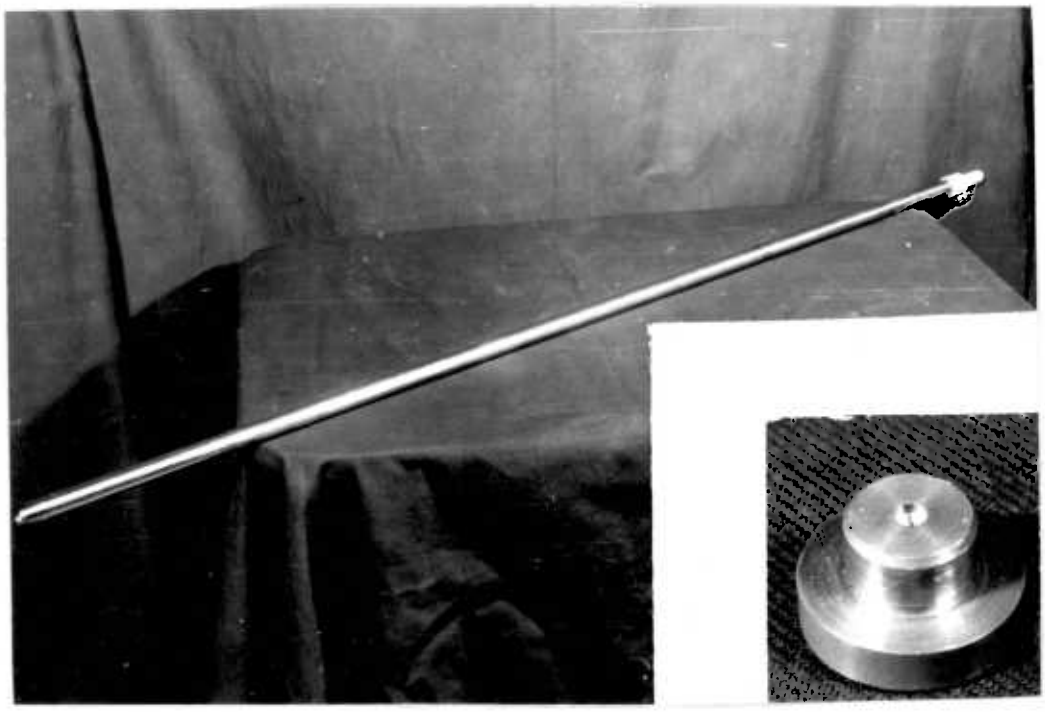
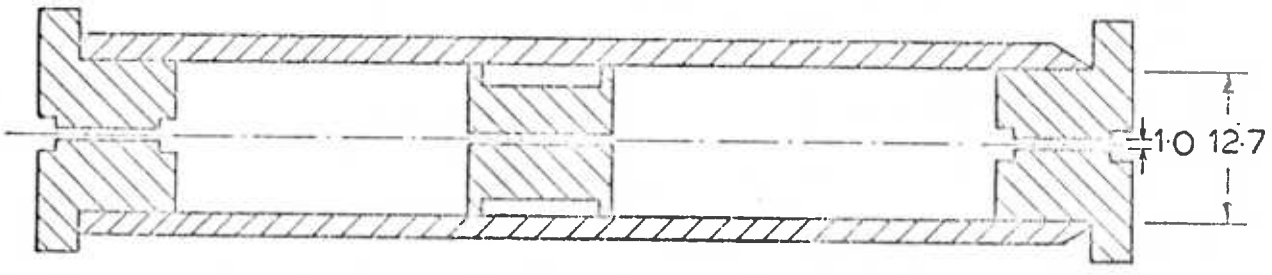


Fig. 2·1a: Burner tube and plug



Dimensions in mm.

Fig. 2·1b: Burner tube and plugs. (Half-sectioned view)

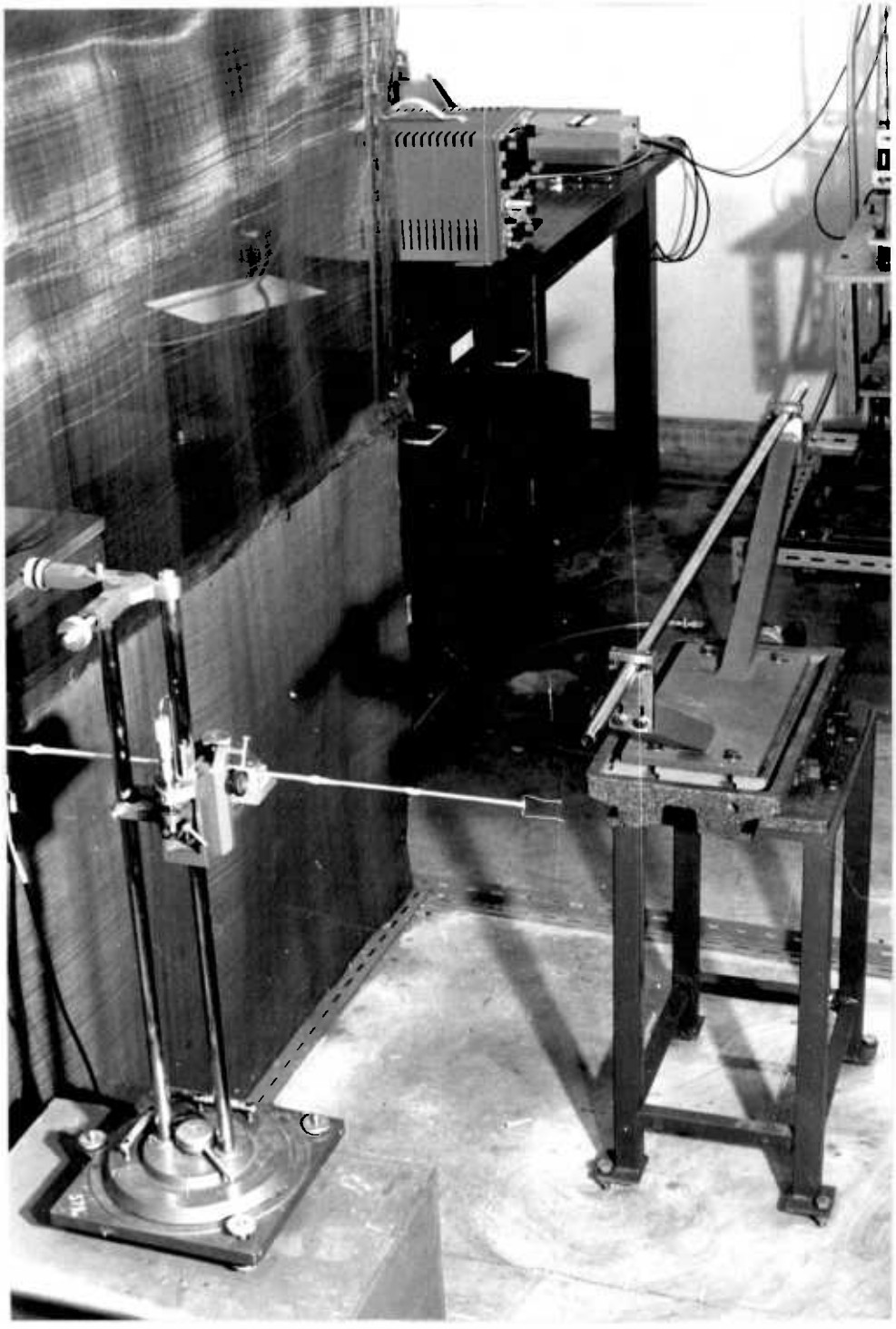


Fig. 2.2: Experimental set up

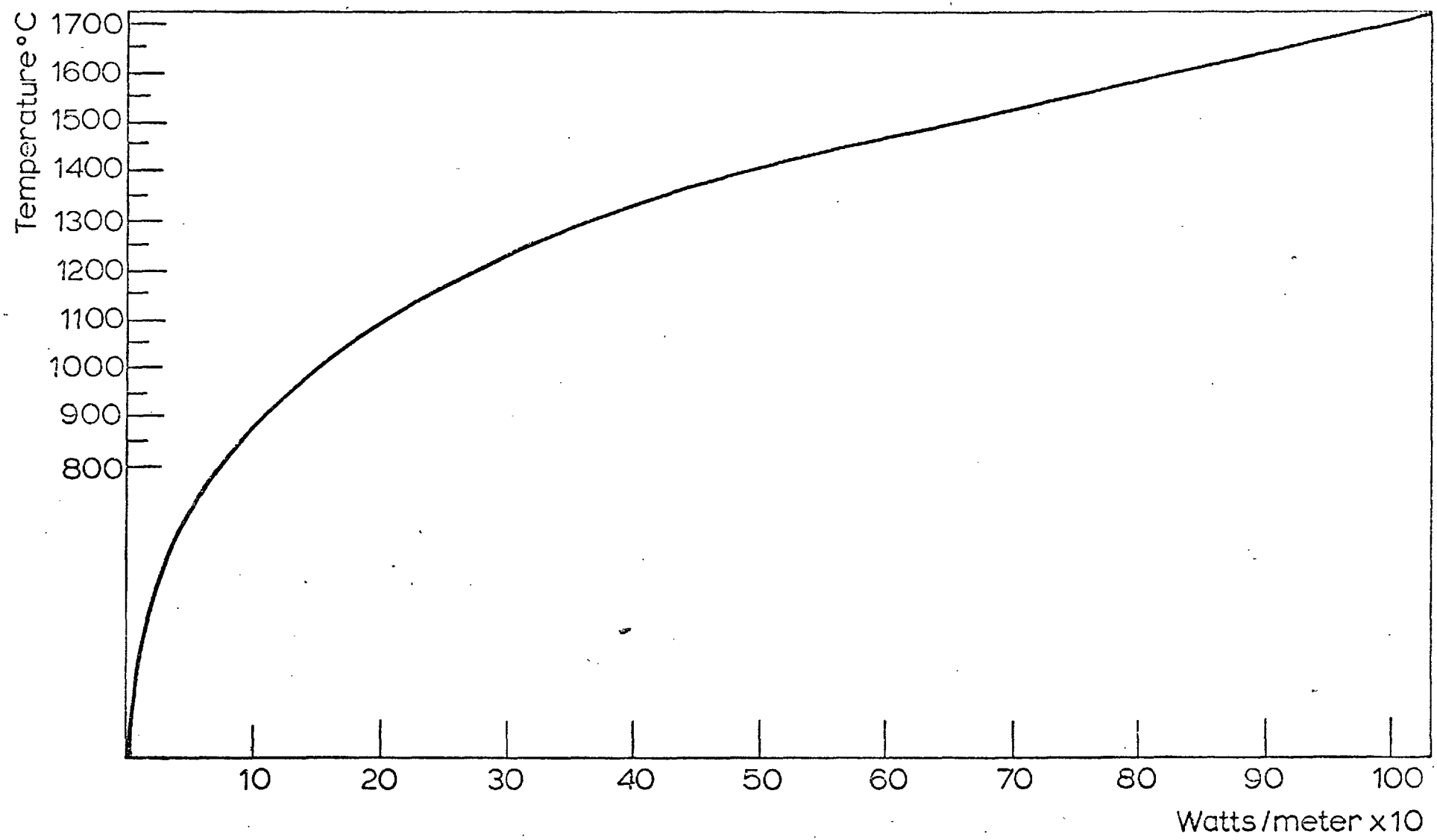


Fig.2.3: Caliberation curve for radiation correction

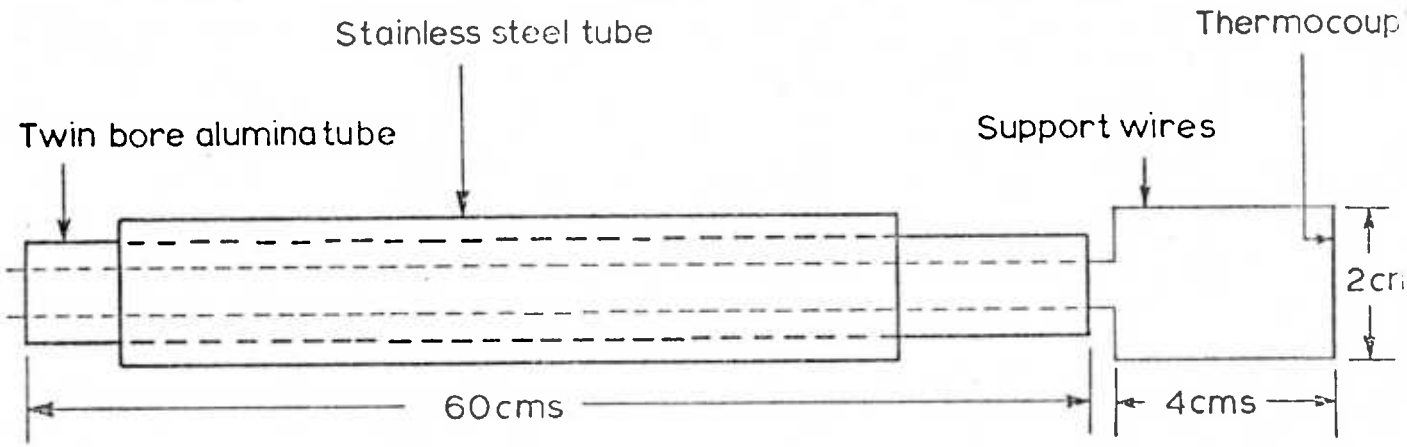


Fig. 2·4a: Thermocouple probe

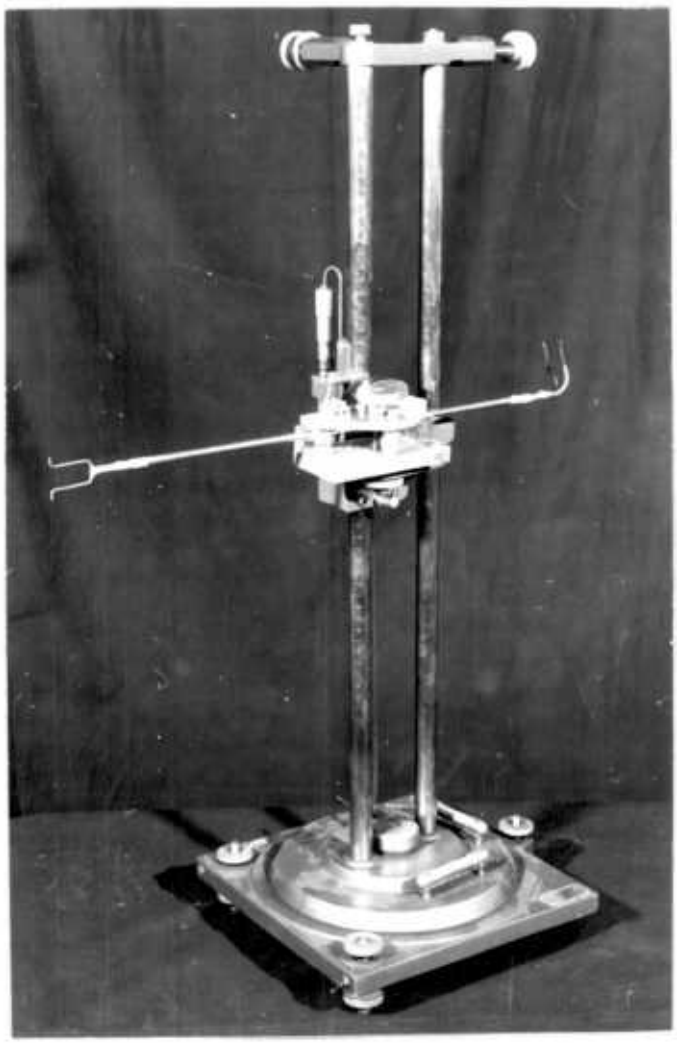


Fig. 2·4b: Thermocouple probe mounted on cathetometer

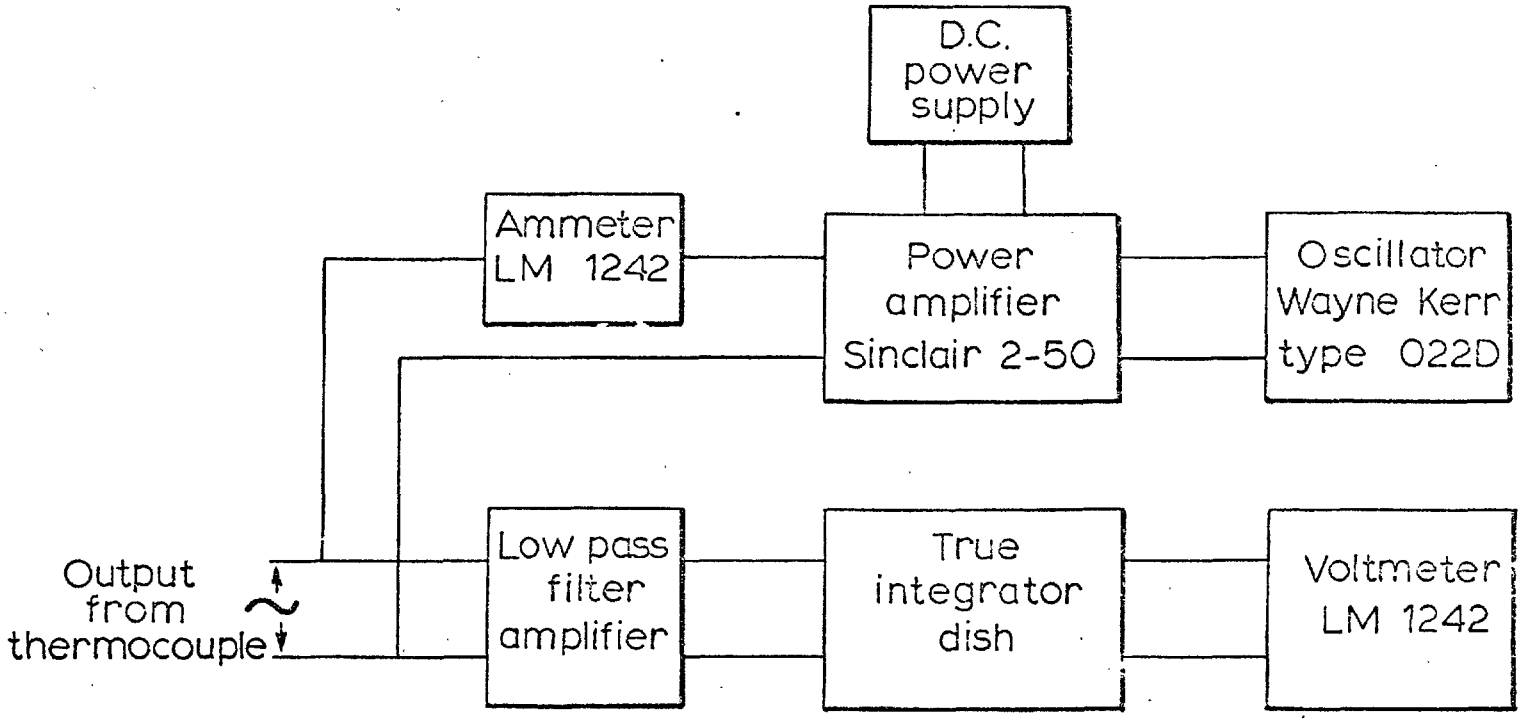


Fig.2·5: Block diagram for temperature measurement.

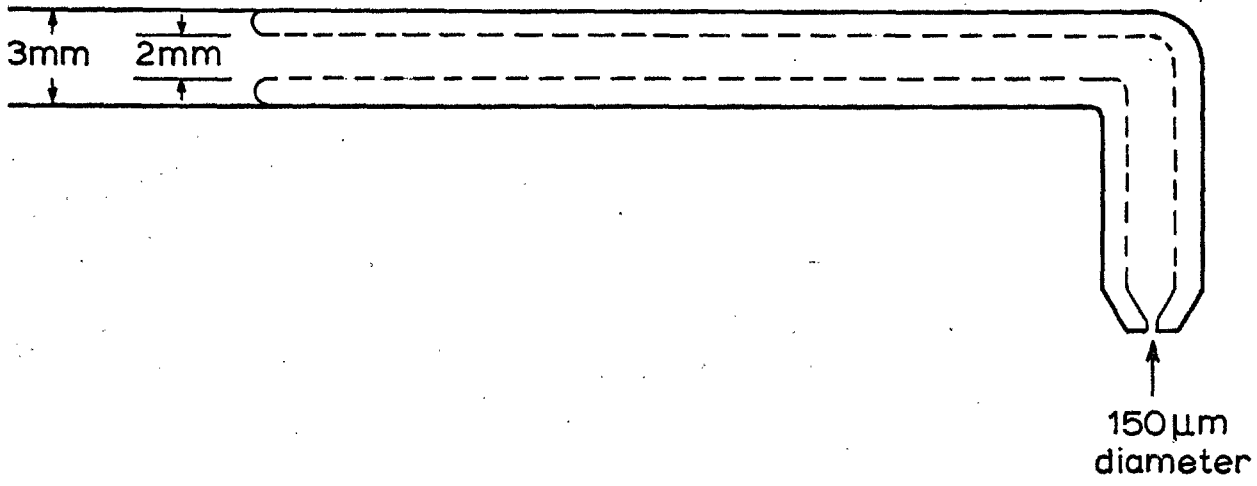


Fig. 2·6: Gas sampling probe

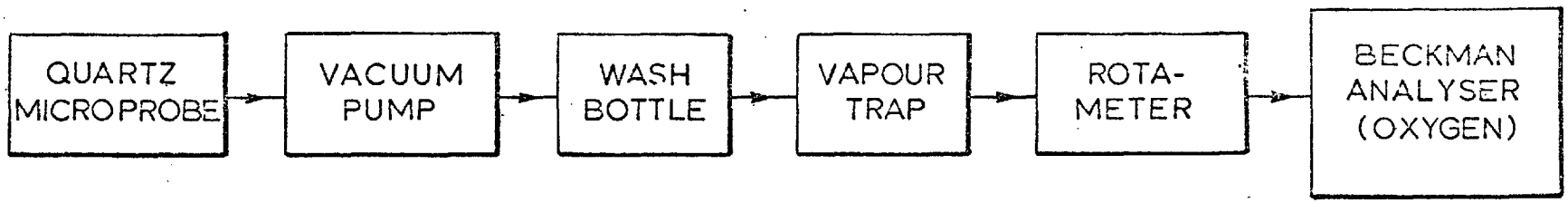


Fig.2·7: Block diagram for oxygen concentration measurement

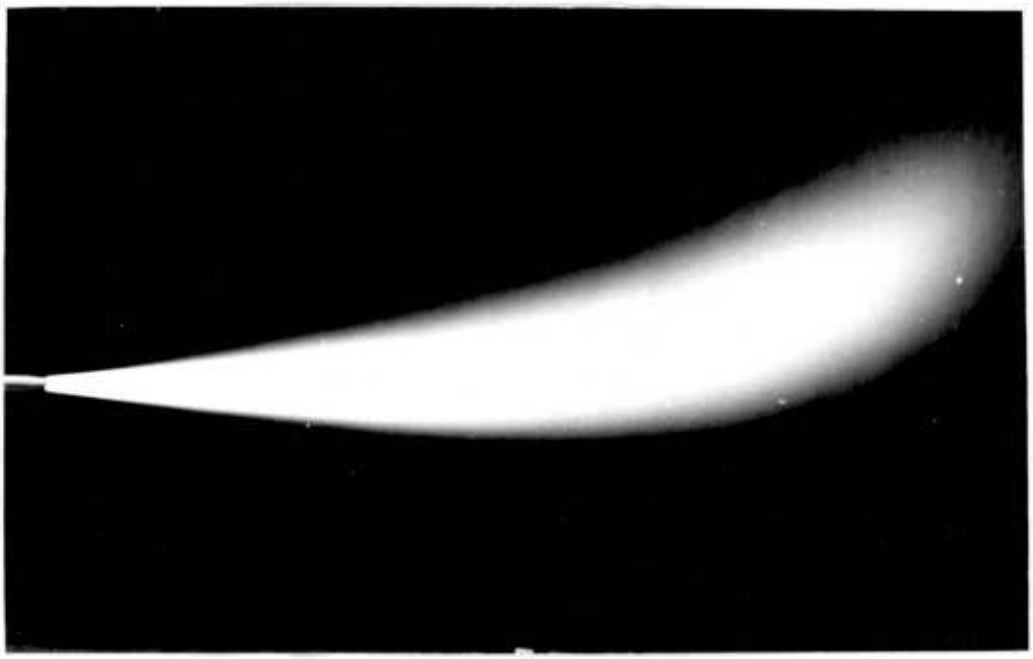


Fig. 2·8a: Long time exposure photograph of Flame I

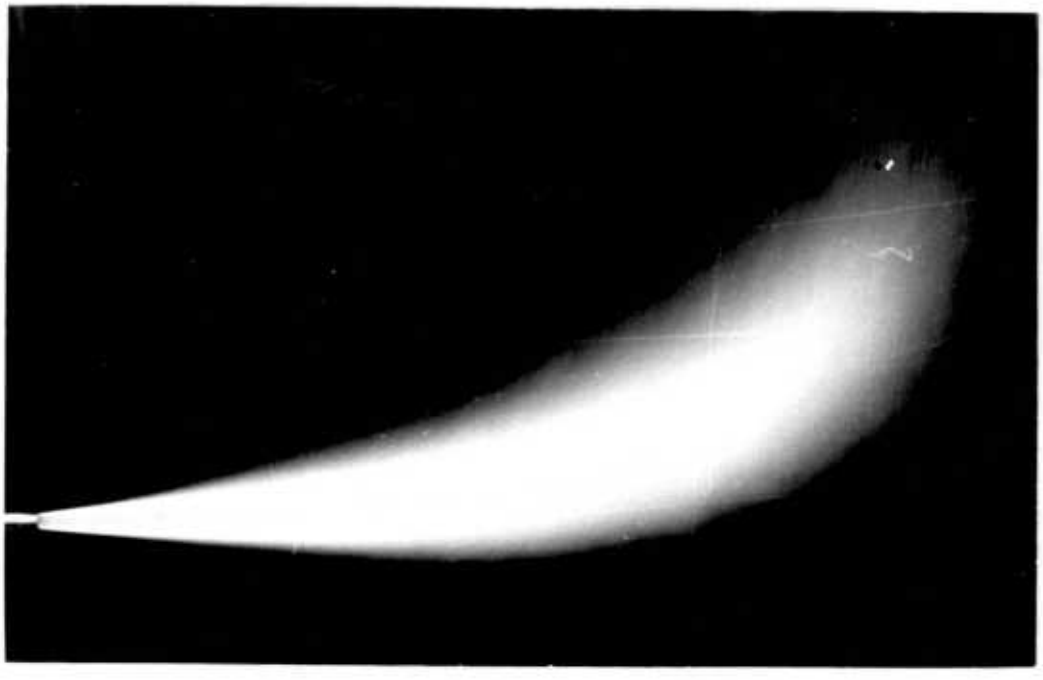


Fig. 2·8b: Long time exposure photograph of Flame II

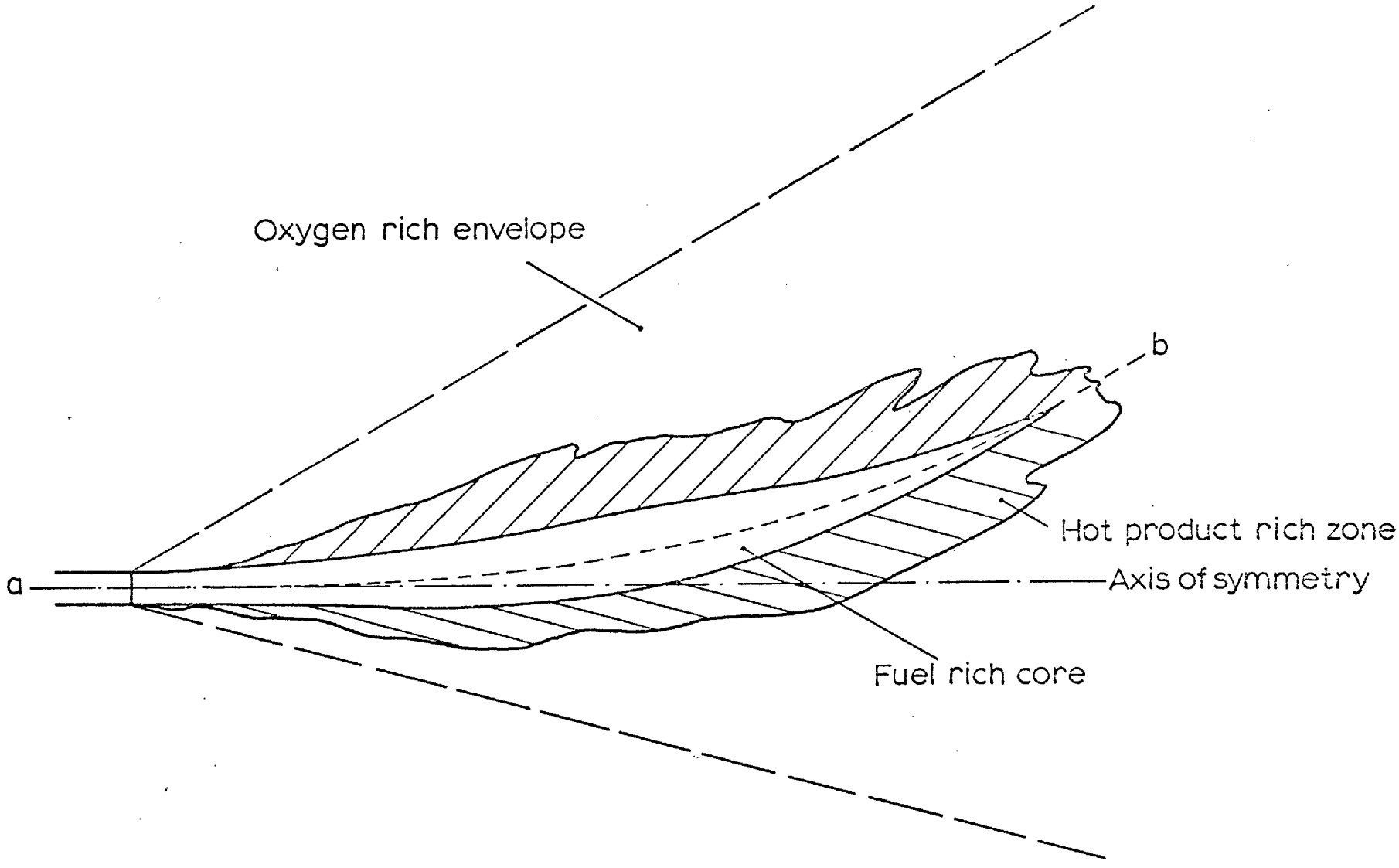


Fig.2·9: Horizontal turbulent diffusion flame

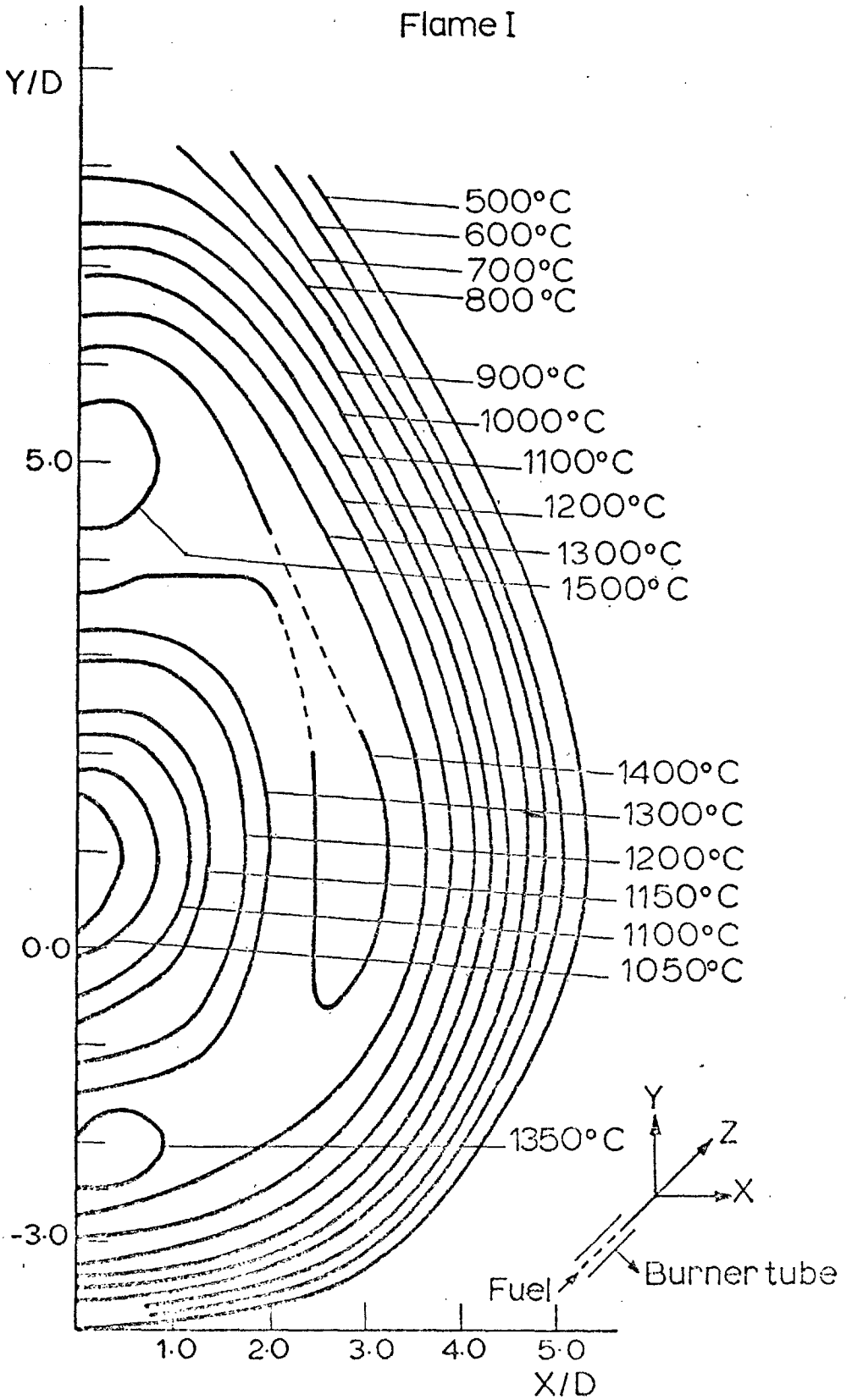


Fig.2·10: Temperature contours at Z/D = 35·4

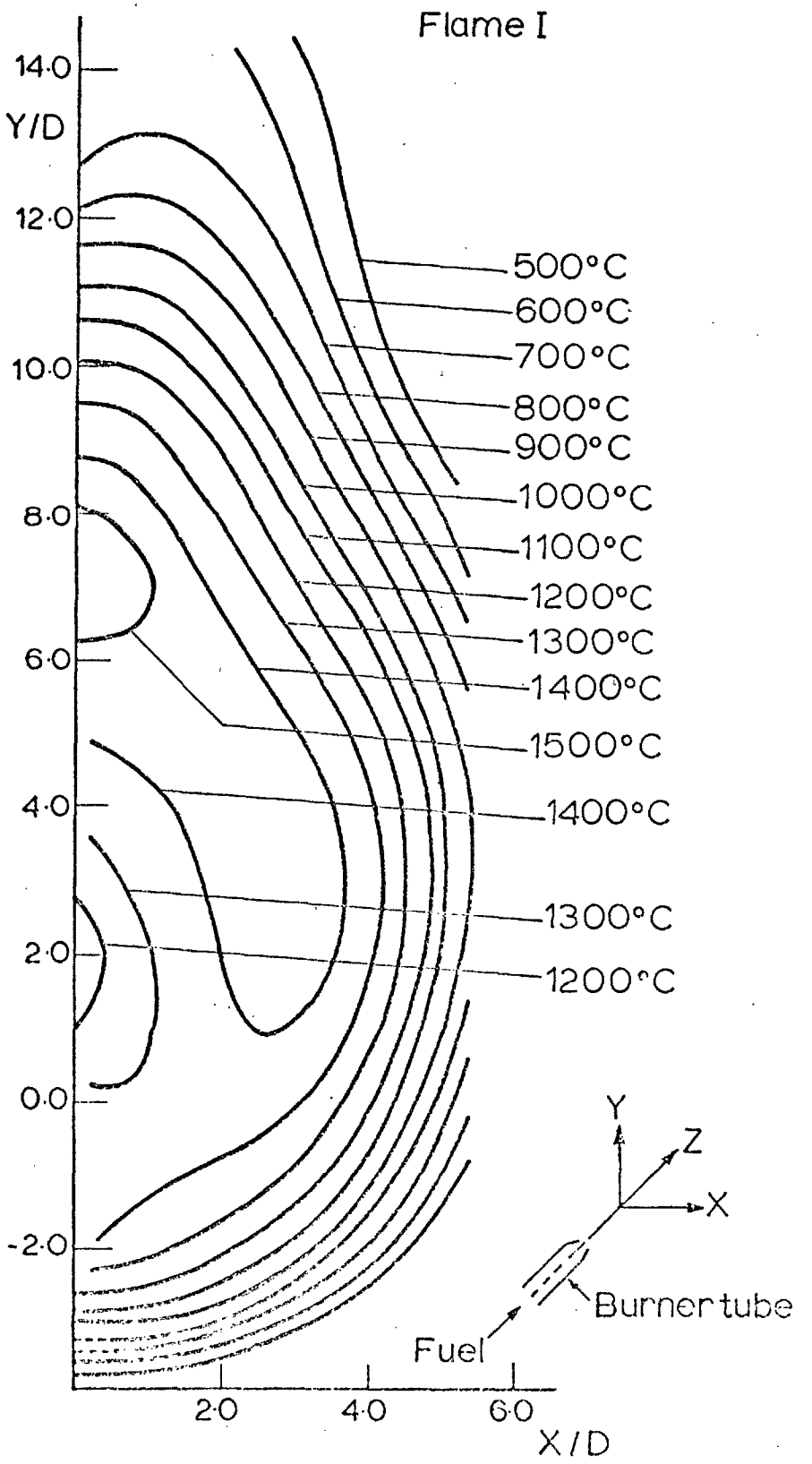


Fig.2·11: Temperature contours at Z/D=47

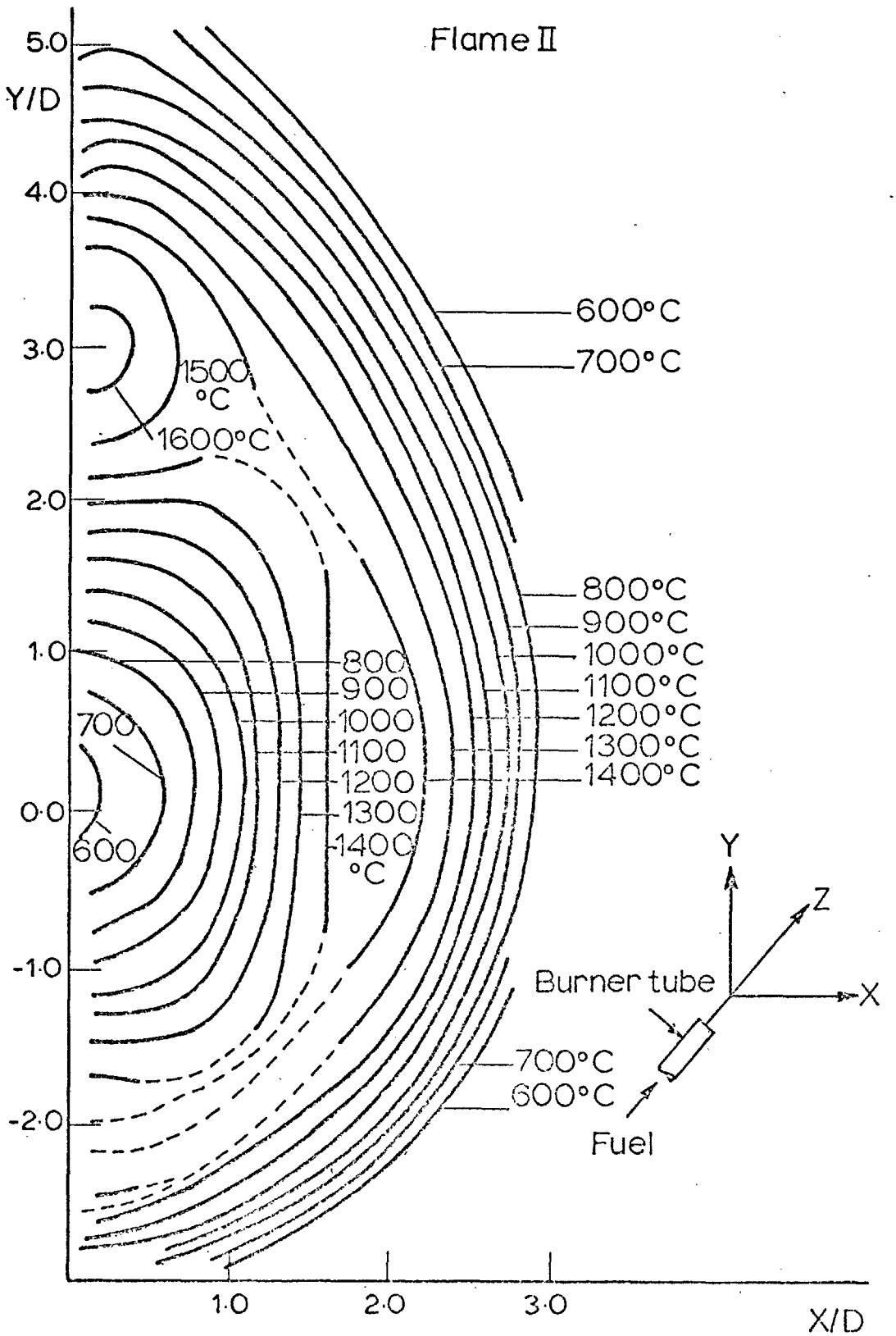


Fig.2.12: Temperature contours at Z/D = 29.0

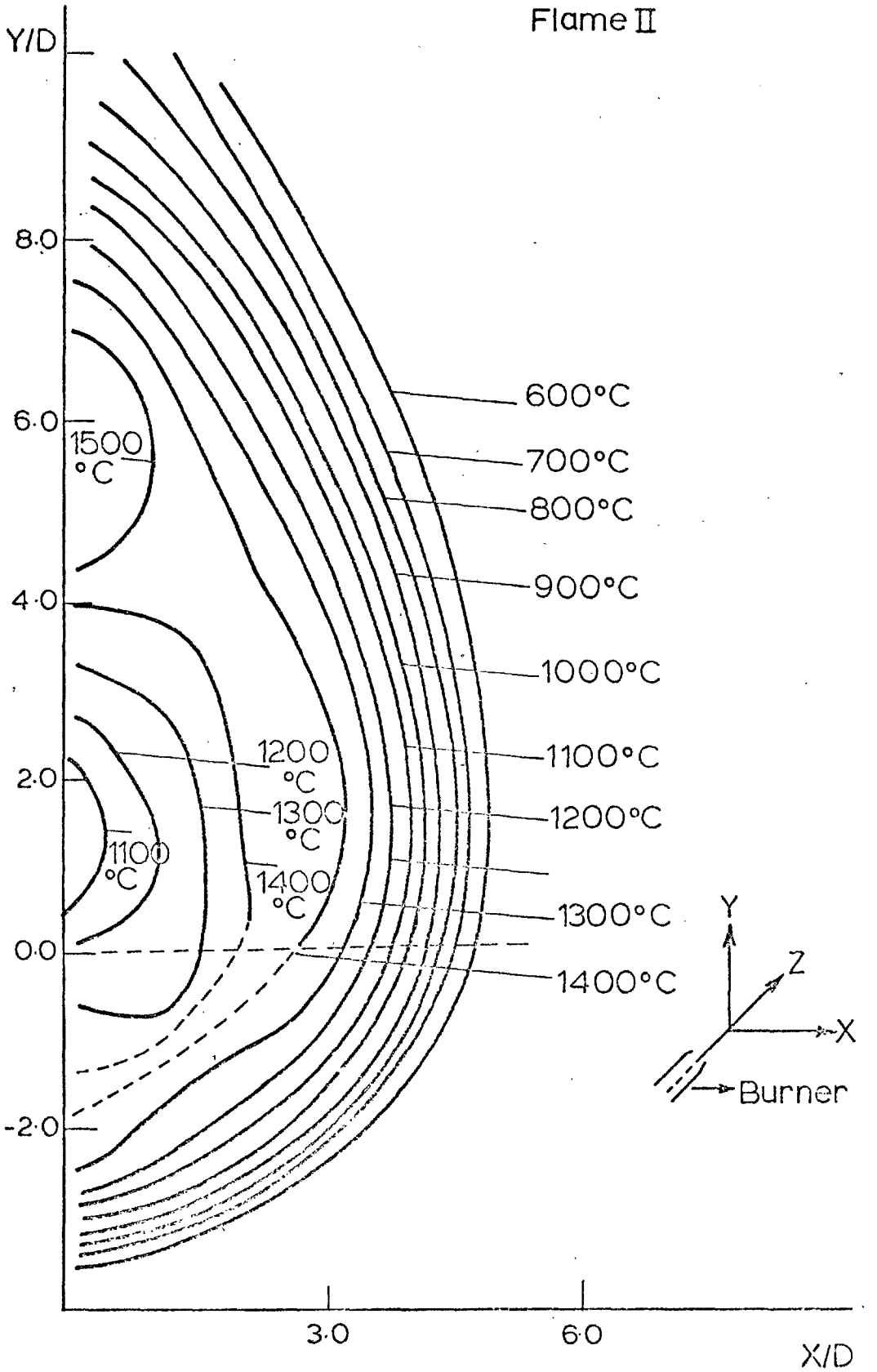


Fig. 2·13: Temperature contours at Z/D = 35·4

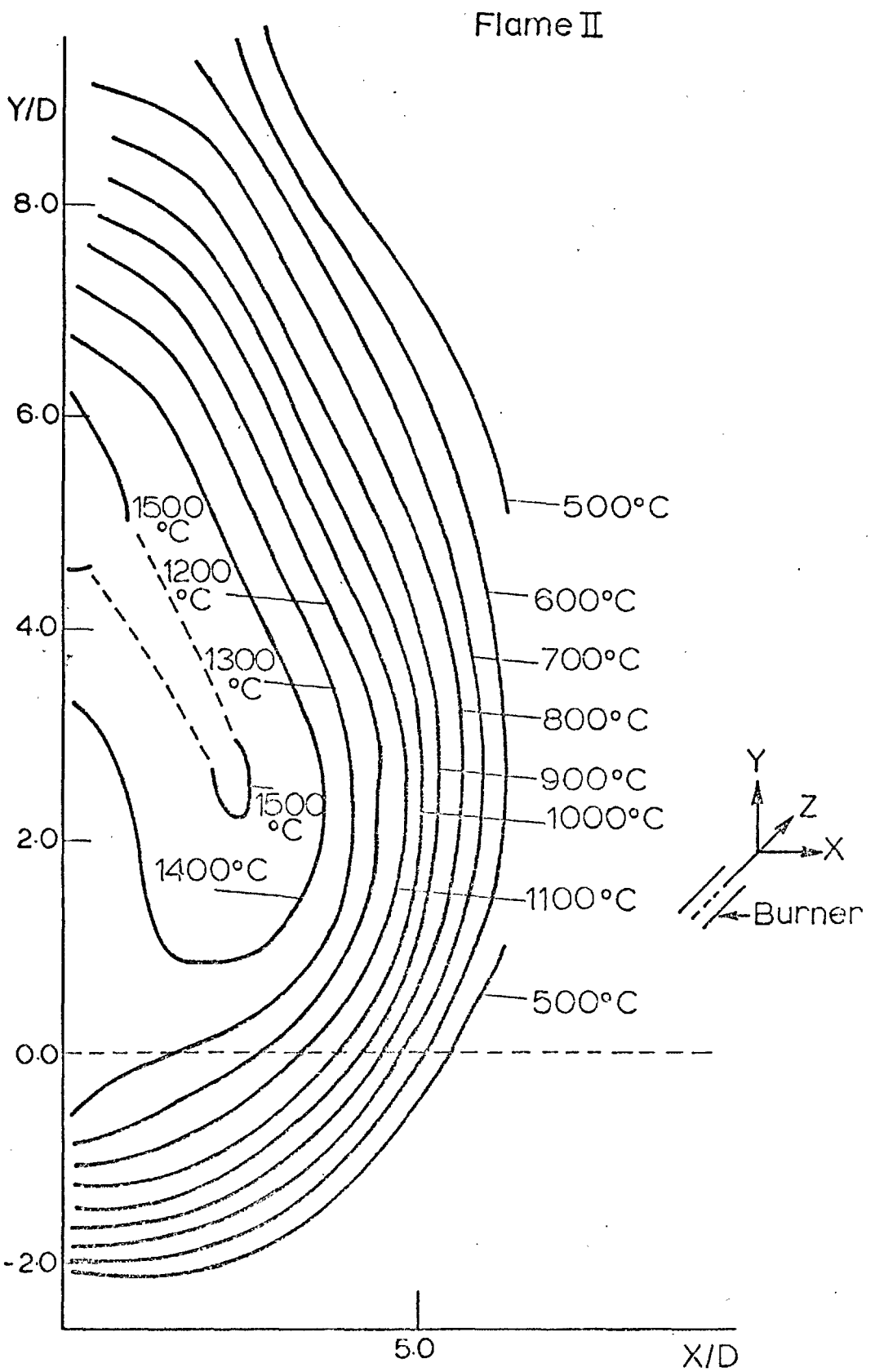


Fig. 2·14: Temperature contours at Z/D = 47·0

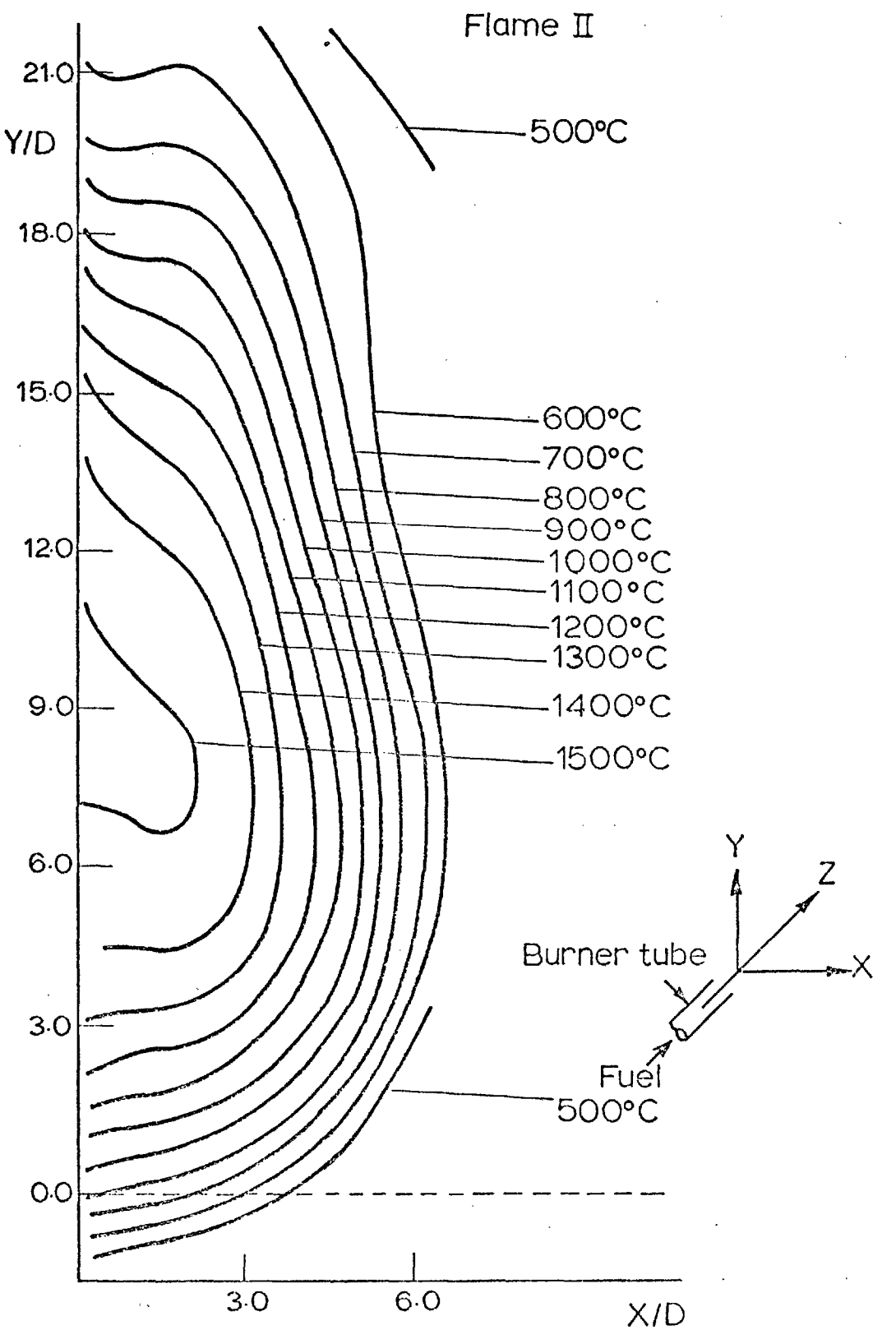


Fig. 2·15: Temperature contours at Z/D = 59

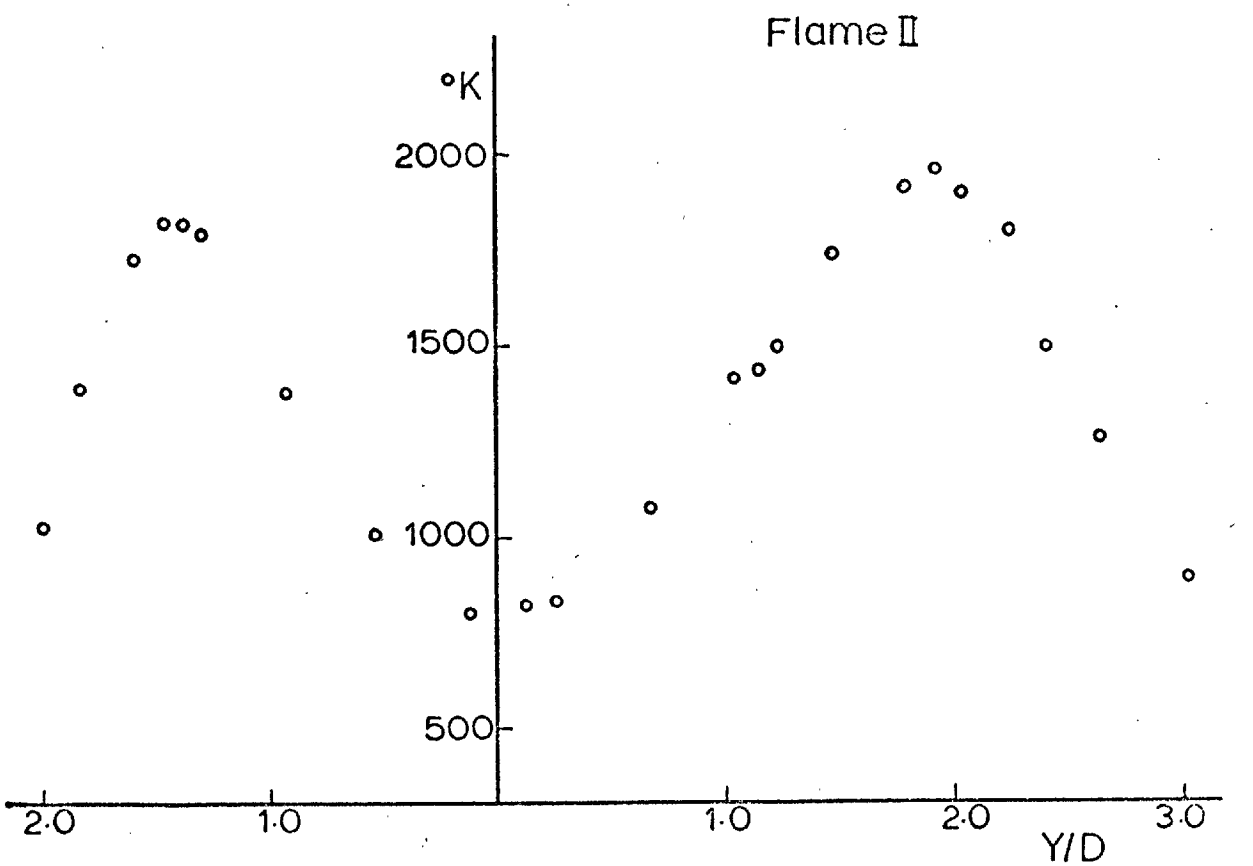


Fig. 2·16a: Temperature profile along Y-axis at Z/D=13

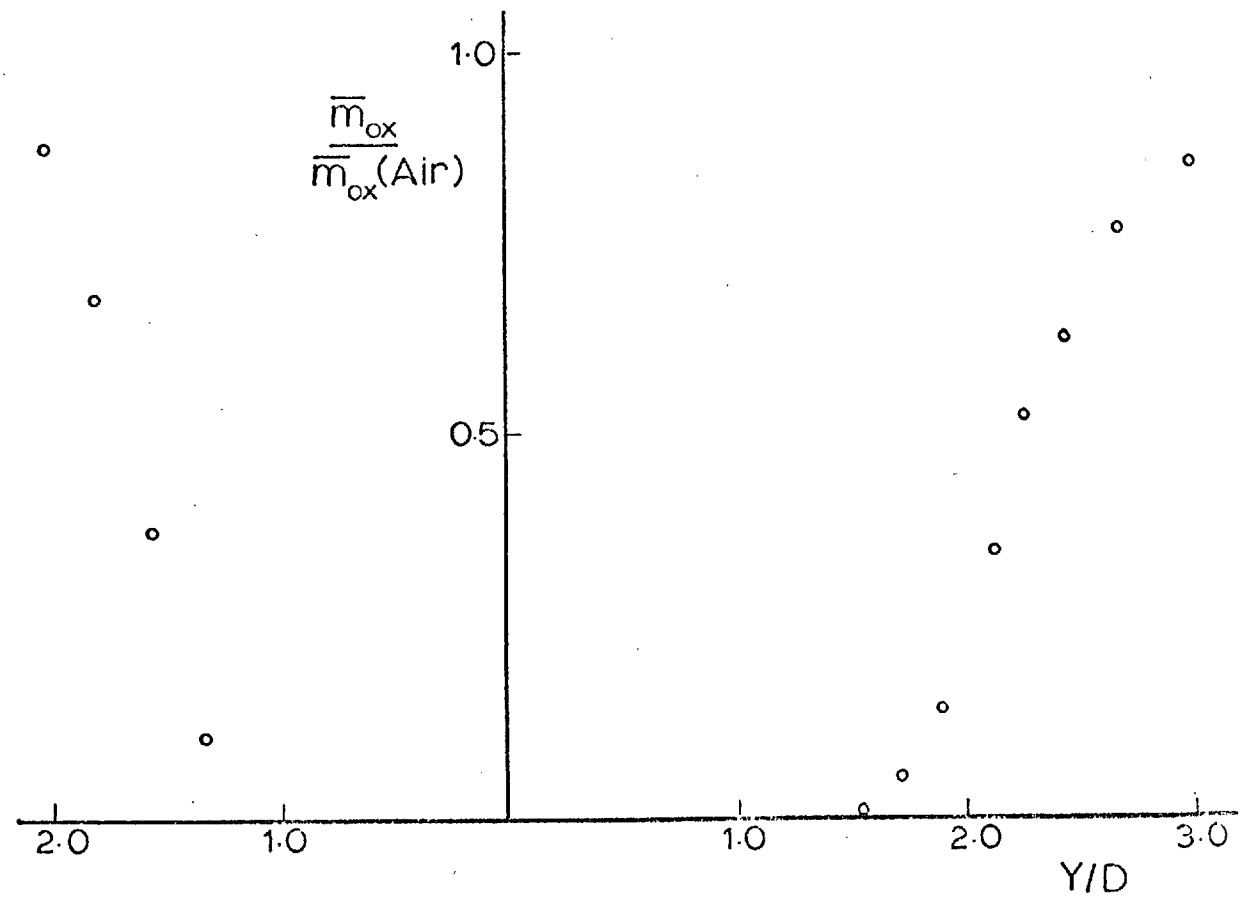


Fig. 2·16b: Oxygen concentration profile along Y-axis at Z/D=13

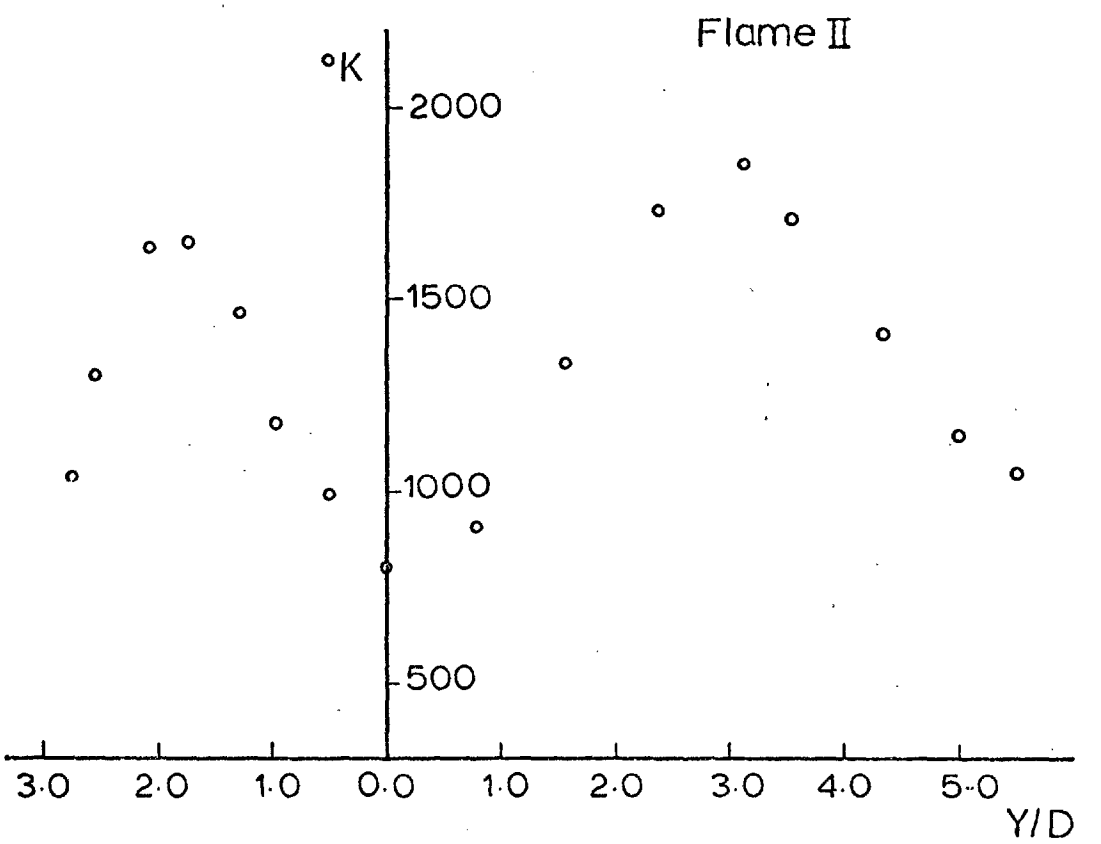


Fig.2·17a: Temperature profile along Y-axis at Z/D = 29

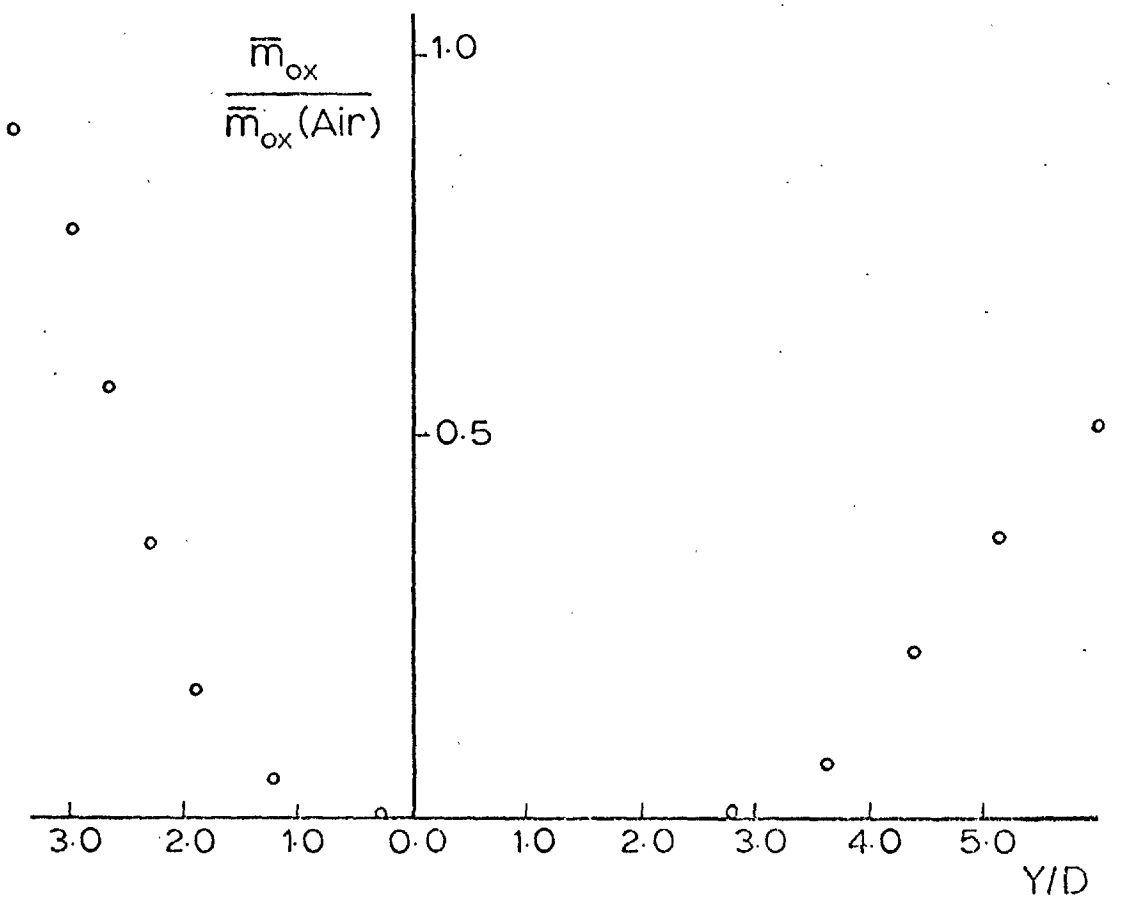


Fig.2·17b: Oxygen concentration profile along Y-axis at Z/D = 29

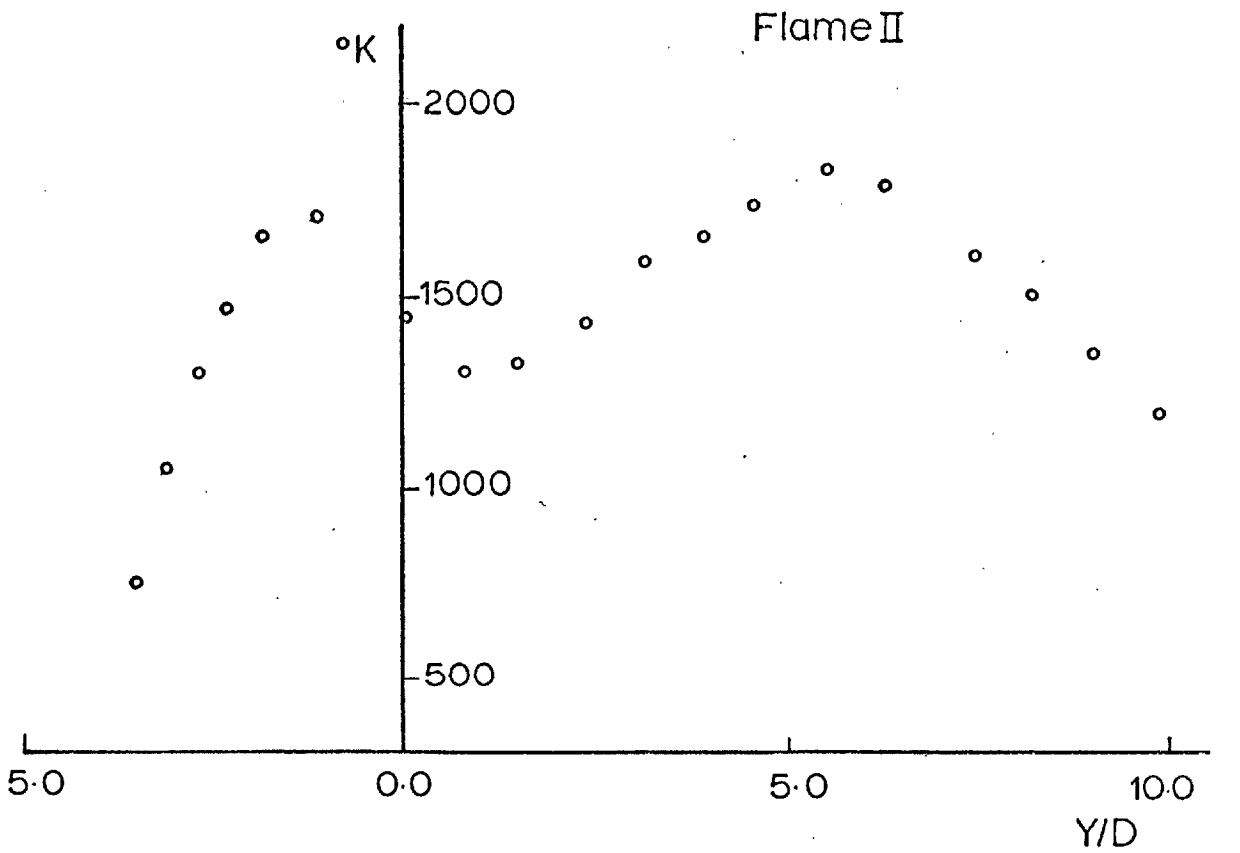


Fig.2·18a: Temperature profile along Y-axis at Z/D=34

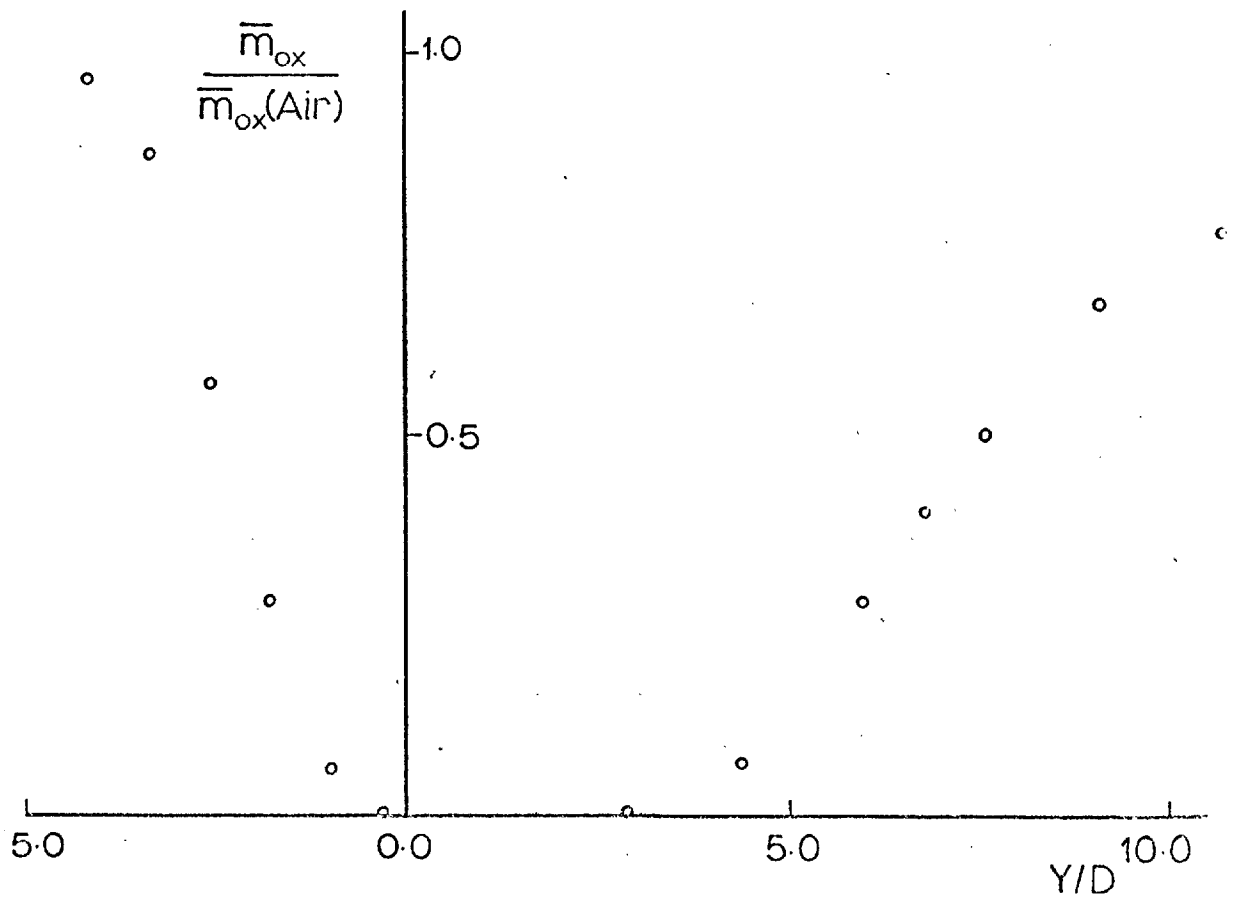


Fig.2·18b: Oxygen concentration profile along Y-axis at Z/D = 34

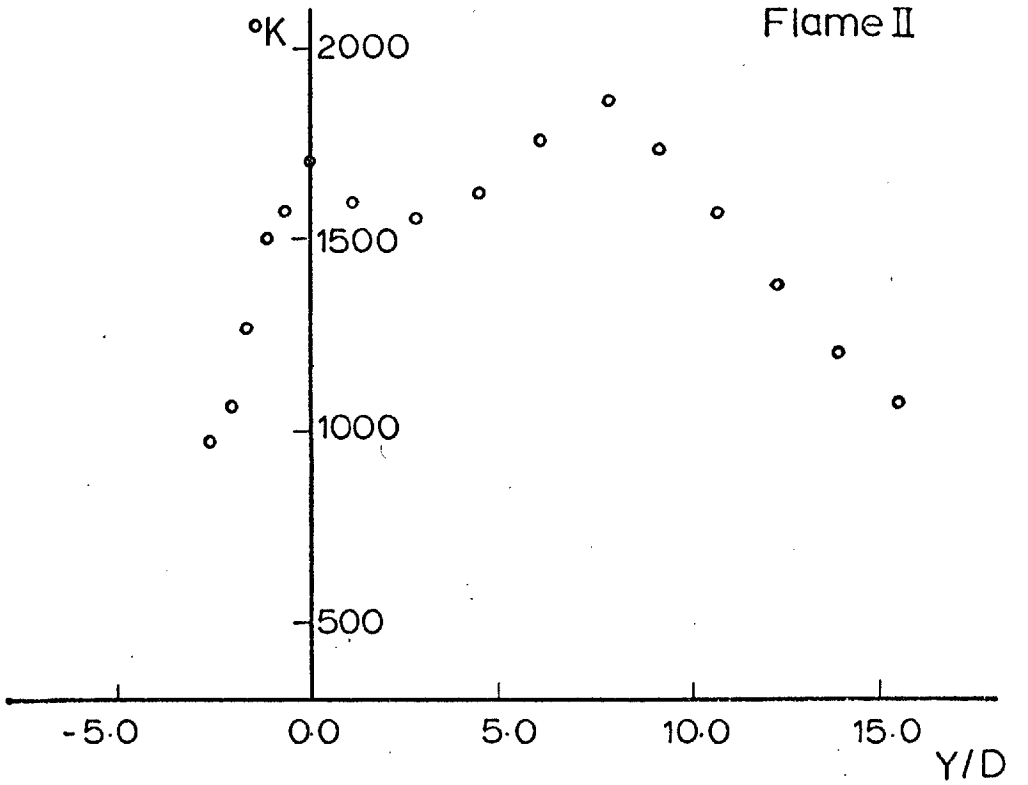


Fig. 2·19a: Temperature profile along Y-axis at Z/D=47·0

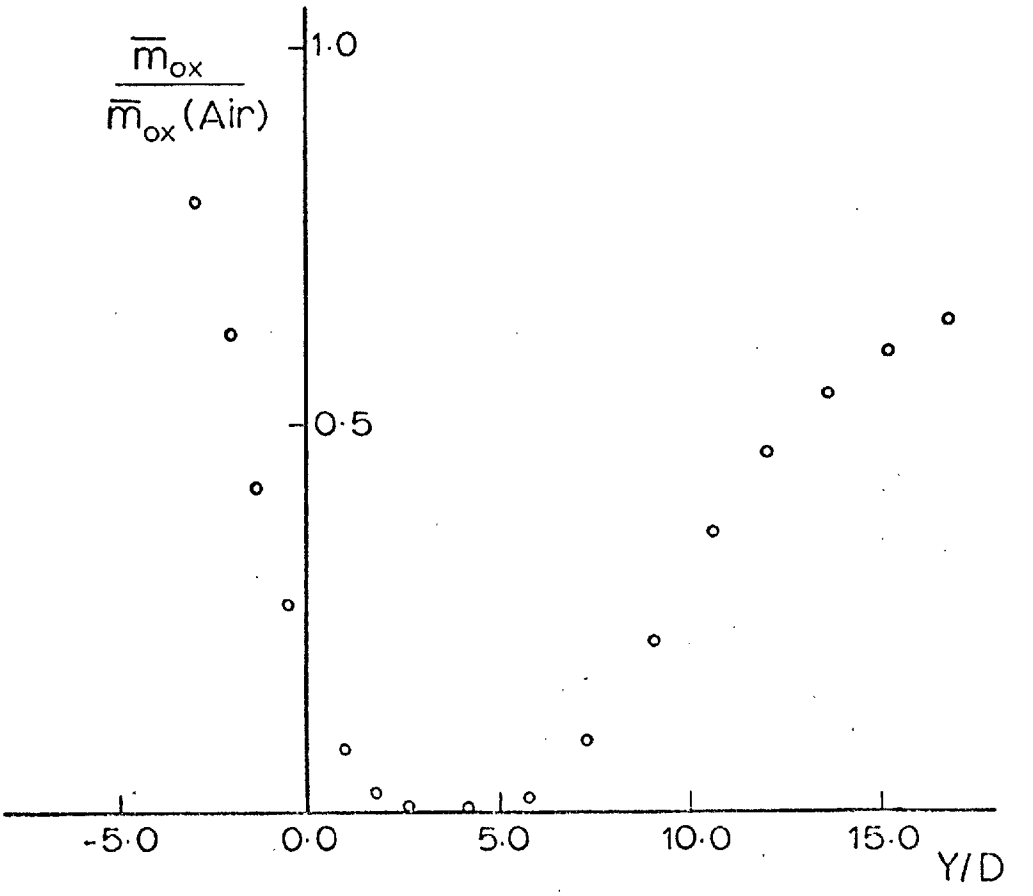


Fig. 2·19b: Oxygen concentration profile along Y-axis at Z/D=47·0

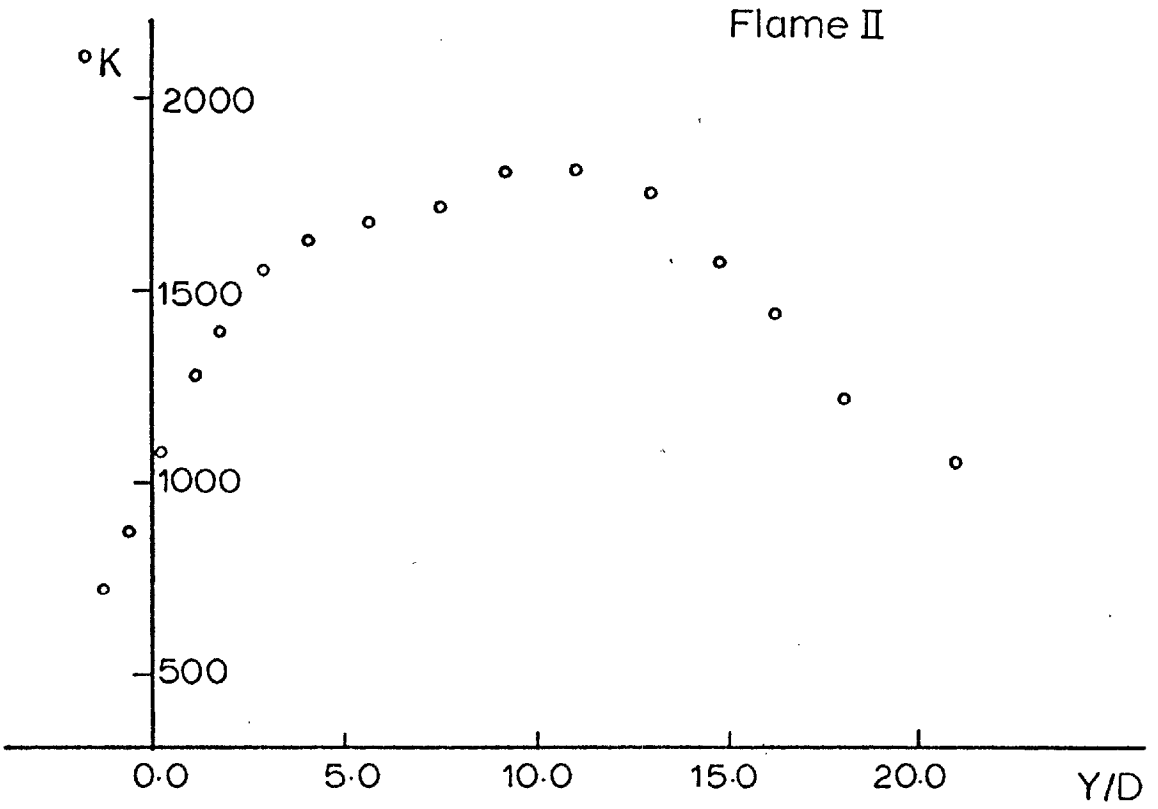


Fig.2·20a: Temperature profile along Y-axis at Z/D = 59

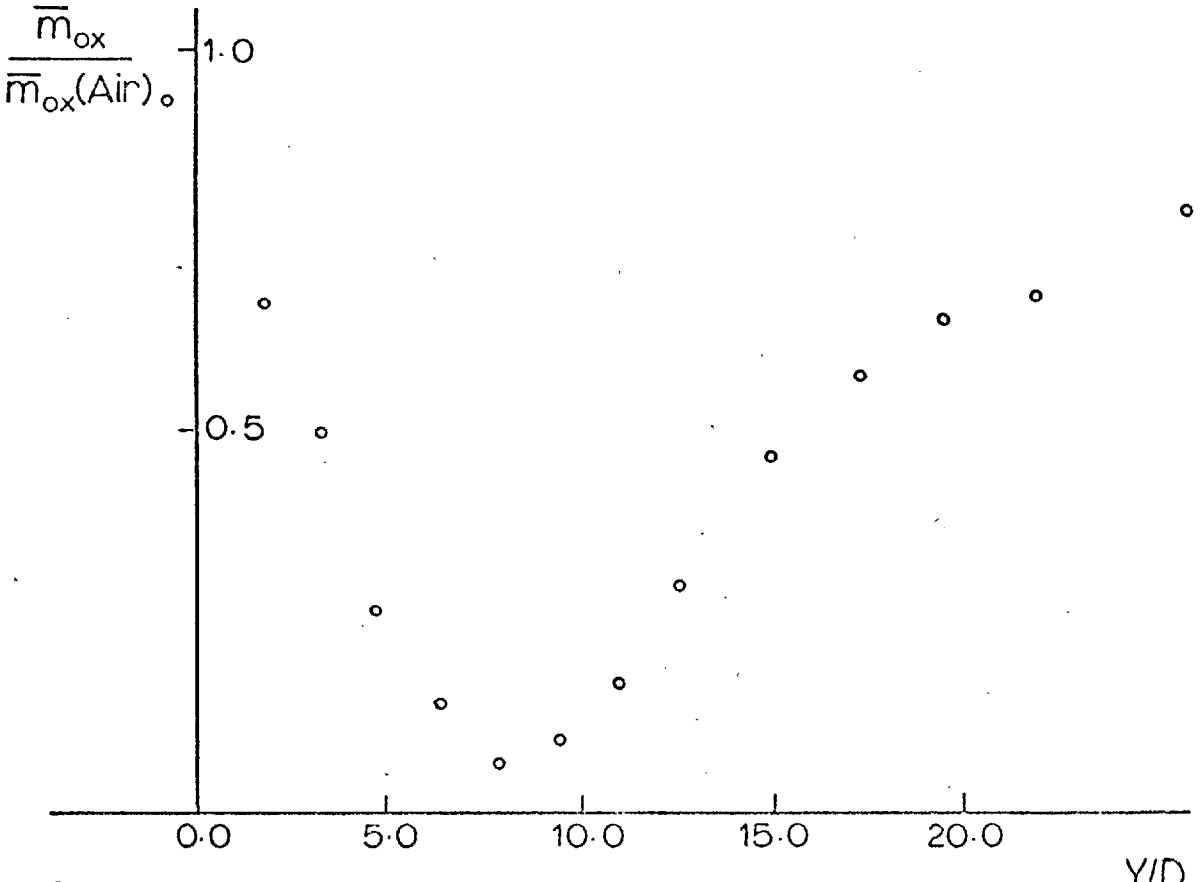


Fig.2·20b: Oxygen concentration profile along Y-axis at Z/D = 59

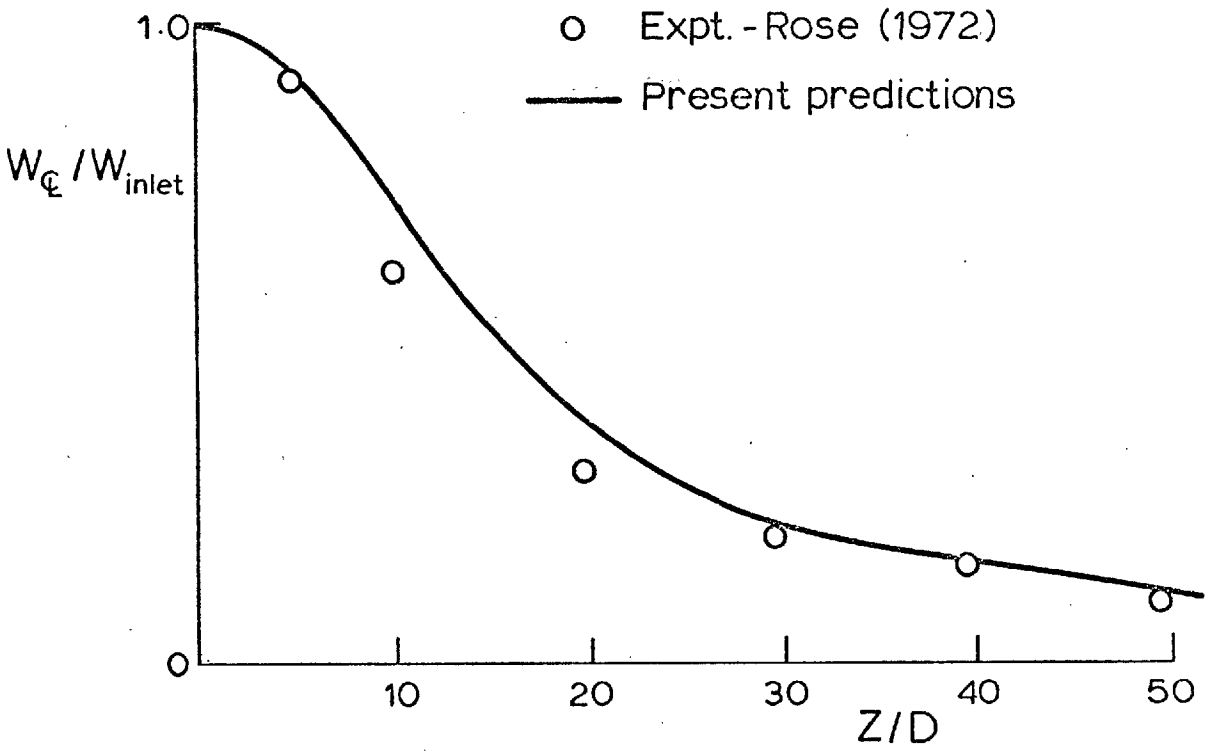


Fig. 4·1: Axial distribution of $W_{\mathbb{C}}/W_{inlet}$

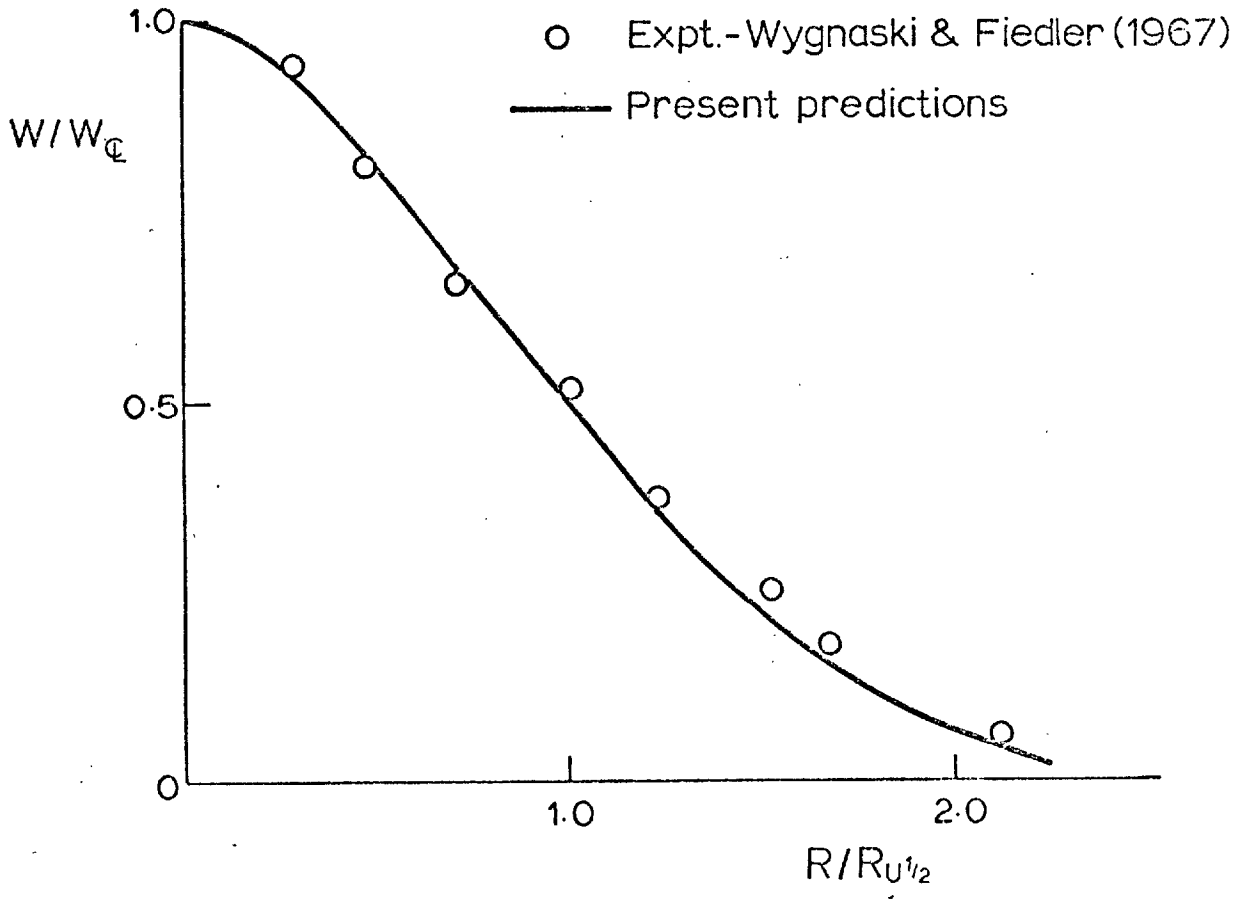


Fig. 4·2: Fully developed velocity profile

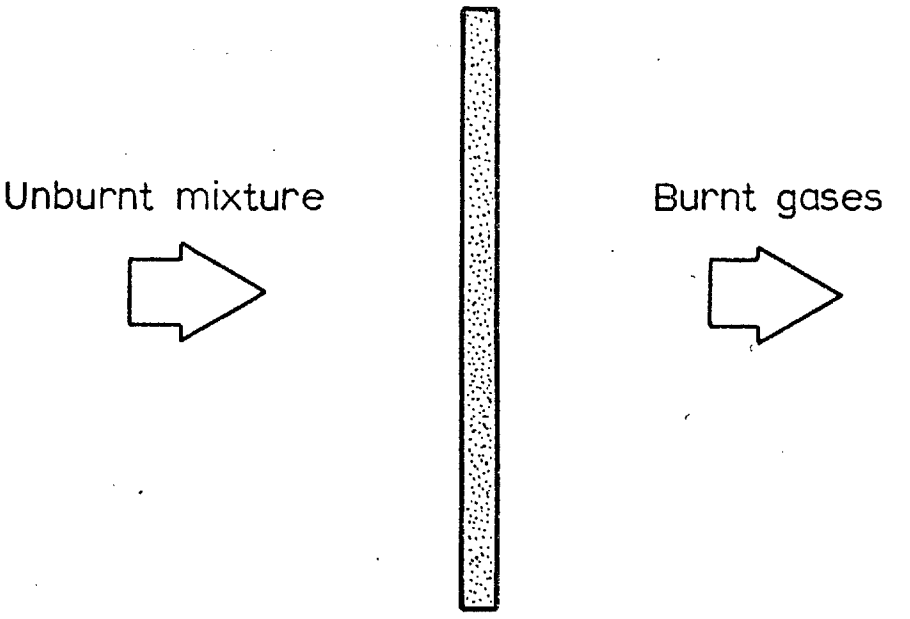


Fig. 5·1a: Laminar flame front

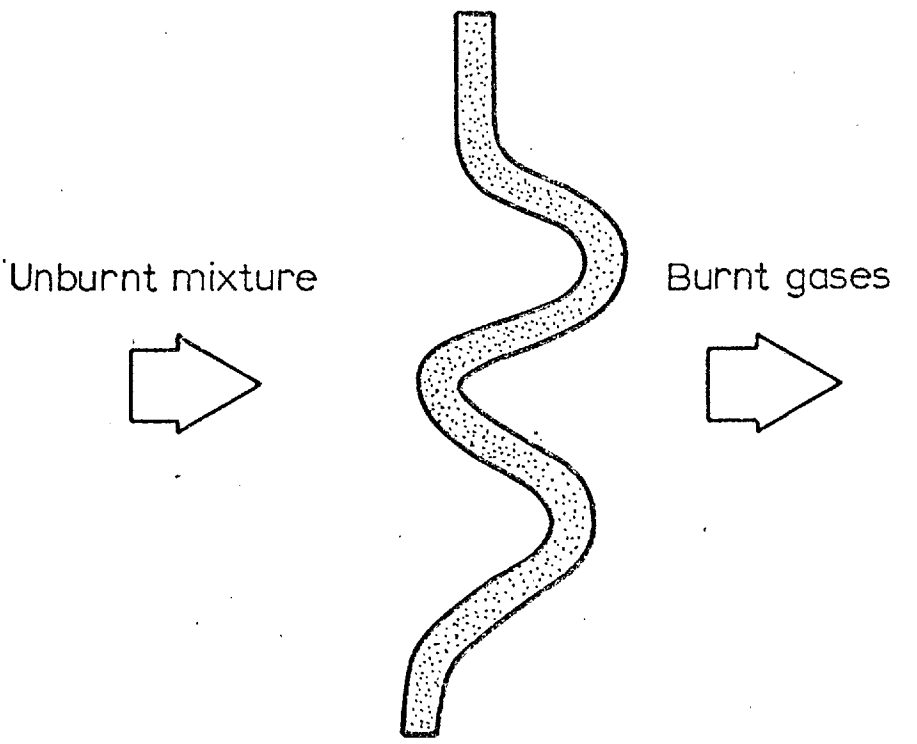


Fig.5·1b: Wrinkled laminar flame

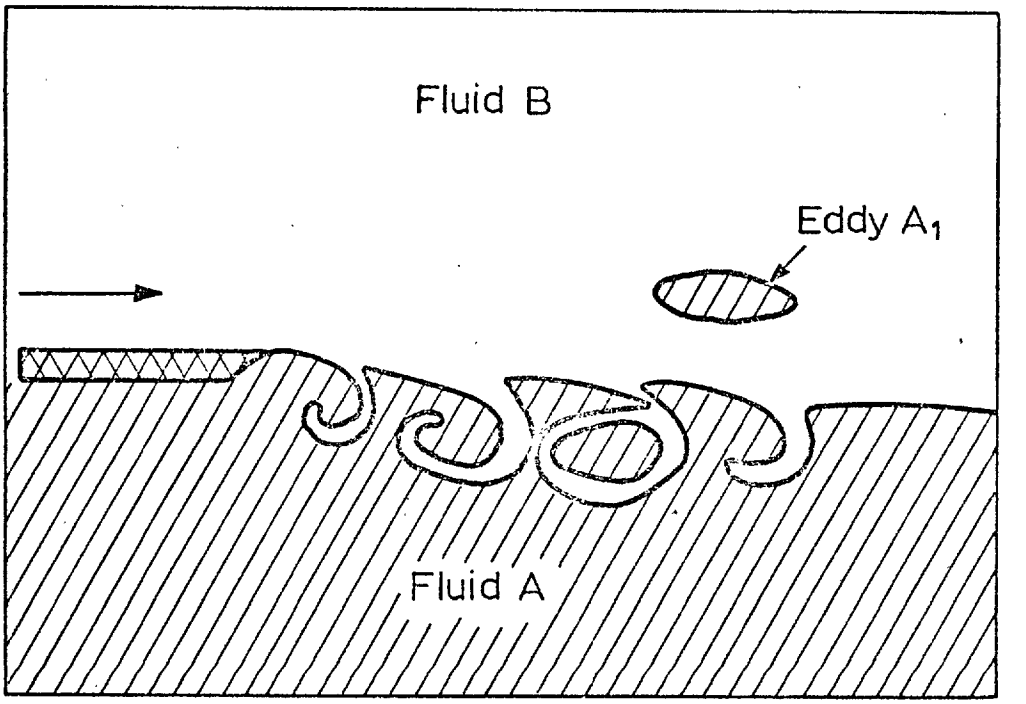


Fig.5·2a: Turbulent mixing of two fluids

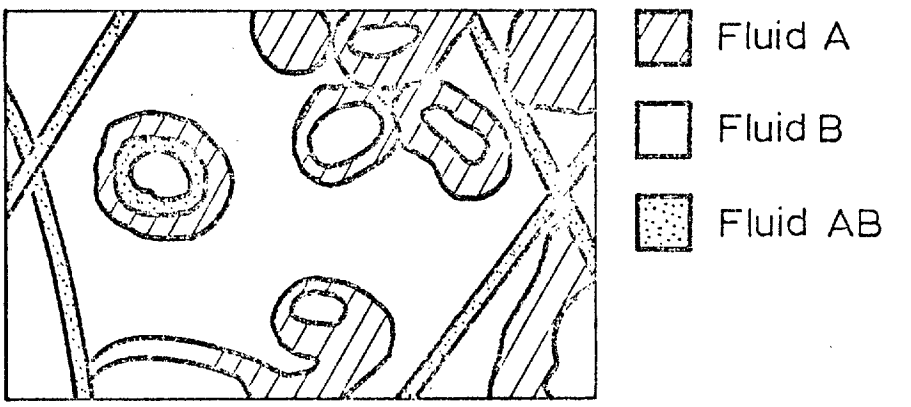


Fig.5·2b: Control volume in a turbulent fluid

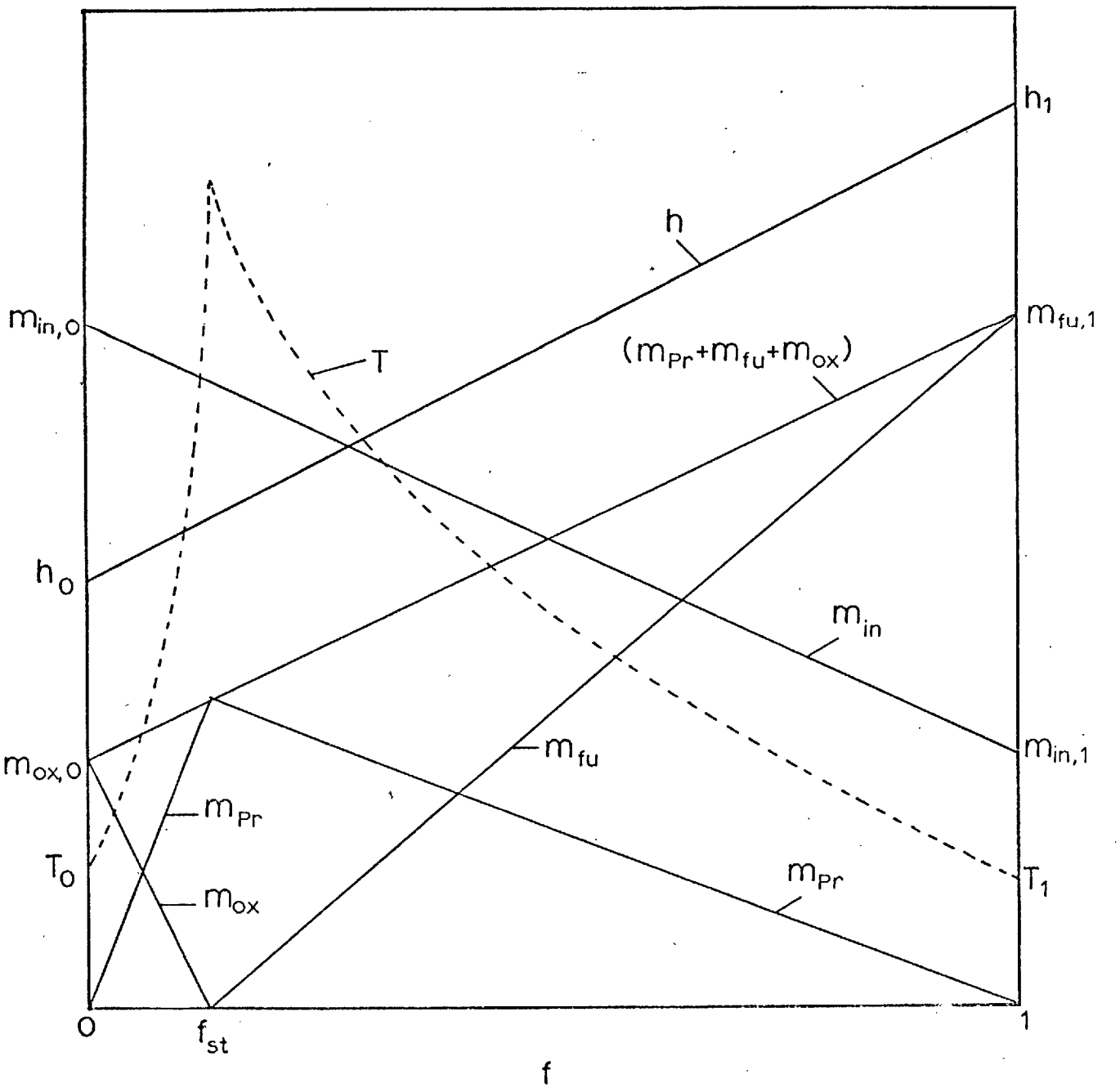


Fig.5.3: Mixture fraction *vs.* various thermodynamic variables

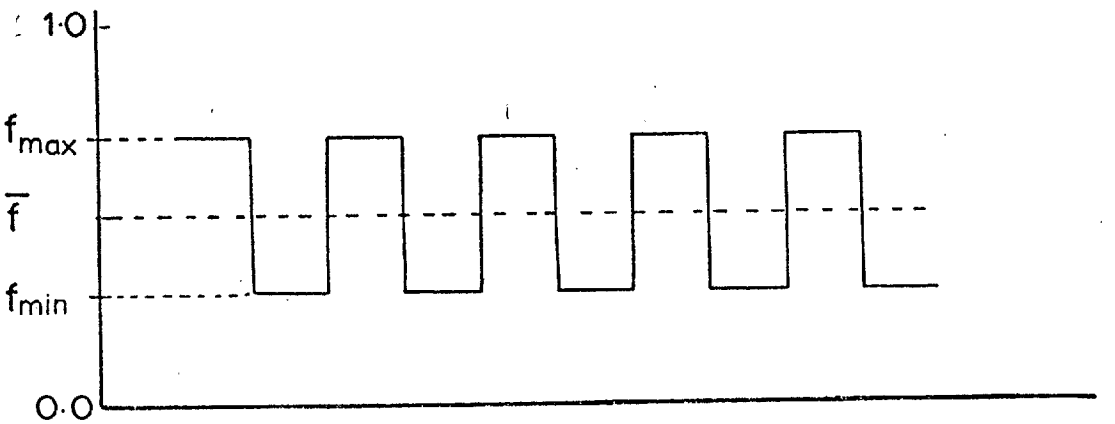


Fig.5·4: Square wave fluctuation

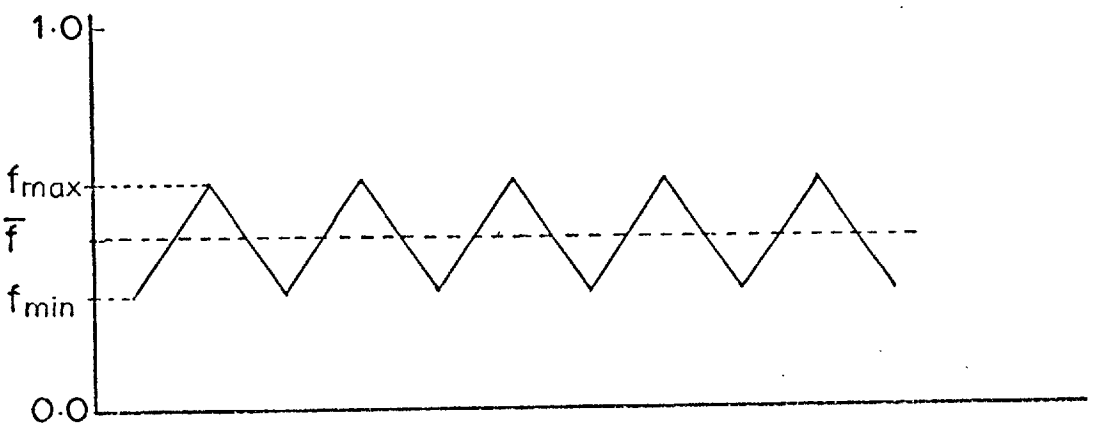


Fig.5·5 : Triangular wave fluctuation

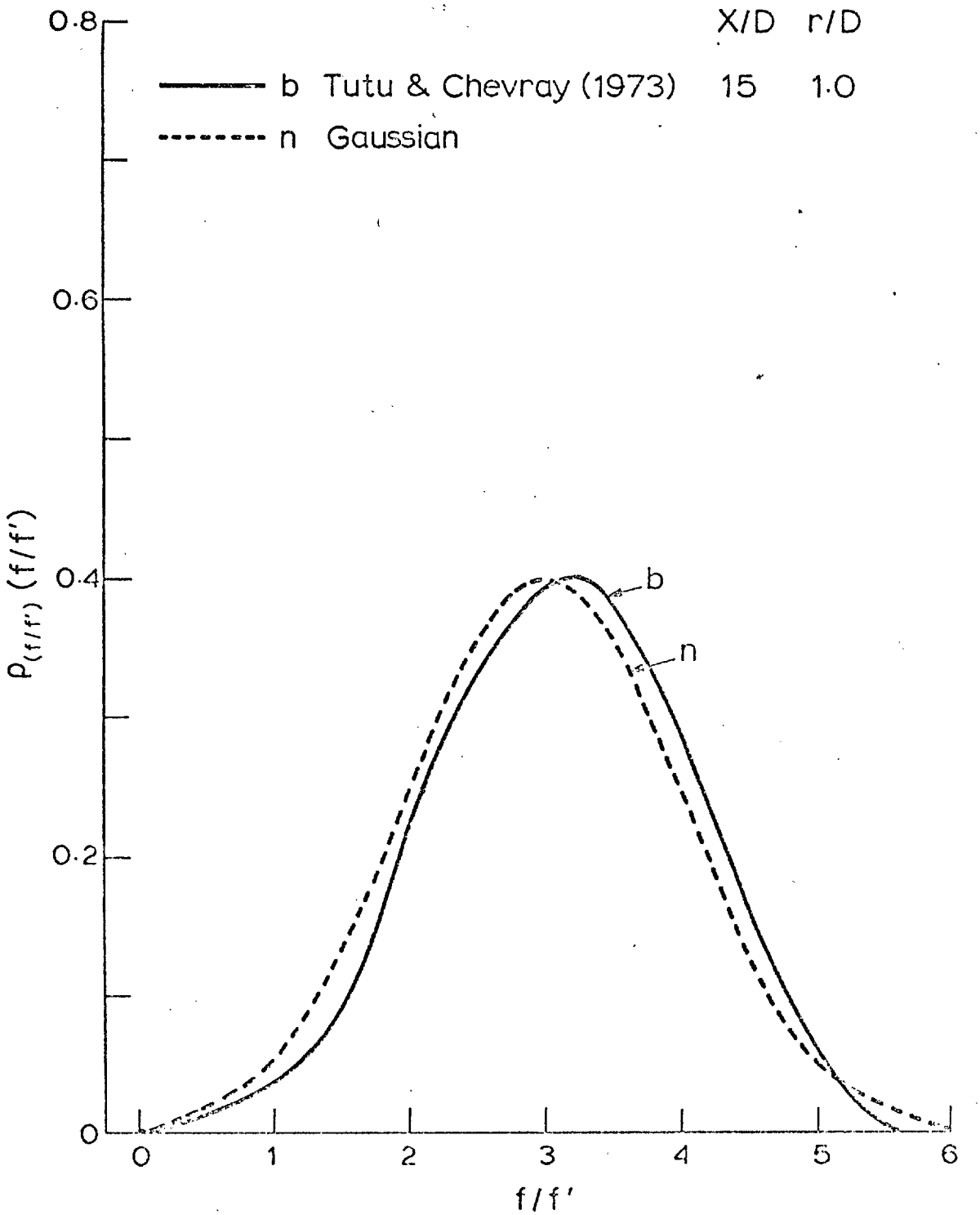


Fig.5·6: Probability density function for a conserved scalar in a slightly heated round jet

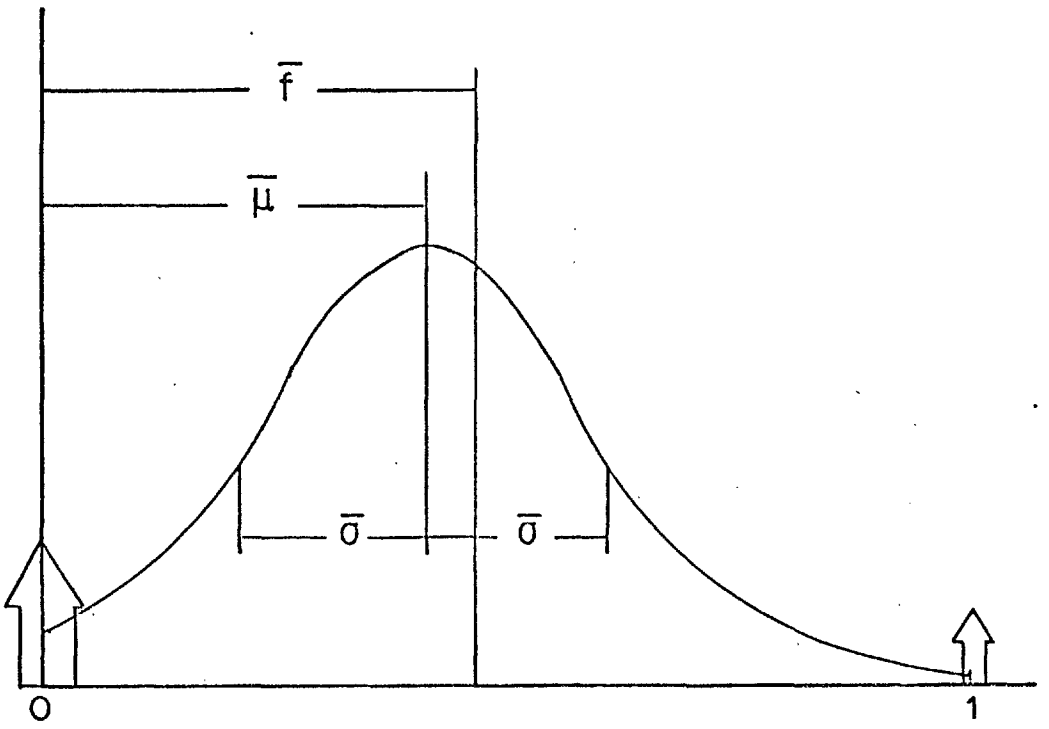


Fig.5·7: Clipped Gaussian distribution function for the mixture fraction.

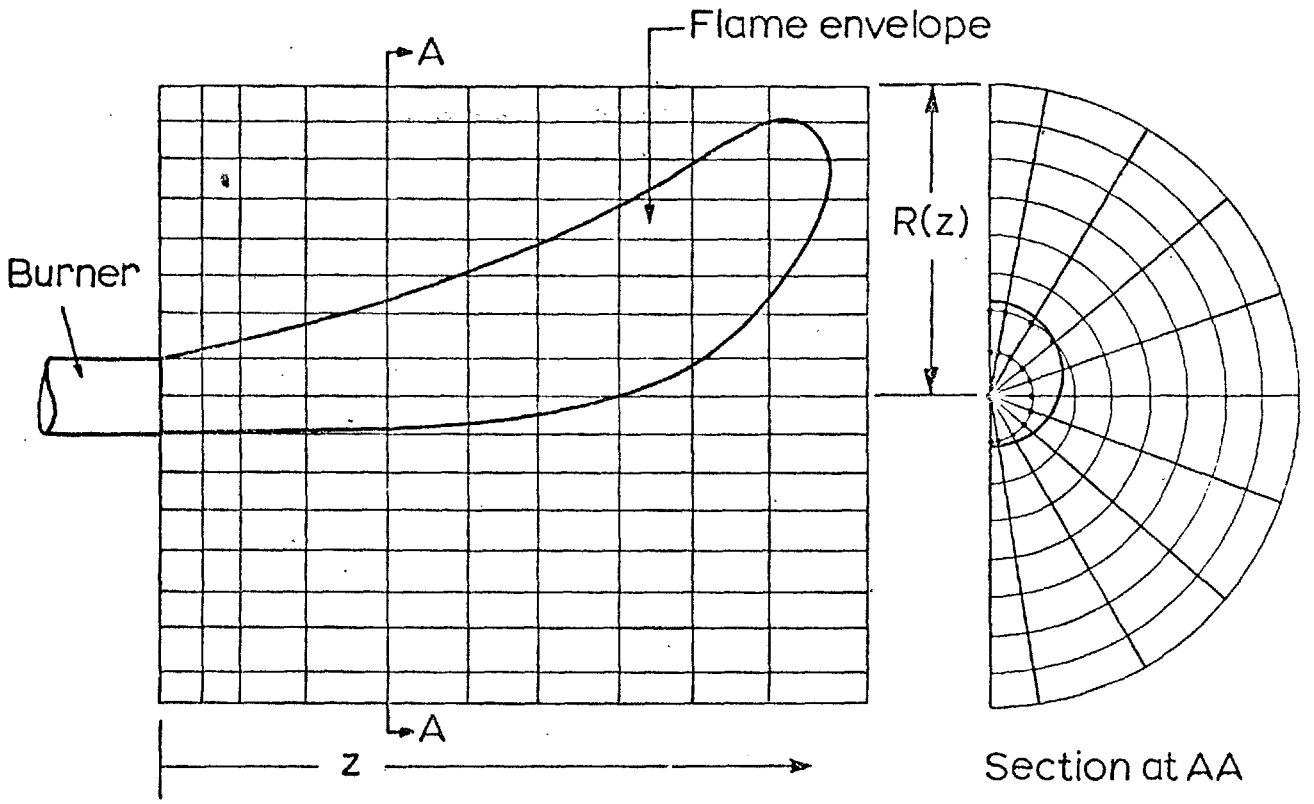


Fig. 6·1: Cylindrical co-ordinate grid system

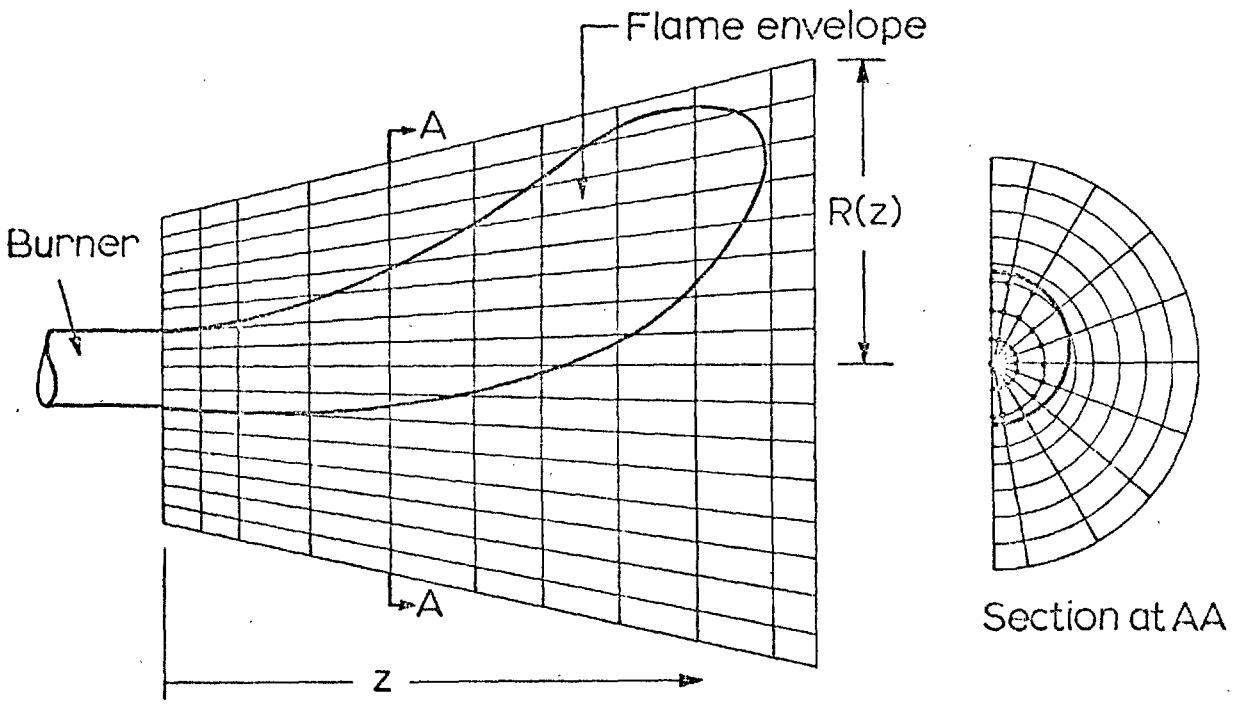


Fig. 6·2: Quasi - orthogonal co-ordinate grid system

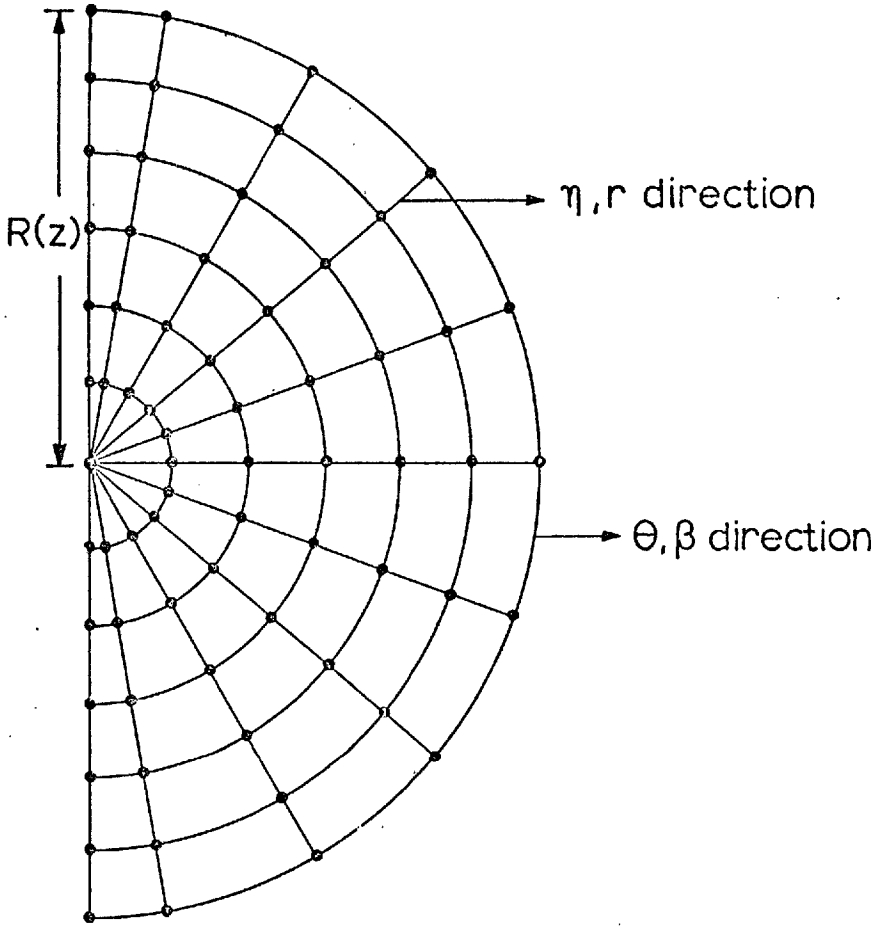


Fig. 6·3: Grid system in $\beta \sim \eta$ plane

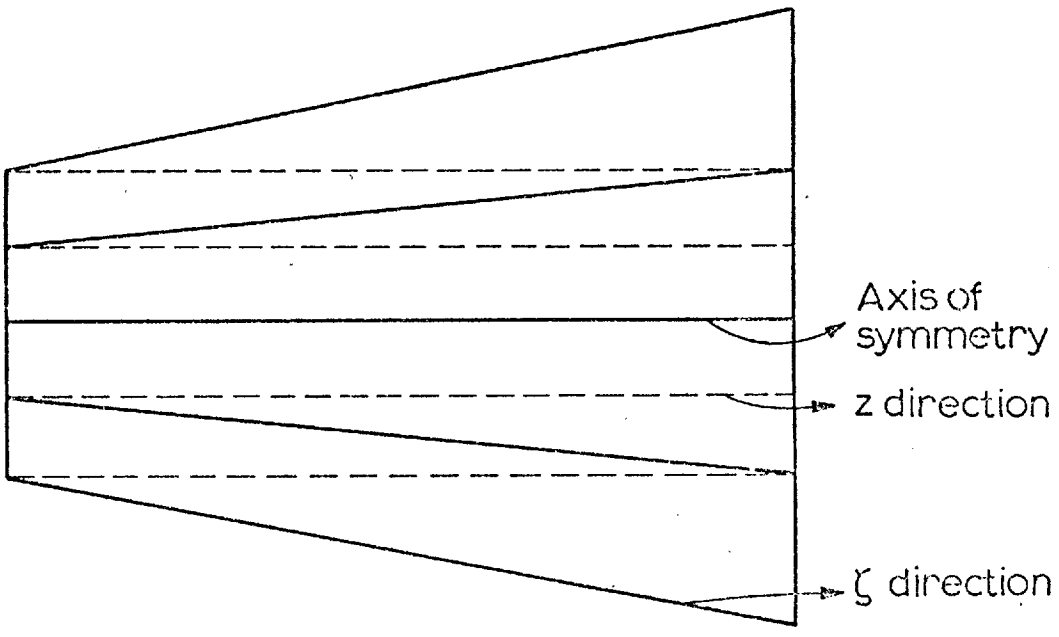
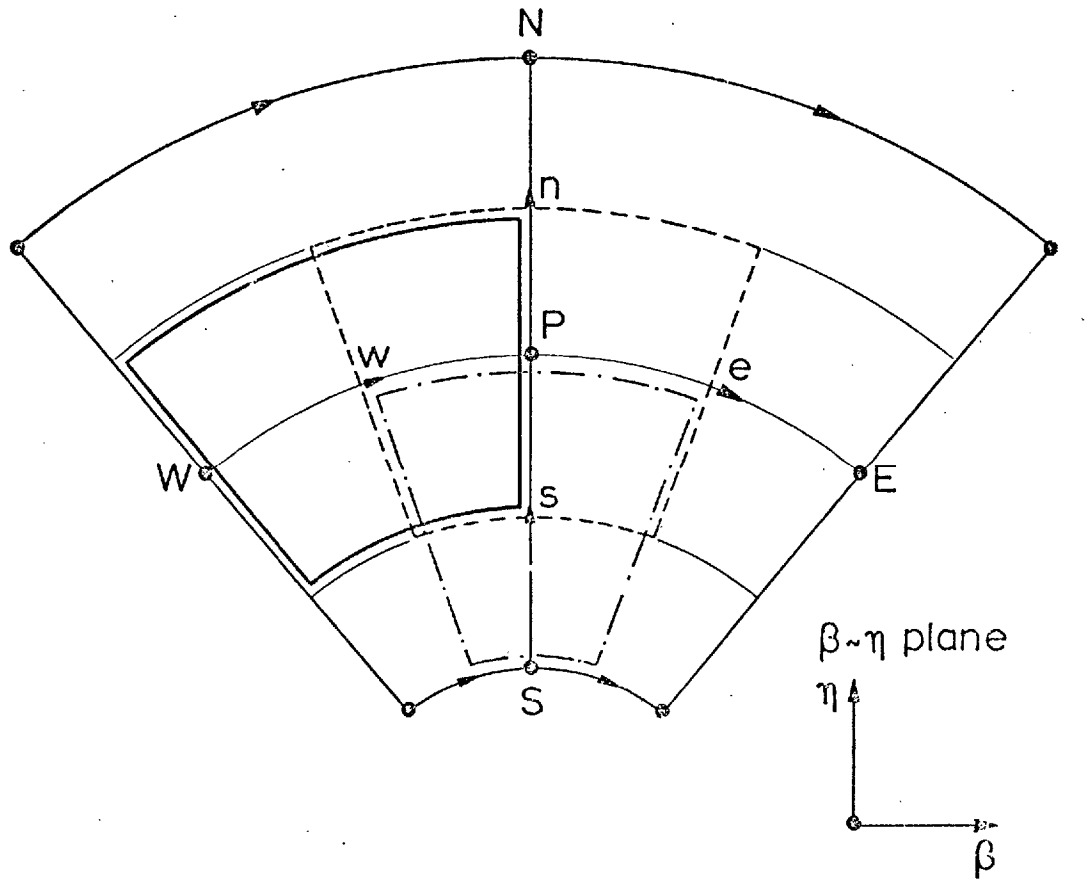


Fig. 6·4: Grid system in $\zeta \sim \eta$ plane



p-cell; p, w, Φ, ρ stored

v-cell; radial velocity $\bar{v}$ stored

u-cell; tangential velocity $\bar{u}$ stored

Fig. 6·5 The staggered grid arrangement

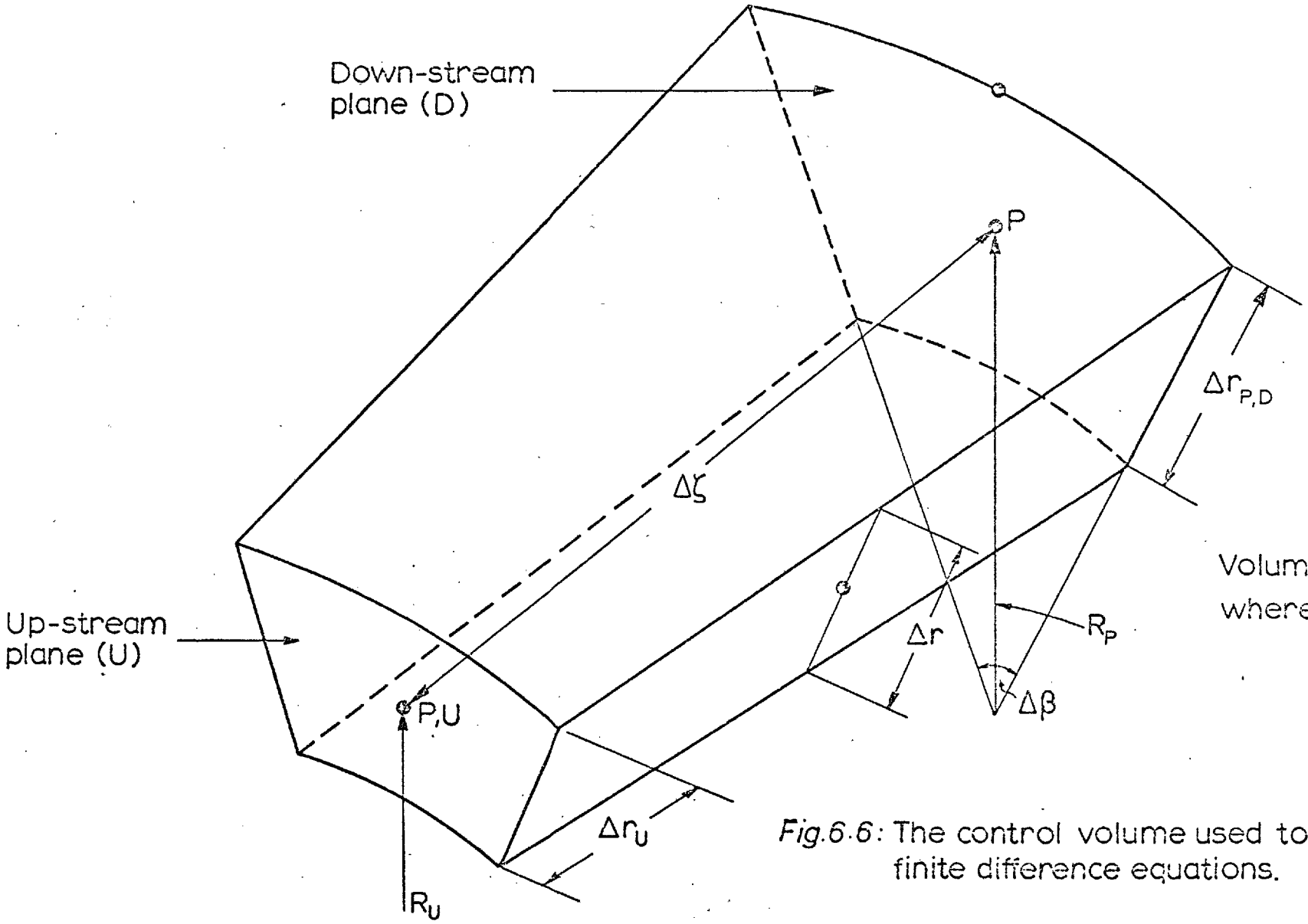


Fig.6.6: The control volume used to derive the finite difference equations.

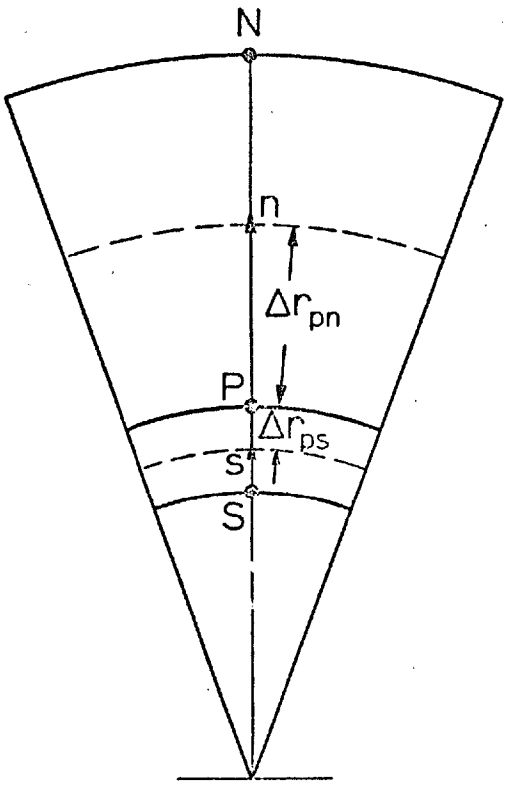


Fig. 6·7: Weighting factor for a non-uniform grid

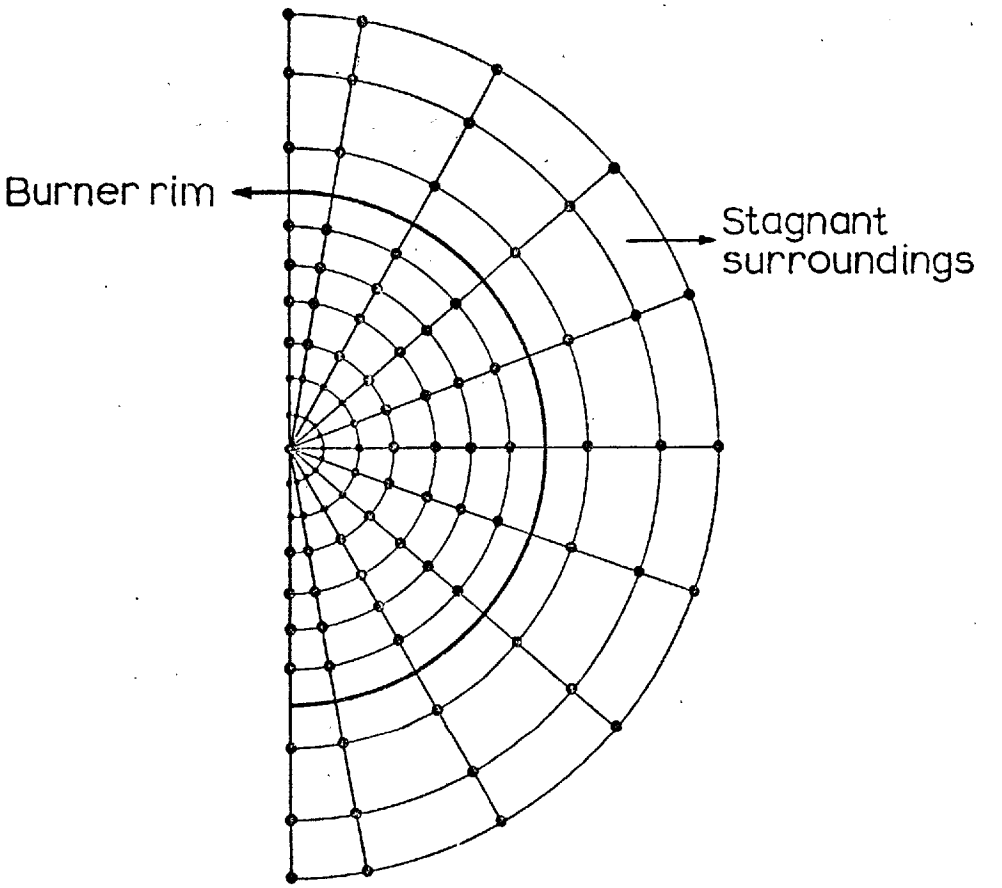


Fig. 6·8a. First cross-stream plane

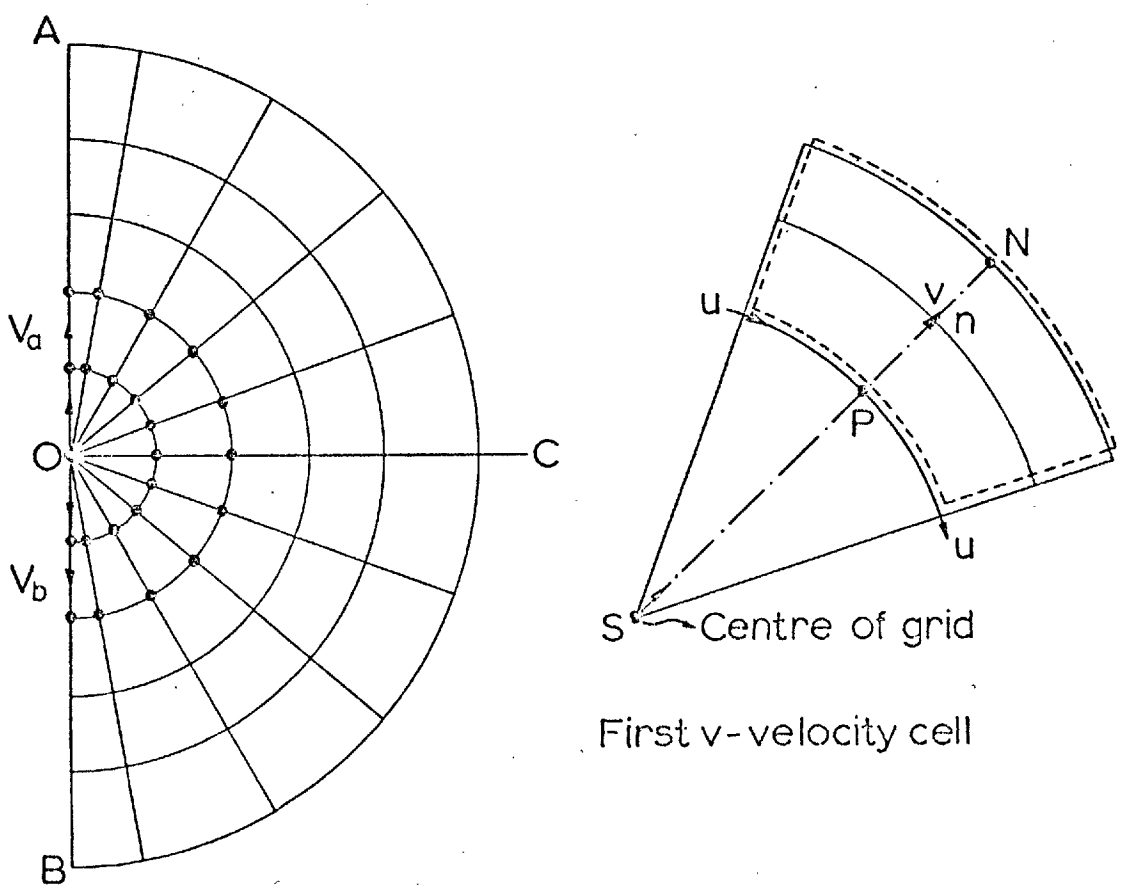


Fig. 6·8b: Boundary conditions for the calculation procedure

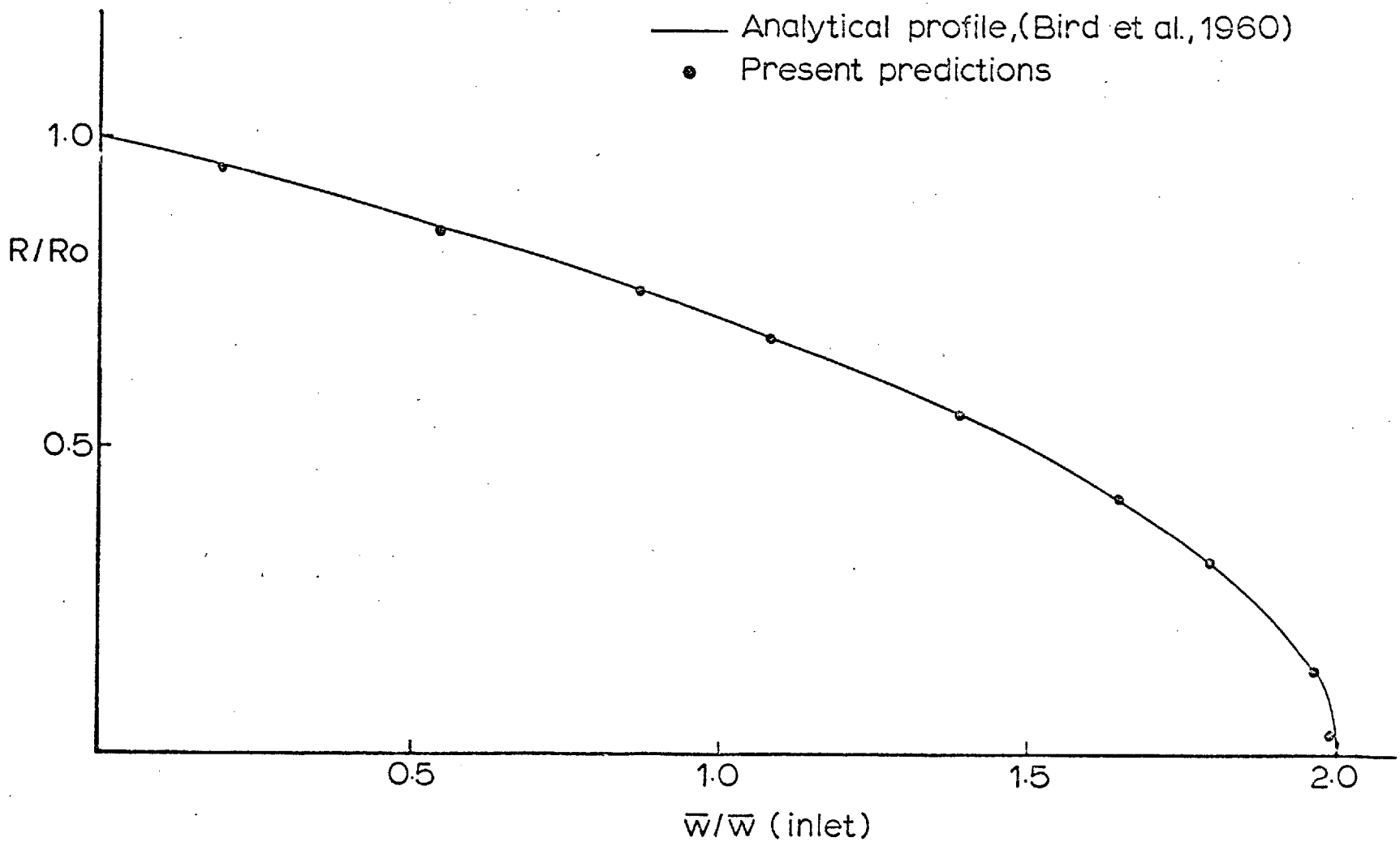


Fig. 6.9: Fully developed profile of axial velocity in a round pipe.

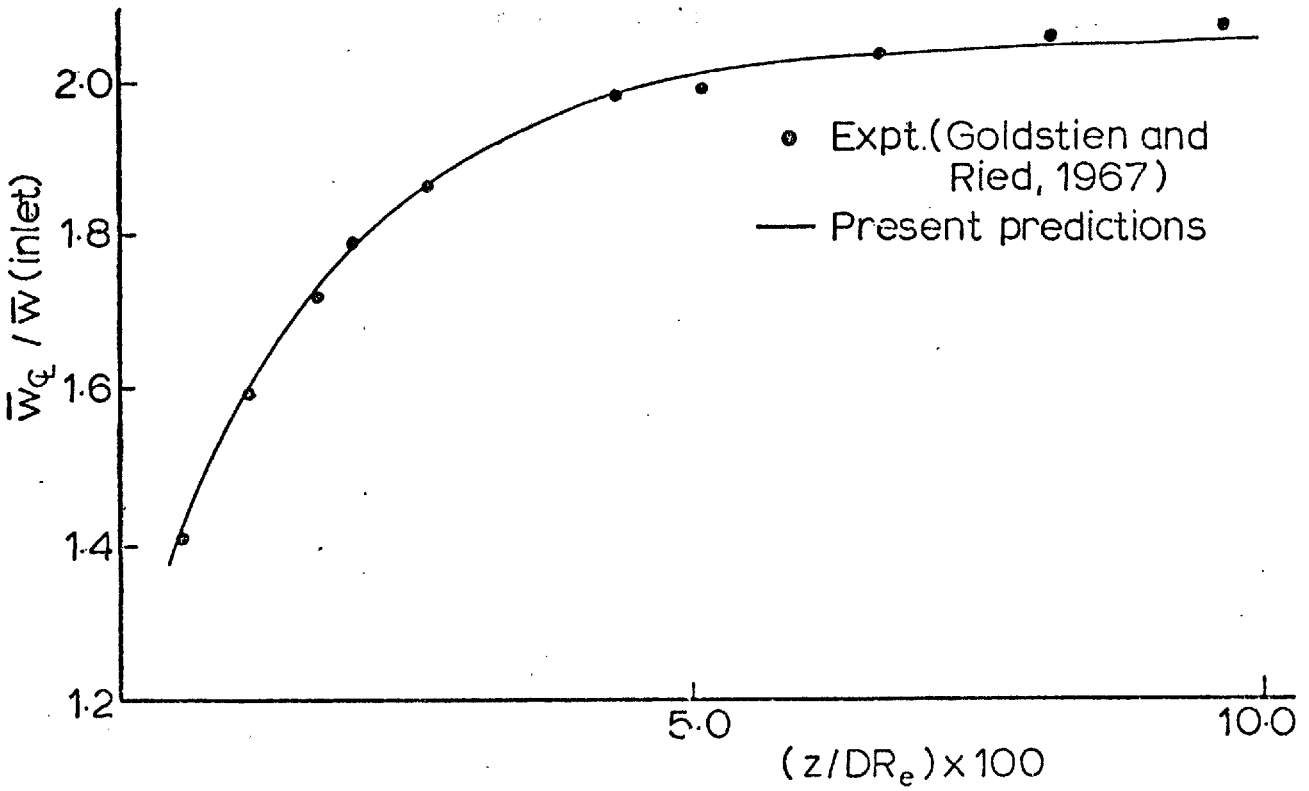


Fig.6·10: Centre-line velocity development in a square duct

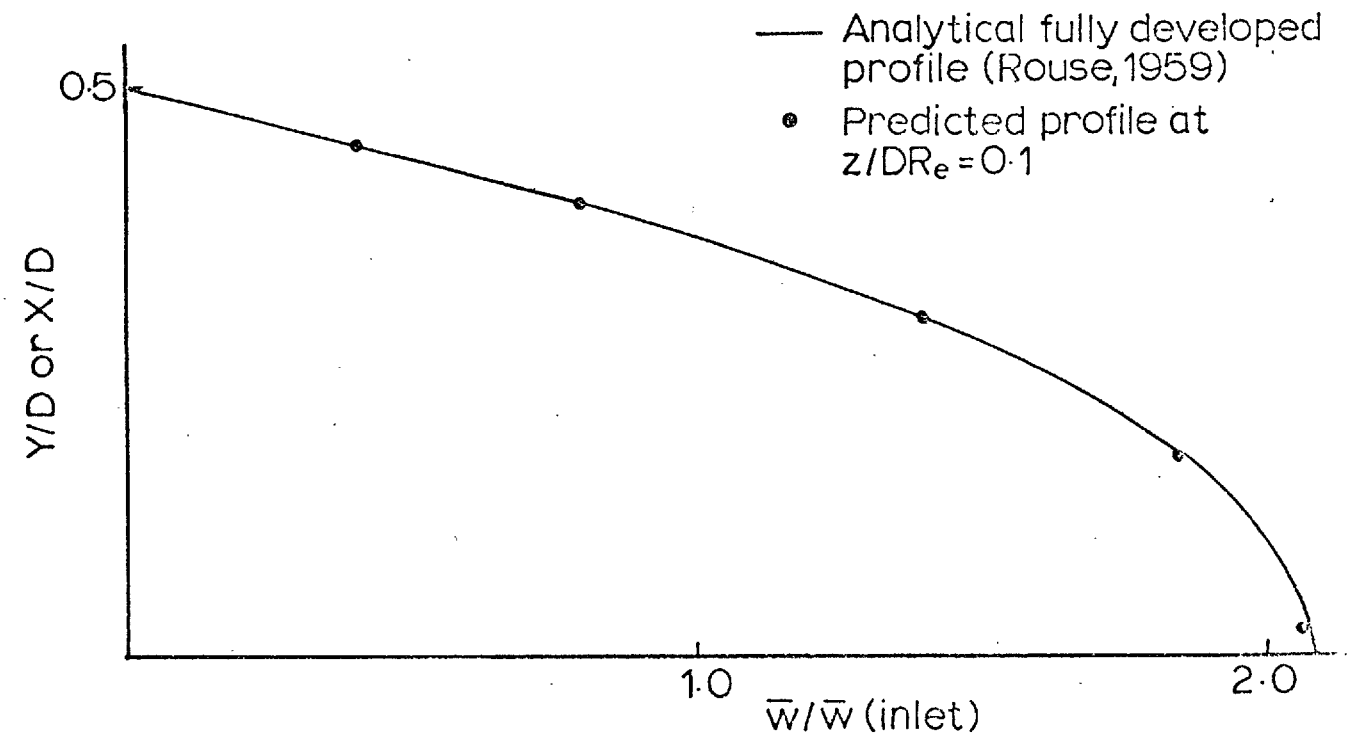
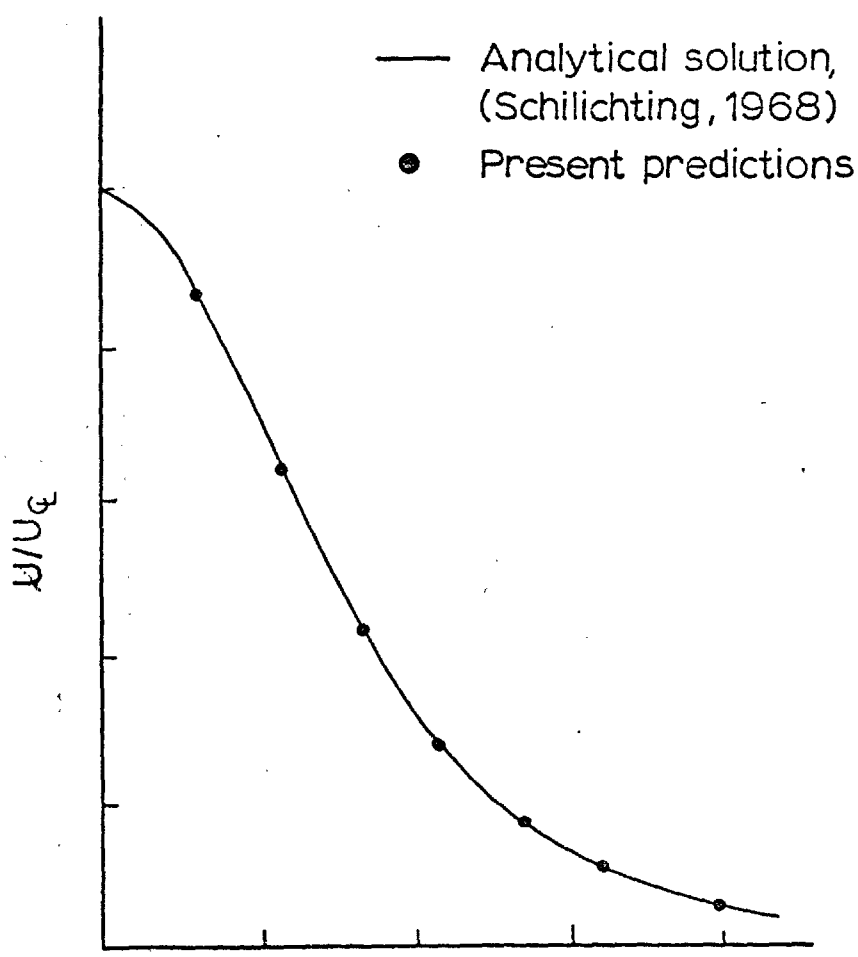


Fig.6·11: Fully developed velocity profile in a square duct (central plane).



Y_{max}= Width of computation grid

Fig. 6·12: Radial distribution of $\bar{U}$

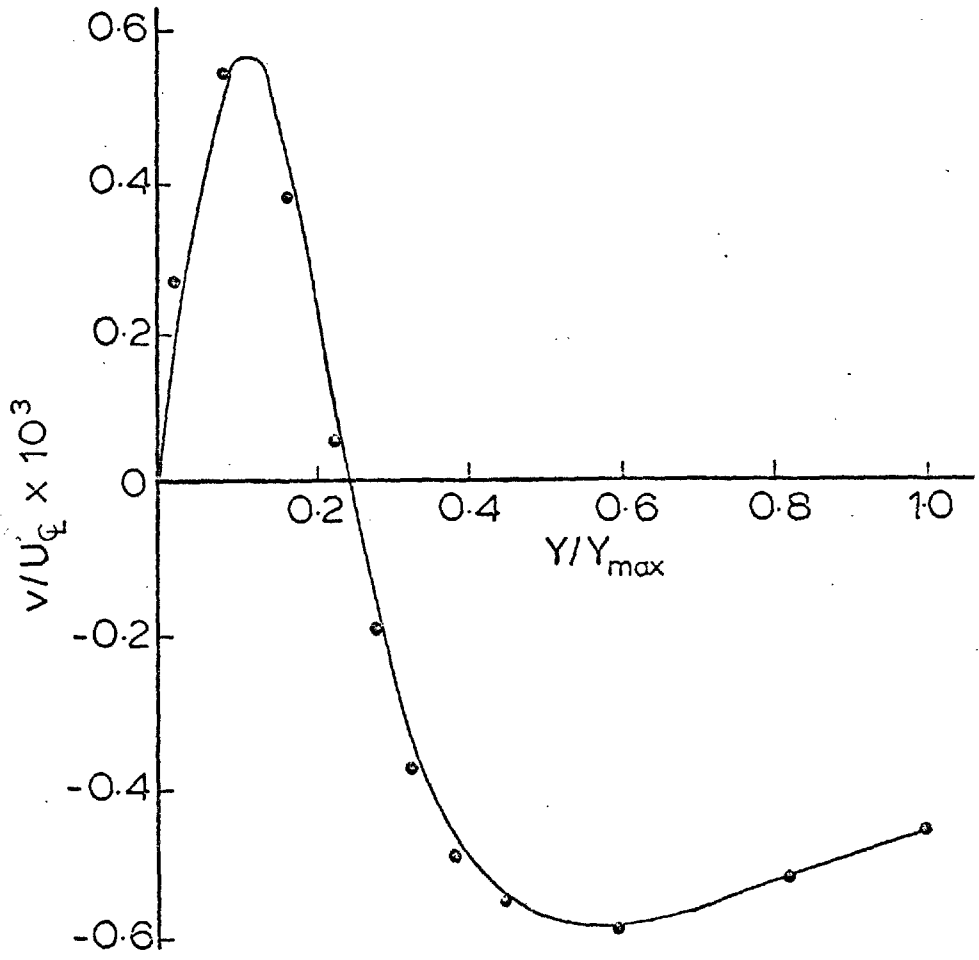


Fig. 6·13: Radial distribution of $\bar{v}$

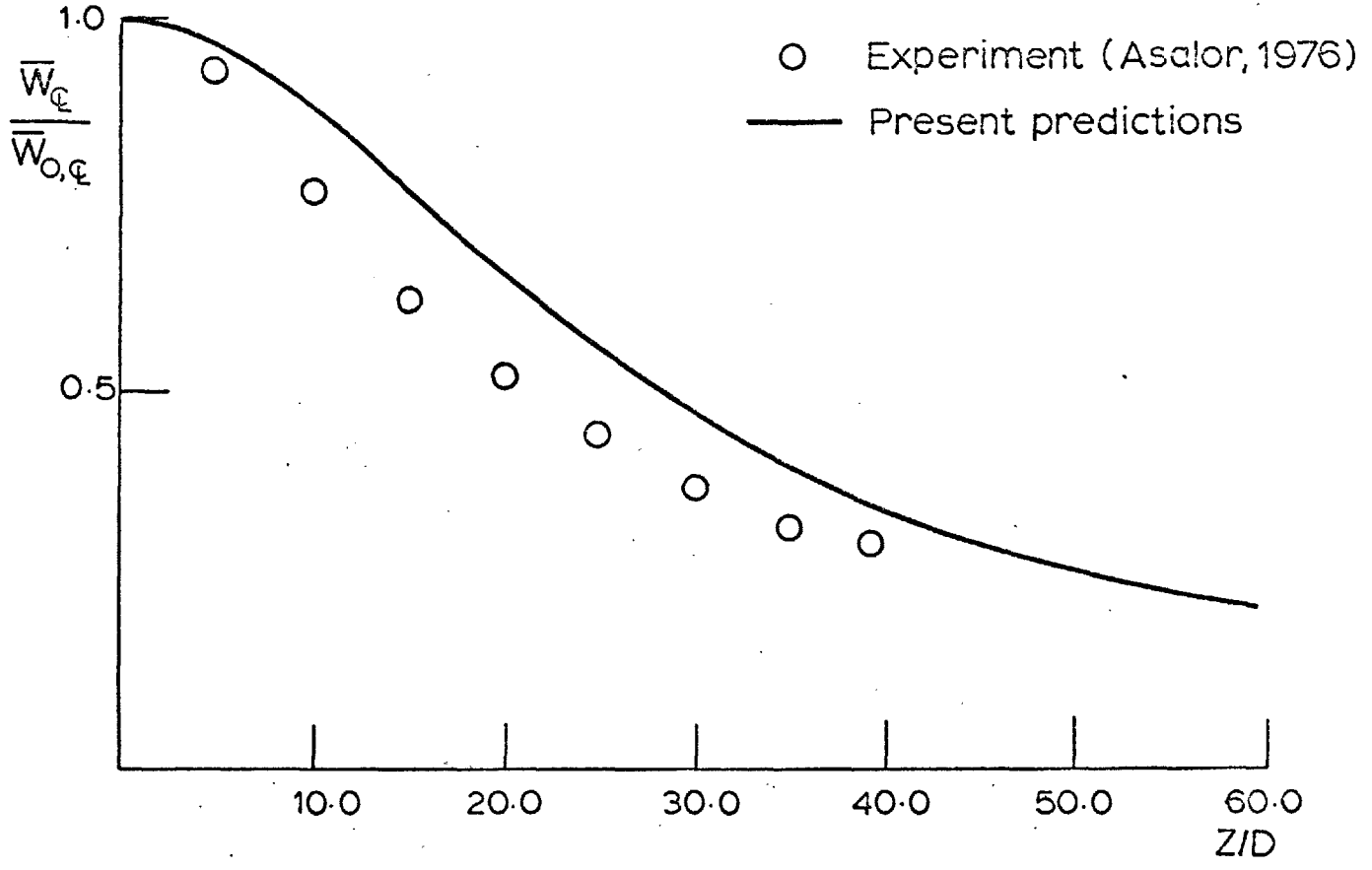


Fig. 7·1 : Axial distribution of $\overline{W}_{\mathfrak{C}} / \overline{W}_{O,\mathfrak{C}}$

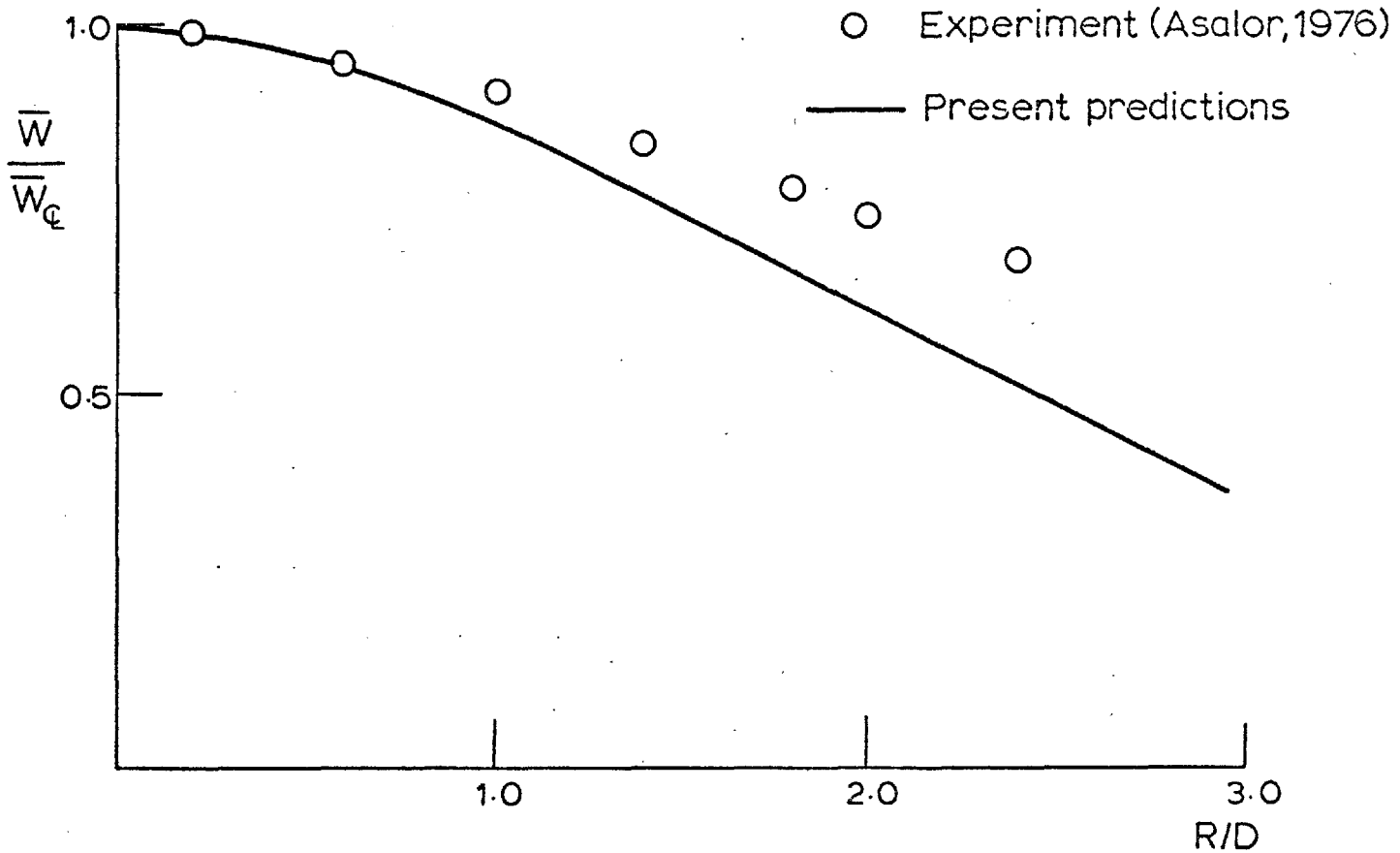


Fig. 7·2: Radial profile of $\overline{W}/\overline{W}_{\mathbb{C}}$ at Z/D=39

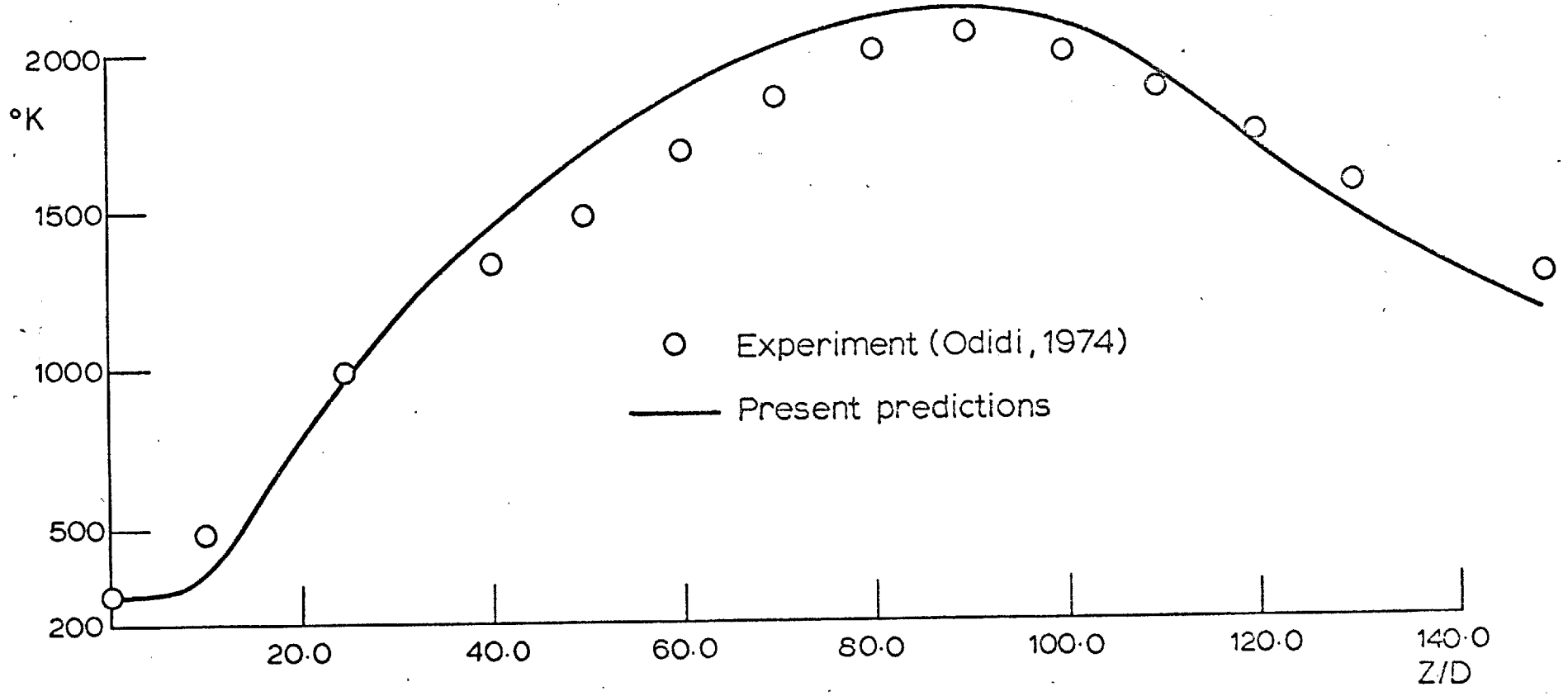


Fig. 7.3: Axial distribution of mean temperature.

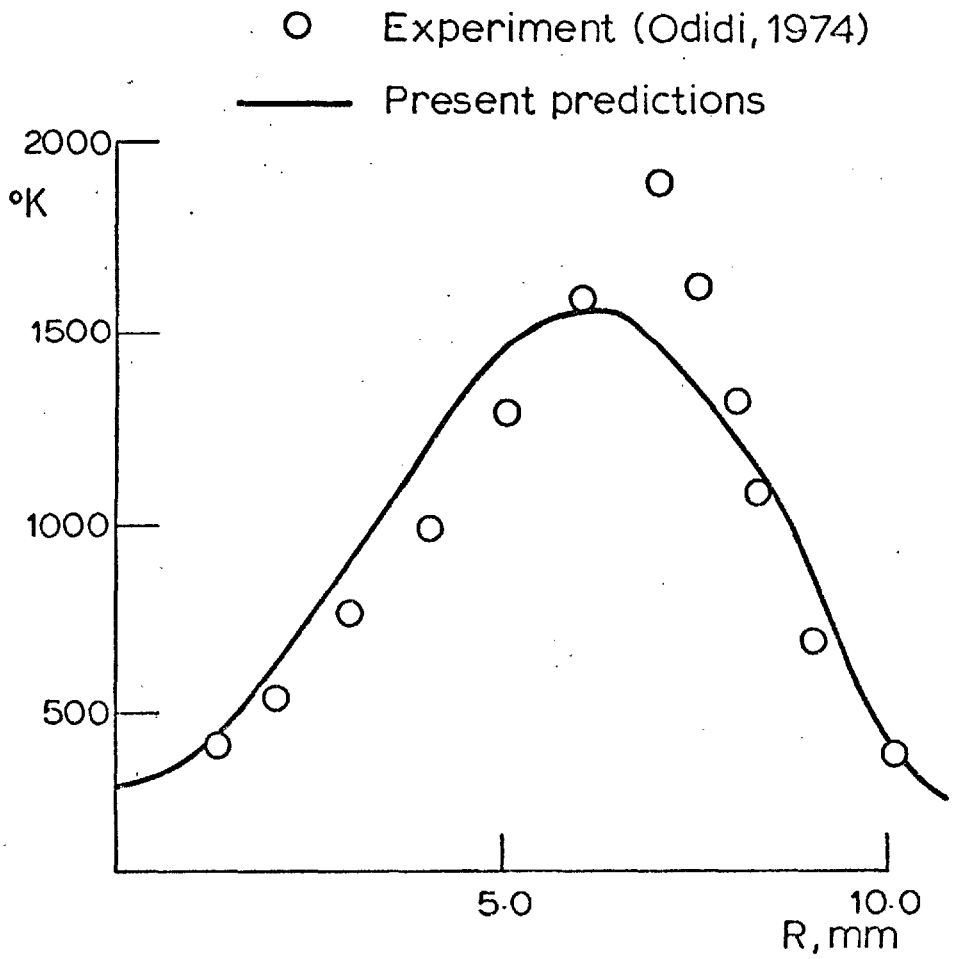


Fig. 7·4: Radial profile of mean temperature at Z/D = 10·0

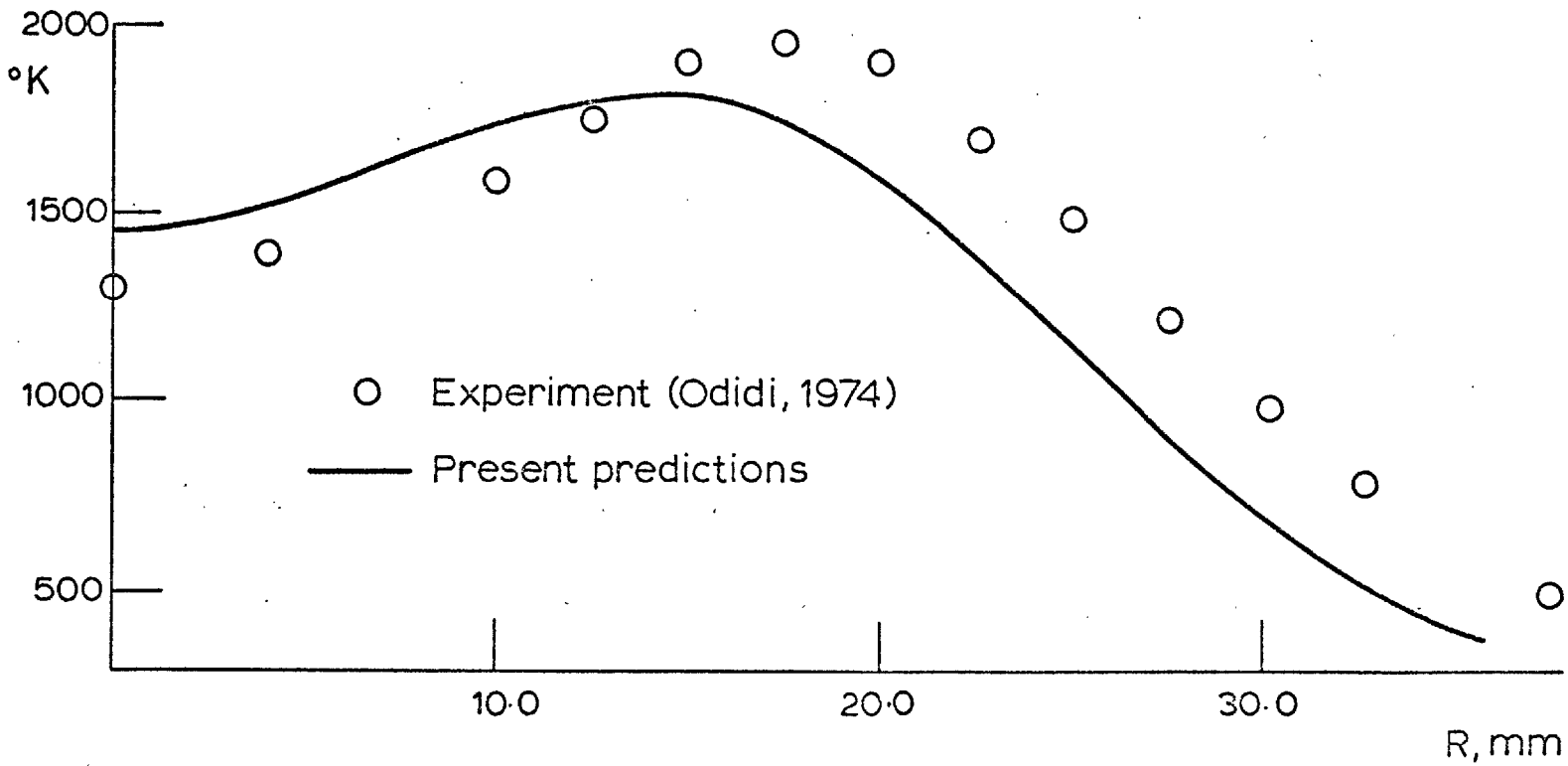


Fig. 7·5: Radial profile of mean temperature at Z/D = 40·0

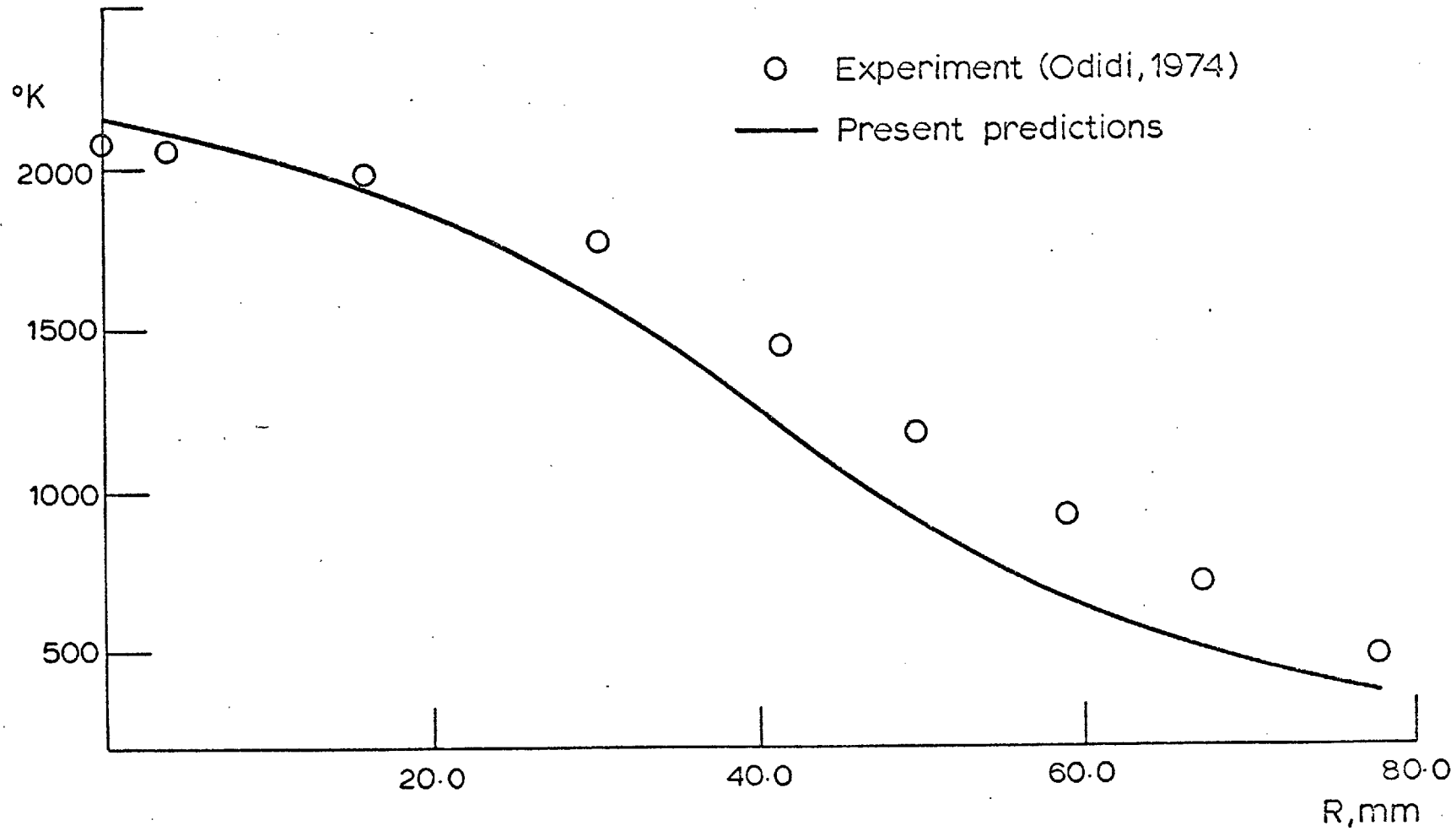


Fig. 7·6: Radial profile of mean temperature at Z/D = 90·0

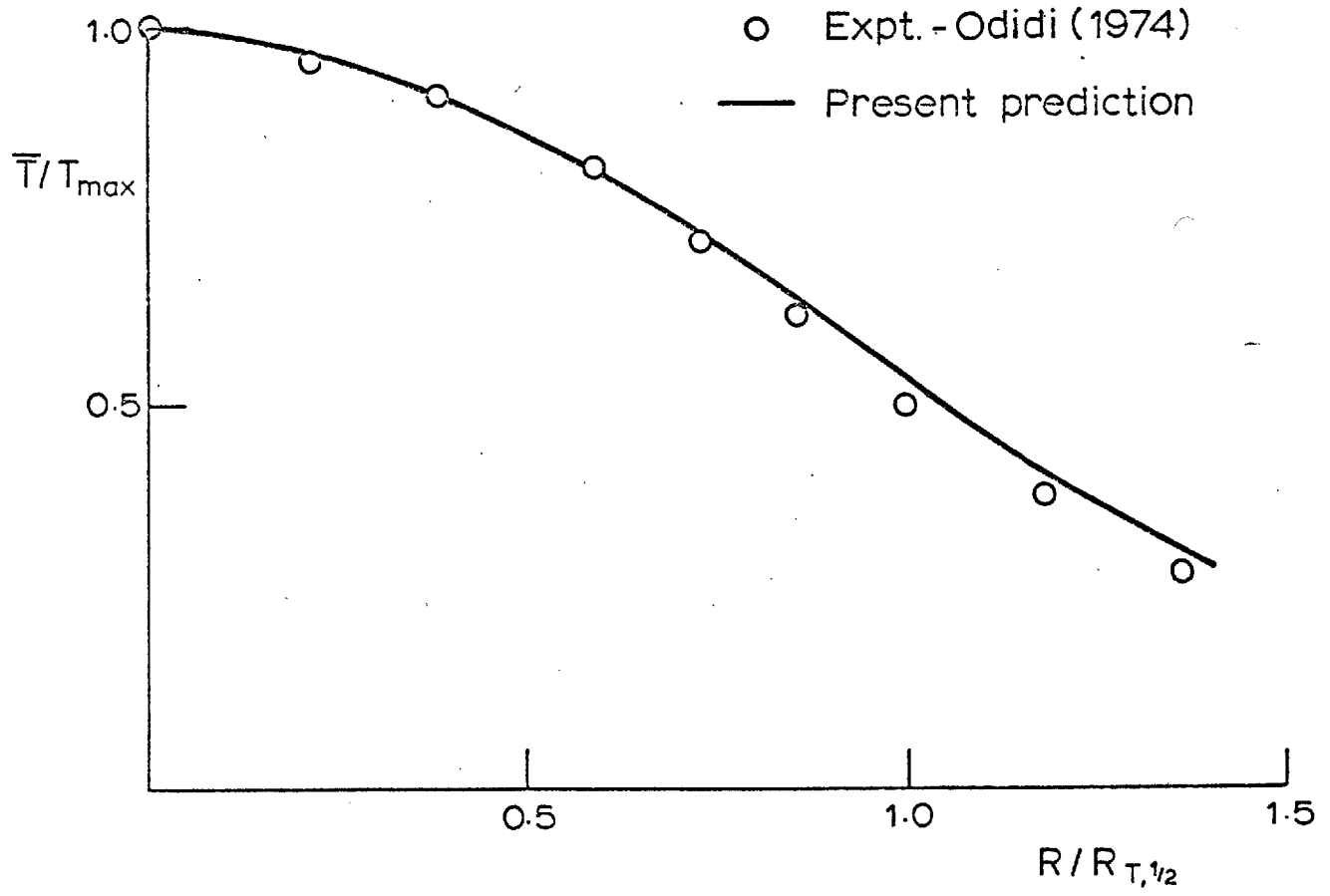


Fig. 7.7: Non-dimensional profile of mean temperature at Z/D = 90.0

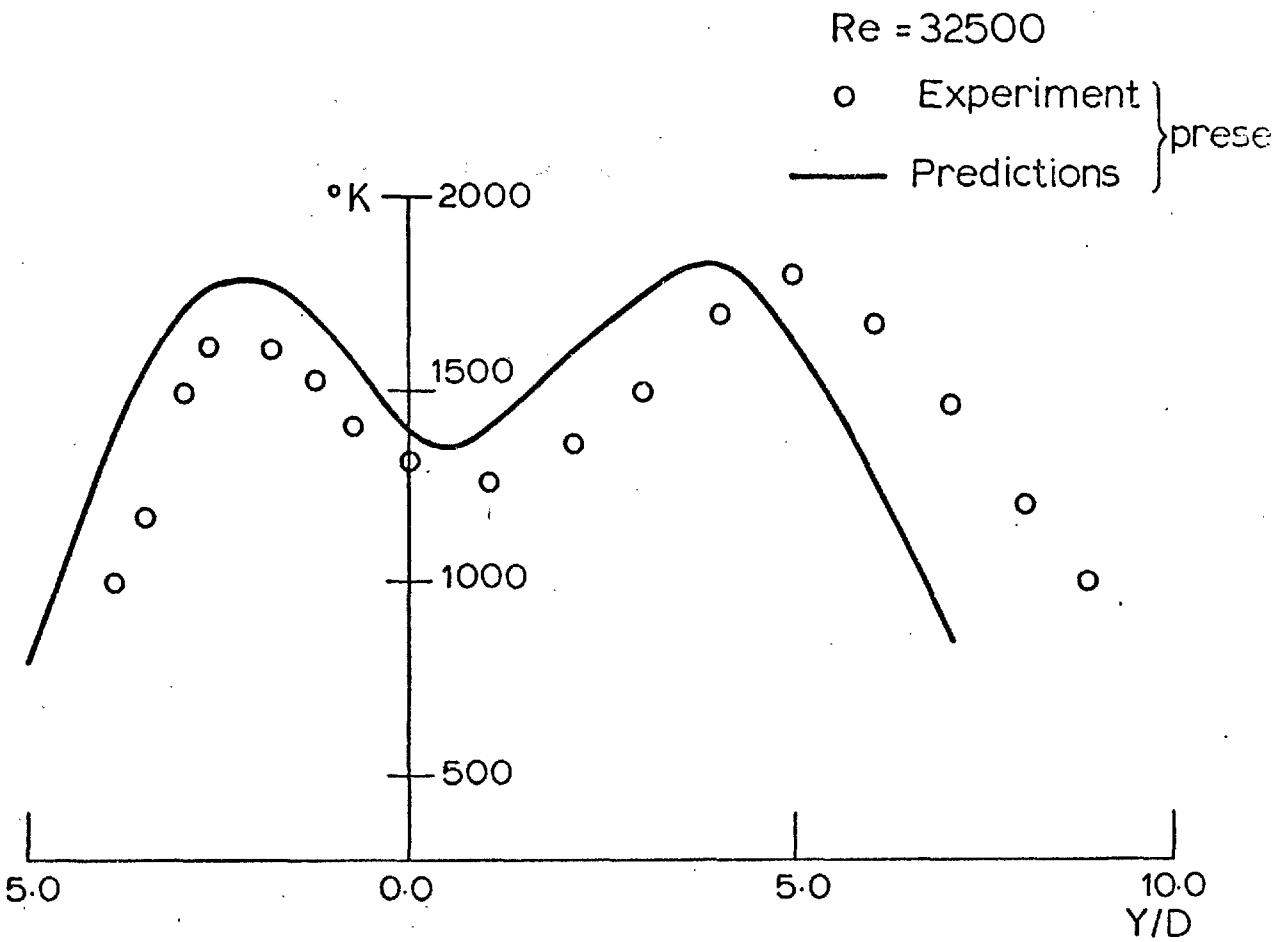


Fig. 7.8: Temperature profile along Y-axis at Z/D = 35·4

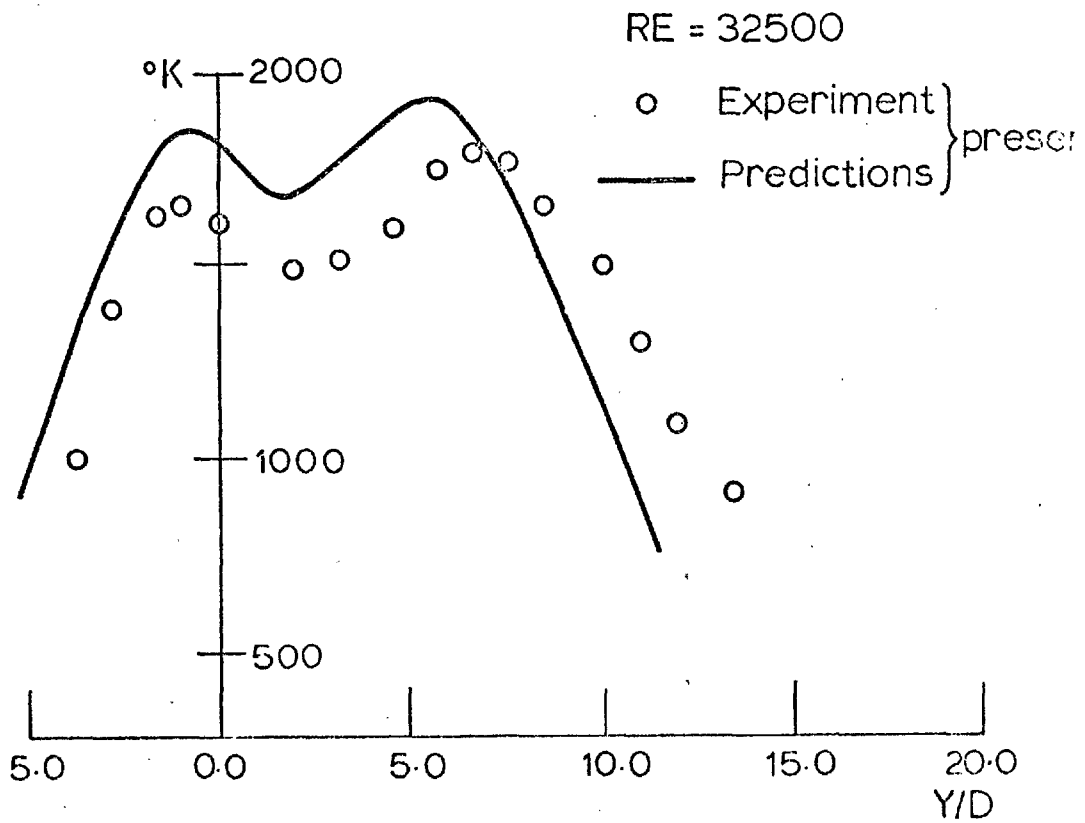


Fig. 7.9: Temperature profile along Y-axis at Z/D = 47

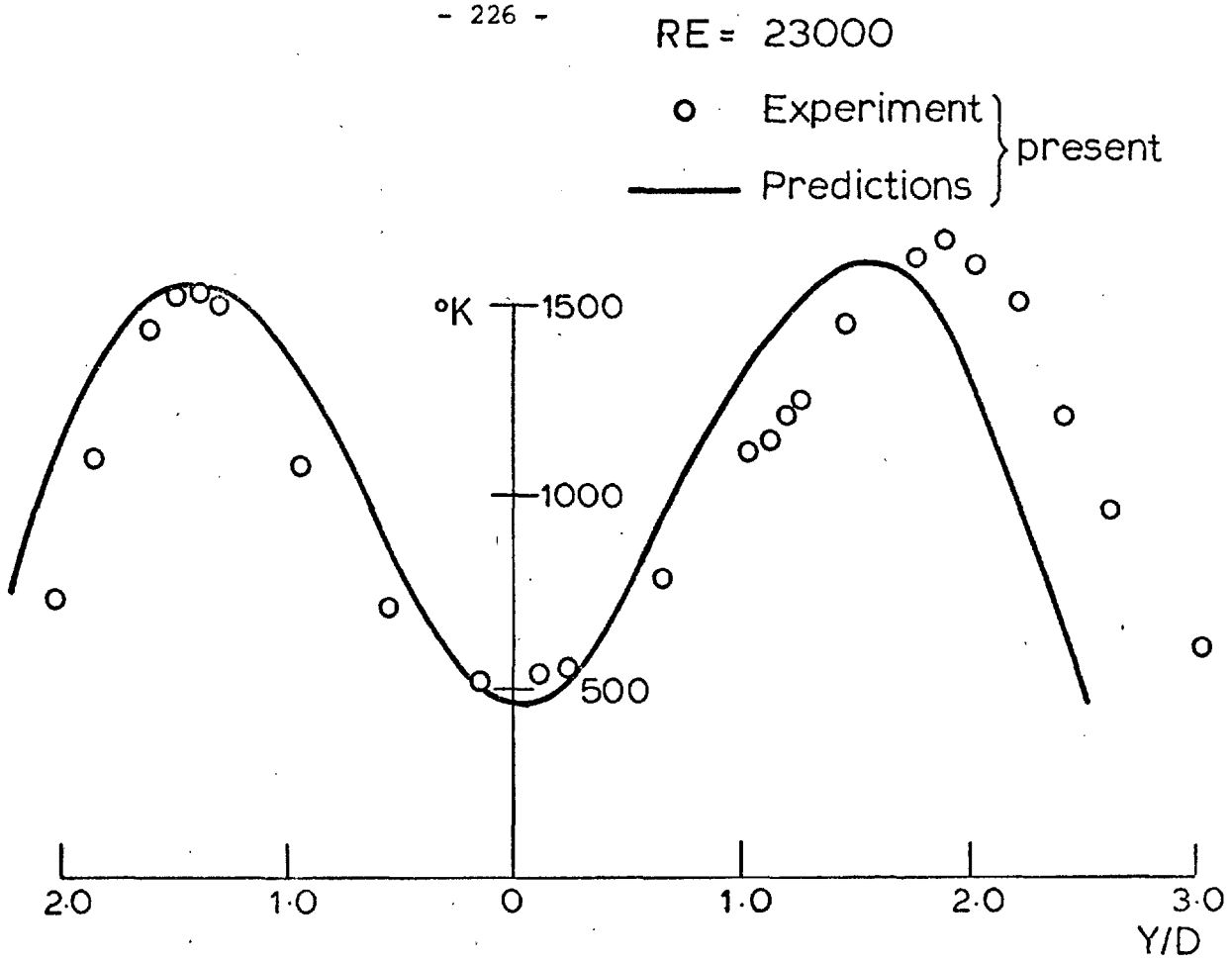


Fig. 7·10a: Temperature profile along Y-axis at Z/D = 13·0

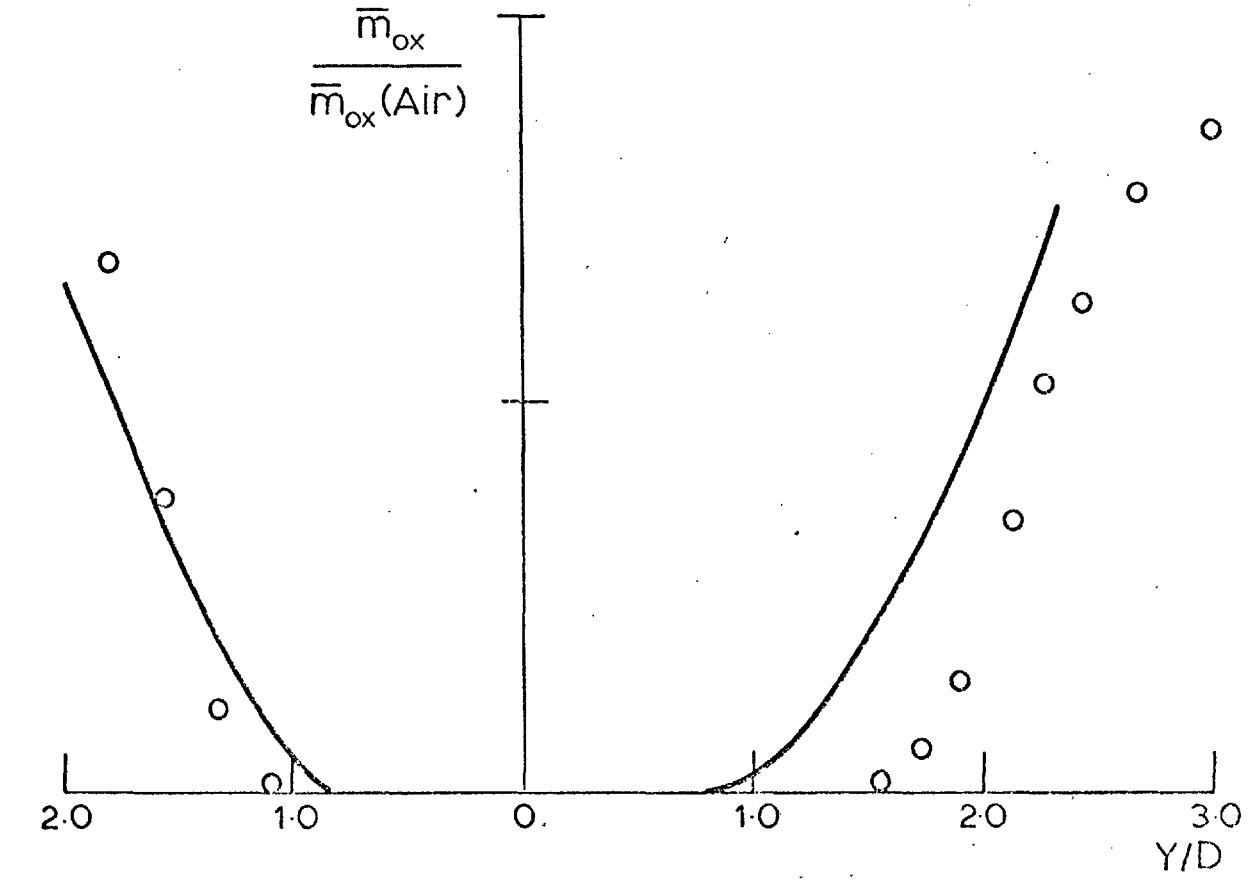


Fig. 7·10b: Oxygen concentration profile along Y-axis at Z/D = 13·0

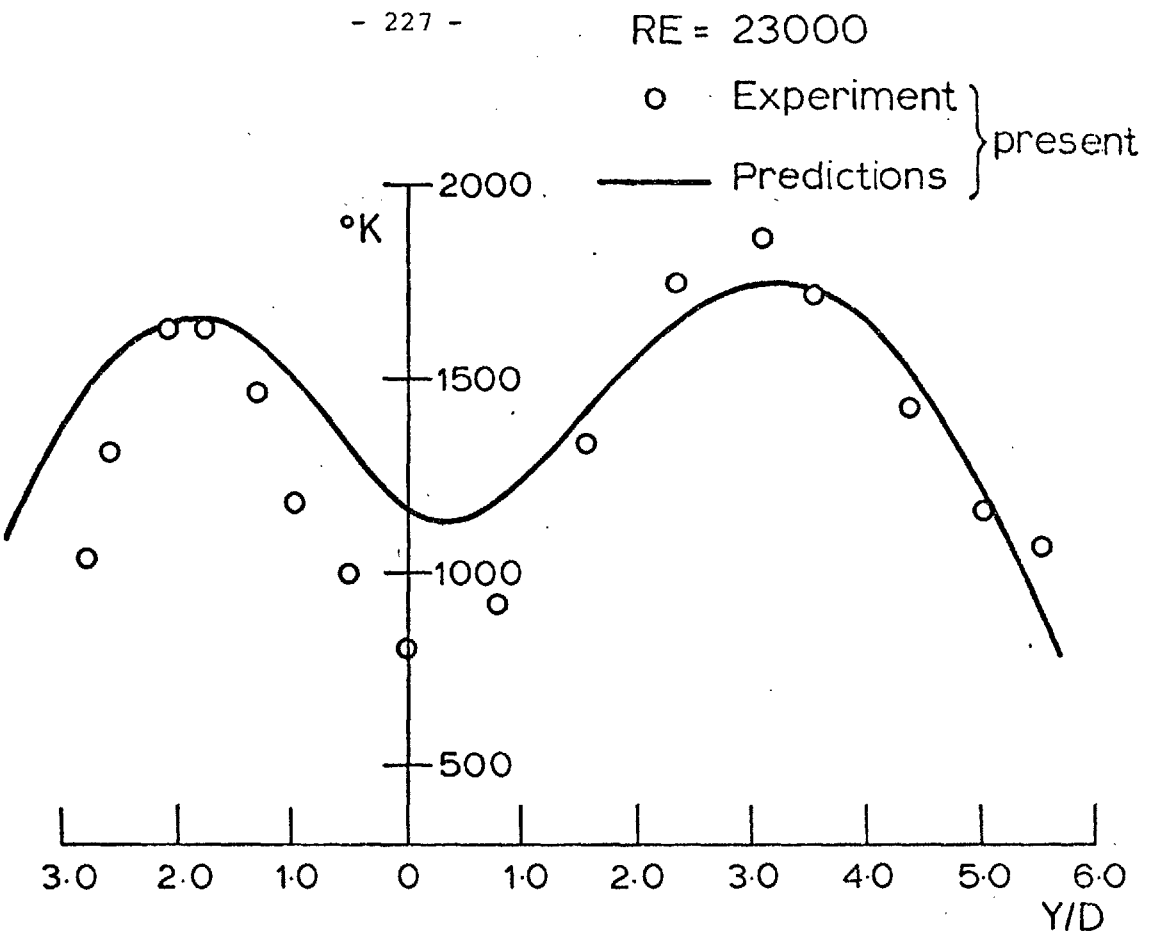


Fig. 7·11a: Temperature profile along Y-axis at Z/D = 29·0

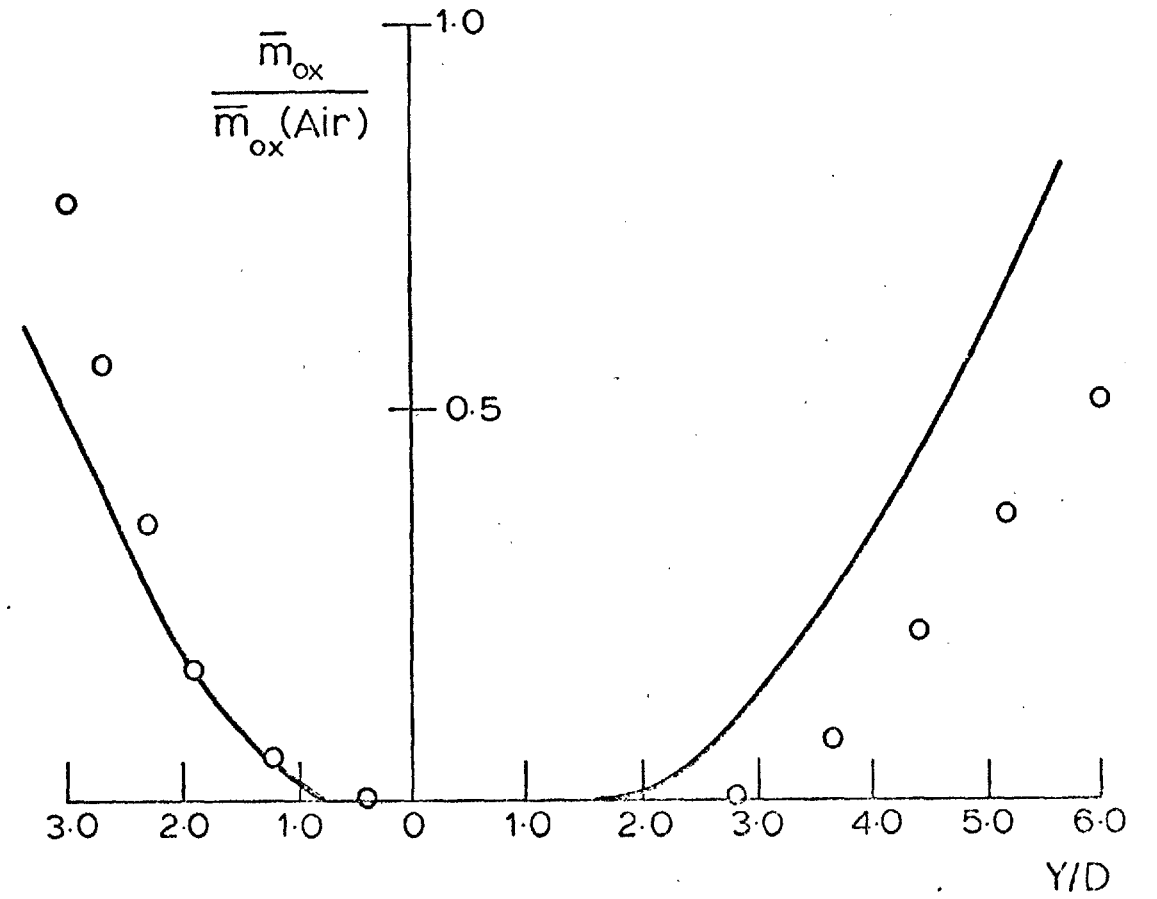


Fig. 7·11b: Oxygen concentration profile along Y-axis at Z/D = 29·0

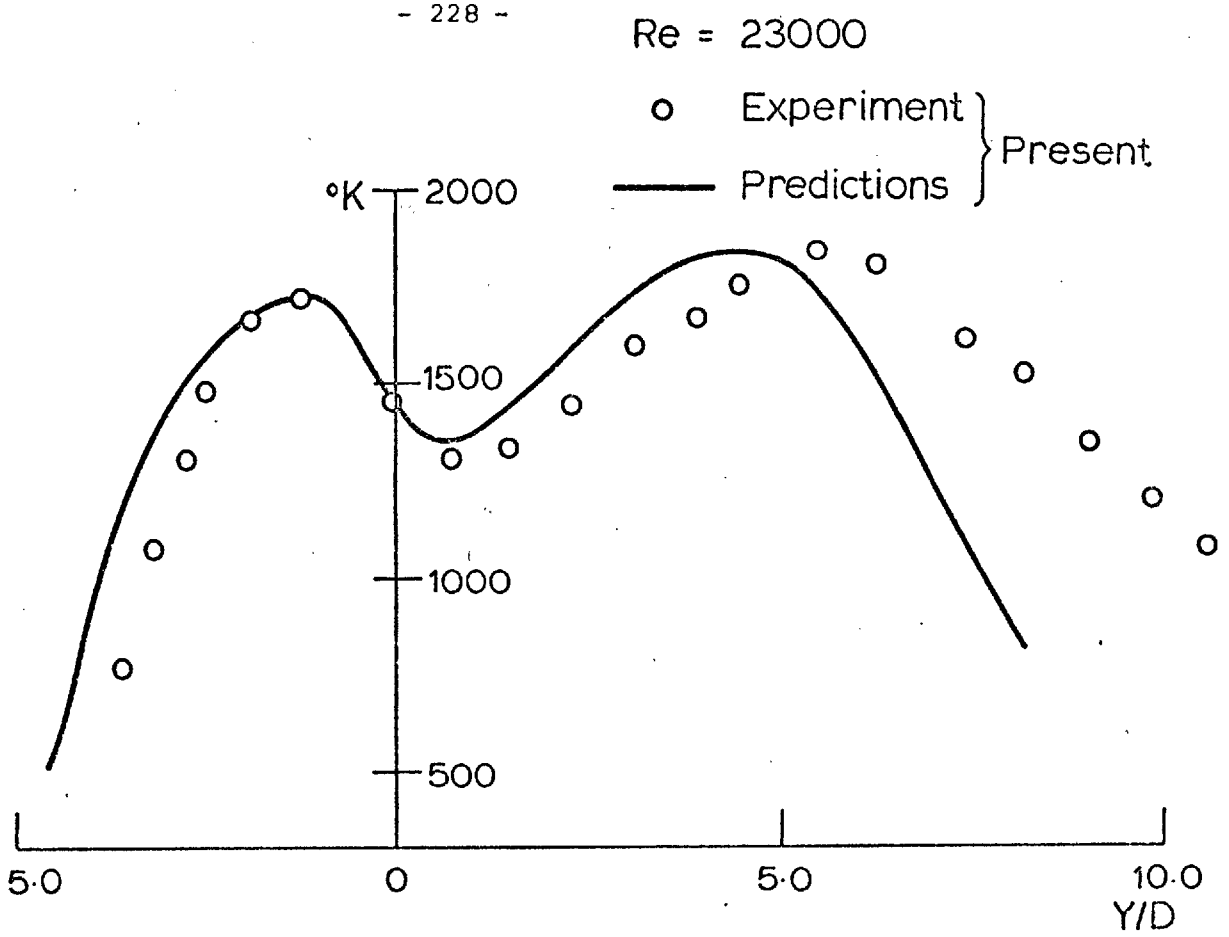


Fig.12a: Temperature profile along Y-axis at Z/D = 35·4

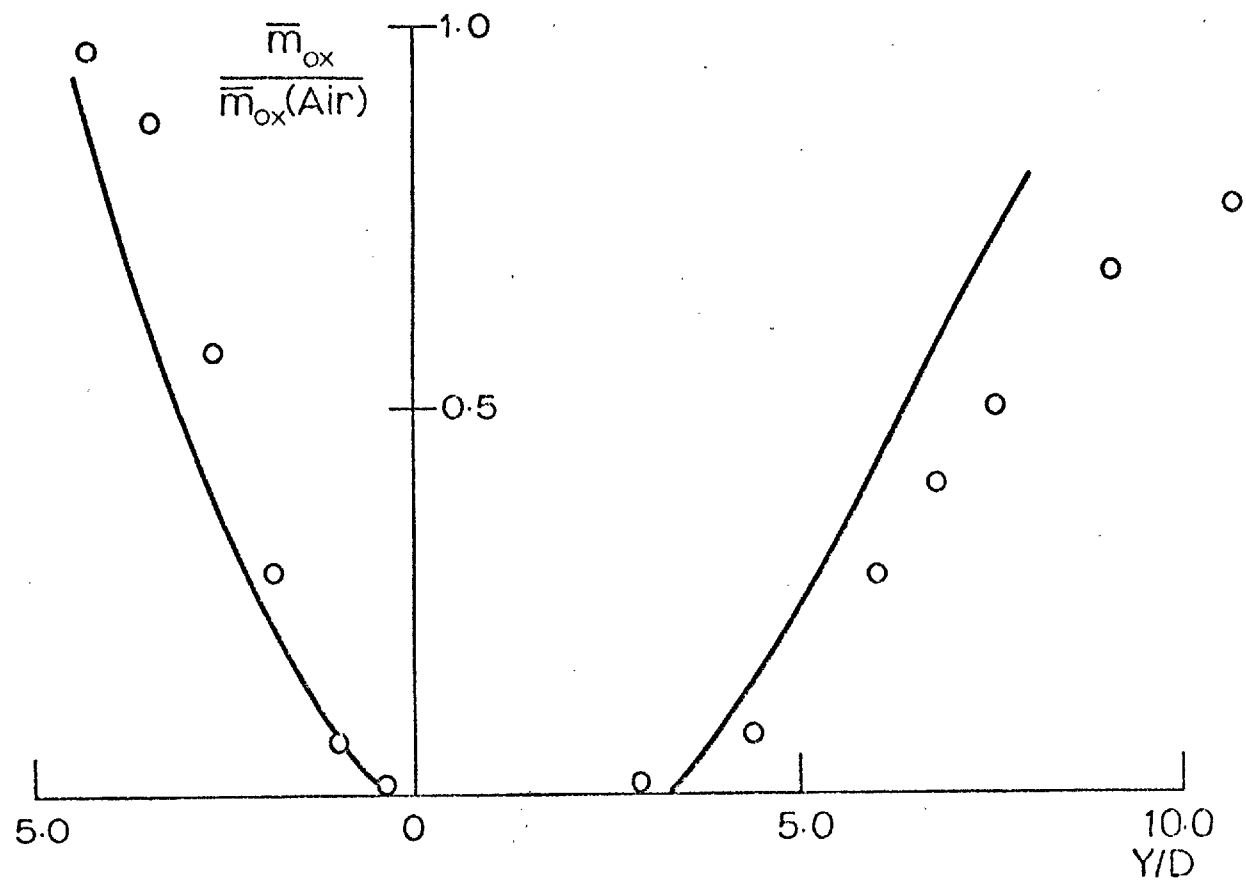


Fig.12b: Oxygen concentration profile along Y-axis at Z/D = 35·4

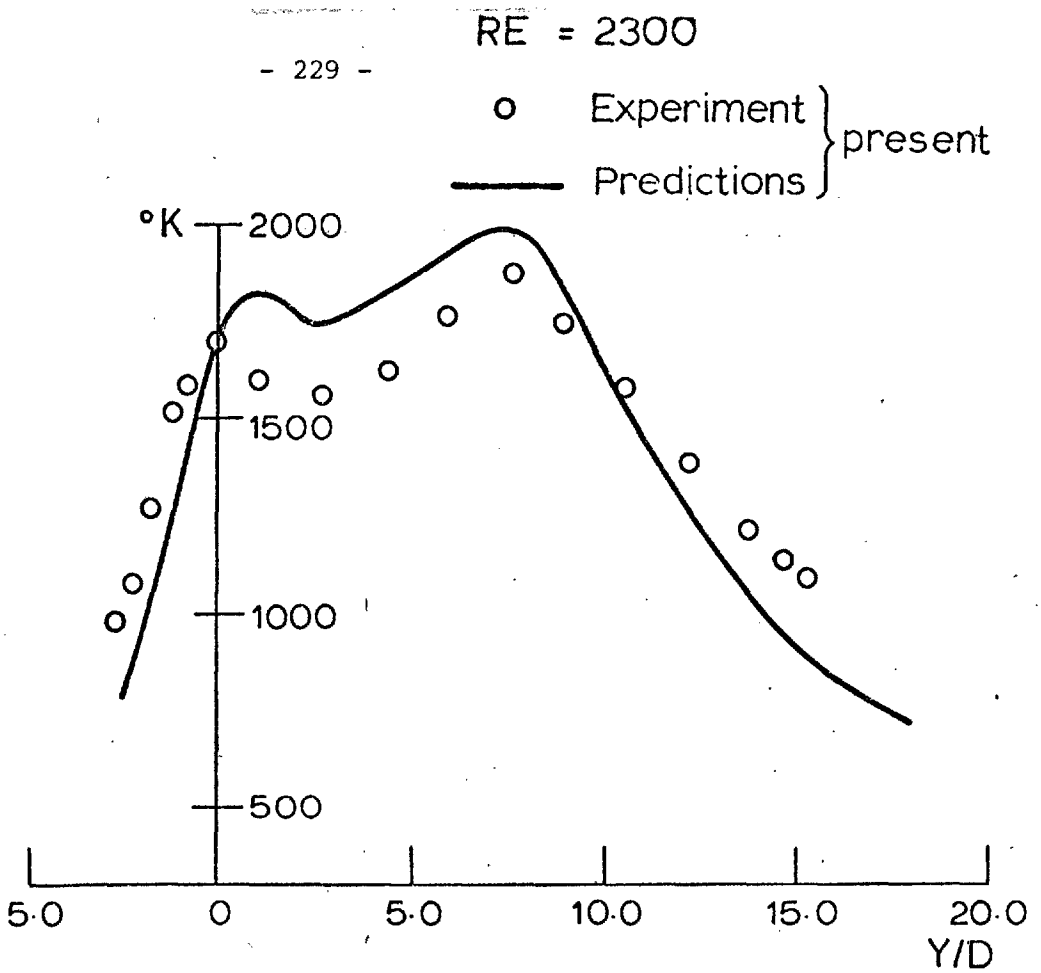


Fig.7·13a: Temperature profile along Y-axis at Z/D = 47·0

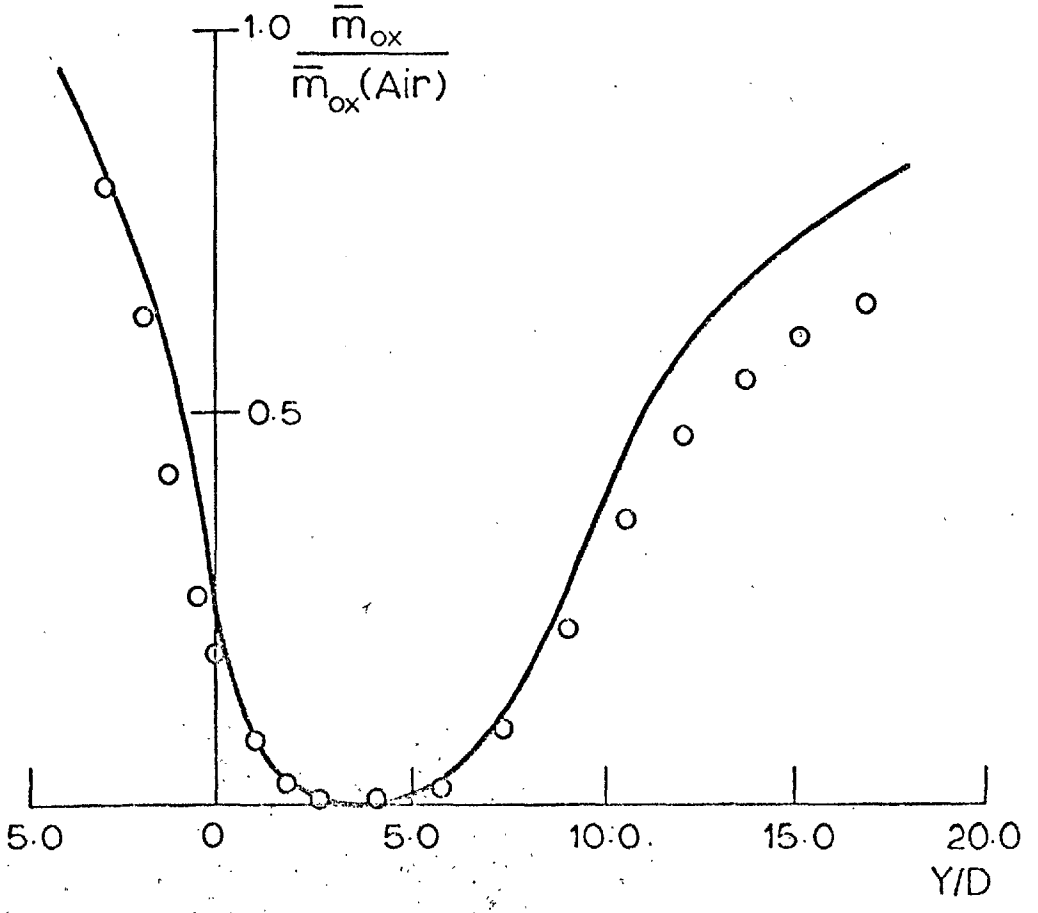


Fig.7·13b: Oxygen concentration profile along Y-axis at Z/D = 47·0

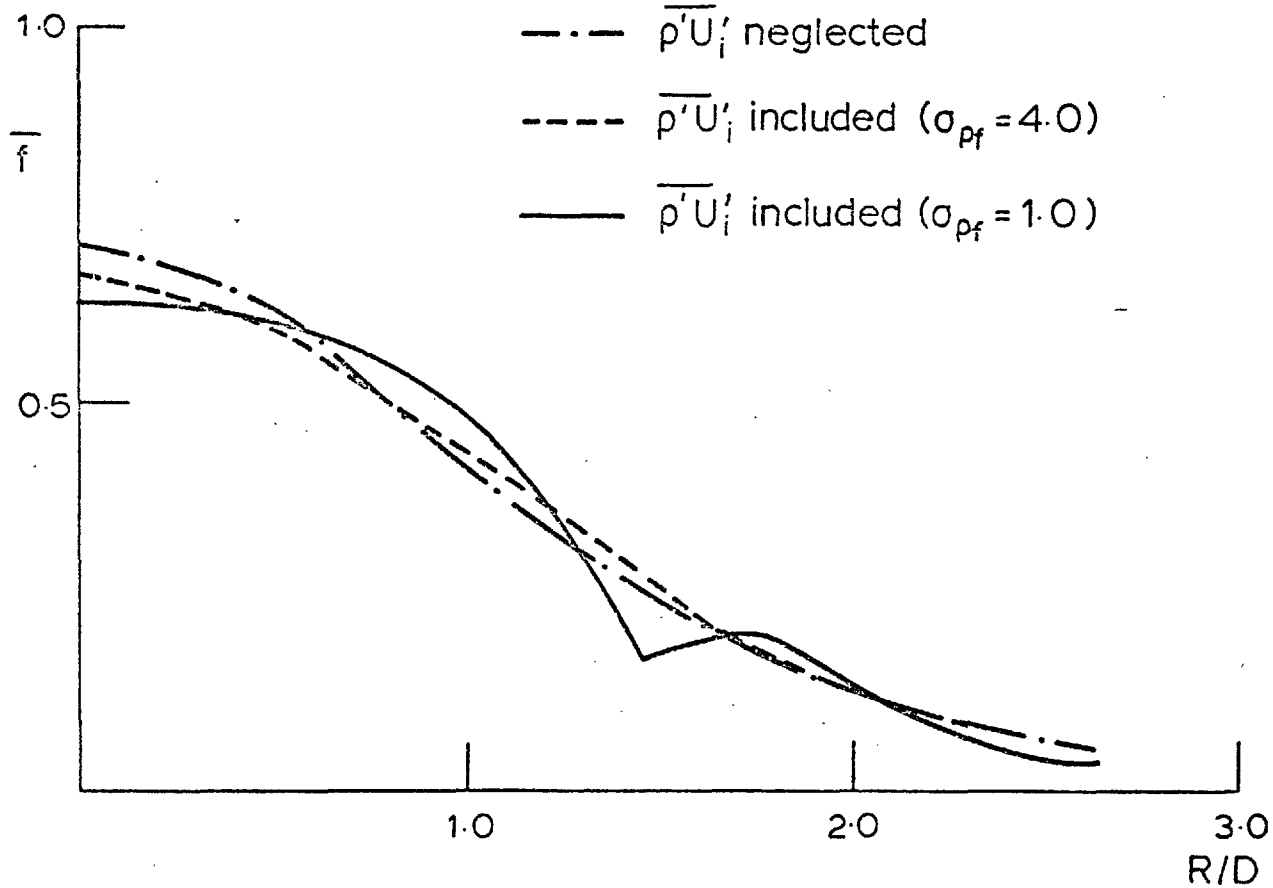


Fig. 7·14: Radial profile of $\overline{f}$ at $Z/D = 20{\cdot}0$

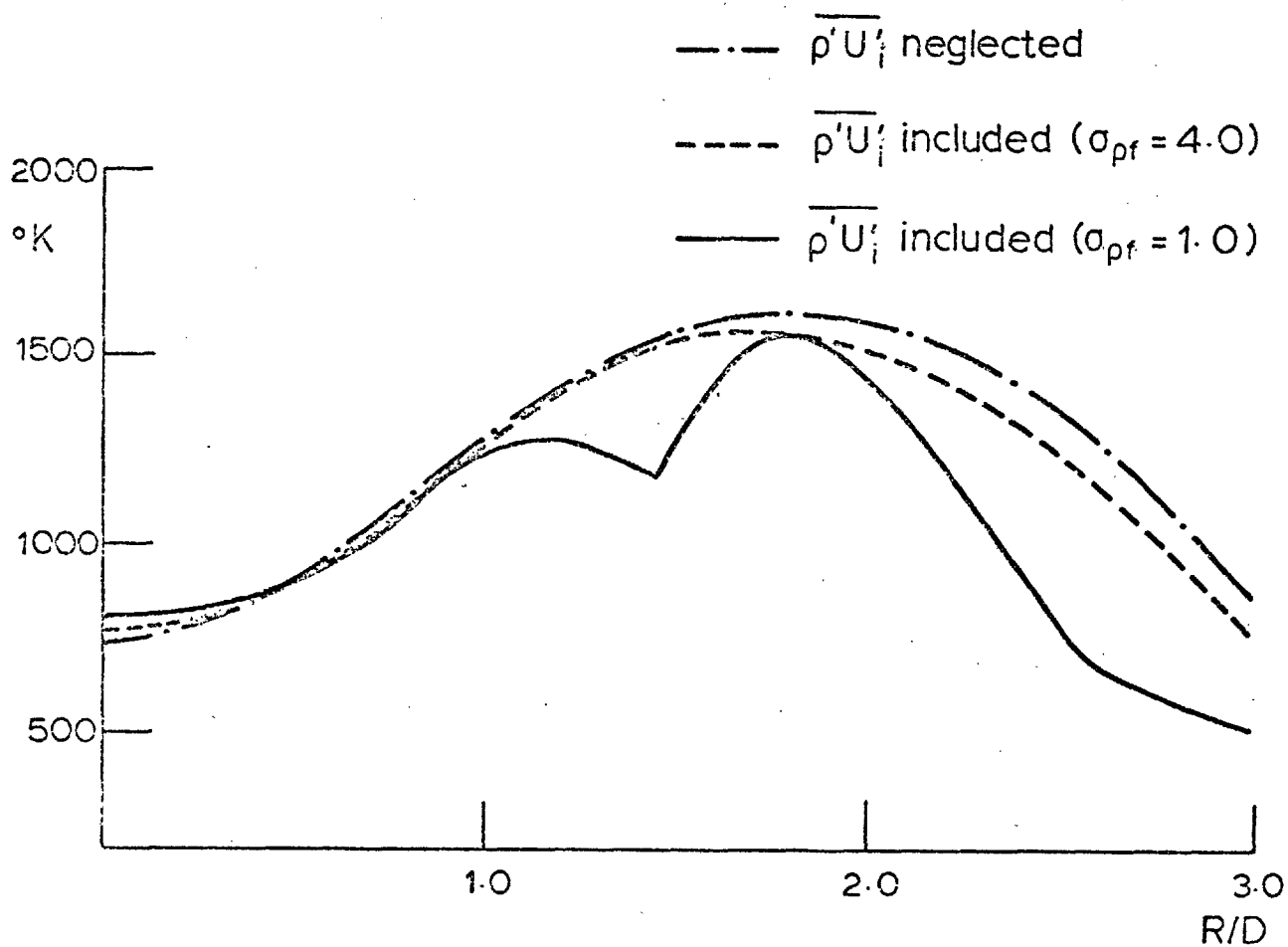


Fig. 7.15: Radial profile of $\overline{T}$ at $Z/D = 20$